Integrable spin, vertex and loop models

Paul Melotti

▶ **To cite this version:**

Paul Melotti. Integrable spin, vertex and loop models. Statistics [math.ST]. Sorbonne Université, 2019. English. NNT : 2019SORUS258 . tel-02277485v2

HAL Id: tel-02277485
https://theses.hal.science/tel-02277485v2

Submitted on 16 Oct 2020

HAL is a multi-disciplinary open access archive for the deposit and dissemination of scientific research documents, whether they are published or not. The documents may come from teaching and research institutions in France or abroad, or from public or private research centers.

L'archive ouverte pluridisciplinaire **HAL**, est destinée au dépôt et à la diffusion de documents scientifiques de niveau recherche, publiés ou non, émanant des établissements d'enseignement et de recherche français ou étrangers, des laboratoires publics ou privés.

THÈSE DE DOCTORAT
DE SORBONNE UNIVERSITÉ

Spécialité : Mathématiques

École doctorale n°386: École doctorale de Sciences Mathématiques de Paris Centre

réalisée

au Laboratoire de Probabilités, Statistique et Modélisation

sous la direction de Cédric BOUTILLIER et Béatrice DE TILIÈRE

présentée par

Paul MELOTTI

pour obtenir le grade de :

DOCTEUR DE SORBONNE UNIVERSITÉ

Sujet de la thèse :

Modèles intégrables de spins, vertex et boucles

Rapporteurs :

M. Vincent BEFFARA
M. Julien DUBÉDAT

soutenue le 28 juin 2019

devant le jury composé de :

Mme	Marie ALBENQUE	Examinatrice
M.	Vincent BEFFARA	Rapporteur
M.	Nathanaël BERESTYCKI	Examinateur
M.	Cédric BOUTILLIER	Directeur de thèse
Mme	Béatrice DE TILIÈRE	Directrice de thèse
M.	Thierry LÉVY	Examinateur
M.	Ioan MANOLESCU	Examinateur
Mme	Sandrine PÉCHÉ	Examinatrice

Table des matières

Introduction **1**
Plan de la thèse / Outline of this thesis . . . 2
1 Bref historique . . . 4
1.1 Mécanique statistique à l'équilibre . . . 4
1.2 Comportements critiques . . . 6
1.3 Intégrabilité... . . . 7
1.4 Universalité . . . 11
2 A few classical models . . . 13
2.1 Ising model . . . 13
2.2 Dimer model . . . 15
2.3 Vertex models . . . 19
2.4 Loop models . . . 23
2.5 Transformations of models . . . 24
3 Six points of view on star-triangle transformations . . . 31
3.1 Simplifying graphs . . . 31
3.2 Coupling relations; locality . . . 32
3.3 Commutation of transfer matrices . . . 35
3.4 Operator form of Yang-Baxter equations . . . 37
3.5 Polynomial relations and spatial recurrence . . . 38
3.6 Geometric embeddings and incidence theorems . . . 42
4 Extended abstracts of presented works . . . 46
4.1 Kashaev's recurrence . . . 46
4.2 The free-fermion 8V-model . . . 52
4.3 Incidence theorems and canonical embeddings of graphs . . . 56
4.4 Long paths in partitions of the divisor graph . . . 58

I Kashaev's recurrence **61**
I.1 Introduction . . . 63
I.2 Free-fermionic $C_2^{(1)}$ loops and double dimers . . . 67
I.2.1 The $C_2^{(1)}$ loop model on a quadrangulation . . . 67
I.2.2 Dimer model on the quad-graph . . . 68
I.2.3 Free-fermion regime . . . 69
I.2.4 Free energy . . . 74
I.3 Cube flip and Kashaev's recurrence . . . 76
I.3.1 Kashaev's recurrence . . . 77

I.3.2 Parametrization of a free-fermionic $C_2^{(1)}$ loop model . . . 78
I.3.3 Cube flip . . . 79
I.4 Taut configurations on stepped surfaces . . . 83
I.4.1 Stepped surfaces . . . 83
I.4.2 Boundary conditions . . . 84
I.4.3 Weights . . . 85
I.4.4 Algebraic consequences . . . 86
I.4.5 Limit shapes . . . 89
I.4.6 Cube groves . . . 93
I.A Calculations for Lemma I.13 . . . 96
I.B Full Kashaev parametrization of free-fermionic $C_2^{(1)}$ loops . . . 97

II Free-fermion 8V model **101**
II.1 Introduction . . . 103
II.2 Definitions . . . 108
II.2.1 Eight-vertex-model . . . 108
II.2.2 Ising model . . . 111
II.2.3 Dimer model . . . 112
II.2.4 Order and disorder variables . . . 112
II.3 Couplings of 8V-models . . . 114
II.3.1 Spin-vertex correspondence . . . 114
II.3.2 Modifications of weights . . . 115
II.3.3 Free-fermion 8V correlators . . . 116
II.3.4 Coupling of free-fermion 8V-models . . . 117
II.4 Kasteleyn matrices . . . 118
II.4.1 Free-fermion 8V to dimers . . . 118
II.4.2 Skew-symmetric real matrix . . . 120
II.4.3 Skew-hermitian complex matrix . . . 122
II.4.4 Eight-vertex partition function and correlations . . . 125
II.4.5 Relations between matrices $K^{-1}_{\alpha,\beta}$ . . . 126
II.5 Z-invariant regime . . . 132
II.5.1 Checkerboard Yang-Baxter equations . . . 133
II.5.2 Lozenge graphs . . . 134
II.5.3 Local expression for $K^{-1}_{k,l}$ . . . 136
II.5.4 Free energy and Gibbs measure . . . 140
II.A 8V-configurations as 1-forms . . . 141
II.A.1 Setup . . . 141
II.A.2 Fourier transform . . . 143
II.A.3 Correlators . . . 144
II.B Proof of Lemma II.34 . . . 145

III Star-triangle transformation on canonical embeddings **151**
III.1 Introduction . . . 153
III.2 The space of α-quads . . . 156
III.3 The star-triangle move for tangential quads . . . 158
III.3.1 Uniqueness . . . 158

III.3.2 Existence 159
III.4 Partial results for α-quads flip 167

IV Path partitions of the divisor graph **169**
IV.1 Introduction 171
IV.2 Notation 173
IV.3 Lemmas 173
IV.4 Proof of the Proposition 176
IV.5 Proof of the Theorem 178

Bibliographie **181**

Introduction

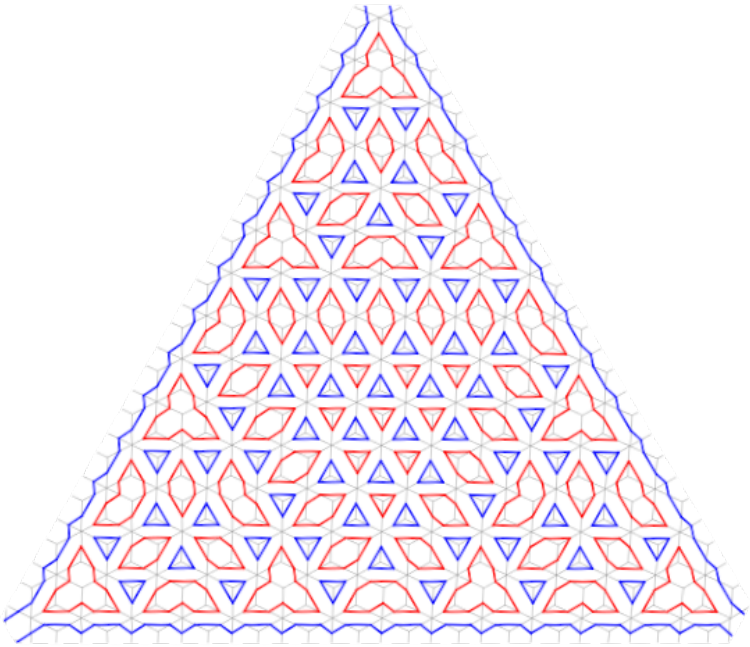

Plan de la thèse

Dans cette thèse, nous étudions plusieurs problèmes de mécanique statistique, liés à l'existence de modèles *intégrables*, ou *exactement solubles*. En introduction, dans la Section 1 (en français), nous proposons un bilan historique des grandes idées de la mécanique statistique, en insistant particulièrement sur les différentes notions d'intégrabilité. Le reste de cette thèse est rédigé en anglais ; dans la Section 2, nous définissons les modèles qui interviennent par la suite : modèle d'Ising, modèle de dimères, modèles "vertex" et modèles de boucles, ainsi que les transformations classiques permettant de passer de l'un à l'autre. Dans la Section 3 nous discutons en détail l'une des acceptions les plus fréquentes de la notion d'intégrabilité : l'existence de *transformations triangle-étoile* ou *équations de Yang-Baxter*, et leurs nombreuses applications. Les résultats obtenus au cours de cette thèse sont résumés en détail dans la Section 4, et démontrés dans les chapitres suivants. Ceux-ci sont organisés comme suit :

- Dans le Chapitre I, nous étudions la transformation triangle-étoile du modèle d'Ising, sous la forme d'une équation d'évolution polynomiale proposée par Kashaev [Kas96]. Nous montrons que cette évolution est encodée par un modèle de boucles appelées *boucles* $C_2^{(1)}$, ce qui résout un problème ouvert de Kenyon et Pemantle [KP16]. Nous donnons plusieurs propriétés statistiques de ce modèle de boucles, comme son *énergie libre* ou l'existence de *formes limites*, qui délimitent les phases du modèle.

  Le contenu de ce chapitre est tiré de [1], publié dans Journal of Combinatorial Theory series A.

- Dans le Chapitre II, nous étudions le modèle des huit sommets ou *eight-vertex model* pour un régime particulier appelé régime des *fermions libres*. Nous exprimons de nouvelles symétries du modèles, qui permettent de le reformuler en termes de dimères sur un graphe biparti, dont l'étude rigoureuse est très avancée. Nous donnons de nouvelles solutions aux équations de Yang-Baxter pour ce modèle, puis nous exprimons des mesures de Gibbs et des corrélations exactes, ainsi que des propriétés de couplage et de *courbes spectrales*.

  Le contenu de ce chapitre est tiré de la prépublication [2], soumis.

- Dans le Chapitre III, nous proposons de réinterpréter la transformation triangle-étoile de certains modèles comme des théorèmes d'incidence en géométrie discrète, via des plongements canoniques de graphes. Les modèles couverts par cette théorie incluent à l'heure actuelle les réseaux de résistance et le modèle d'Ising, et nous proposons de possibles généralisations géométriques.

  Le contenu de ce chapitre est un travail en cours, en commun avec Sanjay Ramassamy et Paul Thévenin.

- Le Chapitre IV concerne un problème de théorie des nombres, sans rapport avec la mécanique statistique : il s'agit d'étudier les partitions du *graphe divisoriel* en un nombre minimal de *chaînes*. Nous montrons que de telles partitions peuvent contenir de très longues chaînes d'ordre $N^{1-o(1)}$.

  Le contenu de ce chapitre est un travail en commun avec Éric Saias [3], à paraître dans Acta Arithmetica.

Outline of this thesis

In this thesis, we study several problems in statistical mechanics, related to the existence of *integrable* or *exactly solvable* models. In the introduction, in Section 1 (in French) we give a historical overview of the main historical ideas of statistical mechanics, with an emphasis on the different notions of integrability. The rest of this thesis is written in English; in Section 2, we define the models that appear later: the Ising model, the dimer model, vertex models and loop models, as well as some classical transformations between them. In Section 3 we discuss one of the most frequent meaning of integrability: the existence of *star-triangle transformations* or *Yang-Baxter equations*, and their numerous applications. The results obtained in this thesis are then summed up in detail in Section 4, and proved in the following chapters. These are organised as follows:

- In Chapter I, we study the star-triangle transformation of the Ising model, stated as a polynomial evolution equation by Kashaev [Kas96]. We show that this evolution is encoded by a loop model known as the $C_2^{(1)}$ *loop model*, thus solving an open problem of Kenyon and Pemantle [KP16]. We give several statistical properties of this loop model, such as its *free energy* or the existence of *limit shapes*, that separate the phases of the model.

  The content of this chapter is taken from [1], published in Journal of Combinatorial Theory series A.

- In Chapter II, we study the *eight-vertex model* in a particular regime known as *free fermions*. We express new symmetries of the model, that let us reformulate it into dimers on a bipartite graph, a model whose rigorous study is extremely advanced. We give new solutions to the Yang-Baxter equations, and we express Gibbs measures and exact correlations, as well as some coupling properties and *spectral curves* of the model.

  The content of this chapter is taken from the preprint [2], submitted.

- In Chapter III, we give interpretations of star-triangle transformations of some models as incidence theorems in discrete geometry, via canonical embeddings of graphs. The models that fall into this theory include resistor networks and the Ising model, and we suggest possible geometric generalisations.

  The content of this chapter is a joint work in progress with Sanjay Ramassamy and Paul Thévenin.

- Chapter IV concerns a problem of number theory, unrelated to statistical mechanics: we study the partitions of the *divisor graph* into a minimal number of *paths*. We show that such partitions can contain very long paths, of order $N^{1-o(1)}$.

  The content of this chapter is a joint work with Éric Saias [3], to be published in Acta Arithmetica.

1 Bref historique

Dresser un historique sérieux de la mécanique statistique, de ses problématiques et de ses méthodes, est un objectif impossible et hors de propos dans cette thèse. Je me propose de donner ici un simple point de vue, très partiel, sur les grandes idées qui ont motivé les objets présentés par la suite. On trouvera plus d'informations dans les sources d'inspiration principales de cette partie, les livres de référence [McC10, DFMS97, BBT03, Bax82].

1.1 Mécanique statistique à l'équilibre

L'objectif général de la mécanique statistique est la description de *systèmes complexes*, c'est-à-dire possédant un grand nombre de degrés de liberté. On peut penser à un système physique composé de nombreuses particules libres : l'air dans la pièce, l'eau dans une casserole, un aimant, etc. Du côté microscopique, on sait décrire avec précision les propriétés des composants élémentaires, par exemple avec les lois de la physique des particules. À l'inverse, à grande échelle, le système est décrit par un champ d'étude tout autre, la thermodynamique. Il se trouve que ces deux descriptions présentent des phénomènes radicalement différents, voire incompatibles. Cette discordance entre monde microscopique et monde macroscopique est illustrée de manière célèbre par le *paradoxe de l'irréversibilité* : bien que les particules élémentaires obéissent à des équations réversibles dans le temps, les phénomènes qu'on observe à grande échelle sont généralement irréversibles.

James Maxwell
(1831 - 1879)

En 1877, en se basant notamment sur des travaux de Maxwell, Boltzmann propose un moyen d'étudier cette question [Bol68]. Lorsque le système est trop complexe, son état microscopique nous est inaccessible. Toutefois, Boltzmann formule les postulats suivants[1] :

- En l'absence d'information sur l'état précis d'un système isolé, on postule qu'il se trouve dans un état aléatoire, choisi uniformément parmi les états accessibles.
- Pour un système isolé, les états accessibles sont ceux qui ont la même énergie que le système initial. Autrement dit, l'énergie totale est la seule quantité conservée au cours du temps.

Ludwig
Boltzmann
(1844 - 1906)

Autrement dit, on va distinguer un *micro-état*, qui est un état possible du système parmi tous les états accessibles, et un *macro-état*, qui est une variable aléatoire à valeurs dans l'ensemble des micro-états.

À partir de ces hypothèses, Boltzmann considère un système non plus isolé, mais mis en contact avec un thermostat qui fixe sa température T. Le système et le thermostat peuvent échanger de l'énergie, donc l'énergie du système n'est plus fixée. À partir des postulats précédents appliqués à l'ensemble du système et du thermostat, Boltzmann montre que la probabilité de trouver le système dans un état microscopique σ vaut

$$\mathbb{P}(\sigma) = \frac{1}{\mathcal{Z}} \mathrm{e}^{-\beta E(\sigma)}, \tag{1}$$

où $E(\sigma)$ est l'énergie du système, et $\beta = \frac{1}{k_B T}$ avec $k_B \simeq 1,38 \times 10^{-23} JK^{-1}$ la *constante de Boltzmann*. Le coefficient de renormalisation $\mathcal{Z}$, qui fait en sorte que (1) soit effectivement

[1] La question de la pertinence de ces postulats fait l'objet de pans entiers de recherche, autant en mathématiques qu'en physique, depuis leur formulation, et nous ne nous y pencherons pas ici. On peut consulter par exemple [Spo91] pour plus d'informations.

une mesure de probabilité, est appelé *fonction de partition*. Dans le cas où l'ensemble des états accessibles σ est dénombrable et où la somme est finie, elle s'exprime comme

$$\mathcal{Z} = \sum_{\sigma} \mathrm{e}^{-\beta E(\sigma)}.$$

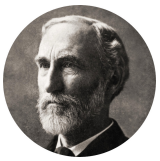

Willard Gibbs (1839 - 1903)

Ce macro-état est connu sous le nom de *mesure de Boltzmann*.

La fonction de partition n'est pas seulement une constante de renormalisation. Vue comme fonction des paramètres du système (par exemple la température β ou les forces d'interaction entre particules), elle contient beaucoup d'information. À titre d'exemple, supposons que l'on veuille connaître l'énergie moyenne du système. Celle-ci s'exprime comme

$$\begin{aligned}\mathbb{E}[E] &= \sum_{\sigma} E(\sigma)\frac{1}{\mathcal{Z}}\mathrm{e}^{-\beta E(\sigma)} \\ &= -\frac{1}{\mathcal{Z}}\frac{\partial \mathcal{Z}}{\partial \beta} \\ &= -\frac{\partial(\ln \mathcal{Z})}{\partial \beta}.\end{aligned}$$

On voit que la connaissance de $\mathcal{Z}$ comme fonction "explicite", "simple" ou "factorisée" des paramètres du système permet de calculer des quantités physiques.

On peut considérer l'article de Boltzmann comme l'acte de naissance de la *mécanique statistique*. La portée de cette idée, initialement réservée à la théorie cinétique des gaz, a été étendue à de nombreux systèmes notamment avec les travaux de Gibbs [Gib02], qui propose une formulation générale de la mesure de Boltzmann. Plus tard, ces concepts ont été appliqués à la physique quantique, avec les travaux notamment de Von Neumann et Landau dans les années 1920. Elle est aujourd'hui un des piliers de la physique moderne et trouve des applications jusqu'à la sociologie ou l'économie.

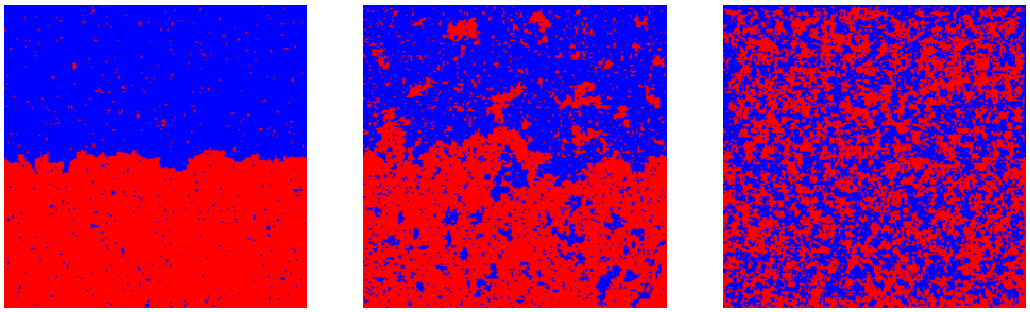

Figure 1: Une simulation du modèle d'Ising sur une portion du réseau carré avec conditions au bord $+$ (rouge) en bas et $-$ (bleu) en haut, pour diverses températures.

Exemple: Le modèle d'Ising

Ernst Ising
(1900 - 1998)

Pour illustrer la mesure de Boltzmann, faisons un saut dans le temps et considérons un des modèles les plus classiques de la mécanique statistique, le modèle d'Ising. Introduit par Lenz et Ising dans les années 1920 [Len20, Isi25], il modélise un métal dont les atomes sont placés sur un réseau. On suppose pour simplifier que chaque atome est représenté par un aimant ou *spin* qui peut pointer vers le Nord (spin +) ou vers le Sud (spin −). Les aimants interagissent de sorte à pointer plutôt dans la même direction ; on parle de *ferromagnétisme*.
On va modéliser cette situation en prenant un graphe fini $\mathscr{G}$, composé de sommets $\mathscr{V}$ reliés par des arêtes $\mathscr{E}$, et un micro état σ est une fonction de $\mathscr{V}$ vers $\{-1,+1\}$. On simplifie encore le problème en supposant que les spins n'interagissent qu'entre plus proches voisins. On définit donc l'énergie de σ par

$$E(\sigma) = -\sum_{e=\{x,y\}\in\mathscr{E}} J_e \sigma_x \sigma_y$$

où les $(J_e)_{e\in\mathscr{E}}$ sont des constantes positive appelées *constantes de couplage*. L'idée est que l'énergie du système est d'autant plus faible que les spins voisins sont alignés. La mesure de Boltzmann est donc

$$\mathbb{P}(\sigma) = \frac{1}{\mathcal{Z}} \mathrm{e}^{\beta \sum J_e \sigma_x \sigma_y} = \frac{1}{\mathcal{Z}} \prod_e \mathrm{e}^{\beta J_e \sigma_x \sigma_y}$$

et la fonction de partition vaut

$$\mathcal{Z} = \sum_\sigma \prod_e \mathrm{e}^{\beta J_e \sigma_x \sigma_y}.$$

Un exemple de quantité d'intérêt, ou *observable*, est la corrélation spin-spin sur une arête $e = \{x, y\}$. Celle-ci s'obtient également en calculant des dérivées partielles de la fonction de partition :

$$\mathbb{E}[\sigma_x \sigma_y] = \frac{1}{\beta} \frac{\partial (\ln \mathcal{Z})}{\partial J_e}$$

1.2 Comportements critiques

Une des motivations essentielles de la mécanique statistique est la compréhension des *transitions de phase*. Ce sont des changements brusques du comportement *macroscopique* du système à une température donnée : passage d'un état solide à un état liquide, d'un liquide à un gaz, ou encore magnétisation spontanée d'un matériau ferromagnétique en dessous de sa température de Curie. Lorsque le système atteint cette température, on parle de comportement *critique*.

En mécanique statistique, le fait que le système soit dans un état critique s'interprète de la façon suivante. Habituellement, dans un système de particules en interaction, on trouve des *longueurs typiques*, comme la longueur de corrélation ξ. Si deux particules se trouvent

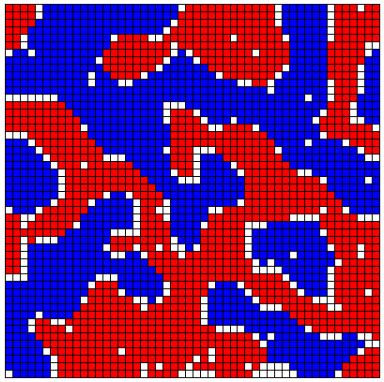

Figure 2: Le modèle de Schelling [Sch71], qui décrit des phénomènes de ségrégation - ici entre des populations bleues et rouges, simulé par Frank McCown - est un modèle de mécanique statistique[2].

en position x et y, on s'attend à ce que la corrélation entre leurs états se comporte comme

$$\langle \sigma_x \sigma_y \rangle \sim \exp\left(-\frac{|x-y|}{\xi}\right). \tag{2}$$

C'est le cas dans la plupart des systèmes, comme on peut le voir avec la taille des "bulles" dans les simulations de droite et de gauche de la Fig. 1. Mais dans la figure centrale, obtenue pour une température critique β_c (telle que $\beta_c J = \frac{1}{2}\log(1+\sqrt{2})$), on trouve des bulles de toutes tailles ; cela n'arrive qu'à la température critique. Il n'y a donc pas de longueur typique de corrélation, ou bien elle devrait être infinie. En réalité, les corrélations à longue portée n'ont plus un comportement exponentiel comme (2), mais en loi de puissance.

On dira donc, informellement, que dans un système critique, la longueur de corrélation ξ devient infinie.

1.3 Intégrabilité...

Pour étudier des phénomènes impliquant un grand nombre de particules élémentaires, une stratégie est donc de concevoir un modèle dont on pense qu'il possède les caractéristiques essentielles du système étudié, lui associer une certaine fonction d'énergie et donc une mesure de Boltzmann, et tenter d'estimer son comportement typique[3]. En pratique, ce dernier but est généralement impossible, c'est pourquoi on doit souvent simplifier le modèle. Mais pour un petit nombre de modèles dits *intégrables*, des calculs exacts peuvent être menés. Pour mieux cerner la notion d'intégrabilité, il est utile de revenir sur le sens que lui ont donné les physicien·ne·s et les mathématicien·ne·s en mécanique classique et en physique quantique.

[2] L'expérimentation ludique de ce modèle sur `https://ncase.me/polygons/` est instructive et donne une bonne idée du genre de phénomène qu'on rencontre en mécanique statistique, notamment les transitions de phase.

[3] Par exemple en calculant "explicitement" sa fonction de partition et en prenant les dérivées partielles appropriées.

a) ...en mécanique classique (intégrabilité au sens de Liouville)

La *mécanique hamiltonienne* est un formalisme général pour la mécanique classique. L'état d'un système est décrit par un ensemble de variables instantanées ou *coordonnées généralisées* $\boldsymbol{q}(t) = (\boldsymbol{q}_i(t))_{i=1\dots N}$, et des *impulsions généralisées* $\boldsymbol{p}(t) = (\boldsymbol{p}_i(t))_{i=1\dots N}$. Elles sont choisies de manière à ce que pour une certaine fonction $H(\boldsymbol{q}, \boldsymbol{p})$ appelée *hamiltonien*, qui généralise l'énergie du système[4], les équations du mouvement s'écrivent

$$\frac{\mathrm{d}q_i}{\mathrm{d}t} = \frac{\partial H}{\partial p_i}, \qquad \frac{\mathrm{d}p_i}{\mathrm{d}t} = -\frac{\partial H}{\partial q_i}.$$

Plus généralement, pour toute fonction $f(\boldsymbol{q}, \boldsymbol{p})$ de l'état du système,

$$\frac{\mathrm{d}f}{\mathrm{d}t} = \{f, H\} \tag{3}$$

où $\{\cdot, \cdot\}$ est le *crochet de Poisson* :

Joseph Liouville
(1809 - 1882)

$$\{A, B\} \;=\; \sum_{i=1}^{N} \left[\frac{\partial A}{\partial q_i}\,\frac{\partial B}{\partial p_i} \;-\; \frac{\partial A}{\partial p_i}\,\frac{\partial B}{\partial q_i} \right].$$

L'équation (3) indique que si $\{f, H\} = 0$, alors f ne varie pas au cours du temps. On parle de *constante du mouvement*. Un exemple de constante du mouvement est le hamiltonien H lui-même : c'est la conservation de l'énergie.

Un système est dit *intégrable au sens de Liouville* s'il existe N constantes du mouvement indépendantes $f_1 = H, f_2, \dots, f_N$ telles que pour tous i, j, $\{f_i, f_j\} = 0$ (on dit qu'elles commutent au sens de Poisson). Dans ce cas, le théorème de Liouville affirme que la trajectoire du système est complètement caractérisée par les valeurs de ces N constantes. Plus précisément, il donne un changement de variable tel que l'équation d'évolution est conjuguée à un produit de translations sur un tore. Nous renvoyons à [BBT03] pour davantage de précisions.

b) ...en mécanique quantique

Bruria Kaufman
(1918 - 1910)

Dans le cas de la physique quantique, l'état du système est représenté par un élément d'un espace de Hilbert, et le hamiltonien est remplacé par un opérateur auto-adjoint agissant sur cet espace. Le crochet de Poisson est alors remplacé par le commutateur de deux opérateurs, $[A, B] = AB - BA$. L'analogue des constantes du mouvement (f_i) est alors un *système complet d'observables qui commutent*.

c) ...au sens des matrices de transfert

Lars Onsager
(1903 - 1976)

L'apparition du terme "intégrabilité" en mécanique statistique est liée à l'utilisation des *matrices de transfert*. Pour comprendre de quoi il s'agit, reprenons l'exemple du modèle d'Ising, et de sa solution pour le réseau carré $\mathbb{Z}^2$ par Kaufman et Onsager au cours des années 1940 [Ons44, Kau49, KO49].

[4] Ici le hamiltonien ne dépend pas du temps, on parle de *système autonome*.

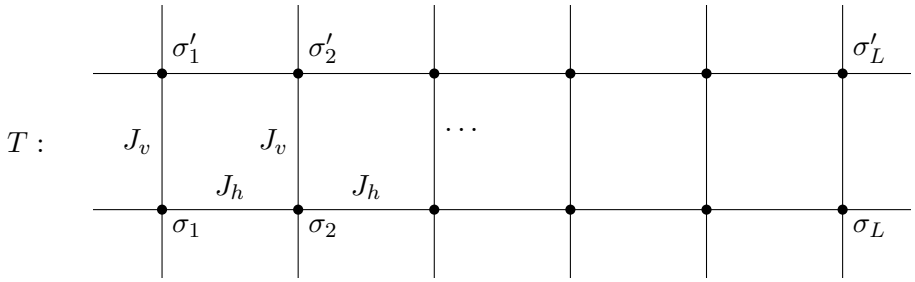

Figure 3: Matrice de transfert du modèle d'Ising sur le réseau carré

Exemple: Matrices de transfert du modèle d'Ising

Considérons le modèle d'Ising sur un tore discret $\mathbb{Z}/L\mathbb{Z} \times \mathbb{Z}/N\mathbb{Z}$, avec des constantes J_h sur les arêtes horizontales et J_v sur les arêtes verticales. Pour deux lignes de spins $\boldsymbol{\sigma} = (\sigma_1, \dots, \sigma_L) \in \{-1, +1\}^L$ et $\boldsymbol{\sigma'} = (\sigma'_1, \dots, \sigma'_L) \in \{-1, +1\}^L$, on note $T_{\boldsymbol{\sigma},\boldsymbol{\sigma'}}$ la contribution de la ligne $\boldsymbol{\sigma}$ et des interactions entre les lignes $\boldsymbol{\sigma}, \boldsymbol{\sigma'}$:

$$T_{\boldsymbol{\sigma},\boldsymbol{\sigma'}} = \exp\left(\beta \sum_{i=1}^{L} J_h \sigma_i \sigma_{i+1} + J_v \sigma_i \sigma'_i\right)$$

avec la convention $\sigma_{L+1} = \sigma_1$. Alors on peut exprimer la fonction de partition en séparant les contributions de chaque ligne, ce qui donne

$$\mathcal{Z}(L, N) = \sum_{\boldsymbol{\sigma}^{(1)}, \dots, \boldsymbol{\sigma}^{(N)} \in \{-1,+1\}^L} T_{\boldsymbol{\sigma}^{(1)},\boldsymbol{\sigma}^{(2)}} \dots T_{\boldsymbol{\sigma}^{(N-1)},\boldsymbol{\sigma}^{(N)}} T_{\boldsymbol{\sigma}^{(N)},\boldsymbol{\sigma}^{(1)}}.$$

En interprétant T comme une matrice 2^L par 2^L, cela donne

$$\mathcal{Z}(L, N) = \mathrm{Tr}(T^N).$$

Par conséquent, l'étude des propriétés spectrales de la *matrice de transfert* T peut donner le comportement de la fonction de partition $\mathcal{Z}(L, N)$ pour N grand. Si λ_1 est la plus grande valeur propre de T, si elle est unique,

$$\lim_{N \to \infty} \frac{1}{N} \log \mathcal{Z}(L, N) = \lambda_1.$$

Plus généralement, si les constantes de couplage J_h et J_v dépendent d'un paramètre complexe u, on note $T(u)$ la matrice de transfert correspondante.

Lorsqu'un modèle admet des matrices de transfert indexées par un paramètre u, on dit qu'il est *intégrable* si les matrices de transfert pour différents paramètres u, v commutent :

$$T(u)T(v) = T(v)T(u). \tag{4}$$

Hans Bethe
(1906 - 2005)

Dans ce cas, si les matrices sont diagonalisables, elles le sont dans une base commune, et on peut rechercher leurs valeurs propres pour adapter le raisonnement fait dans l'encadré précédent. Une méthode puissante pour deviner la forme des vecteurs propres a été développée

par Bethe en 1931 [Bet31] et porte désormais le nom d'Ansatz de Bethe.

En réalité, cette notion d'intégrabilité n'est pas si différente de celle de Liouville. En effet, si on suppose que $T(u)$ peut se développer en série, par exemple pour u voisin de 0 :

$$T(u) = \sum_k T_k u^k$$

alors (4) donne

$$\forall k, l,\ [T_k, T_l] = 0$$

qui rappelle l'équation satisfaite par les constantes du mouvement.

d) ...au sens d'une solution exacte

Rodney Baxter (1940 -)

En mécanique statistique, la notion d'intégrabilité est en général inspirée par les définitions que nous venons de voir, mais est parfois utilisée de manière plus floue. On dira qu'un système est intégrable s'il possède "suffisamment de symétries" pour être caractérisé totalement par ces symétries. On parle aussi de modèles *exactement solubles* lorsque les quantités d'intérêt, comme la fonction de partition, peuvent s'exprimer explicitement sous une forme analytique ; c'est notamment le sens que lui donne Baxter dans [Bax82].

Ce caractère intégrable d'un modèle est communément lié à l'existence de structures algébriques sous-jacentes, bien qu'il n'existe pas de théorie unifiant tous les cas où de telles structures apparaissent ; on en verra des exemples avec le modèle de dimères au paragraphe 2.2 ou dans la reformulation du modèle à huit sommets au chapitre II.A.

D'un point de vue algorithmique, il signifie aussi que le calcul de la fonction de partition peut s'effectuer en temps polynomial, alors que l'algorithme naïf qui consiste à énumérer toutes les configurations est exponentiel en la taille du système.

e) ...au sens de Yang-Baxter

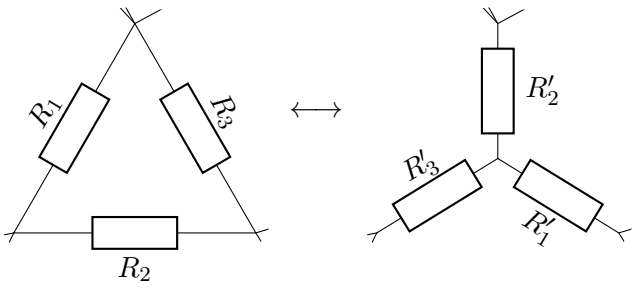

$$R'_1 = \frac{R_2 R_3}{R_1+R_2+R_3} \qquad R'_2 = \frac{R_1 R_3}{R_1+R_2+R_3} \qquad R'_3 = \frac{R_1 R_2}{R_1+R_2+R_3}$$

Figure 4: Transformation "triangle-étoile" pour les réseaux de résistance (Kennelly, 1899 [Ken99]).

Le sens qui sera utilisé dans cette thèse est l'existence de *transformations triangle-étoile*, ou *équations de Yang-Baxter*, pour le modèle. Nous reviendrons en détail dans le paragraphe 3 sur les différentes interprétations de ces transformations, mais mentionnons déjà qu'elles

Yang Chen-Ning
(1922 -)

fournissent une condition **suffisante** à la commutation des matrices de transfert. Pour cette raison, l'existence de solutions aux équations de Yang-Baxter est souvent confondue avec l'intégrabilité d'un modèle, mais là aussi, aucune théorie générale n'établit ce fait.

Il est également troublant que pour de nombreux modèles, les régimes correspondant à des solutions aux équations de Yang-Baxter sont exactement ceux pour lesquels une notion *d'holomorphie discrète* existe pour les observables du système.

f) ...dans d'autres domaines

Il existe encore d'autres définitions de l'intégrabilité dans différents domaines des mathématiques et de la physique. Citons pêle-mêle l'existence d'une paire de Lax (issu de [Lax68], expliqué par exemple au chapitre 2.4 de [BBT03]) et la méthode de la transformation de diffusion inverse ("inverse scattering transform") dans les équations aux dérivées partielles [GGKM67, GGKM74] et sa version *quantique* par Faddeev et toute "l'école de Leningrad" [Fad95], ou la formulation de problèmes de Riemann-Hilbert en probabilités et en matrices aléatoires (voir par exemple le chapitre 5 de [BDS16]).

Face à cette diversité de points de vue il n'est pas toujours simple de cerner ce que l'on entend quand on dit qu'un système est intégrable, et cette notion n'est certainement pas fixée : elle dépend de la machinerie technique dont on dispose. Ainsi la liste des "systèmes intégrables" s'allonge avec le temps. Comme dit dans un entretien entre McKean et Flaschka rapporté par Deift [Dei19], que je traduis[5] :

> Comme ça tu veux savoir ce qu'est un système intégrable ? Eh bien je vais te le dire ! Tu ne pensais pas que je pourrais le résoudre. Mais je peux !

Remarque. Pour conclure cet aperçu des idées liées à l'intégrabilité, on peut tout de même objecter que les modèles intégrables semblent être en contradiction avec l'un des postulats de Boltzmann : ils possèdent un nombre maximal de quantités préservées, là où Boltzmann faisait l'hypothèse que seule l'énergie se conserve. Pour citer McCoy [McC10], que je traduis[5] :

> Si le chaos est une hypothèse nécessaire à l'utilisation de la mécanique statistique à l'équilibre, pourquoi pouvons-nous fonder des intuitions sur des modèles intégrables, totalement dépourvus de chaos ?

Une réponse possible réside dans l'idée d'*universalité*.

Leo Kadanoff
(1937 - 2015)

1.4 Universalité

L'idée d'universalité semble avoir été introduite sous sa forme moderne par Kadanoff dans les années 1960. Elle désigne le fait que les comportements "à grande échelle" d'un système ne dépendent pas des détails du système (comme la forme précise des interactions ou le choix d'un réseau sur lequel les particules se placent), mais de quelques caractéristiques essentielles, comme la dimension ou les groupes d'invariance des configurations.

La première manifestation de ce phénomène est l'existence *d'exposants critiques* universels. Lorsqu'un système à une température inverse β approche son point critique β_c, certaines

[5] Merci à Paul Galvan pour son aide !

observables $a(\beta)$ deviennent infinies (ou nulles), en suivant typiquement un comportement du type

$$a(\beta) \sim C(\beta - \beta_c)^{\alpha}.$$

La constante C (ainsi que d'éventuelles corrections polynomiales) dépend des détails du système, mais l'exposant α est très robuste aux modifications du modèle. Le calcul de ces *exposants critiques* et l'émergence de *classes d'universalité* est un des objets d'étude essentiels de la mécanique statistique depuis les années 1960. Une technique de calcul puissante, mais en général non rigoureuse, est l'utilisation de *groupes de renormalisation*, dont le développement a culminé avec les travaux de Wilson au cours des années 1970.

Kenneth Wilson
(1936 - 2013)

Exemple: Un exposant critique du modèle d'Ising

On a déjà mentionné la longueur de corrélation ξ d'un système non-critique ; celle-ci dépend de la température β, et devient infinie pour une température critique β_c. Plus précisément, pour le modèle d'Ising, au voisinage de β_c on peut montrer (voir [Bax82], chapitre 7)

$$\xi(\beta) \sim (\beta - \beta_c)^{-1}.$$

On dit que $\nu = 1$ est l'exposant critique de longueur de corrélation dans la classe d'universalité du modèle d'Ising. On verra ce même exposant apparaître dans le modèle à huit sommets (voir la Section 4.2), ce qui peut s'interpréter par le fait que l'espace de ses configurations a le même groupe d'invariance $\mathbb{Z}/2\mathbb{Z}$ que le modèle d'Ising.

Pour la mécanique statistique en dimension 2, les objets limites universels constituent des sujets d'étude d'une grande importance, et rassemblent des communautés de mathématicien·ne·s et de physicien·ne·s. On peut citer les courbes SLE (Schramm-Loewner evolution) étudiées notamment par Lawler, Schramm, Smirnov, Werner [Sch00, LSW04, Wer04, Smi10] le champ libre gaussien ou GFF, et la gravité quantique de Liouville, avec les travaux de Duplantier, Miller, Sheffield, Rhodes, Vargas, [She07, DS11, RV14, DRSV14, MS16], etc. La compréhension de ces limites d'échelle permet, entre autres, de deviner d'un seul coup les comportements critiques de tous les modèles dans leur classe d'universalité.

Crédits photos, par ordre d'apparition :

- G. J. Stodart ;
- Uni Frankfurt ;
- Éditions H. A. Bumstead and R. G. Van Name ;
- Thomas Ising ;
- Stony Brook Mathematics Department and Institute for Mathematical Sciences ;
- Kibbutz Mishmar HaEmek Archive, Israel ;
- The Nobel Prize Foundation ;
- Los Alamos National Laboratory ;
- George M. Bergman ;
- U.S. Department of Energy ;
- Dan Dry - The University of Chicago ;
- The Nobel Prize Foundation.

2 A few classical models

We introduce the models studied in this thesis. To make this exposition simpler, we define them only on finite graphs. However, extensions to infinite graphs typically exist, and are obtained by constructing Gibbs measures as appropriate limits.

Let $\mathscr{G}$ be a finite graph, that is a finite set of vertices $\mathscr{V}$ linked by non-oriented edges $\mathscr{E}$. We suppose that $\mathscr{G}$ is either a planar graph or a toric graph, that is, it can be embedded on a sphere (resp. the torus) with non-intersecting edges, such that the connected components of the complement of this embedding, or *faces*, are homeomorphic to disks. We suppose that such a proper embedding is fixed, and we denote by $\mathscr{F}$ the set of faces.

Starting from $\mathscr{G}$, we can define a few objects *via* simple constructions. These objects will carry the statistical mechanics models that we define thereafter. Examples are shown in Figure 5.

- The *dual* graph $\mathscr{G}^*$ has vertices $\mathscr{V}^* = \mathscr{F}$, and its edges $\mathscr{E}^*$ are in bijection with $\mathscr{E}$: for every edge $e \in \mathscr{E}$, let $f, g \in \mathscr{F}$ be the faces adjacent to e (which might be equal), then we define its dual edge e^* as joining f and g in $\mathscr{G}^*$.

  In contrast to the dual graph, $\mathscr{G}$ is often called the *primal* graph.

- The *diamond* graph $\mathscr{G}^\diamond$ has vertices $\mathscr{V}^\diamond = \mathscr{V} \cup \mathscr{F}$ and edges $\mathscr{E}^\diamond$ that link every face $f \in \mathscr{F}$ to the vertices v on the boundary of f (once for every time v is met in a clockwise trajectory around the boundary of f).

  This gives a quadrangulation, meaning that the faces of $\mathscr{G}^\diamond$ have degree 4. In fact Tutte proved that this procedure gives a bijection between 2-colored quadrangulation and graphs $\mathscr{G}$ [Tut63a], considered up to homomorphism (*i.e.* as *maps*).

- The *medial* graph $\mathscr{G}^m$ is the dual of $\mathscr{G}^\diamond$. It is therefore a 4-regular graph: all its vertices have degree 4. Its vertices $\mathscr{V}^m$ are in bijection with $\mathscr{E}$.

- A *train-track* associated to $\mathscr{G}$ is a path that crosses the faces of $\mathscr{G}^\diamond$ in such a way that it always exits a face by the edge opposite to the one it entered from. It is therefore completely determined by one edge of $\mathscr{G}^\diamond$ that it crosses.

  We denote by $TT(\mathscr{G})$ the set of all train-tracks associated to $\mathscr{G}$.

  Since we embed $\mathscr{G}$ on a closed surface, all train-tracks are closed loops; if we do the same for a graph with a boundary, they will be either paths joining two boundary edges of $\mathscr{G}^m$, or internal loops.

2.1 Ising model

The Ising model might be the most studied model in statistical mechanics. It is a quintessential *spin* model: the degrees of freedom or *spins* live on the vertices of a graph, and they interact on the edges.

To give a brief overview, after its introduction by Lenz [Len20] and its solution in dimension 1 by Ising [Isi25], the existence of a phase transition in dimension 2 was shown by Peierls [Pei36]. An analytic expression was then found by Kaufman and Onsager [Ons44,

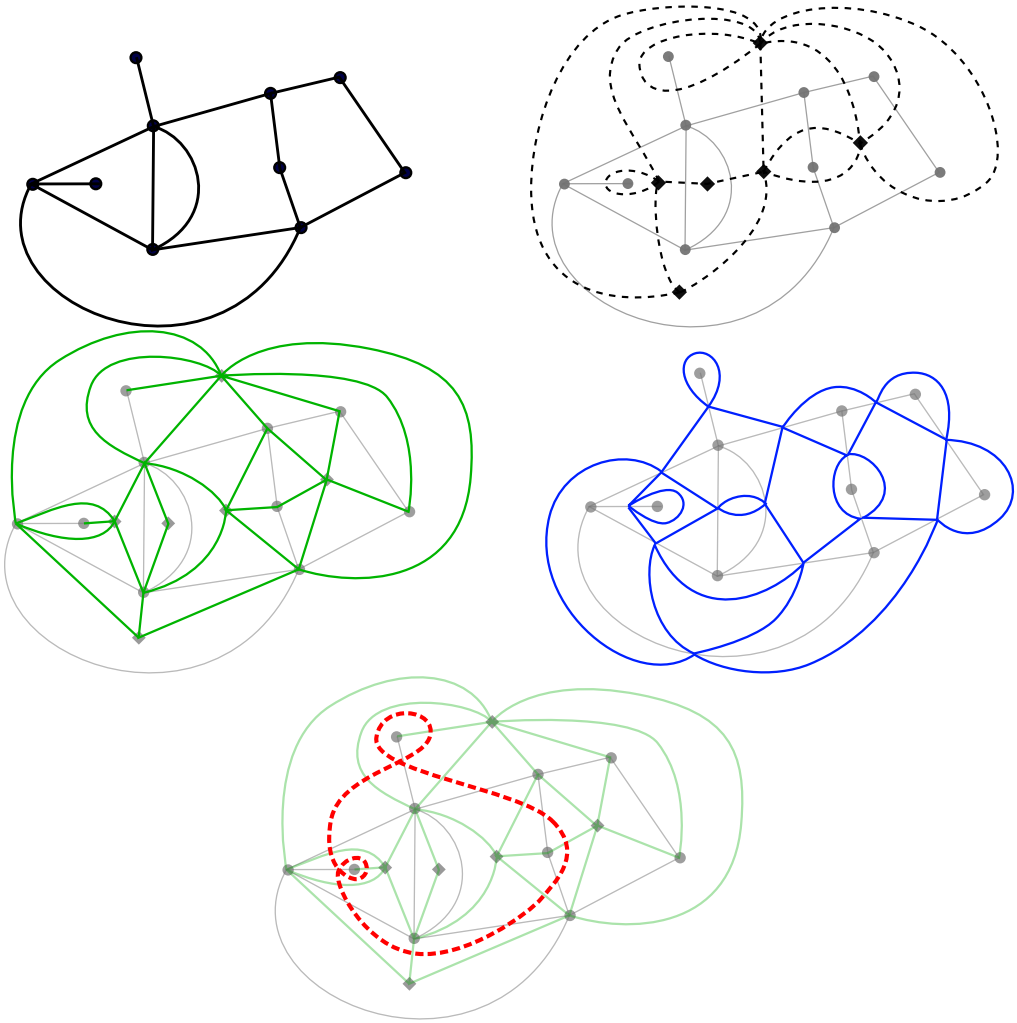

Figure 5: Top left: the *primal* graph $\mathscr{G}$. Top right: its *dual* graph $\mathscr{G}^*$ (dashed). Middle left: its *diamond* graph $\mathscr{G}^\diamond$ (green). Middle right: its *medial* graph $\mathscr{G}^m$ (blue). Bottom: a *train-track* (red).

Kau49, KO49]. The behaviour of the model on the square lattice attracted a lot of attention, with important discoveries such as the exact formulas for correlation by Yang, Wu and McCoy, see [MW14]. Methods based on conformal field theory appeared in the 1960s and until the 1980s, with notable contributions of the "Russian school" of Kadanoff, Belavin, Polyakov, Zamolodchikov [BPZ84], etc; see the introduction of [DFMS97]. Alternative approaches, using correspondence with dimers on decorated graph, were developed by Kasteleyn and Fisher in the 1960s [Kas63, Fis61]. Recent techniques from the mathematics community use tools of analytic geometry, such as the breakthroughs of Smirnov and coauthors [Smi01, SW01, Smi10, CS12], who proved conformal invariance for specific lattices and linked interfaces of the Ising model to SLE curves.

A *spin configuration* σ is an element of $\{-1,+1\}^{\mathscr{V}}$. Let us equip $\mathscr{G}$ with positive *coupling constants* $(J_e)_{e\in\mathscr{E}}$ on the edges. The associated *Boltzmann distribution* of the Ising model

consists in taking σ in $\{-1,+1\}^{\mathscr{V}}$ distributed as[6]

$$\mathbb{P}_{\text{Ising}}(\sigma) = \frac{1}{\mathcal{Z}_{\text{Ising}}(\mathscr{G},J)} \exp\left(\sum_{e=\{uv\}\in\mathscr{E}} J_e\sigma_u\sigma_v\right) \tag{5}$$

with the *partition function*

$$\mathcal{Z}_{\text{Ising}}(\mathscr{G},J) = \sum_{\sigma\in\{-1,1\}^{\mathscr{V}}} \exp\left(\sum_{e=\{uv\}\in\mathscr{E}} J_e\sigma_u\sigma_v\right).$$

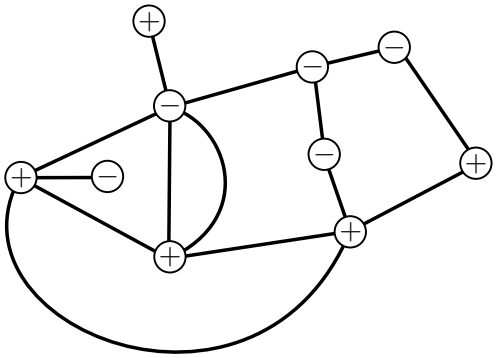

Figure 6: A spin configuration on $\mathscr{G}$.

2.2 Dimer model

This model was initially introduced in 1937 by Fowler and Rushbrooke [FR37] to model the adsorption of diatomic molecules on a regular surface. It has found many other interpretations since, such as double bonds position in fullerenes or, in mathematics, as tiling problems; see for instance [RHHB98, Ken09].

A *dimer configuration* on $\mathscr{G}$, also called a *perfect matching*, is a subset $m \subset \mathscr{E}$ such that every vertex of $\mathscr{G}$ belongs to exactly one edge of m. We denote by $\mathcal{M}(\mathscr{G})$ the set of dimer configurations on $\mathscr{G}$.

Let $\nu = (\nu_e)_{e\in\mathscr{E}}$ be a set of positive real weights on the edges. Then the Boltzmann weight of a dimer configuration is defined as, for every $m \in \mathcal{M}(\mathscr{G})$:

$$w_{\text{dim}}(m) = \prod_{e\in m} \nu_e.$$

We similarly define the partition function for dimers:

$$\mathcal{Z}_{\text{dim}}(\mathscr{G},\nu) = \sum_{m\in\mathcal{M}(\mathscr{G})} w_{\text{dim}}(m).$$

Thus the Boltzmann probability on $\mathcal{M}(\mathscr{G})$ is $\mathbb{P}_{\text{dim}}(m) = \frac{w_{\text{dim}}(m)}{\mathcal{Z}_{\text{dim}}(\mathscr{G},\nu)}$.

[6]Contrary to the historical introduction, we do not write the inverse temperature β; we suppose that it is included into J.

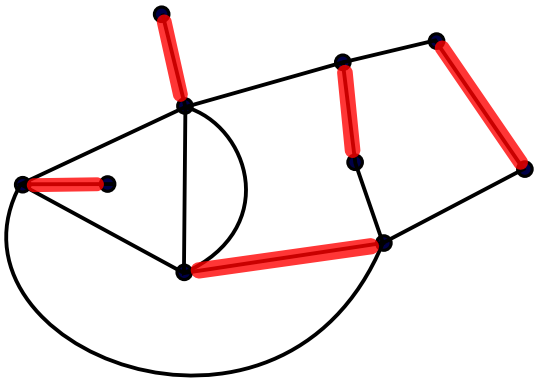

Figure 7: A dimer configuration on $\mathscr{G}$.

a) On a finite planar graph

An exact solution of the dimer model on planar graphs was discovered by Kasteleyn [Kas61, Kas67], Temperley and Fisher [TF61]. An *orientation* of $\mathscr{G}$ is a choice of direction for every edge $e \in \mathscr{E}$. An orientation is said to be *admissible* if every face is *clockwise-odd*, that is, it has an odd number of co-oriented edges if we travel its boundary clockwise.

If $\mathscr{G}$ has an admissible orientation, we define its *Kasteleyn matrix* as the $|\mathscr{V}| \times |\mathscr{V}|$ skew-symmetric matrix K such that

$$\forall u, v \in \mathscr{V}, \quad K_{u,v} = \begin{cases} 0 & \text{if } \{u,v\} \notin \mathscr{E}, \\ \nu(e) & \text{if } u \xrightarrow{\ e\ } v, \\ -\nu(e) & \text{if } u \xleftarrow{\ e\ } v. \end{cases}$$

As K is skew-symmetric, it admits a *Pfaffian*, which is a combinatorial quantity that can be defined in the following way. We suppose that $|\mathscr{V}|$ is even (otherwise, there is no dimer configuration), and we write $\mathscr{V} = \{v_1, \dots, v_{2n}\}$. Then,

$$\mathrm{Pf}(K) = \frac{1}{2^n n!} \sum_{\sigma \in \mathfrak{S}_{2n}} \mathrm{sgn}(\sigma) \prod_{i=1}^{n} K_{v_{\sigma(2i-1)}, v_{\sigma(2i)}}.$$

For a skew-symmetric matrix, the Pfaffian satisfies Cayley's identity:

$$\mathrm{Pf}(K)^2 = \det(K)$$

which makes it easily computable.

Theorem 1 ([Kas61, Kas67, TF61])**.** *For any finite planar graph $\mathscr{G}$, there exists an admissible orientation. Moreover, its Kasteleyn matrix satisfies*

$$\mathscr{Z}_{dim}(\mathscr{G}, \nu) = |\mathrm{Pf}(K)|\,.$$

One can also compute correlations of the model by using the Kasteleyn matrices, as noted by Kenyon [Ken97].

Theorem 2 ([Ken97]). *Let $e_1 = \{u_1, v_1\}, \dots, e_n = \{u_n, v_n\}$ be edges of the graph $\mathscr{G}$. Then the probability that they are all present in M is*

$$\mathbb{P}_{dim}(\{e_1, \dots, e_n\} \in M) = \pm \left(\prod_{i=1}^{n} K_{u_i, v_i} \right) \mathrm{Pf}\left(K^{-1}_{\{u_1, v_1, \dots, u_n, v_n\}} \right),$$

where $K^{-1}_{\{u_1, v_1, \dots, u_n, v_n\}}$ is the sub-matrix of K^{-1} restricted to rows and columns in $\{u_1, v_1, \dots, u_n, v_n\}$. The sign ± 1 can also be explicitly computed.

A remarkable property of the dimer model on planar graphs is its sensitivity to boundary conditions, and the occurrence of limit shapes. To illustrate this, we represent dimer configurations on pieces of $\mathbb{Z}^2$ as colored tilings by dominoes, using an underlying bipartite coloration of $\mathbb{Z}^2$ and the transformation of Figure 8. In Figure 9 we show a random dimer configuration taken uniformly, for subgraphs of $\mathbb{Z}^2$ that both discretize a large square, one being a standard N by N square and the other being tilted by $\pi/2$ and then discretized[7], giving a graph known as the *Aztec diamond*. It is evident that they have extremely different behaviours. For the Aztec diamond, the existence of a limiting curve between two phases of the model, or *arctic circle*, was first shown by Jockusch, Propp and Shor [JPS98], and can be established using the *variational principle* approach of Cohn, Keynon and Propp [CKP01], and other methods such as *orthogonal polynomials* and *Airy processes* [Joh05, BCJ18] or the *octahedron recurrence* [Spe07, DFSG14]. We use tools inspired by this last method to prove limit shape results for a loop model in Section I.4.5.

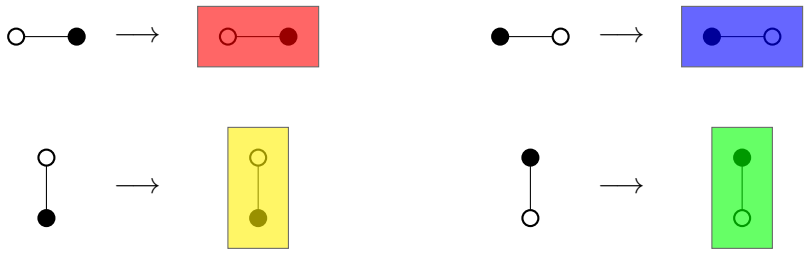

Figure 8: Transformation of edges occupied by dimers into dominoes, using an underlying bipartite coloring of $\mathbb{Z}^2$. More generally, the dimer model on $\mathscr{G}$ can be transformed into a tiling of $\mathscr{G}^*$.

Those exact results illustrate the integrable nature of the dimer model. They can be extended to graphs embedded on higher genus surfaces [Kas61, Kas63, DMS+96, GL99, Tes00, CR07, CR08], by taking linear combinations of Pfaffians of appropriately modified Kasteleyn matrices. In the next section, we review some results of Kenyon, Okounkov and Sheffield [KOS06] that apply when $\mathscr{G}$ is embedded on a torus, which is important to study infinite periodic graphs.

b) On a bipartite bi-periodic graph

In this paragraph, we assume that $\mathscr{G}$ is an *infinite* graph embedded in the plane, and is $\mathbb{Z}^2$-periodic: it is invariant under translations by the two vectors of the canonical basis of

[7] More precisely it is the set of (i, j) such that $|i| + |j| \leq N$.

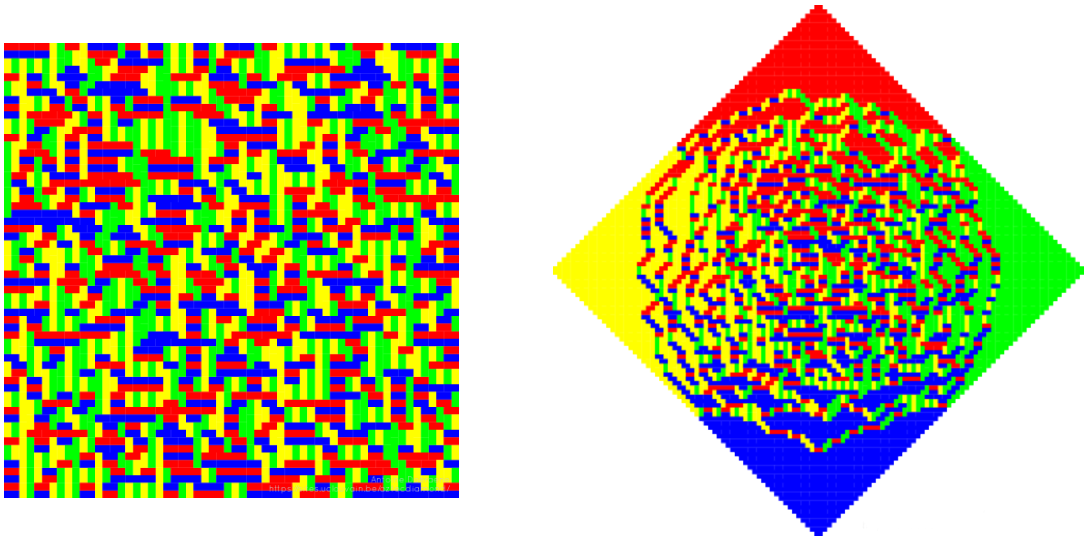

Figure 9: A domino tiling taken uniformly at random on a square (left) and on the Aztec diamond (right). Simulations by Antoine Doeraene.

$\mathbb{R}^2$. Also assume that its weights $(\nu_e)_{e\in\mathscr{E}}$ are $\mathbb{Z}^2$-periodic. Then for any $n \in \mathbb{N}^*$, define $\mathscr{G}_n = \mathscr{G}/n\mathbb{Z}^2$ as a graph embedded in the torus, that inherits the weights ν_n.

An important question is to compute the *free energy*, or growth rate of the partition function:

$$f = -\lim_{n\to\infty} \frac{1}{n^2} \log \mathcal{Z}(\mathscr{G}_n, \nu_n).$$

This can be done by introducing the *characteristic polynomial* of the dimer model. Consider the toric graph $\mathscr{G}_1$, and fix two cycles γ_x, γ_y that wind once horizontally (resp. vertically) on the torus. Then for any $z, w \in \mathbb{C}$, for every entry $K_{u,v}$ of the Kasteleyn matrix of $\mathscr{G}_1$, multiply it by z (resp. z^{-1}) if the edge $\{u, v\}$ crosses γ_x from left to right (resp. right to left), and similarly for w and γ_y.

When $\mathscr{G}$ is a periodic bipartite graph, we can chose $\mathscr{G}_1$ to also be bipartite. If we decompose its edges $\mathscr{V}_1$ into two proper sets of black and white vertices, B_1 and W_1, then the Kasteleyn matrix takes the form

$$K(z,w) = \begin{array}{c} \begin{matrix} W_1 & B_1 \end{matrix} \\ \begin{pmatrix} 0 & \mathcal{K}(z,w) \\ -{}^t\mathcal{K}_k(z^{-1}, w^{-1}) & 0 \end{pmatrix} \end{array} \begin{matrix} W_1 \\ B_1 \end{matrix}.$$

Define the *characteristic polynomial* as the (Laurent) polynomial

$$P(z,w) = \det\left(\mathcal{K}(z,w)\right). \tag{6}$$

By taking the limit of Boltzmann probabilities on $\mathscr{G}_n$, Cohn, Kenyon, Propp, Okounkov and Sheffield show that these objects encode the statistical properties of the model on the infinite graph $\mathscr{G}$. In the following theorem, an explicit construction of an *ergodic Gibbs measure* for the infinite graph is given; this a translation-invariant measure on the whole infinite graph, that satisfies the DLR (Dobrushin [DF68], Lanford, Ruelle [LR69]) conditions, and ergodicity means that translation-invariant events have probability 0 or 1.

Theorem 3 ([CKP01, KOS06]). *Let $\mathscr{G}$ be a **bipartite** bi-periodic planar graph, such that $P(z,w)$ has a finite number of zeros on the torus $\mathbb{T}^2 = \{(z,w) \mid |z| = |w| = 1\}$.*

There exists an ergodic Gibbs measure μ on $\mathcal{M}(\mathscr{G})$, such that for every subset of edges $\{e_1, \dots, e_k\} \subset \mathscr{E}$ with $e_i = \{b_i, w_i\}$, the probability of occurrence of these edges is

$$\mu(e_1, \dots, e_k \in m) = \left(\prod_{i=1}^{k} K_{w_i,b_i} \right) \det \left(K^{-1}_{b_i,w_j} \right)_{1 \le i,j \le k}$$

where K^{-1} is an inverse of the operator K on the whole graph $\mathscr{G}$, given for every $b, w \in \mathscr{V}_1$ and $(x,y) \in \mathbb{Z}^2$ by

$$K^{-1}_{b,w+(x,y)} = \frac{1}{(2i\pi)^2} \int_{\mathbb{T}^2} \frac{\left[{}^t \operatorname{Com} \mathcal{K}(z,w)\right]_{b,w}}{P(z,w)} z^x w^y \frac{dz}{z} \frac{dw}{w}.$$

The free energy of the model is

$$f = \frac{-1}{(2i\pi)^2} \int_{\mathbb{T}^2} \log |P(z,w)| \frac{dz}{z} \frac{dw}{w}.$$

The seminal work [KO06, KOS06] goes well further and also establishes:

- a classification of ergodic Gibbs measures, that form a two-parameter family;
- a correspondence between dimers' spectral curves $\{(z,w) \in \mathbb{C}^2 \mid P(z,w) = 0\}$ and objects of algebraic geometry known as *Harnack curves*.

The extension of these results to non-bipartite graphs is one of the biggest open problems in the field.

2.3 Vertex models

Those are, generally, models where degrees of freedom are carried by edges, and interactions happen on the vertices. The most famous one is probably the six-vertex, or 6V model. It was introduced by Pauling [Pau35] in 1935 to model the arrangement of water molecules in ice.

a) Classical case: six-vertex and eight-vertex models on $\mathbb{Z}^2$

Each water molecule is made of a big oxygen atom, and two smaller hydrogen atoms. Imagine that the oxygen atoms are arranged on a regular, planar quadrangulation, say $\mathbb{Z}^2$. Each oxygen atom has two neighbouring hydrogen atoms, and every edge of the graph has to contain exactly one hydrogen atom, giving a configuration like the one shown in Figure 10. There are six possible configurations at every site, hence the name six-vertex model.

This model is nicely represented by an orientation of the graph, where arrows point towards the hydrogen atom. By the condition on ice, every vertex has to have 2 incoming (and 2 outgoing) edges.

Exact solutions of the 6V-model on the square lattice have been found by Lieb [Lie67] and Sutherland [Sut67]; see also Chapter 8 of [Bax82]. The model has played an important role in the formulation of the general theory of lattice statistical mechanics throughout the

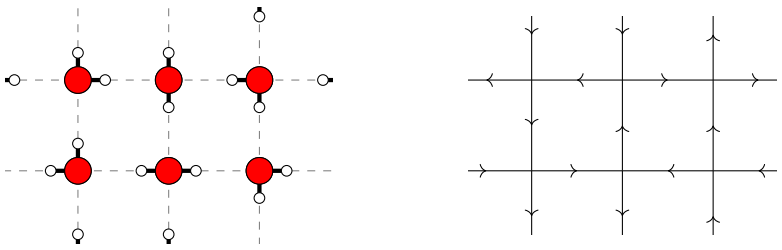

Figure 10: Left: an arrangement of water molecules on the square lattice, with oxygen atoms in red and hydrogen atoms in white. Right: the corresponding orientation of edges, or 6V-configuration.

20th century, with the definition of transfer matrices, Yang-Baxter equations, Bethe Ansatz, etc.

Before defining the Boltzmann measure properly, we extend configurations to the more general 8V-model, by letting the orientation contain *defects*: "sinks" and "sources", that is, vertices with 4 incoming (resp. outgoing) edges. This was done first by Fan, Wu [FW69] and Sutherland [Sut70]. There are several reasons to extend the 6V-model to get such a *8V-model*: it gives a richer phase diagram, with more complete and physically coherent behaviours, as we explain later; it lets us rephrase many spin models (such as interacting Ising models) with the *spin-vertex* correspondence, see Section 2.5 a); it is, generally, more symmetric.

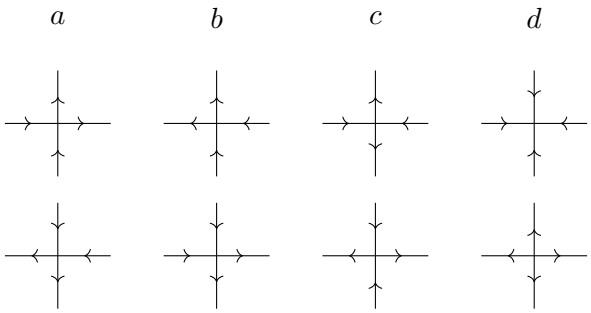

Figure 11: Local configurations of the 8V-model on $\mathbb{Z}^2$, and their *type* a, b, c, d shown above.

Consider a finite portion of $\mathbb{Z}^2$, and let τ be an orientation of its edges, such that every vertex has an even number of incoming edges. Every vertex has to be of one of the eight types shown in Figure 11. Fix four numbers $a, b, c, d \in \mathbb{R}^+$, not all of them being zero, and define the Boltzmann weight of τ as

$$w_{8V}(\tau) = a^{N_a} b^{N_b} c^{N_c} d^{N_d}$$

where N_i is the number of configurations of type i in τ.

In this paragraph, we discuss the $d = 0$ case, *i.e.* 6V-model, or square ice. By taking the limit of the 6V-model with periodic boundary conditions (*i.e.* on $(\mathbb{Z}/N\mathbb{Z})^2$ and letting $N \to \infty$), it has been argued by physicists that the limiting distribution of the model should depend on $a/c, b/c$ with the phase diagram shown in Figure 12; we again refer to [Bax82].

The *frozen* phases[8] of type a, b, c are such that the configuration on the infinite graph $\mathbb{Z}^2$ contains only vertices of type a (resp. b, c) (there are only two such frozen configurations); they are characterized by the fact that one of the weights a, b, c is greater than the sum of the other two. The *disordered* phase make all the vertex types appear with positive density. However, it is also argued that in the disordered phase, correlations of distant edges should decay as a power law and not as an exponential (2).

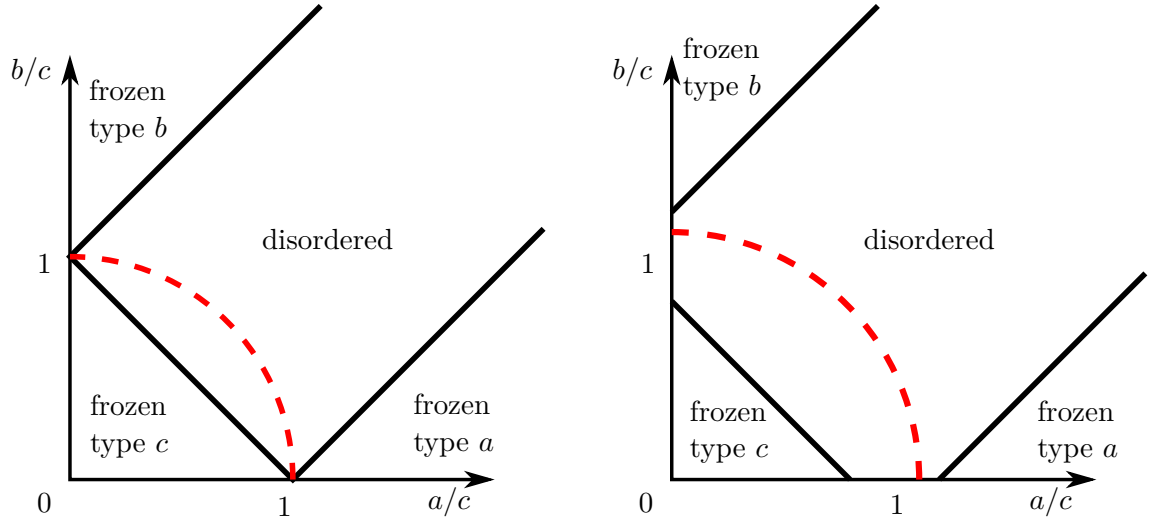

Figure 12: Phase diagram of the 6V-model (left) and 8V-model (right, with $0 < d < c$). The *free-fermion* line $a^2 + b^2 = c^2 + d^2$ is indicated in dashed red.

This last behavior is peculiar in statistical mechanics, as correlations are supposed to typically happen at a characteristic scale (the ξ in (2)), which naturally implies an exponential decay, except for very special *critical* points. This shows that the 6V-model is in some sense too rigid, and motivates the consideration of the case $d > 0$. However, the six-vertex model itself has many interesting integrable features; we refer to the lecture notes [Res10].

When $d > 0$, if we consider d as a fixed parameter the phase diagram is given in the right of Figure 12. It still contains frozen phases (characterized by the fact that one of the weights a, b, c, d is bigger than the sum of the three others), and a disordered phase. However, in that case, correlations should typically have exponential decay. In Chapter II, we give partial results towards this, by considering the 8V-model in the *free-fermion* regime $a^2+b^2 = c^2+d^2$, with the help of the dimer model. It is to be noted that quantities of interest, such as the free energy, should be analytic throughout the disordered phase, so that the free-fermion regime should be enough to guess the whole behaviour of disordered 8V-models.

b) Generalisation

In the hope of understanding the 8V-model more intrinsically, we generalise the previous definitions in two ways: we define the 8V-model on a generic 4-regular graph, and we let the local weights a, b, c, d depend on the site.

[8] They are generally called *(anti)-ferroelectric* phases.

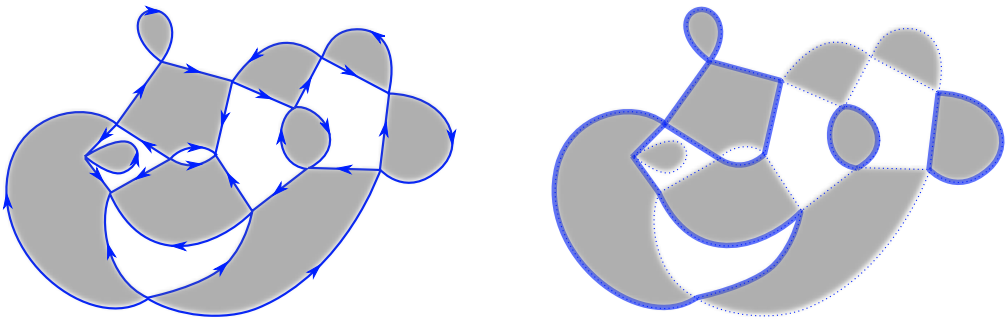

Figure 13: The medial graph $\mathscr{G}^m$, with its faces corresponding to vertices of $\mathscr{G}$ shaded in gray, equipped with an 8V-configuration shown as an orientation of edges (left), or as a subset of edges (right).

On the medial graph $\mathscr{G}^m$ (see Figure 5), faces are in bijection with the initial vertices and faces $\mathscr{V} \cup \mathscr{F}$. This corresponds to a bipartite coloring of the faces. Thus, if we have an orientation of the edges $\mathscr{E}^m$, we can transform it into a subset of edges by keeping, say, the edges that have an element of $\mathscr{F}$ on their left. An example is shown in Figure 13. Orientations that satisfy the 8V-rule are transformed into subsets of edges that are even at every vertex in $\mathscr{V}^m$, and vice-versa. We will use this "subgraph" representation.

Thus we define an eight-vertex configuration on $\mathscr{G}^m$ as a subset of edges τ such that every vertex of $\mathscr{V}^m$ has even degree in τ. Every vertex $v \in \mathscr{V}^m$ is equipped with 4 positive weights A_v, B_v, C_v, D_v. The local weight[9] of τ at v is defined as the value among these 4 that corresponds to the local configuration of τ at v, as in Figure 14; we denote it by $w_v(\tau)$. The total weight of τ is

$$w_{8\mathrm{V}}(\tau) = \prod_{v \in \mathscr{V}^m} w_v(\tau).$$

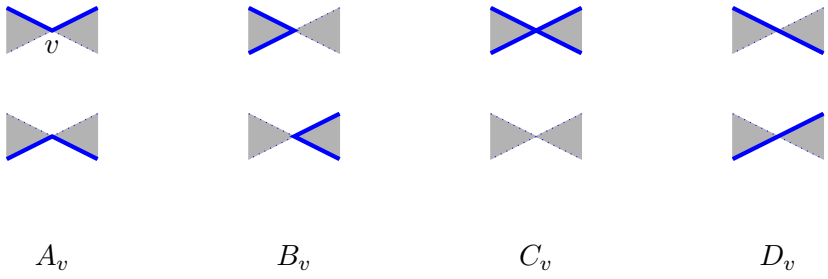

Figure 14: The eight possible local 8V-configuration at a vertex $v \in \mathscr{V}^m$, with the corresponding local weights shown below.

Let $X = (A_v, B_v, C_v, D_v)_{v \in \mathscr{V}^m}$ be the complete set of weights. The partition function of the 8V-model is

$$\mathscr{Z}_{8\mathrm{V}}(\mathscr{G}^m, X) = \sum_{\tau} w_{8\mathrm{V}}(\tau).$$

[9]Notice that this assignation of weights to configuration is only well-defined because of the bipartite coloring of the faces of $\mathscr{G}^m$. To be able to distinguish between complementary configuration, we would need to break another symmetry, for instance by fixing directions of the train-tracks. This would give so-called *rapidities* that define the model's weights.

Where the sum is over 8V-configurations. By following the successive transformations, we see that the 6V-model sub-case is obtained by setting $D = 0$.

The free energy of the 8V-model has been computed on $\mathbb{Z}^2$ and a few other lattices, see for instance [Bax82]. But many properties, such as the behaviour of correlations in generic cases, still need rigorous investigation.

2.4 Loop models

In this class of models, the configurations are sets of closed loops on a graph, with some local interactions, and global factors depending on the number of loops. In this exposition, I will present the loops as going through the edges of the diamond graph $\mathscr{G}^\diamond$ and winding inside its quadrangular faces $\mathscr{F}^\diamond$ (see Figure 5), but other cases exist such as the loops on hexagonal lattices.

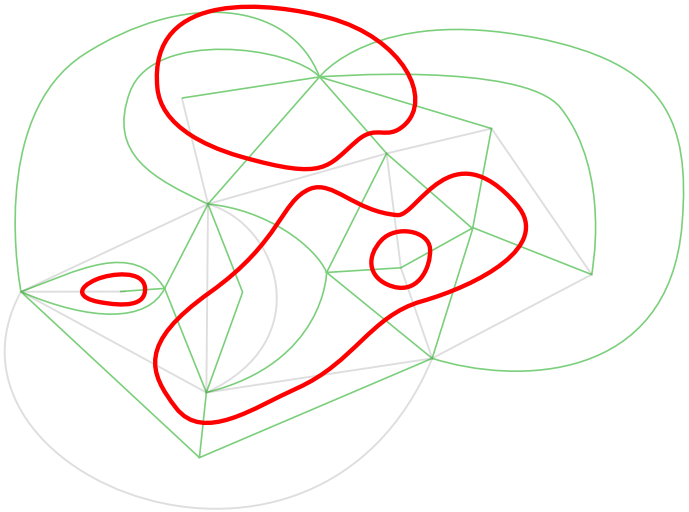

Figure 15: A loop configuration ω on $\mathscr{G}^\diamond$. Here $N(\omega) = 4$.

Thus in a loop configuration ω, every face of $\mathscr{G}^\diamond$ has to be of one of the "plaquette" types shown in Figure 16, with the condition that adjacent faces have to agree on their boundary. Just like for vertex models, every local configuration at $f \in \mathscr{F}^\diamond$ is assigned a weight $w_f(\omega)$. We also fix a positive parameter n called *fugacity*. Let N_ω be the total number of loops in ω. Then its weight, and the partition function, are given by

$$w_{\text{loop}}(\omega) = n^{N_\omega} \prod_{f \in \mathscr{F}^\diamond} w_f(\omega),$$

$$\mathcal{Z}_{\text{loop}} = \sum_{\omega} w_{\text{loop}}(\omega).$$

Many interesting models exist in this class, and the terminology referring to them may vary. The generic model we just described is often called the *(dilute) $O(n)$ loop model*, a name that comes from a spin model where spins take values on an n-dimensional sphere, that admits a combinatorial expansion into loops [DMNS81]. When only *fully packed* configurations are allowed, *i.e.* the right-most plaquettes of Figure 16, it is sometimes called a *Temperley-Lieb (TL) loop model*. In some variants, loops can exist in different flavours or

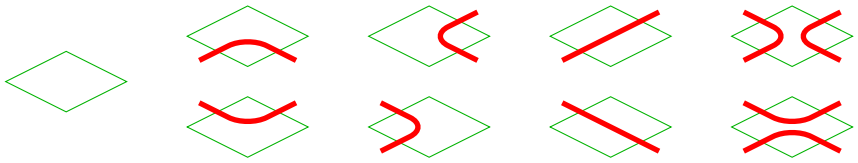

Figure 16: Possible configurations of a loop models, or "plaquettes", around a face $f \in \mathscr{F}^\diamond$.

colors. We will see such an example with the $C_2^{(1)}$ loop model, due to Warnaar and Nienhuis [WN93], in Chapter I where we show that is has a combinatorial link with the Ising model.

More generally, loop models are often used as convenient tools to find strong relations between known models, such as the coupling of Random Cluster models and 6V-models by Baxter, Kelland and Wu [BKW76]. They are also closely related to the graphical expansion of *quantum spin chains*; see for instance [AN94].

2.5 Transformations of models

This section is devoted to the problem of transforming a model into another. As we saw before, some models can be deeply understood, both analytically and geometrically, such as the bipartite dimer model. So when we are faced with a new model, it is tempting to transform it into, say, bipartite dimers. The game of finding relations between models constitutes a connection of statistical mechanics with combinatorics, and sometimes other fields like algebra and discrete geometry.

Let us show a few examples, and try to give a general picture of available techniques. First we relate the Ising model of Section 2.1 and the eight-vertex model of Section 2.3.

a) Ising and vertex models

There is a transformation from a pair of Ising models to an 8V-model, called the *spin-vertex correspondence*. Its complete form seems to be due to Wu [Wu71], Kadanoff and Wegner [KW71].

Suppose that $\mathscr{G}$ is a planar graph, *i.e.* it has been drawn on the sphere. Consider two independent Ising models, one on $\mathscr{G}$ with weights J and one on $\mathscr{G}^*$ with weights J'. Given two spin configurations, σ on $\mathscr{V}$ and σ' on $\mathscr{F}$, draw the edges of $\mathscr{G}^m$ that separate a $+$ spin from a $-$ spin. This gives a subset of edges that has even degree at every vertex of $\mathscr{V}^m$, that is, an 8V-configuration τ.

This transformation from (σ, σ') to τ is two-to-one, because flipping the spins of both σ and σ' would result in the same τ. Moreover, the image measure on τ can be expressed as an 8V-Boltzmann measure, simply by looking at the form of local weights and translating from the spin weights to vertex weights. Every primal edge $e \in \mathscr{E}$ corresponds to a vertex of the medial graph, denoted $v_e \in \mathscr{V}^m$. If we define the 8V-weights as

$$\begin{aligned} A_{v_e} &= \exp\left(J_e - J'_{e^*}\right), \\ B_{v_e} &= \exp\left(-J_e + J'_{e^*}\right), \\ C_{v_e} &= \exp\left(J_e + J'_{e^*}\right), \\ D_{v_e} &= \exp\left(-J_e - J'_{e^*}\right), \end{aligned} \tag{7}$$

then we have:

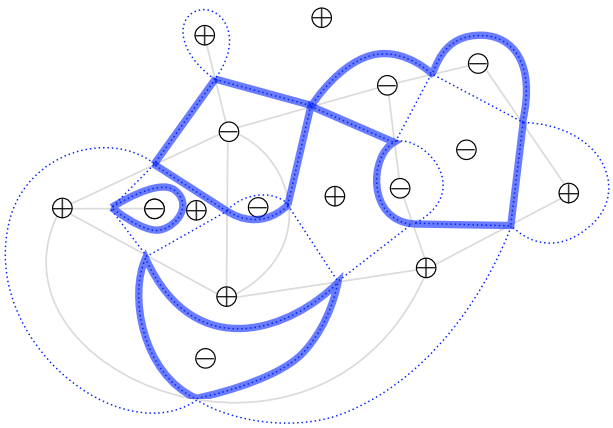

Figure 17: A spin configuration on $\mathscr{G} \cup \mathscr{G}^*$ and its image as an 8V-configuration on the medial graph $\mathscr{G}^m$.

Proposition 4 ([Wu71, KW71])**.** *For the 8V-weights X on $\mathscr{G}^m$ defined in* (7)*,*

$$\mathcal{Z}_{Ising}(\mathscr{G}, J)\ \mathcal{Z}_{Ising}(\mathscr{G}^*, J') = 2\mathcal{Z}_{8V}(\mathscr{G}^m, X).$$

Conversely, any 8V-model on $\mathscr{G}^m$ such that at every vertex $AB = CD$ can be expressed as two independent Ising models. When this condition is not satisfied, it corresponds to two *coupled* Ising models, as for example the Ashkin-Teller model [AT43].

b) Vertex models and dimers

We may want to transform vertex models on $\mathscr{G}^m$ from Section 2.3 into the dimer of Section 2.2, to use the strong integrability structures available there. Optimally, we would like to get dimers on a bipartite graph. An idea that dates back to the 1960s and 1970s [Kas63, Fis66, FW69, WL75] is to replace every vertex v of $\mathscr{G}^m$ with a small *decoration*. This technique is also named *holographic reduction* in the computer science literature [Val04].

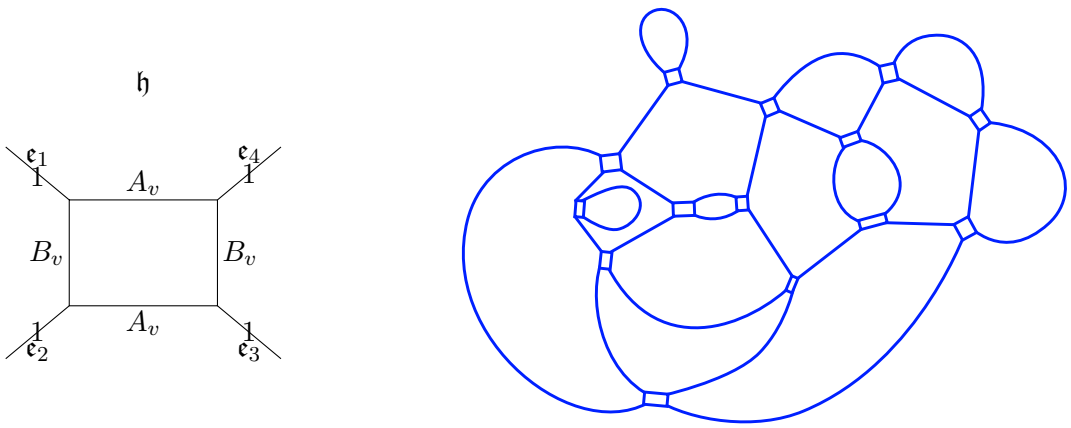

Figure 18: Left: a simple decoration $\mathfrak{h}$, due to Wu and Lin [WL75], with its dimer weights ν_v. Right: the corresponding decorated graph $\mathscr{G}^{\mathfrak{h}}$ (sometimes also denoted $\mathscr{G}^{\mathcal{Q}}$.

Let $\mathfrak{h}$ be a finite embedded graph, with four external edges or *legs*, denoted in direct cyclic order by $\mathfrak{e}_1, \mathfrak{e}_2, \mathfrak{e}_3, \mathfrak{e}_4$. For every $v \in \mathscr{V}^m$, let ν_v be weights on the edges of $\mathfrak{h}$, with the weights of the legs $\mathfrak{e}_i$ set to be 1. For a fixed 8V-model on $\mathscr{G}^m$ with weights $X = (A_v, B_v, C_v, D_v)_{v\in\mathscr{V}^m}$, we say that $(\mathfrak{h}, (\nu_v)_{v\in\mathscr{V}^m})$ is a *dimer-to-vertex* decoration if

1. all dimer configurations on $\mathfrak{h}$ use an even number of the 4 external edges;
2. for any even subset $I \subset \{1,2,3,4\}$, let $\mathcal{Z}^I$ be the sub-partition function of dimer configurations on $\mathfrak{h}$ that contain the leg $\mathfrak{e}_i$ *iff* $i \in I$:

$$\mathcal{Z}^I = \mathcal{Z}^I_{\mathrm{dim}}(\mathfrak{h}, \nu_v) := \sum_{m \text{ s.t. } \forall i, \mathfrak{e}_i \in m \Leftrightarrow i \in I} w_{\mathrm{dim}}(m).$$

   Then it is equal to the weight among A_v, B_v, C_v, D_v that corresponds to the local 8V-configuration that uses the edges $(\mathfrak{e}_i)_{i\in I}$, that is

$$\begin{aligned}\mathcal{Z}^{14} = \mathcal{Z}^{23} &= A_v,\\ \mathcal{Z}^{12} = \mathcal{Z}^{34} &= B_v,\\ \mathcal{Z}^{1234} = \mathcal{Z}^{\emptyset} &= C_v,\\ \mathcal{Z}^{13} = \mathcal{Z}^{24} &= D_v.\end{aligned}$$

We denote by $\mathscr{G}^{\mathfrak{h}}$ the decorated graph obtained by replacing every vertex v of $\mathscr{G}^m$ with a copy[10] of $\mathfrak{h}$, with the weights ν_v. We also denote the complete set of weights on $\mathscr{G}^{\mathfrak{h}}$ by ν.

Example 5. *The graph of Figure 18 is a dimer-to-vertex decoration for a 6V-model such that $A_v^2 + B_v^2 = 1 = C_v$. This is illustrated in Figure 19. The condition $C_v = 1$ on the 6V-model can be relaxed by multiplying all the local weights at a face by a same constant, which does not affect the ratio of Boltzmann weights, but one should still have $A_v^2 + B_v^2 = C_v^2$.*

Lemma 6. *If $(\mathfrak{h}, (\nu_v)_{v\in\mathscr{V}^m})$ is a dimer-to-vertex decoration for the 8V-weights X on $\mathscr{G}^m$, then*

$$\mathcal{Z}_{8V}(\mathscr{G}^m, X) = \mathcal{Z}_{dim}(\mathscr{G}^{\mathfrak{h}}, \nu).$$

Proof. For any dimer configuration m on $\mathscr{G}^{\mathfrak{h}}$, by Condition 1, the set of legs covered by m is an 8V-configuration τ. We denote this as $m \mapsto \tau$. By Condition 2 and the fact that legs have weight 1, for any 8V-configuration τ,

$$w_{8\mathrm{V}}(\tau) = \sum_{m \text{ s.t. } m\mapsto\tau} w_{\mathrm{dim}}(m)$$

and the equality of partition functions follows. □

Proposition 7. *For any* planar *decoration $\mathfrak{h}$ and any set of weights ν_v,*

$$\mathcal{Z}^{14}\mathcal{Z}^{23} + \mathcal{Z}^{12}\mathcal{Z}^{34} = \mathcal{Z}^{1234}\mathcal{Z}^{\emptyset} + \mathcal{Z}^{13}\mathcal{Z}^{24}. \tag{8}$$

[10] More precisely, this can be done by first fixing a cyclic order of the 4 medial edges around v and identifying these edges with $\mathfrak{e}_1, \mathfrak{e}_2, \mathfrak{e}_3, \mathfrak{e}_4$.

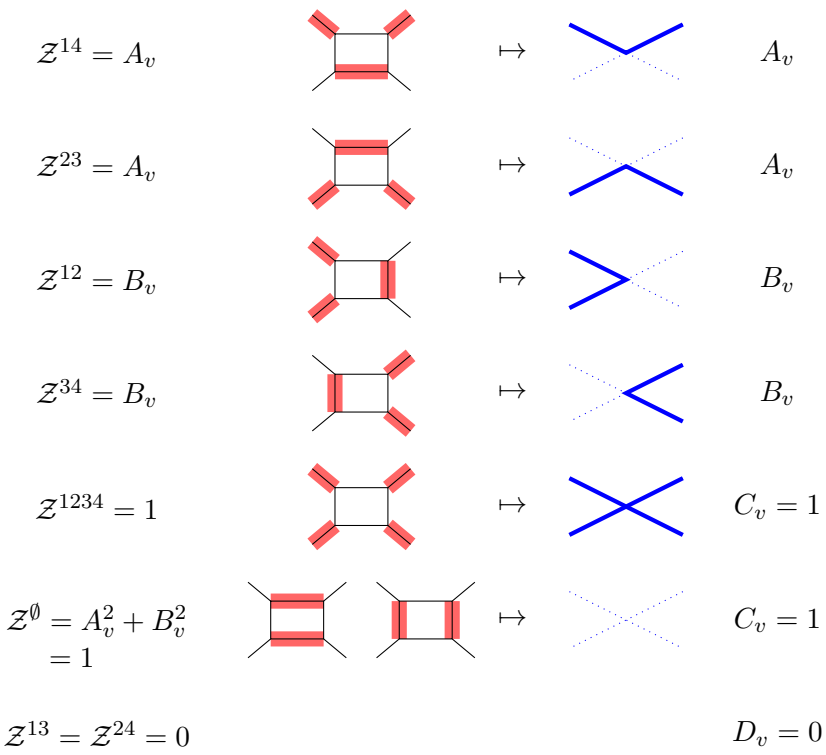

Figure 19: Local transformation of a dimer model into a 6V-configuration, for all possible dimers on the decorated graph of Figure 18, and the corresponding local weights for the two models.

Proof. The term $\mathcal{Z}^{14}\mathcal{Z}^{23}$ can be represented as a sum over couples of dimer configurations, one containing the legs $\mathfrak{e}_1, \mathfrak{e}_4$ and the other containing $\mathfrak{e}_2, \mathfrak{e}_3$. Let us call the first ones the black dimers, and the second ones the white dimers. If we start from the black dimer on $\mathfrak{e}_1$ and follow successively the white and black dimers, we get a path that has to end on another leg. Because of the planarity condition, it cannot be $\mathfrak{e}_3$, otherwise the other path would have no way to go from $\mathfrak{e}_2$ to $\mathfrak{e}_4$. Thus the first path has to end either at $\mathfrak{e}_2$ and have even length (because of the alternating color of dimers), or end at $\mathfrak{e}_4$ and have odd length. The situation is summed up in the left-most two diagrams of Figure 20; "e" stands for even and "o" for odd.

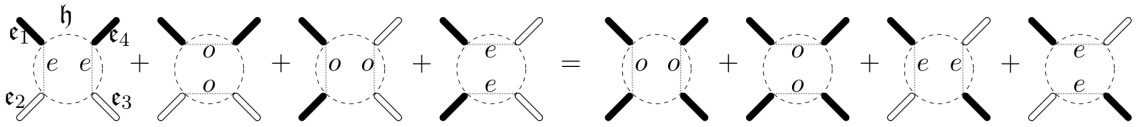

Figure 20: Double-dimer paths inside $\mathfrak{h}$

All the other cases can be decomposed similarly, as we do in Figure 20. There is a bijection between the left-hand side and the right-hand side, obtained by flipping the color of dimers in the path containing $\mathfrak{e}_3$. □

As a result of this Proposition, we can only hope to use dimers on decorated graphs when the 8V-model satisfies (implicitly, at every $v \in \mathscr{V}^m$)

$$A^2 + B^2 = C^2 + D^2.$$

This is known as the *free-fermion* regime of the 8V-model. This terminology comes from the fact that the Pfaffians arising in dimers (see Section 2.2) can be written as integrals of anti-commuting variables (see for instance [DFMS97], chapter 2.B), and those variables are interpreted physically as non-interacting fermions. Conversely, at least when $\forall v \in \mathscr{V}^m, C_v \neq 0$, any free-fermion 8V-model can be represented as a dimer model, using the decoration of Figure 21 [FW69].

Equation (8) can also be seen as a *Plücker relation*, which is a relation satisfied by generic minors of matrices. The existence of this necessary condition is actually a consequence of the determinantal (or Pfaffian) structure of dimers.

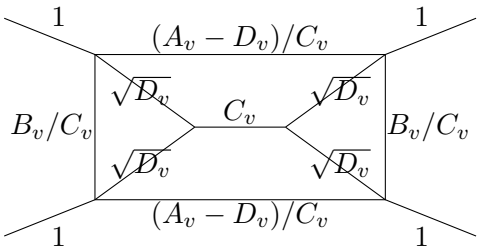

Figure 21: A decoration due to Fan and Wu [FW69]. This is a dimer-to-vertex decoration for any free-fermion 8V-model under the condition $\forall v \in \mathscr{V}^m, C_v \neq 0$.

Proposition 8. *For any* bipartite *decoration* $\mathfrak{h}$ *and any set of weights* ν_v*, one of the* 4 *products in* (8) *has to be zero.*

Proof. Suppose that we have fixed a bipartite coloring of $\mathfrak{h}$ into black and white vertices. Consider the case where the internal endpoints of $\mathfrak{e}_1$ and $\mathfrak{e}_3$ are black, and the internal endpoints of $\mathfrak{e}_2$ and $\mathfrak{e}_4$ are white. We interpret again the term $\mathcal{Z}^{13}\mathcal{Z}^{24}$ as a sum over couples of dimer configurations, one being black and the other being white. By following the dimers' alternating path starting from $\mathfrak{e}_1$ and looking at the alternation of vertices and dimers colors, it is easy to see that this path cannot exit the graph $\mathfrak{h}$ by any leg. Hence the sum is empty and this term is null.

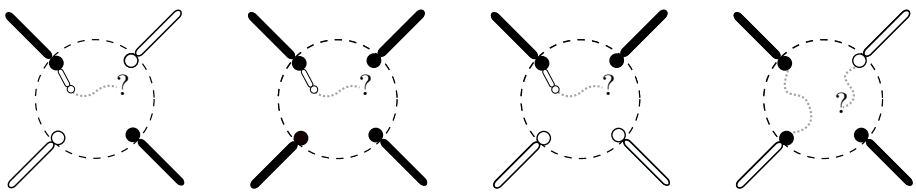

Figure 22: Proof of impossibility of certain double-dimer combinations for a bipartite $\mathfrak{h}$.

All the other cases can be treated similarly. A graphical representation of the proofs is given in Figure 22. □

This result basically reduces the scope of planar bipartite dimers to free-fermion 6V-models, that is models for which $D = 0$ and

$$A^2 + B^2 = C^2.$$

For instance, in that case, the decoration of Figure 21 reduces into the bipartite one of Figure 18 after a proper reparametrization.

The result of Proposition 8 is an obstacle to the rigorous study of the 8V-model even in the free-fermion regime, since we cannot use the theory of bipartite dimers to get, say, explicit Gibbs measures on infinite graphs from Theorem 3. In Chapter II we develop a solution to this issue, with an indirect method to find bipartite dimers and use the technology of [BdTR18].

c) Generic principles

In an attempt to sum up the kind of techniques that are used to relate models, we can distinguish four kinds (that are actually included into one another):

1. **Bijections.** The most simple case is when there is a bijection from the configuration space of model A, denoted $\Omega(A)$, to that of model B, denoted $\Omega(B)$.

   For instance, if we fix the spin of a vertex to always be $+1$, then the spin-vertex correspondence of Proposition 4 is a bijection.

2. **Surjective (many-to-one) mappings.** If there is a surjective map $f : \Omega(A) \to \Omega(B)$, such that the Boltzmann weights of the models, w_A and w_B, are such that

   $$\forall \omega_B \in \Omega(B), \quad w_B(\omega_B) = \sum_{\omega_A \in f^{-1}\{\omega_B\}} w_A(\omega_A)$$

   then the partition functions are equal. This is the case in the dimer-to-vertex correspondence of Lemma 6.

3. **Random mappings, or *couplings*.** When we can get the Boltzmann probability of model B as the image of that of model A by a function, that might use some extra randomness, it defines a strong *coupling* of the two models. For instance, the Edwards-Sokal coupling relates the random cluster and Potts models [ES88]. In some sense, this plays the role of a "many-to-many" mapping.

4. **Combinatorial identities.** Sometimes, the correspondence of two partition functions is shown by purely combinatorial means and does not seem to carry any information about how the models can be coupled. This is *a priori* the case for the duality relations of the Ising model [KW41] and of the 8V-model [Wu69] (although in these cases interpretations can be given by extending the configuration space and considering *order and disorder* variables [KC71]).

Those classes are more and more generic, but give less and less information about the actual behaviour of the models. In the worst-case scenario, we only know that the partition functions are equal. In that case, it is often an interesting question to try to know how strongly the two models can be coupled.

The panorama of relations between models is fascinating and constantly evolving. In the convoluted map of Figure 23, I try to sum up some of the relations I encountered.

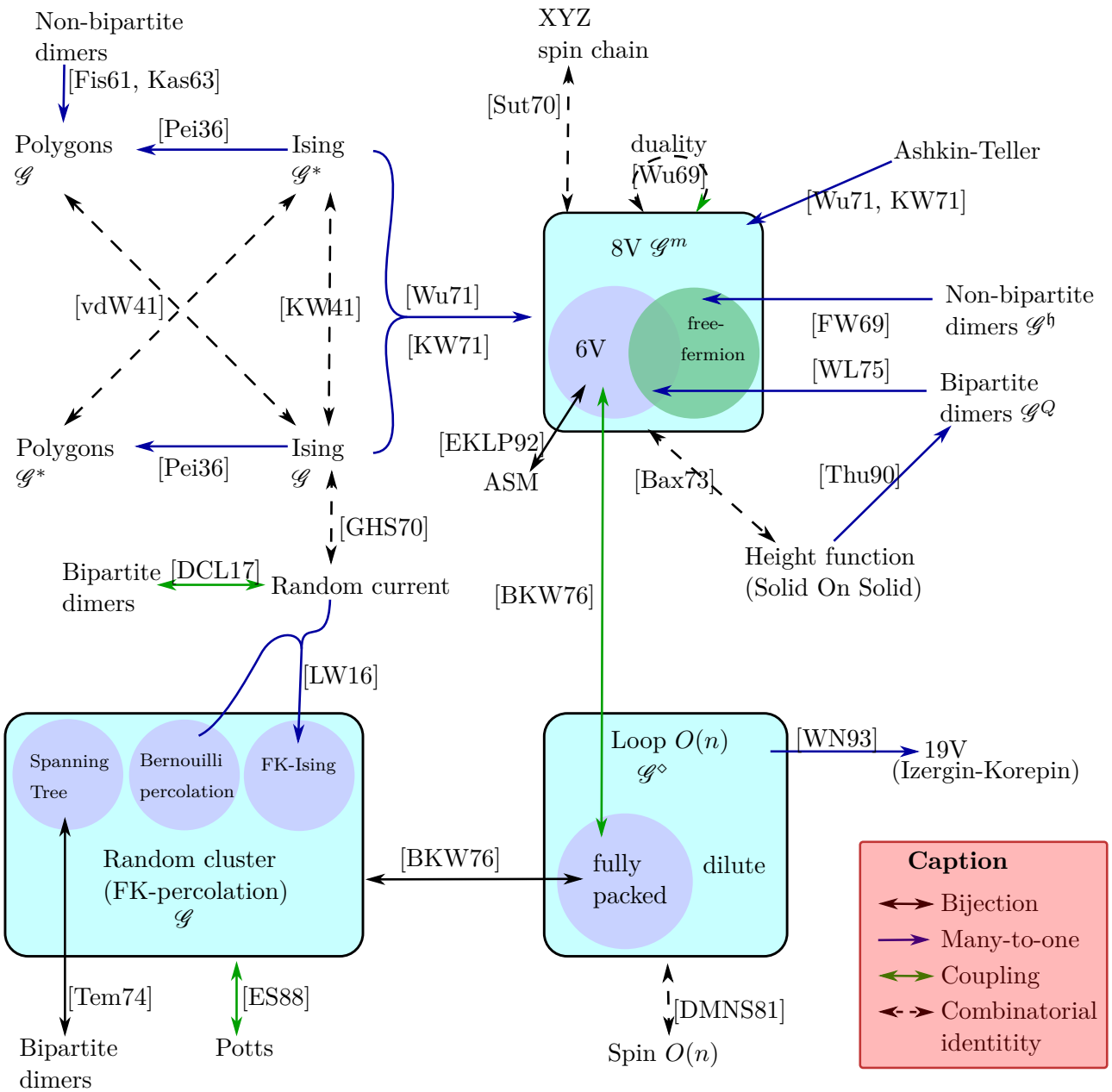

Figure 23: Some existing transformations of models (sometimes with the corresponding graph).

3 Six points of view on star-triangle transformations

We now turn our attention to a common feature of integrability, which is the existence of a *star-triangle* transformation. If the graph $\mathscr{G}$ contains a triangle, we can get a new graph $\mathscr{G}'$ by removing the edges of this triangle, adding a vertex at the center, and linking it to the vertices of the previous triangle. Thus we get a vertex of degree 3, or a *star*. This is also known as a Y-Δ move ; of course the converse transformation (*triangle-star*, or Δ-Y) can also be performed. On the diamond graph $\mathscr{G}^\diamond$, this induces a "cube flip", and on train-tracks, it performs a crossing, that is analogous to the Reidemeister move of type III [Rei27, AB26].

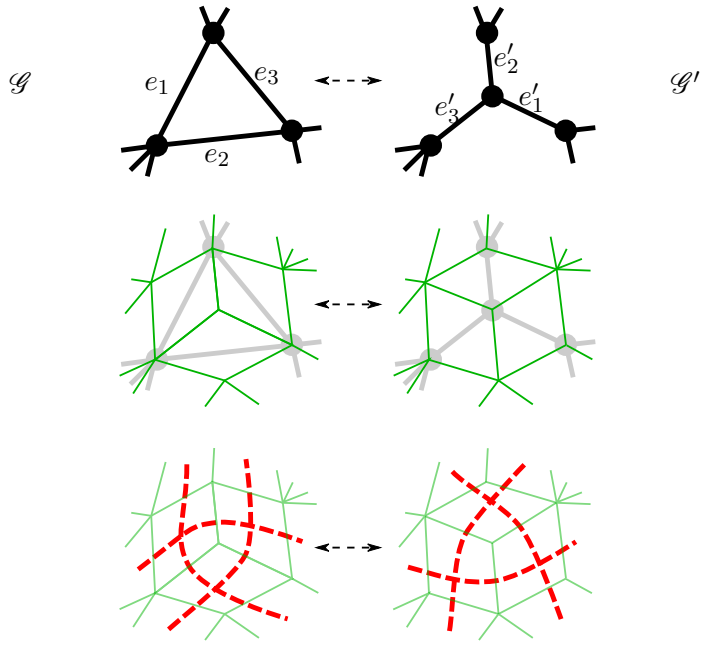

Figure 24: The star-triangle move and its effect on $\mathscr{G}$, on $\mathscr{G}^\diamond$, and on $TT(\mathscr{G})$.

As we will see, this is a powerful topological move. The next idea is to find models for which the partition function is unchanged when we perform a star-triangle move: this is called a *Z-invariant regime*. Such regimes have been found for a number of models, such as the Ising model [Ons44, Wan45], 6-vertex and 8-vertex models [Bax78, Bax82], spanning trees and spanning forests [Ken19], percolation [GM13] and FK-percolation [DCLM18], chiral Potts model [BPAY88], etc.

3.1 Simplifying graphs

The first appearance of star-triangle transformation is in the context of resistor networks, with the work of Kennelly [Ken99], see Figure 4. This transformation is such that the equivalent resistance between any two points of the graph (excluding the center vertex of the star) is left unchanged. Other simplifications of the graph have the same property, provided that we correctly update the resistance on the edges; they are represented in Figure 25. The most famous ones are the simplification of two resistors directly in series or in parallel.

All these transformation are enough to compute equivalent resistances whenever the

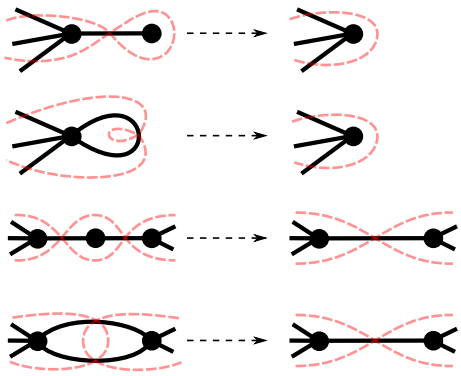

Figure 25: Simplifications of a graph $\mathscr{G}$ (with its train-tracks displayed): suppression of a vertex of degree 1, suppression of a loop, reduction in series and in parallel.

network is planar; this is due to Epifanov [Epi66].

Theorem 9 ([Epi66])**.** *Let $\mathscr{G}$ be a planar graph, with two distinguished vertices on the boundary, u and v. Using the star-triangle move and the simplifications of Figure 25, it is possible to transform $\mathscr{G}$ into a graph with just one edge between u and v.*

This is not such a surprise. Consider the set of train-tracks of the graph. Then the star-triangle move lets us take one train-track and make it cross an intersection of two train-tracks: we can essentially take one train-track and move it freely around the graph. With some care and with the help of the simplifications of Figure 25, this makes the task of reducing the graph to a single edge more or less equivalent to that of untangling a messy pool of cables.

Later, Feo and Provan published an algorithm of complexity $O(|\mathscr{V}|^2)$ that achieves this simplification [FP93] . This can be related to a "computational" point of view on integrability: for any Z-invariant model, on a finite planar graph, the partition function can be computed in a complexity which is polynomial in the size of the graph.

3.2 Coupling relations; locality

The star-triangle transformation is often phrased as a coupling relation. We will consider the examples of the Ising and the 8V-models. This is the analogous statement to the fact that in the resistor network, equivalent resistances do not change.

a) Star-triangle for the Ising model

Suppose that the graph $\mathscr{G}$ is equipped with an Ising model (see Section 2.1), with coupling constants $J = (J_e)_{e\in\mathscr{E}}$. We want to find weights J' on $\mathscr{G}'$, equal to J everywhere except on the edges involved in the star-triangle move, such that the Ising models on $\mathscr{G}$ and $\mathscr{G}'$ can be *coupled* in the strongest possible way. More precisely, we want to define a random variable (σ, σ') on $\{-1,+1\}^{\mathscr{V}} \times \{-1,+1\}^{\mathscr{V}'}$, with the marginals distributed as the Boltzmann measure (5) on $(\mathscr{G}, J)$, resp. $(\mathscr{G}', J')$, and such that almost surely $\sigma_v = \sigma'_v$ for every $v \in \mathscr{V}$ (i.e. for all vertices except the center of the star).

If we condition on the spins on the boundary of the star-triangle, the conditional probabilities are proportional to local Boltzmann weights. Thus by listing all boundary conditions (up to symmetry), the desired coupling exists *iff* the following quantities are proportional, with the same constant of proportionality. We denote for simplicity $J_i = J_{e_i}$ and $J'_i = J'_{e'_i}$.

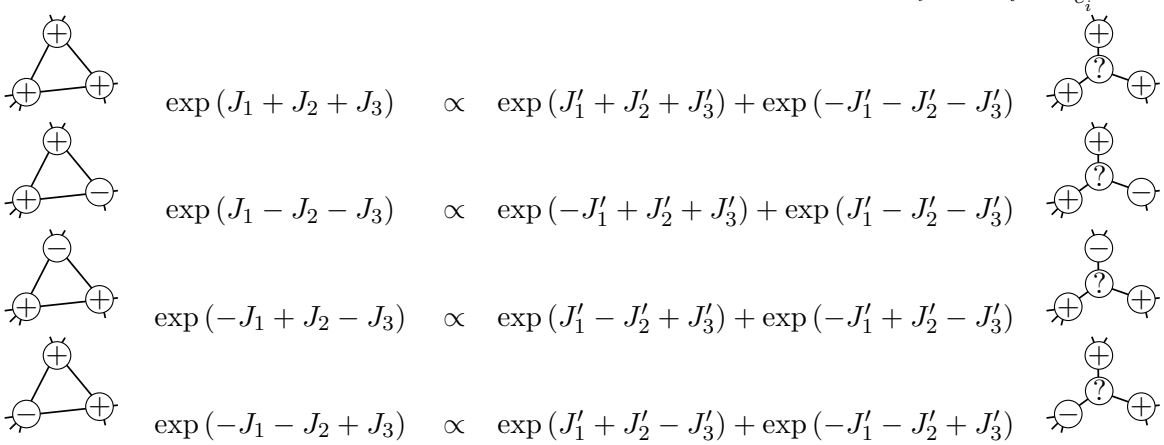

$$\exp(J_1+J_2+J_3) \quad \propto \quad \exp(J'_1+J'_2+J'_3)+\exp(-J'_1-J'_2-J'_3)$$

$$\exp(J_1-J_2-J_3) \quad \propto \quad \exp(-J'_1+J'_2+J'_3)+\exp(J'_1-J'_2-J'_3)$$

$$\exp(-J_1+J_2-J_3) \quad \propto \quad \exp(J'_1-J'_2+J'_3)+\exp(-J'_1+J'_2-J'_3)$$

$$\exp(-J_1-J_2+J_3) \quad \propto \quad \exp(J'_1+J'_2-J'_3)+\exp(-J'_1-J'_2+J'_3)$$

We call these the *coupling relations* for the Ising model. These equations can be solved, in the sense that one can express the J'_i in terms of the J_i, or the converse. Thus the transformation can be made as a triangle-to-star or as a star-to-triangle move, while keeping the Ising model "constant". The exact formulas can be found in different forms in several references [Bax82, KP16, BdTR18]. We will cite a solution, due to Baxter [Bax82] and reparametrized by Boutillier, de Tilière and Raschel [BdTR18], that expresses the coupling constants in terms of Jacobi elliptic functions.

Let k be an *elliptic modulus*, that is a complex number with $k^2 \in (-\infty, 1]$. The Jacobi elliptic functions $\mathrm{sn}(\cdot|k), \mathrm{cn}(\cdot|k)$ are generalisations of the trigonometric functions sin and cos; the special trigonometric case corresponds to $k = 0$. See [Law89] for an introduction and useful properties of these functions. We also use the complete elliptic integral of the first kind $\mathrm{K}(k)$, that plays the role of the *quarter-period* of elliptic functions (for $k = 0$, it is equal to $\frac{\pi}{2}$):

$$\mathrm{K}(k) = \int_0^{\frac{\pi}{2}} \frac{d\theta}{\sqrt{1-k^2\sin^2\theta}}.$$

Proposition 10 ([Bax82, BdTR18])**.** *Let J_1, J_2, J_3 be three positive numbers. Then there exists a unique elliptic modulus k such that for all $i \in \{1,2,3\}$,*

$$J_i = \frac{1}{2}\log\left(\frac{1+\mathrm{sn}(\tau_i \mid k)}{\mathrm{cn}(\tau_i \mid k)}\right), \tag{9}$$

and the parameters τ_i satisfy $\tau_1+\tau_2+\tau_3 = \mathrm{K}(k)$.

Then the solution of the coupling relations for the Ising model is

$$J'_i = \frac{1}{2}\log\left(\frac{1+\mathrm{sn}(\mathrm{K}(k)-\tau_i \mid k)}{\mathrm{cn}(\mathrm{K}(k)-\tau_i \mid k)}\right).$$

Notice that the new coupling constants are simply obtained by changing τ_i into $\mathrm{K}(k)-\tau_i$. We will see a geometric interpretation of these expressions in Section 3.6.

b) Star-triangle for 8V-models

For the eight-vertex model defined in Section 2.3b), the line of reasoning is exactly the same: we want to couple the models on $\mathscr{G}^m$ and $(\mathscr{G}')^m$, such that they agree everywhere except on the medial edges that have been modified during the star-triangle move. The coupling relations on the 8V-weights $(A_i, B_i, C_i, D_i)_{i\in\{1,2,3\}}$ and $(A'_i, B'_i, C'_i, D'_i)_{i\in\{1,2,3\}}$ can still be written by conditioning on boundary conditions. They can be found in [Bax82], and also in Section II.5.

An important difference with the Ising case is that the coupling equations for the 8V-model cannot be solved for generic values of $(A_i, B_i, C_i, D_i)_{i\in\{1,2,3\}}$, and we have to assume that they take a certain form to perform the transformation; see again [Bax82] for more details. We state the result as an elliptic parametrization, adapted from Baxter's expression. Since the Boltzmann measure is unchanged when we multiply all the 8V weights at a site by the same constant, the solution can be written in homogeneous coordinates.

Proposition 11 ([Bax82])**.** *Suppose that there exists an elliptic modulus k and a real number λ such that for all $i \in \{1,2,3\}$, in homogeneous coordinates,*

$$\begin{aligned}[A_i : B_i : C_i : D_i] = [&\operatorname{sn}(\lambda\tau_i|k) : \\ &\operatorname{sn}(\lambda(\mathrm{K}(k) - \tau_i)|k) : \\ &\operatorname{sn}(\mathrm{K}(k)\lambda|k) : \\ &k\operatorname{sn}(\lambda\tau_i|k)\ \operatorname{sn}(\lambda(\mathrm{K}(k) - \tau_i)|k)\ \operatorname{sn}(\mathrm{K}(k)\lambda|k)],\end{aligned} \tag{10}$$

and such that $\tau_1 + \tau_2 + \tau_3 = \mathrm{K}(k)$. Then the solution of the 8V-model coupling relations are

$$\begin{aligned}[A'_i : B'_i : C'_i : D'_i] = [&\operatorname{sn}(\lambda(\mathrm{K}(k) - \tau_i)|k) : \\ &\operatorname{sn}(\lambda\tau_i|k) : \\ &\operatorname{sn}(\mathrm{K}(k)\lambda|k) : \\ &k\operatorname{sn}(\lambda\tau_i|k)\ \operatorname{sn}(\lambda(\mathrm{K}(k) - \tau_i)|k)\ \operatorname{sn}(\mathrm{K}(k)\lambda|k)].\end{aligned}$$

c) Locality

It has been argued by Baxter in [Bax78] that when a model is Z-invariant, *i.e.* when we can perform a star-triangle coupling wherever we want, it should also be *local*. The idea is again that we can move train-tracks freely around the graph, without changing the statistical properties such as two-point correlations (provided that we do not cross one of the points while moving the train-tracks). We present this in the context of vertex models, but it should hold for any Z-invariant model.

Suppose that each train-track (see Figure 5) or *rapidity* $t \in TT(\mathscr{G})$ carries a parameter θ_t, and that the 8V-weights at the intersection of two train-tracks t, t' are a function of $(\theta_t, \theta_{t'})$. For a well chosen function [Bax78], the 8V-coupling relations of Proposition 11 are automatically satisfied. This is known as a Z-invariant regime. Then for any medial edges $e, e' \in \mathscr{E}^m$, we can chose a path on the medial graph that goes from e to e', crossing rapidities with parameters $\theta_1, \dots, \theta_p$. Baxter argues that if τ is distributed as the Boltzmann measure of the 8V-model, the correlations can be written as

$$\langle 1_{e\in\tau} 1_{e'\in\tau}\rangle = g(\theta_1, \dots, \theta_p)$$

where g is some universal function, symmetric in the parameters. Similar formulas should also exist for correlations involving more edges. This property is surprising, since correlations should depend on the geometry of the whole graph. Here it depends only on a path (*any* path) between the two edges.

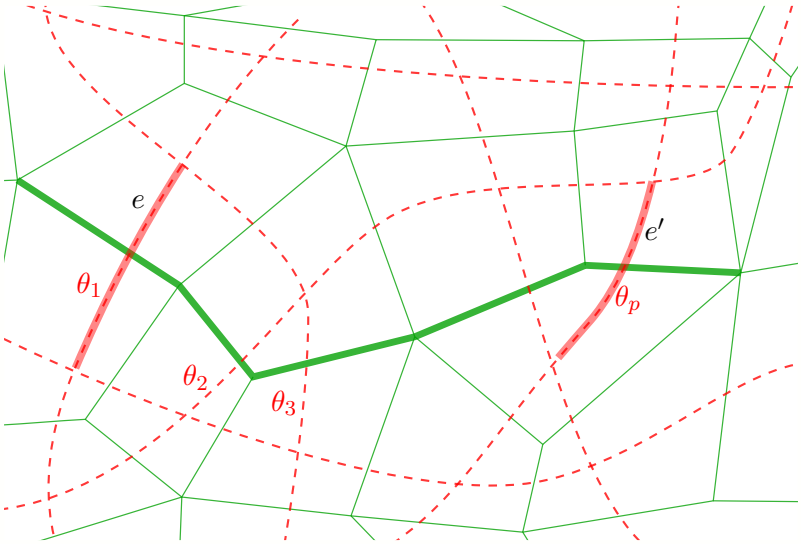

Figure 26: Two medial edges e and e', with the diamond graph $\mathscr{G}^\diamond$ in green. A path linking e and e' is represented in bold green. It crosses train-track, or rapidities, with parameters $\theta_1, \dots, \theta_p$.

The justification that Baxter gives is unfortunately non-rigorous in general: it involves creating train-tracks "at infinity" and bringing them around the path using star-triangle transform. If the path has been isolated from the rest of the graph with sufficiently many rapidities, the correlations should no longer depend on the rest of the graph.

However, it is a strong indication, and explicit expressions of this function g have indeed been found for the Z-invariant Green function [Ken02] and massive Green function [BdTR17], for the correlations of some Z-invariant bipartite dimers [Ken02, dT18], for the Ising model at criticality [BdT11] and away from criticality [BdTR18]. In Section II.5.3 we find such a function g for Z-invariant free-fermion 8V-models.

3.3 Commutation of transfer matrices

Perhaps the most common use of star-triangle relations is to provide a sufficient condition for the commutation of transfer matrices. Again we take the example of the 8V-model, but more details and models can be found in [McC10]. It is customary and more convenient to present these proofs graphically.

We represent the set of local 8V-weights at a medial vertex by a single lowercase letter. The existence of star-triangle coupling means that for any local weights u and v, there exists local weights w such that we have the first diagram of Figure 27.

Another useful property is the existence of *inversion relations*. This means that for any local weights w, there exists a choice of local weights w' such that the second diagram of Figure 27 holds. Then the commutation of transfer matrices is hopefully illustrated by the graphical proof of Figure 28.

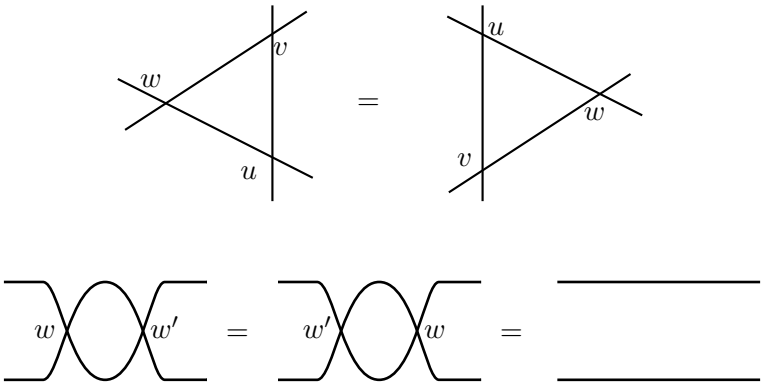

Figure 27: Diagrammatic representation of star-triangle and inversion relations.

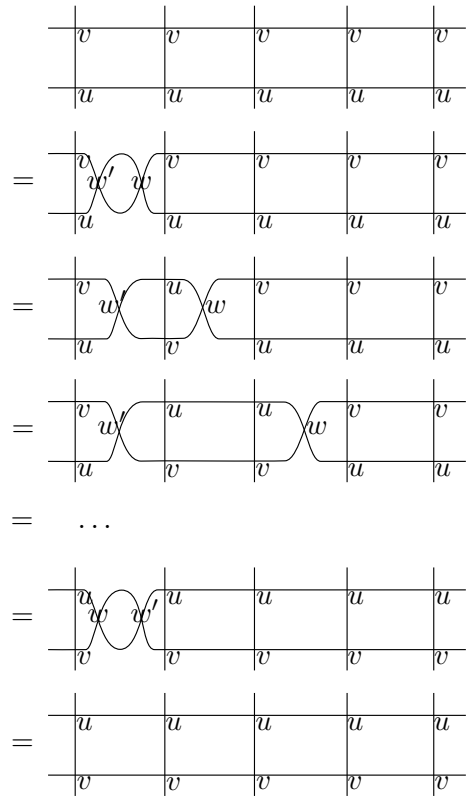

Figure 28: Proof of commutation of transfer matrices.

3.4 Operator form of Yang-Baxter equations

Although we present them as a coupling condition that encapsulates several equations, the star-triangle relations can also be stated as single relation on matrices, constructed on a tensor product. We present this formalism for vertex models, and we refer to [PAY06] for a more complete panorama.

It will be more convenient for this exposition to define the local weights in a slightly different way compared to Section 2.3. First we orient every train-track $t \in TT(\mathscr{G})$ and we equip it with a parameter q_t. At every medial vertex, two oriented train tracks t, t' intersect; we can assume that they are as in the configuration of Figure 29. The values of i, j, k, l are equal to 1 when the corresponding medial edge is occupied, and 0 otherwise. Then the local 8V-weight is set to be a function of the parameters $q_t, q_{t'}$ and of the four occupation values, denoted $w_{i,j}^{k,l}(q_t, q_{t'})$.

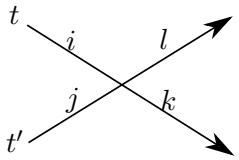

Figure 29: Two oriented train-tracks or *rapidities* crossing.

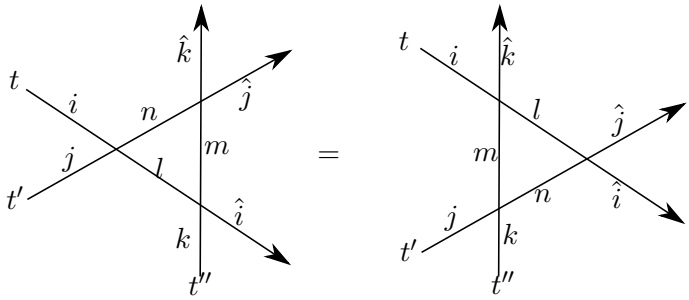

Figure 30: A star-triangle move on the oriented train-tracks t, t', t''.

Recall that the coupling relations amount to requiring that for any boundary conditions, the sum of local Boltzmann weights are proportional. Then, in the configuration of Figure 30, this is equivalent to saying that for any $i, j, k, \hat{i}, \hat{j}, \hat{k}$,

$$\begin{aligned} &\sum_{l,m,n} w_{i,j}^{l,n}(q_t, q_{t'})\, w_{l,k}^{\hat{i},m}(q_t, q_{t''})\, w_{n,m}^{\hat{j},\hat{k}}(q_{t'}, q_{t''}) \\ \propto &\sum_{l,m,n} w_{j,k}^{n,m}(q_{t'}, q_{t''})\, w_{i,m}^{l,\hat{k}}(q_t, q_{t''})\, w_{l,n}^{\hat{i},\hat{j}}(q_t, q_{t'}), \end{aligned} \tag{11}$$

with the same constant of proportionality.

This can be interpreted as an operator product. First define $R(t, t')$ as the 4×4 matrix with rows (resp. columns) identified with the possible values of (i, j) (resp. (k, l)), so that its entries are the $w_{i,j}^{k,l}(q_t, q_{t'})$. We can consider these matrices as elements of $\mathrm{End}(\mathscr{V} \otimes \mathscr{V})$, where $\mathscr{V}$ is a vector space of dimension 2. Then for any $u, v \in \{1, 2, 3\}$ with $u < v$, we define $R_{i,j}(t, t')$ as the element of $\mathrm{End}(\mathscr{V} \otimes \mathscr{V} \otimes \mathscr{V})$ (or 8×8 matrix) that acts as $R(t, t')$ on the

components u, v of the tensor product, and as the identity on the other one. For instance, the matrix $R_{1,2}(t,t')$ has rows indexed by the values of (i_1,j_1,k_1) and columns by (i_2,j_2,k_2), and the corresponding matrix element is

$$w_{i_1,j_1}^{i_2,j_2}(q_t,q_{t'})\delta_{k_1,k_2}.$$

Then the whole set of coupling relations (11) is equivalent to

$$R_{1,2}(t,t')R_{1,3}(t,t'')R_{2,3}(t',t'') \propto R_{2,3}(t',t'')R_{1,3}(t,t'')R_{1,2}(t,t').$$

This is often called the (quantum[11]) Yang-Baxter equation. The abstract construction and classification of solutions to this equation has motivated the construction of important objects related to Lie algebras, such as *quantum groups*, independently by Drinfeld [Dri88] and Jimbo [JM94]. Other approaches can be taken to the classification of their solutions, such as the *consistency* approach [ABS03, ABS04], *differential* approaches [Vie18], methods based on algebraic geometry [Kri81], on Lie algebra [Baz85], etc.

3.5 Polynomial relations and spatial recurrence

In some cases, there is another way to sum up all the coupling relations into a single, *polynomial* one, via a well-chosen change of variables. This idea seems to be due to Kashaev [Kas96]. The polynomial relations we obtained can be considered as evolution equations, and have attracted interest in cluster algebra [FZ02b, GK13, KP16, Yam18, Lea19], combinatorics [Spe07, CS04, KP16], [1] and limit shapes phenomena [DFSG14, PS05, KP16, Geo17], [1].

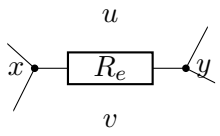

Figure 31: An edge e carrying a resistor, adjacent to vertices x, y and faces u, v.

Example 12 (Resistor networks and Hirota equation)**.** *Consider the star-triangle equations for resistor networks (or equivalently, for the discrete Laplacian or for random walks, see e.g. [Ken12]) of Figure 4. Suppose that there is a set of positive variables on the vertices and faces of $\mathscr{G}$, denoted $(f_x)_{x\in\mathscr{V}\cup\mathscr{F}}$, such that for every edge $e\in\mathscr{E}$, there is a resistor whose value is given, in the notation of Figure 31, by*

$$R_e = \frac{f_u f_v}{f_x f_y}.$$

Then the star-triangle relations of the resistor network are equivalent to the f variables satisfying, in the notation of Figure 32 [Kas96],

$$f_0' = \frac{f_1 f_4 + f_2 f_5 + f_3 f_6}{f_0}. \tag{12}$$

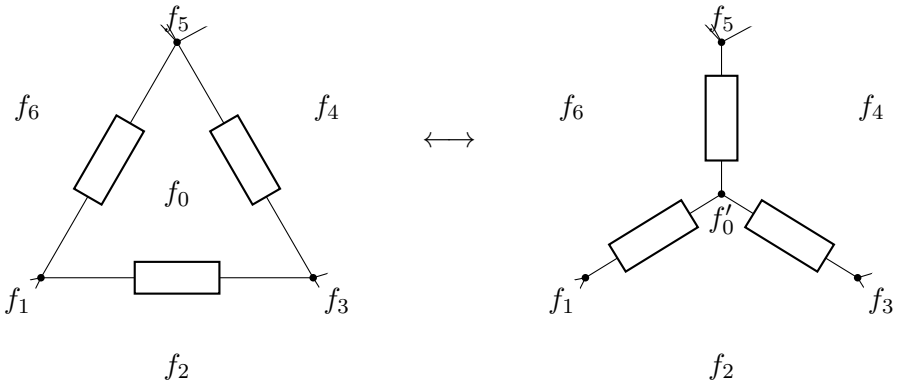

Figure 32: The star-triangle move on the f variables.

Equation (12) is known, in discrete integrable systems, as the discrete Hirota equation [Hir77], and was also named *the cube recurrence* by Propp [Pro01]. This last terminology comes from the fact that we can imagine the eight values of the f parameters as being embedded on the vertices of a cube, so that (12) lets us define the value at a given vertex in terms of the seven other. We can go a step further and start with a large subset of $\mathbb{Z}^3$ for which the values of f are fixed, that will play the role of *initial condition*. Then by building cubes and using (12), we can define f on further vertices of $\mathbb{Z}^3$. Thus we have transformed (12) into a *spatial recurrence*.

Let us give a more formal setting. We say that a function f from $\mathbb{Z}^3$ to $\mathbb{C}^*$ satisfies the cube recurrence if, for every $(i,j,k) \in \mathbb{Z}^3$,

$$f_{i,j,k}f_{i+1,j+1,k+1} = f_{i+1,j,k}f_{i,j+1,k+1} + f_{i,j+1,k}f_{i+1,j,k+1} + f_{i,j,k+1}f_{i+1,j+1,k}.$$

For a vertex $(i,j,k) \in \mathbb{Z}^3$, we define its *cone* as

$$\mathcal{C}_{i,j,k} = \{(i',j',k') \in \mathbb{Z}^3 \mid i' \leq i, j' \leq j, k' \leq k\}.$$

We say that a subset $\mathcal{L} \subset \mathbb{Z}^3$ is *monotone* if $\forall (i,j,k) \in \mathcal{L}, \mathcal{C}_{i,j,k} \subset \mathcal{L}$. We fix such a monotone subset. Then its *surface boundary* $\mathcal{I}$, defined by

$$\mathcal{I} = \{(i,j,k) \in \mathcal{L} \mid (i+1,j+1,k+1) \notin \mathcal{L}\},$$

can play the role of an initial condition for the cube recurrence. If $z \in \mathbb{Z}^3$ is such that $\mathcal{C}_z \cap \mathcal{L}^c$ is finite, and if f satisfies the cube recurrence, then f_z is a function of the $(f_y)_{y\in\mathcal{I}}$, and even of the $(f_y)_{y\in\mathcal{I}\cap\mathcal{C}_z}$. It is clear that this is a rational function. But Fomin and Zelevinsky proved that it is, unexpectedly, a Laurent polynomial [FZ02b], *i.e.* a polynomial in the f_y and the f_y^{-1}; they actually prove this for the much wider class of *cluster algebras*.

A Laurent polynomial is an object that strongly resembles a partition function. In the case of the cube recurrence, it is a sum of weights that are products of the initial variables $(f_y)_{y\in\mathcal{I}\cap\mathcal{C}_z}$; this might be interpreted as the total weight of some configuration, and we would like these configurations to be in bijection with the different terms of the Laurent polynomial.

[11] In contrast, the *classical* Yang-Baxter equation is the equation obtained when R is a first-order perturbation of the identity; see [PAY06].

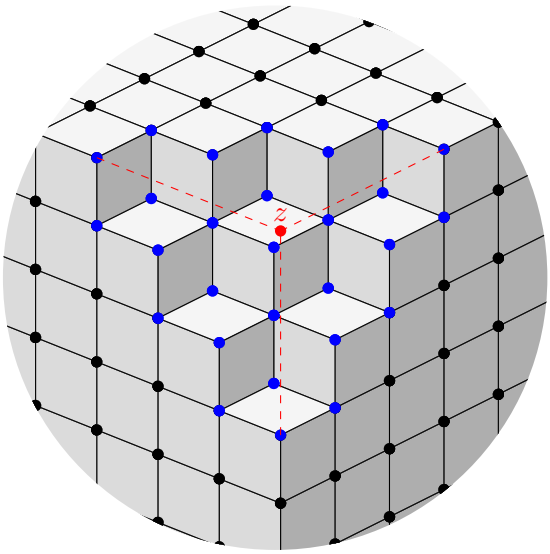

Figure 33: A monotone set $\mathcal{L}$ intersected with the cone $\mathcal{C}_z$, with the vertices of $\mathcal{I}$ in blue. In that case, we have set $\mathcal{L} = \{(i,j,k) \mid i+j+k \leq 0\}$, so $\mathcal{I} = \{(i,j,k) \mid i+j+k = 0, -1 \text{ or } -2\}$, and $z = (1,1,1)$.

Such an interpretation was found by Carroll and Speyer [CS04], with the introduction of *cube groves*.

A cube grove on $\mathcal{I} \cap \mathcal{C}_z$ is choice of one diagonal for each unit square at the surface of $\mathcal{I} \cap \mathcal{C}_z$, such that the resulting graph is a spanning forest of the vertices (*i.e.* it has no loop and touches every vertex), with every tree of the forest connected to the boundary, and with an extra condition on the boundary vertices connection that can hopefully be guessed from Figure 34. If $\mathfrak{g}$ is a grove, and $y \in \mathcal{I} \cap \mathcal{C}_z$, we denote by $\deg_{\mathfrak{g}}(y)$ the degree of y in the forest $\mathfrak{g}$. Then the weight of $\mathfrak{g}$ is defined as

$$w(\mathfrak{g}) = \prod_y f_y^{\deg_{\mathfrak{g}}(y)-2}.$$

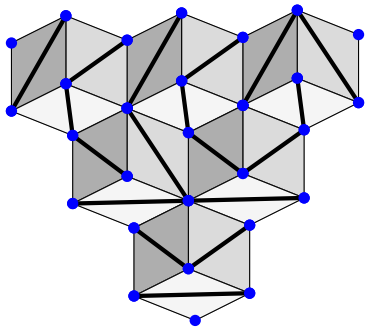

Figure 34: A cube grove on $\mathcal{I} \cap \mathcal{C}_z$.

Theorem 13 ([CS04]). *With the previous notation,*

$$f_z = \sum_{\mathfrak{g}} w(\mathfrak{g})$$

where the sum is over cube groves on $\mathcal{I} \cap \mathcal{C}_z$. Moreover, there is a one-to-one correspondence between such cube groves and monomials of f_z, seen as a Laurent polynomial in the formal variables $(f_y)_{y \in \mathcal{I} \cap \mathcal{C}_z}$.

This is not the only occurrence of combinatorial objects in the iteration of a statistical mechanics transformation. Speyer proved a similar results for the *octahedron recurrence* (that can be seen as an expression of the *urban renewal* move for dimers) and dimer configurations on certain graphs [Spe07]. Kenyon and Pemantle found an analogous relation between double-dimer configurations and the *hexahedron recurrence* [KP16], while investigating a recurrence due to Kashaev [Kas96], which we introduce now.

Example 14 (Ising star-triangle and Kashaev's relation). *Suppose that there is a set of positive variables on the vertices and faces of $\mathscr{G}$, denoted $(g_x)_{x \in \mathscr{V} \cup \mathscr{F}}$, and equip every edge $e \in \mathscr{E}$ with an Ising coupling constant J_e defined, in the notation of Figure 31, by*

$$\sinh^2(2J_e) = \frac{g_x g_y}{g_u g_v}.$$

Then, in the notation of Figure 32, the Ising model satisfies the star-triangle relations of Section 3.2a) iff g satisfies

$$2(a^2 + b^2 + c^2 + d^2) - (a + b + c + d)^2 - 4(s + t) \tag{13}$$

where

$$a = g_0 g_0', \quad b = g_1 g_4, \quad c = g_3 g_6, \quad d = g_5 g_2,$$
$$s = g_0 g_2 g_4 g_6, \quad t = g_0' g_1 g_3 g_5.$$

Equation (13) is known in tensor algebra as Cayley's $2 \times 2 \times 2$ *hyperdeterminant* [Cay61], but for our purposes we will call it *Kashaev's relation*. It can also be embedded on the vertices of a cube, and the value at one point be defined in terms of the others, with some care since we have to take the root of a polynomial of degree 2. By always taking the + root, we ensure that the values of g stay positive. Thus we also have a spatial recurrence: we say that $g : \mathbb{Z}^3 \to \mathbb{C}^*$ satisfies *Kashaev's* (positive) *recurrence* if at every vertex $(i, j, k) \in \mathbb{Z}^3$, by denoting $g_{abc} = g_{i+a, j+b, k+c}$, we have

$$g_{111} = \frac{A + 2\sqrt{D}}{g_{000}^2}$$

where

$$A = 2g_{100}g_{010}g_{001} + g_{000}(g_{100}g_{011} + g_{010}g_{101} + g_{001}g_{110})$$
$$D = (g_{000}g_{011} + g_{010}g_{001})(g_{000}g_{101} + g_{100}g_{001})(g_{000}g_{110} + g_{100}g_{010}).$$

The solution of this recurrence also has a Laurentness property, with a connection to cluster algebra [KP16].

Theorem 15 ([KP16]). *If g satisfies Kashaev's positive recurrence, for any monotone $\mathcal{L} \subset \mathbb{Z}^3$ with surface boundary $\mathcal{I}$, and any z such that $\mathcal{C}_z \cap \mathcal{L}^c$ is finite, g_z is a Laurent polynomial in the variables $(g_y)_{y \in \mathcal{I} \cap \mathcal{C}_z}$, and $\left(\sqrt{g_x g_y + g_u g_v}\right)_{x,y,u,v \in \mathcal{I} \cap \mathcal{C}_z}$ where x, u, y, v are the boundary of a unit square.*

In fact Kenyon and Pemantle obtained this result by showing that g_z is the partition function of a *double-dimer model* on a decorated graph, but the configurations are not in bijection with monomials of g_z. Such an identification was made later [1] by defining $C_2^{(1)}$ loop configurations on $\mathcal{I} \cap \mathcal{C}_z$. For exact definitions of the configurations and weights, see Section 4.1 and Chapter I; let us just say now that it gives a theorem analogous to Theorem 13 in the case of Kashaev's recurrence.

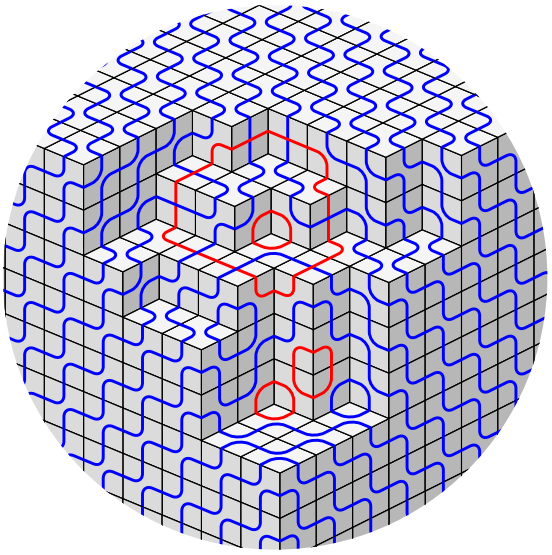

Figure 35: A loop configuration on $\mathcal{I} \cap \mathcal{C}_z$.

3.6 Geometric embeddings and incidence theorems

All the interpretations given so far used the embedding of $\mathscr{G}$ as a *map*, *i.e.* up to homomorphism, or combinatorial interpretations on a regular lattice. In other words, they were rather *topological*. The last point of view that we mention is a *geometric* one: it deals with an actual realisation of $\mathscr{G}$ as an embedded graph.

a) Isoradial embeddings

Suppose that $\mathscr{G}$ is embedded in the plane in such a way that each of its internal faces can be inscribed in a circle of radius 1, and the center of this circle is inside the face. Such a graph is called *isoradial* [Mer01, Ken02]; it is equivalent to the fact that the internal faces of $\mathscr{G}^\diamond$ are rhombi with edge-length 1. We say that $\mathscr{G}^\diamond$ is a *lozenge graph*. Each edge $e \in \mathscr{E}$ corresponds to a rhombus, and we denote by $\theta_e \in (0, \frac{\pi}{2})$ the half-angle of this rhombus at the primal vertices, see Figure 36.

The class of isoradial graphs is preserved by star-triangle moves, as illustrated in the simple geometric property of Figure 36. Moreover, the action of this geometric transformation on

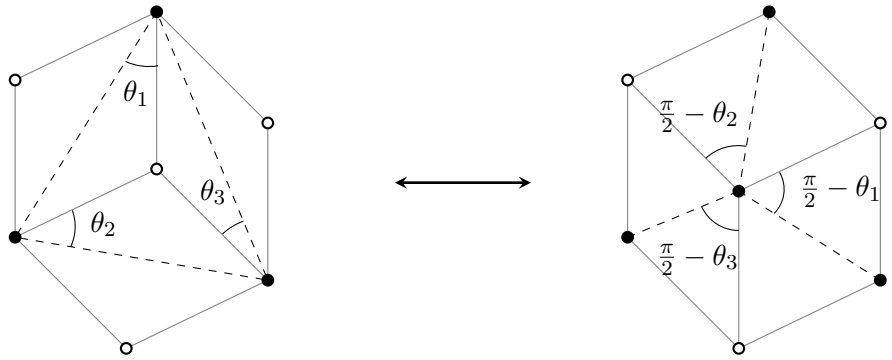

Figure 36: Star-triangle move on an isoradial graph $\mathscr{G}$ (with its vertices in black and its edges dashed, and the dual vertices in white), and its action on the lozenge graph $\mathscr{G}^\diamond$. The angles satisfy $\theta_1 + \theta_2 + \theta_3 = \frac{\pi}{2}$.

the θ variables is very similar to the transformation of τ variables in Propositions 10 and 11. Indeed, if we fix an elliptic modulus k, and if for every edge we define $\tau_e = \frac{2\mathrm{K}(k)}{\pi}\theta_e$ and we fix the coupling constants of the Ising model (resp. 8V-model) accordingly using (9) (resp. (10)), then the weights after a star-triangle move are exactly what we would have designed for the graph $\mathscr{G}'$. In other words, this parametrization yields the coupling equations automatically.

This is known as a Z-invariant regime on isoradial graphs, and it has been defined for a large number of models [Ken02, BdT10, BdT11, BdT12, GM13, CGS16, DCLM18, BdTR17, BdTR18, dT18, Ken19], [2], etc. In fact it might be true that every solution of the star-triangle relations can be geometrically interpreted on isoradial graphs by a proper geometric parametrization, although this still requires investigation for some integrable models such as the chiral Potts model.

Isoradial embeddings are an important class of graph on which integrable models can be defined, but not all graphs are isoradial (see [KS05] for a characterization in terms of train-tracks). To study the integrability of a model on a generic graph, one can hope to find *canonical* embeddings that work for any graph, and are stable by star-triangle moves. We now present such embeddings, again for resistor networks and for the Ising model.

b) Harmonic embeddings

When $\mathscr{G}$ is a planar graph equipped with a resistor network, every edge $e \in \mathscr{E}$ carries a resistance $R_e > 0$. We define the *conductance* as $c_e = \frac{1}{R_e}$, and the *discrete Laplacian* as the operator Δ on functions $f : \mathscr{V} \to \mathbb{C}$ as

$$\forall v \in \mathscr{V}, \quad \Delta f(v) = \sum_{e=\{u,v\}\in\mathscr{E}} c_e \left(f(u) - f(v)\right).$$

A *harmonic embedding* of $\mathscr{G}$ is an injective function $f : \mathscr{V} \to \mathbb{C}$ such that $\Delta f = 0$, and such that f defines an embedding (*i.e.* edges do not intersect when each vertex v is sent to $f(v)$). Under weak hypothesis and boundary conditions, the existence of a harmonic embedding was proved by Tutte [Tut63b].

Recently, Kenyon, Lam, Ramassamy and Russkikh [KLRR18] noted that we can also embed $\mathscr{G}^*$ naturally. By harmonicity of the embedding, it is possible to define f on $\mathscr{F}$ so

that for every edge $e = \{u, v\} \in \mathscr{E}$, let $x, y \in \mathscr{F}$ be the adjacent faces, with x to the right and y to the left of the oriented edge $\overrightarrow{uv}$, then

$$f(y) - f(x) = ic_e(f(v) - f(u)).$$

This gives an embedding of $\mathscr{G}$ and $\mathscr{G}^*$, such that the diamond graph $\mathscr{G}^\diamond$ is made of *orthodiagonal* quadrilaterals, meaning that their diagonals are orthogonal. Moreover, the conductances of the model have a geometric interpretation (as a ratio of diagonals).

This class of graph is also stable by star-triangle transformation, and the new conductances satisfy the transformation of resistor networks of Figure 4 [KLRR18]. The result of planar geometry that encodes this transformation is known as Steiner's theorem, see Figure 37: if we start with three orthodiagonal quadrilaterals $APCB'$, $CPBA'$, $BPAC'$, then there is a new point P' such that $C'P'B'A$, $B'P'A'C$, $A'P'C'B$ are orthodiagonal quadrilaterals. This is exactly the effect of the star-triangle move on the diamond graph.

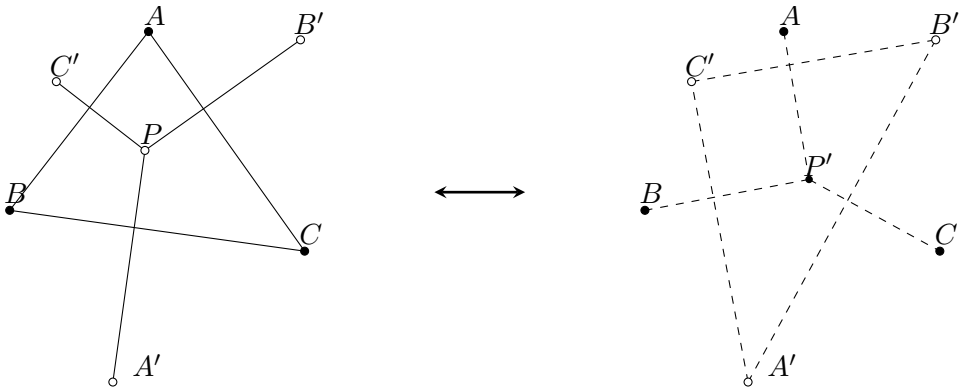

Figure 37: Steiner's theorem: the perpendicular to (AB) through C', the perpendicular to (BC) through A' and the perpendicular to (AC) through B' (solid lines) are concurrent *iff* the perpendicular to $(A'B')$ through C, the perpendicular to $(B'C')$ through A and the perpendicular to $(A'C')$ through B (dashed lines) are concurrent.

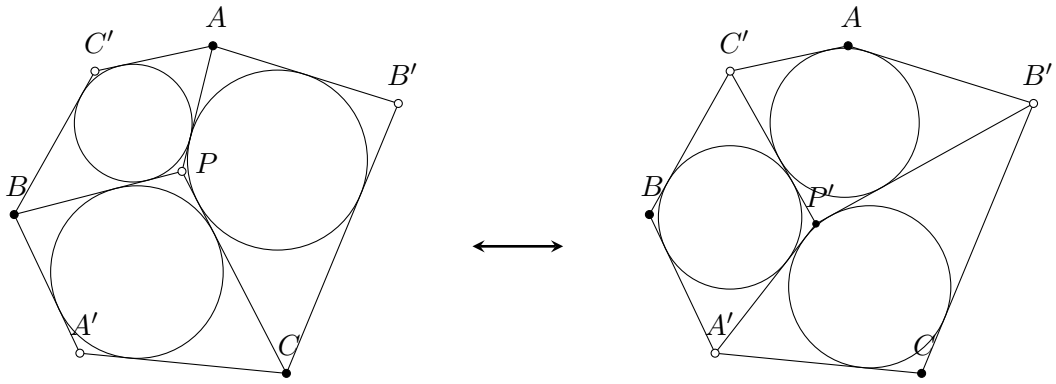

Figure 38: Star-triangle transformation on the diamond graph in the case of s-embeddings.

c) s-embeddings

Regarding the Ising model, Chelkak [Che17] introduced a canonical embedding of $\mathscr{G}$ and $\mathscr{G}^*$, when the graph is equipped with coupling constants $(J_e)_{e\in\mathscr{E}}$, called *s-embedding*. This embedding is such that every face of the diamond graph is a *tangential* quadrilateral, meaning that its sides are all tangent to a circle within the quadrilateral. The incidence theorem of geometry that encodes the star-triangle transformation on this class of embeddings is investigated in Chapter III; see Figure 38.

4 Extended abstracts of presented works

4.1 Kashaev's recurrence

Chapter I is devoted to the study of Kashaev's recurrence [1], already mentioned in Section 3.5. The first result is the solution to an open problem of Kenyon and Pemantle [KP16], summarized below in Theorem 16.

A *taut loop configuration* on $\mathcal{I} \cap \mathcal{C}_z$ is a fully packed loop model configuration, where the loops can be either red or blue, loops of the same color cannot intersect, and loops on the three "flat" sides of $\mathcal{C}_z$ have to be blue and internally connected as in the schematic view of Figure 39, see also Figure 35. This kind of two-color loop configurations appeared in work by physicists [WN93, JK04, IC09], without the boundary conditions defined here. We name them $C_2^{(1)}$ loops, following the terminology of [WN93].

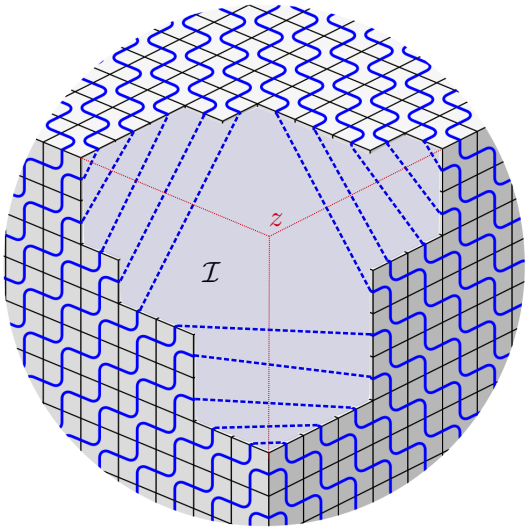

Figure 39: Rule of connections of the infinite loops in a taut loop configuration on $\mathcal{I} \cap \mathcal{C}_z$.

In such a configuration ω, there are 10 local possible configurations at a face f, which are shown in Figure 40. Let $w_f(\omega)$ be the corresponding weight, shown at the right of the corresponding configuration, which is a function of the g variables at the vertices of f. The total weight of ω is defined as

$$w(\omega) = 2^{N_\omega} \prod_{f \in \mathscr{F}} w_f(\omega) \prod_{x \in \mathcal{I} \cap \mathcal{C}_z} g_x^{-2}$$

where N_ω is the number of *finite* loops in ω. Notice that the configuration ω is infinite, as it continues on the faces of $\mathcal{C}_z$, far enough from z, but the boundary conditions are such that this extension to the faces of $\mathcal{C}_z$ is unique. The product of variables g_x^{-2} compensates the local weights of this extension, so that $w(\omega)$ is a finite expression in the g variables.

The partition function is then

$$\mathcal{Z}_{\text{loop}}(g, \mathcal{I}, z) = \sum_\omega w(\omega),$$

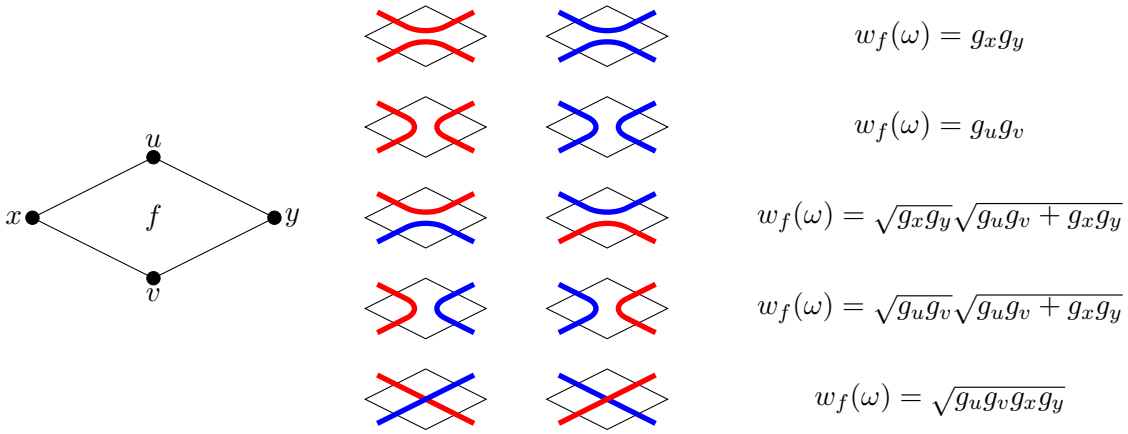

Figure 40: The 10 local configurations at a face f and their weight.

where the sum is over taut loop configurations on $\mathcal{I} \cap \mathcal{C}_z$.

We can now state the main result:

Theorem 16 ([1])**.** *With the previous notation,*

$$g_z = \mathcal{Z}_{loop}(g, \mathcal{I}, z).$$

Moreover, there is a one-to-one correspondence between taut loop configurations and monomials of g_z.

Idea of proof of Theorem 16. The proof goes by induction on the number of unit cubes in $\mathcal{C}_z \setminus \mathcal{L}$ (or "holes" in the pile of cubes). If there is a hole, it is possible to add a unit cube to $\mathcal{L}$, thus getting a new lattice $\mathcal{L}'$, with surface boundary $\mathcal{I}'$ obtained by "pushing" the hole into a new cube. We want to prove that when g satisfies Kashaev's positive recurrence,

$$\mathcal{Z}_{\text{loop}}(g, \mathcal{I}, z) = \mathcal{Z}_{\text{loop}}(g, \mathcal{I}', z). \tag{14}$$

If this is true, then by adding successive cubes, we will eventually reach a lattice that contains $\mathcal{C}_z$, *i.e.* where there is no hole; see Figure 41. In this case, the boundary conditions are such that there is a unique taut loop configuration, and its weight is g_z. All in all, we initially have the quantity $\mathcal{Z}_{\text{loop}}(g, I, z)$ and we show by adding successive cubes that in the end, it is equal to g_z.

To prove (14), we proceed as in the coupling equations for the star-triangle transformation: we condition on boundary conditions (colors and connections of loops) and show that the sums of local weights are equal. These coupling equations are schematically represented in Figure 42. They are satisfied *iff* g satisfies Kashaev's positive recurrence on the vertices of the added cube.

Finally, we show that the configurations are in bijection with the monomials of g_z, *i.e.* that two different configurations have different weights (as formal expressions in the g variables). This is done by an explicit reconstruction algorithm, that takes a weight and returns the configuration. The idea is to discover new faces successively: we already know the configuration far away from z, so the "unknown region" is finite. We can also show that if the unknown region contains a vertex of degree 2 on its boundary, then we can discover the configuration on one new face. By geometric means, we prove the following (see Lemma I.20):

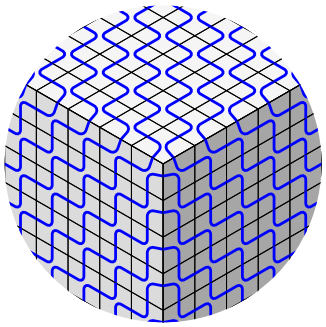

Figure 41: Taut loop configuration when the lattice contains $\mathcal{C}_z$.

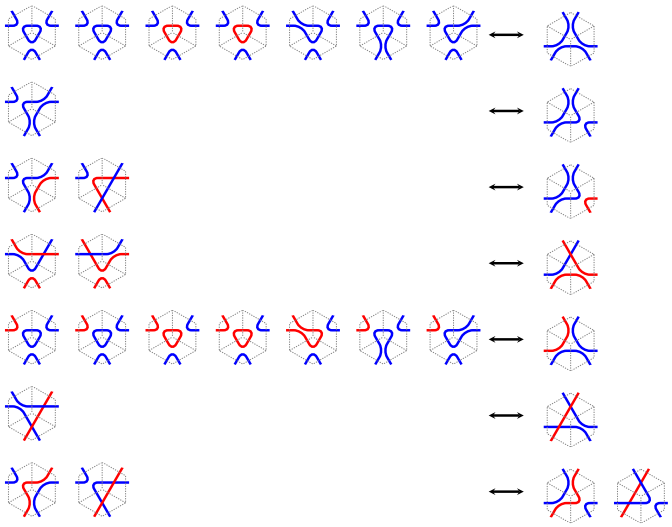

Figure 42: Coupling equations for loop configurations when we add a cube.

Lemma 17. *Any non-empty graph whose faces are non-degenerate rhombi has at least three vertices of degree* 2 *on its outer boundary.*

This allows one to guarantee that the algorithm finishes. □

From there, we prove some limit shapes results. Suppose that the lattice is $\mathcal{L} = \{(i, j, k) \mid i + j + k \leq 0\}$. Chose three numbers $a, b, c > 0$ and fix the initial conditions g on $\mathcal{I}$ to be periodic, as in Figure 43. Then sample a random taut loop configuration, proportionally to its weight, on $\mathcal{I} \cap \mathcal{C}_z$, for a "large" $z = (i, j, k)$. When $|z| = i + j + k$ becomes large, the behaviour of the model changes at boundaries that become deterministic when rescaled by $|z|$, called *limit shapes*, see Figure 44. In this case the limit shapes are algebraic curves of degree 8 than can be computed explicitly, and there are three different behaviors or *phases*: solid (the three "corners"), liquid (the "annulus") and gas (the central "facet").

Let us give a loose statement of the characterization of the limit shape that we prove; see Section I.4.5 for precise results. For any $z \in \mathbb{N}^3$, we define an *observable* ρ_z that is the expectation of a local random variable depending on the loops around the point $(0, 0, 0)$ (which belongs to $\mathcal{I}$); see (I.17) for its exact meaning. If we fix $(u, v, w) \in (0, 1)^3$ such

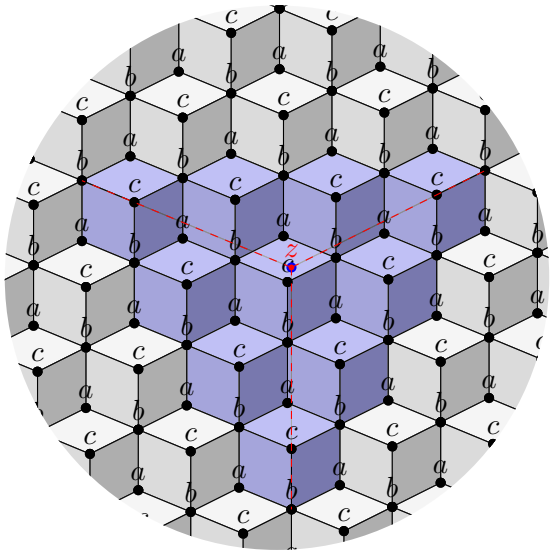

Figure 43: Periodic initial conditions.

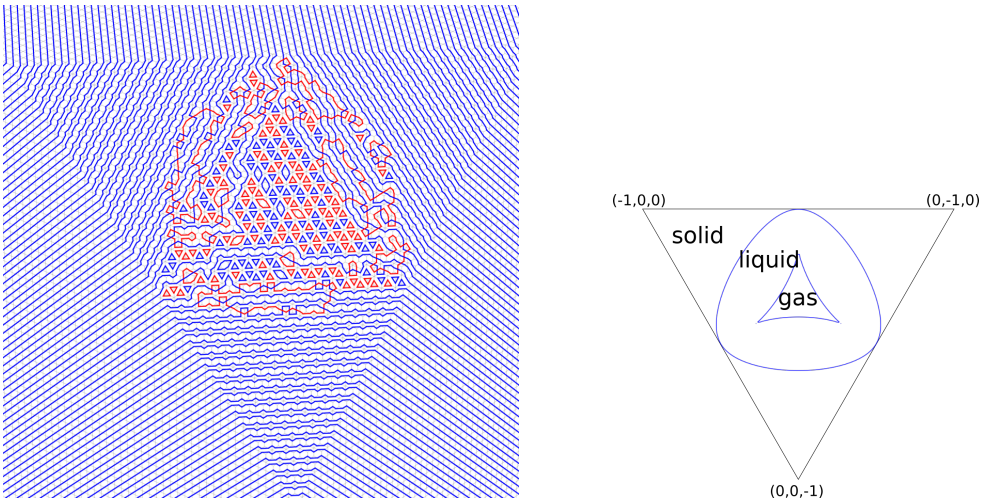

Figure 44: Left: a random taut loop configuration when $|z|$ is large. Right: the algebraic limit shape, represented in the plane $x + y + z = -1$, with the three expected phases of the model.

that $u + v + w = 1$ and set z to be $(\lfloor ku \rfloor, \lfloor kv \rfloor, \lfloor kw \rfloor)$, with $k \to \infty$, then the observable ρ_z will probe the asymptotic behaviour of the model around the point corresponding to $(-u, -v, -w)$ in the right-hand side of Figure 44.

Theorem 18 ([1])**.** *Let $(u, v, w) \in (0, 1)^3$ be such that $u + v + w = 1$, and set $z = (\lfloor ku \rfloor, \lfloor kv \rfloor, \lfloor kw \rfloor)$. As $k \to \infty$, ρ_z has the following asymptotic behaviour:*

- *If $(-u, -v, -w)$ is in the frozen region of Figure 44, then ρ_z tends to 0 exponentially fast in k.*
- *If $(-u, -v, -w)$ is in the liquid region of Figure 44, then ρ_z tends to 0 as a power of*

k.

- *If $(-u,-v,-w)$ is in the gaseous region of Figure 44, then ρ_z tends to $\frac{1}{3}$.*

Together with some heuristics on the possible behaviour of the random variable whose expectation is ρ_z, this result on a single observable is enough to guess the actual behaviour of the loops in the three phases. For instance, notice that in the loop configuration of Figure 44, the interface between the solid and liquid phases corresponds to the first occurrence of red loops, and the interface between liquid and gas phases corresponds to the position of the "center-most" infinite blue loops.

Idea of proof of Theorem 18. The idea follows the technique of [DFSG14] and uses the results of analytic combinatorics stated in the reference [PW13]; the proof itself is very similar to that of [KP16].

If we let the value of z vary, we now know that $\mathcal{Z}_{\text{loop}}(g,\mathcal{I},z)$ satisfy Kashaev's relation. By taking the logarithmic derivative of this relation with respect to the value of one initial condition (say $g_{0,0,0}$), this gives a *linear* relation among the

$$\rho_z = g_{0,0,0}\frac{\partial\left(\ln \mathcal{Z}_{\text{loop}}(g,\mathcal{I},z)\right)}{\partial g_{0,0,0}}.$$

As for several examples mentioned before, this logarithmic derivative of the partition function has a probabilistic meaning, as the expectation of a local random variable related to the loops around the point $(0,0,0)$. Since the variables ρ_z satisfy a linear relation, we can show that their generating function (in z) is algebraic:

$$F(x,y,z) := \sum_{i,j,k} \rho_{(i,j,k)} x^i y^j z^k = \frac{P(x,y,z)}{H(x,y,z)},$$

for some polynomials in three variables P, H.

From there, analyzing the singularities of H and using the powerful theory of *analytic combinatorics* developed in [PW13] allows us to deduce the behavior of ρ_z for $|z|$ large. □

Theorem 16 is combinatorial in nature. However, recall that Kashaev's originates from the study of the Ising model. Hence we might be able to find an interpretation in statistical mechanics: the loop model introduced here might have some natural relation with an Ising model, even on generic graphs $\mathscr{G}$ that do not come from a cubic lattice. We present such a relation now.

Let $\mathscr{G}$ be graph embedded on the sphere, with Ising coupling constants J (see Section 2.1). We consider $C_2^{(1)}$ loop configurations on $\mathscr{G}^\diamond$, where the local weights are given in the following way: for every "diamond" face $f \in \mathscr{F}^\diamond$, in the notation of Figure 40, suppose that $x, y \in \mathscr{V}$ are the primal vertices and $u, v \in \mathscr{F}$ are the dual vertices. Let $e = \{x, y\} \in \mathscr{E}$. Then, in the order of Figure 40, the local weights at f are set to be $a_e^2, b_e^2, a_e, b_e, a_e b_e$, where $a_e = \tanh 2J_e$ and $b_e = (\cosh 2J_e)^{-1}$. Let $\mathcal{Z}_{\text{loop}}(\mathscr{G}^\diamond, J)$ denote the corresponding partition function.

Theorem 19 ([1])**.**

$$\left(\mathcal{Z}_{Ising}(\mathscr{G},J)\right)^4 = \left(2^{|\mathscr{V}|}\prod_{e\in\mathscr{E}}\cosh 2J_e\right)^2 \mathcal{Z}_{loop}(\mathscr{G}^\diamond, J).$$

Idea of proof. The proof uses a relation between the Ising model and a 6V-model, that was written explicitly in [Dub11a] and uses argument of [Nie84, WL75]; see also [BdT14]. Consider the 6V-model on $\mathscr{G}^m$, where for every $e \in \mathscr{E}$ the local weights at the corresponding medial vertex are given, in the notation of Figure 14 and identifying the medial vertex with e, by $A_e = a_e, B_e = b_e, C_e = 1$ and of course $D_e = 0$. Note that $a_e^2 + b_e^2 = 1 = c_e^2$ so this model is actually free-fermionic. Then we have [Dub11a]

$$(\mathcal{Z}_{\text{Ising}}(\mathscr{G}, J))^2 = C\ \mathcal{Z}_{\text{6V}}(\mathscr{G}^m, J),$$

for an explicit constant C. Hence it is sufficient to prove that for this 6V-model, $(\mathcal{Z}_{\text{6V}}(\mathscr{G}^m, J))^2 = \mathcal{Z}_{\text{loop}}(\mathscr{G}^\diamond, J)$. This is done by a series of mapping, which is summed up in Figure 45.

First, given a loop configuration ω, we can orient every loop to get an *oriented* loop configuration $\overrightarrow{\omega}$. If we define the weight of $\overrightarrow{\omega}$ by

$$w(\overrightarrow{\omega}) = \prod_{f \in \mathscr{F}} w_f(\omega)$$

(notice that there is no factor 2^{N_ω}), then there is a weight-preserving (many-to-one) mapping from oriented loop configurations to loop configurations, simply obtained by forgetting the orientation.

On the other hand, starting from an oriented loop configuration, one can forget the *connection* information and simply look at the orientation and color of every medial edge. This gives what we call a $C_2^{(1)}$ *vertex* configuration. See the left of Figure 46.

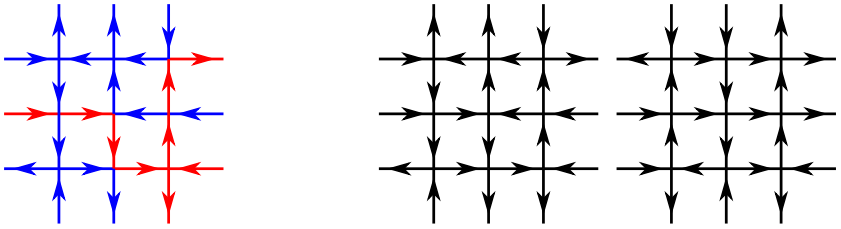

Figure 45: Left: an example of a $C_2^{(1)}$ vertex configuration on a piece of $\mathbb{Z}^2$. Right: the corresponding couple of 6V-configurations.

Finally, we show that there is a weight-preserving bijection between $C_2^{(1)}$ vertex configurations and couples of 6V-configurations (seen here as orientations of the medial edges). Let τ be a $C_2^{(1)}$ vertex-configuration, then the first 6V-configuration is obtained by forgetting the colors of τ, and the second is obtained by reverting every blue arrow and then forgetting the colors. It is easy to check that this is a bijection.

All in all, we get all the transformations shown in Figure 46, which proves the equality of partition functions, as well as some more precise information about the statistics of loops in terms of interfaces of the Ising models.

$$\text{Ising}^4 \dashleftarrow\dashrightarrow \text{6V}^2 \longleftrightarrow C_2^{(1)}\ \text{vertex} \longleftarrow \text{oriented loops} \longrightarrow \text{loops}$$

Figure 46: The series of transformation, from Ising to loops.

□

In Chapter I and in [1], the previous transformations are stated in a slightly different way: we use a dimer model instead of the 6V-ones, and instead of using orientations on the loops we put two different kinds of *markers*. This is done to make the transformation to the *double-dimers* of [KP16] more transparent. However, it is completely equivalent to the previous idea of proof.

4.2 The free-fermion 8V-model

Chapter II is devoted to the study of the eight-vertex model [2]. We will use the the content of Sections 2.3 and 2.5. Recall that we want to give rigorous results on the 8V-model, defined on the dual of a bipartite quadrangulation $\mathcal{Q}$; to do so, we suggest transforming it into a *dimer model* (see 2.2). This is possible only for a *free-fermion* regime for which at every face of the quadrangulation $f \in \mathcal{F}$, $A_f^2 + B_f^2 = C_f^2 + D_f^2$. Such a regime is included into the *disordered* phase of the expected phase diagram of Figure 12 and, by analyticity, should give an idea of the model in the whole disordered phase. However, the dimer model we obtain cannot be bipartite, except in degenerate cases (for which $\forall f \in \mathcal{F}, A_f B_f C_f D_f = 0$, such as the free-fermion 6V-model of Example 5).

In Chapter II we describe a procedure that avoids this issue. Namely, we show:

Theorem 20 ([2])**.** *Let $\mathcal{Q}$ be a quadrangulation of the sphere, and let $(A_f, B_f, C_f, D_f)_{f\in\mathcal{F}}$ be non-degenerate, free-fermion 8V-weights on the faces of $\mathcal{Q}$. Then there exists two sets of free-fermion 6V-weights, $(A_f^{(1)}, B_f^{(1)}, C_f^{(1)}, 0)_{f\in\mathcal{F}}$ and $(A_f^{(2)}, B_f^{(2)}, C_f^{(2)}, 0)_{f\in\mathcal{F}}$, such that*

$$\mathcal{Z}_{8V}\left(\mathcal{Q}, (A, B, C, D)\right)^2 = \mathcal{Z}_{6V}\left(\mathcal{Q}, (A^{(1)}, B^{(1)}, C^{(1)})\right) \mathcal{Z}_{6V}\left(\mathcal{Q}, (A^{(2)}, B^{(2)}, C^{(2)})\right).$$

This relation gives a link between generic free-fermion 8V-models and bipartite dimers. It is stated at the level of partition functions, but more precise objects can be related:

- *Kasteleyn matrices*: The (non-bipartite) Kasteleyn matrix K of dimers for the 8V-model, and the (bipartite) Kasteleyn matrices K_1, K_2 of dimers for the 6V models are related via a simple local permutation matrix T:

  Theorem 21 ([2])**.**

  $$K^{-1} = \frac{1}{2}\left(K_1^{-1} + K_2^{-1} + T(K_1^{-1} - K_2^{-1})\right).$$

  This implies that the correlations of the 8V-model can be expressed in terms of the two 6V-ones. Thus we can get explicit correlations, and an explicit Gibbs measure in the appropriate limit.

- *Characteristic polynomials*: In the case of a toric quadrangulation, consider the characteristic polynomials (see (6)) P of dimers for the 8V-model, and P_1, P_2, of dimers for the 6V-model. Then we have

  Theorem 22 ([2])**.**

  $$P(z, w) = P_1(z, w)P_2(z, w).$$

This is quite surprising: the characteristic polynomial of a natural non-bipartite dimer model is in fact reducible. Algebraically, this implies that the zero locus of P in $\mathbb{C}^2$ is the union of two Harnack curves.

- *Couplings*: Some statistical information can be kept between the models. Let τ, τ' bet two 8V-configurations, seen as subset of edges, then we denote their XOR (or symmetric difference) by $\tau \oplus \tau'$.

  Theorem 23 ([2]). *In the notation of Theorem 20, consider τ, τ' distributed as the Boltzmann 8V-measure (A, B, C, D), and τ_1, τ_2 distributed as the Boltzmann 6V-measures $(A^{(1)}, B^{(1)}, C^{(1)})$, $(A^{(2)}, B^{(2)}, C^{(2)})$ respectively, all of them being independent. Then $\tau \oplus \tau'$ and $\tau_1 \oplus \tau_2$ are equal in distribution.*

  This is proved using the formalism of *order-disorder* variables for the 8V-model [KC71, Dub11a]. These objects generalise usual probabilistic correlations, and can be tracked throughout the proof of Theorem 20 of which we give a sketch below. To go back to the probabilistic statement of Theorem 23, we use techniques of discrete Fourier theory; see Section II.A for more details.

Example 24 (Classical case). *Let us show in an example how the transformation from free-fermion 8V to free-fermion 6V can be computed in practice. Consider the case of the "classical" 8V-model from Section 2.3a), defined on $\mathbb{Z}^2$ (represented with vertical and horizontal edges) according to four constant weights a, b, c, d. Suppose that we are in the free-fermion regime $a^2 + b^2 = c^2 + d^2$. Then the corresponding 6V-models are obtained as follows: first, one can find $\alpha, \beta \in \mathbb{R}/2\pi\mathbb{Z}$ such that in homogeneous coordinates*

$$\left[a : b : c : d\right] = \left[\sin\left(\tfrac{\alpha+\beta}{2}\right) : \cos\left(\tfrac{\alpha+\beta}{2}\right) : \cos\left(\tfrac{\alpha-\beta}{2}\right) : \sin\left(\tfrac{-\alpha+\beta}{2}\right)\right].$$

Then the corresponding free-fermion 6V-models have weights that alternate between even and odd sites of $\mathbb{Z}^2$; the first one corresponds to the dimer model on the periodic graph of Figure 47 (using the correspondence with dimers, this is exactly the decorated graph shown in Figure 18 when the initial graph is $\mathbb{Z}^2$), and the second 6V-model is obtained by switching the roles of α and β (or equivalently of even and odd sites).

We give elements of the proof of Theorem 20. These also form the basis to the proofs of Theorems 21, 22, 23.

Idea of proof of Theorem 20. Let $\mathcal{V}$ denote the vertices of the quadrangulation $\mathcal{Q}$. We fix a bipartite coloration of $\mathcal{V}$ into black vertices $\mathcal{B}$ and white vertices $\mathcal{W}$.

1. Suppose that we have an Ising model on $\mathcal{B}$, with interaction on the diagonals of the faces of $\mathcal{Q}$, with coupling constants J_1 and another one on $\mathcal{W}$ with coupling constants J_2. We can use the spin-vertex correspondence (see Proposition 4) to get an 8V-model, which we denote by $8V_{12}$.

2. From there, we apply a *duality* result to the model $8V_{12}$. This duality was discovered by Wu [Wu69] and stated on more generic graphs in [Dub11a].

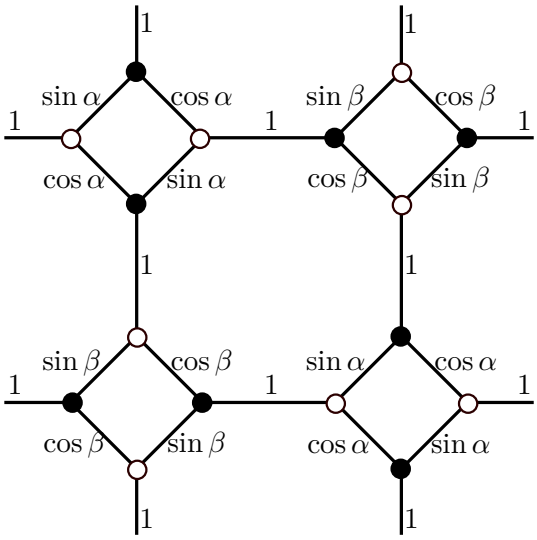

Figure 47: The periodic, bipartite dimer model associated with one of the 6V-models, obtained from the "classical" free-fermion model on $\mathbb{Z}^2$.

Proposition 25 ([Wu69, Dub11a]). *Let $(A, B, C, D) : \mathcal{F} \to \mathbb{R}^4$ be 8V-weights. Define $(\tilde{A}, \tilde{B}, \tilde{C}, \tilde{D})$ by*

$$\forall f \in \mathcal{F}, \quad \begin{pmatrix} \tilde{A}(f) \\ \tilde{B}(f) \\ \tilde{C}(f) \\ \tilde{D}(f) \end{pmatrix} = \frac{1}{2} \begin{pmatrix} 1 & -1 & 1 & 1 \\ -1 & 1 & 1 & 1 \\ 1 & 1 & 1 & -1 \\ 1 & 1 & -1 & 1 \end{pmatrix} \begin{pmatrix} A(f) \\ B(f) \\ C(f) \\ D(f) \end{pmatrix}.$$

Then

$$\mathcal{Z}_{8V}(\mathcal{Q}, A, B, C, D) = \mathcal{Z}_{8V}(\mathcal{Q}, \tilde{A}, \tilde{B}, \tilde{C}, \tilde{D}).$$

This is a linear involution on the weights. This relation can be proved in several ways; in Section II.A, extending on results of [Dub11a, Dub11b], we describe how it can be seen as a Poisson summation formula in discrete Fourier theory.

It happens that applying this duality on the model $8V_{12}$ gives a *free-fermion* model, which we call $8V_{12}^{\Delta}$.

3. By taking two Ising models on $\mathcal{B}$ and two others on $\mathcal{W}$, arranging them as in Figure 48, we create four 8V-models, that we can transform into free-fermion ones by duality. As a result, those satisfy the "switching" relation:

$$\mathcal{Z}_{8V_{12}^{\Delta}} \mathcal{Z}_{8V_{34}^{\Delta}} = \mathcal{Z}_{8V_{14}^{\Delta}} \mathcal{Z}_{8V_{32}^{\Delta}}.$$

In the special subcase where the Ising models J_1 and J_4 are *dual* of each other in the sense of [KW41], the model $8V_{12}^{\Delta}$ turns into a $6V$-model; this was shown in [Dub11a]. As a result, in the previous identity, if we set J_1, J_4 (resp. J_2, J_3) to be dual Ising models, it is easy to get

$$\mathcal{Z}^2_{8V_{12}^{\Delta}} = \mathcal{Z}_{6V_1^{\Delta}} \mathcal{Z}_{6V_2^{\Delta}}.$$

The theorem follows from the fact that the model $8V_{12}^{\Delta}$ that we constructed is in fact a completely generic free-fermion 8V-model.

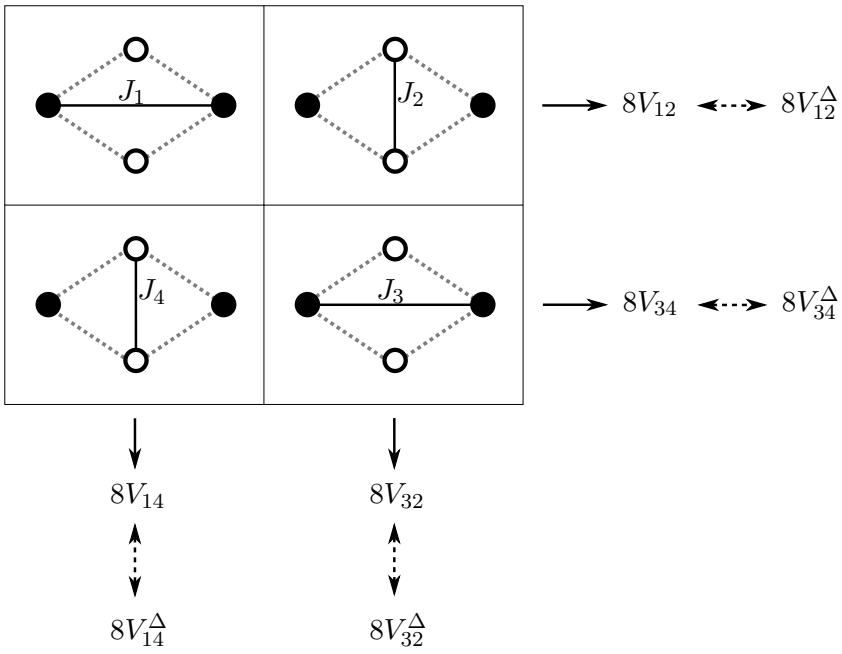

Figure 48: Transformation from Ising models to free-fermion 8V-models, shown at a face of $\mathcal{Q}$.

□

In the rest of Chapter II, we investigate Z-invariant free-fermion models on isoradial graphs, defined in Section 3.6a). We show that there exists a two-parameter family of weights that satisfy the star-triangle relations, indexed by two elliptic moduli k, l (the notations related to elliptic functions are introduced in Section 3.2a)). In the isoradial embedding, every face f of the quadrangulation is a rhombus; let θ be its half-angle at the black vertices, and let $\tau_k = \frac{2\mathrm{K}(k)}{\pi}\theta$, and similarly for τ_l. Then we set

$$\begin{aligned} A(f) &= \mathrm{sn}\,(\tau_k|k) + \mathrm{sn}\,(\tau_l|l) \\ B(f) &= \mathrm{cn}\,(\tau_k|k) + \mathrm{cn}\,(\theta_l|l) \\ C(f) &= 1 + \mathrm{sn}\,(\tau_k|k)\,\mathrm{sn}\,(\tau_l|l) + \mathrm{cn}\,(\tau_k|k)\,\mathrm{cn}\,(\tau_l|l) \\ D(f) &= \mathrm{cn}\,(\tau_k|k)\,\mathrm{sn}\,(\tau_l|l) - \mathrm{sn}\,(\tau_k|k)\,\mathrm{cn}\,(\tau_l|l)\,. \end{aligned} \tag{15}$$

Note that when $k = l$ this is a 6V-model (*i.e.* $D(f)$ vanishes), and that exchanging k and l does not change the regime.

Theorem 26 ([2])**.** *On any finite of infinite isoradial graph, the weights* (15) *satisfy the star-triangle relations of the 8V-model.*

It might be a bit surprising that these weights are not present in Baxter's derivation of Z-invariant weights stated in Proposition 11. This comes from the fact that our definitions

break the symmetry between black and white vertices of the quadrangulation, thus giving more solutions to the star-triangle equations. This is sometimes called a *checkerboard* setting. The proof of Theorem 26 is a computation, that uses identities on elliptic functions from [Law89, AS64].

By starting with these Z-invariant weights and applying the procedure to transform them into 6V-models, we recover models that have been studied in [BdTR18]. This allows for the computation of explicit correlations, that satisfy the *locality* property of Section 3.2c). These correlations can be analysed precisely, to show that:

- When $k = 0$ or $l = 0$, the coefficients of the inverse Kasteleyn matrix decay as a power law.
- When $0 < k < l$, they decay exponentially; essentially $\langle \tau_e \tau_{e'} \rangle \sim \exp\left(\frac{|e-e'|}{\xi_k}\right)$ for faraway edges e, e'. The correlation length ξ_k tends to infinity as $k \to 0$, which is the critical parameter of this model. More precisely, ξ_k is of order k^{-2} for small k; this gives the critical exponent for the correlation length, and this exponent is the same as that of the Ising model.

The results on exact correlations of [2] are summed up in the phase diagram of Figure 49. The point $k = l = 0$ corresponds to the trigonometric 6V-model, which is a special case of the critical bipartite dimer model on an isoradial graph defined in [Ken02].

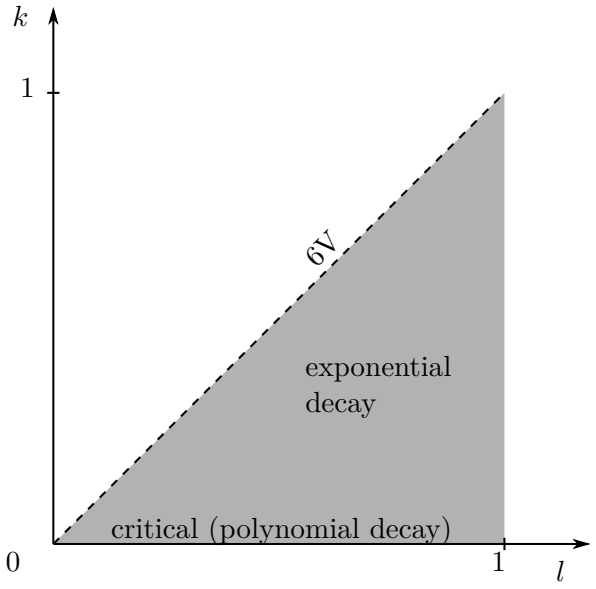

Figure 49: Phase diagram of the Z-invariant free-fermion 8V-models, in the parameters k, l and in the regime $0 \leq k \leq l < 1$.

4.3 Incidence theorems and canonical embeddings of graphs

The goal of Chapter III is to give elements towards the definition of *canonical* embeddings of graphs equipped with a model, such that observables of the model have a direct interpretation in the embedding. Examples of such embeddings are given in Section 3.6; one should add

the correspondence between the dimer model and *circle patterns*, see [KLRR18]. We propose the following framework.

Let $f : (0, \infty)^2 \to \mathbb{R}$ be a symmetric, homogeneous function. A non-crossed quadrilateral with successive sides a, b, c, d is said to be an *f-quad* if it satisfies

$$f(a, c) = f(b, d).$$

For instance, a *kite*, which is a quadrilateral such that $\{a, c\} = \{b, d\}$, is an f-quad for any function f. Embeddings of graphs made of kites have been studied in [Lis17], equipped with a critical Ising model. This is generalised by the definition of s-embeddings in [Che17].

For a planar graph $\mathcal{G}$, an *f-embedding* of $\mathcal{G}$ is a proper embedding of both $\mathcal{G}$ and $\mathcal{G}^*$, such that all faces of $\mathcal{G}^\diamond$ are f-quads.

Example 27.
- *For $f(x, y) = x^2 + y^2$, being an f-quad is equivalent to being an* orthodiagonal *quadrilateral. Those are the quadrilaterals appearing in the harmonic embeddings for resistor networks.*
- *For $f(x, y) = x + y$, being an f-quad is equivalent to being a* tangential *quadrilateral. Those are the ones that appear in the s-embeddings of the Ising model [Che17].*

We are define a particular sub-family of f-quads. For $f(x, y) = x^\alpha + y^\alpha$, where $\alpha \in \mathbb{R}^*$, we dub the f-quads as *α-quads*. The definition can be naturally extended to $\alpha \in \bar{\mathbb{R}} = [-\infty, \infty]$, by setting 0-quads to correspond to $f(x, y) = xy$, $+\infty$-quads to $f(x, y) = \max(x, y)$, and $-\infty$-quads to $f(x, y) = \min(x, y)$.

We explore the space of such quadrilaterals. For instance,

Proposition 28. *If a quadrilateral is an α-quad and an α'-quad for two different values α, α' in $\bar{\mathbb{R}}$, then it is a kite.*

We then turn to the star-triangle transformations for f-embeddings. Our hope is to generalise the incidence theorems exemplified in Figures 36, 37, 38. We say that f satisfies the *flip property* if, for every proper embedding of three f-quads $A_0A_1A_2A_3$, $A_0A_3A_4A_5$ and $A_0A_5A_6A_1$ as in Figure 50, there exists a point A_7 such that $A_7A_2A_3A_4$, $A_7A_4A_5A_6$ and $A_7A_6A_1A_2$ are proper f-quads.

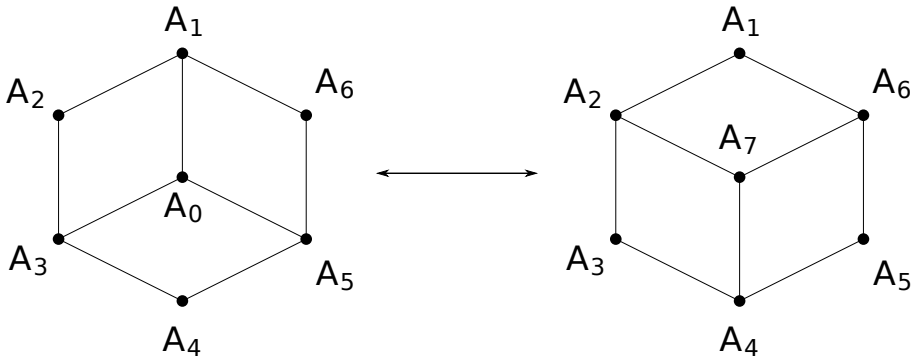

Figure 50: The flip property.

The existence of such a flip is a strong indication that f-embeddings form an integrable system, and hint at the existence of an underlying statistical model.

Conjecture 29. *Any continuous, symmetric, homogeneous function $f : (0,\infty)^2 \to \mathbb{R}$ satisfies the flip property.*

The conjecture holds for $f(x,y) = x^2 + y^2$ by Steiner's theorem. We show that it holds for $f(x,y) = x + y$, proving the property observed in Figure 38.

Theorem 30. *The function $f(x,y) = x + y$ satisfies the flip property, moreover, the points A_0, A_7 are unique.*

Our goal in the future of this project is to establish this property for more functions f, and hopefully to understand these flip properties in terms of integrable models.

4.4 Long paths in partitions of the divisor graph

This chapter is dedicated to the study of optimal partitions of the *divisor graph* [3]. The divisor graph of order N is the graph with vertices indexed by the integers $\{1,\dots,N\}$, and edges linking any two distinct integers that are multiple (or divisor) of one another, see Figure 51. The original definition of this graph goes back to Erdős, Freud and Hegyvári [EFH83]. Several questions can be asked about this graph:

- What is the longest *path*, *i.e.* the longest sequence of distinct integers in $\{1,\dots,N\}$ such that one divides or is a multiple of the next? This is denoted $f(N)$ and it has been shown by Saias [Sai98] that
$$f(N) \asymp \frac{N}{\log N}.$$
- What is the minimal number of paths needed to partition the divisor graph? After several successive improvements [ES95, Sai03, Maz06, Cha08, McN18], it is known that this number $F(N)$ satisfies
$$F(N) \sim cN, \tag{16}$$
where $c \in (0.176488, 0.2289)$.
- A partition is said to be *optimal* if it contains $F(N)$ paths. We address the question of knowing what an optimal partition can look like. We denote by $L(N)$ the length of the longest possible path *appearing in an optimal partition.* Clearly, we have $L(N) \le f(N)$, and by a pigeonhole principle, for N large enough we have $L(N) \ge \frac{1}{c} > 4$ where c is the constant of (16). In Chapter IV we prove that $L(N)$ can be very large, of order $N^{1-o(1)}$. More precisely,

  Theorem 31 ([3])**.** *There exists a constant $A > 0$ such that for all $N \ge 3$,*
$$\log L(N) \ge \log N - \frac{(\log\log N)^2}{\log 2} - A \log\log N.$$

Example 32. *For $N = 7$, the divisor graph is shown in Figure 51. One can check that $f(7) = 6$, with an example of a maximal path being $(5,1,3,6,2,4)$. One has $F(7) = 2$, as we can just add the path (7) to the previous one to get a partition of the divisor graph. Thus, in that case, $L(7) = f(7) = 6$. Note that we could have optimal partitions with shorter paths, such as $(7,1,5),(3,6,2,4)$.*

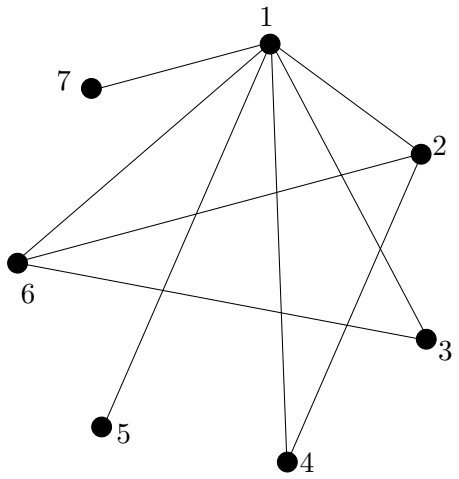

Figure 51: The divisor graph for $N = 7$.

Tools for the proof.

- *Self-similarity*: For $k \geq 2$, consider the prime numbers in $\left(\frac{N}{k+1}, \frac{N}{k}\right]$. By the prime number theorem, there is an order constant $\times \frac{N}{\log N}$ of them. For every such prime number p, in an optimal partition of N, there are k multiples of p, and each of these can be connected either with other multiples of p, or to a number smaller than k. But there is far less numbers smaller than k than prime numbers in $\left(\frac{N}{k+1}, \frac{N}{k}\right]$, hence for "almost all" p, the multiples of p are only connected to other multiples of p. Hence they form an optimal partition of $\left[\frac{N}{p}\right] = k$. This can lead to "bootstrap" functional equations between $L(N)$ and the $L(k)$ for different values of k. This line of reasoning can be adapted to prime numbers of order as small as $\sqrt{N \log N}$.

- *Extraction*: In an optimal partition, the integer 1 belongs to some path. We can remove 1 from this path and use it to connect two different paths; in doing so, the total number of paths has augmented and then decreased by 1, so the final partition is still optimal. This is very useful, for instance with the previous argument it implies that for any fixed k, for N large enough, $L(N) \geq 2L(k) + 1$. By bootstrapping, this shows that $L(N) \to \infty$.

  We can actually extract numbers different from 1, provided we know that there exists paths ending with multiples (or divisors) of these numbers.

- *Buchstab's inequality*: To get better lower bounds on $L(N)$, we want to be able to apply extraction on many numbers. For that reason, we introduce $L_{a,b}(N)$ as the maximal length of a path having a and b as endpoints and belonging to an *optimal* partition of $\{1, \ldots, N\}$ and we work with the "uniform" quantity

$$H(N) = \min L_{r',r}(N)$$

  where the min is over prime numbers $\frac{N}{3} < r \leq \frac{N}{2} < r' \leq N$. Working with all these possible endpoints "at once" gives more freedom in the construction of long paths.

Bootstrap inequalities on $H(N)$ are analogous to Buchstab's inequality, see [Sai93], and give the bound on $L(N)$ after some computations.

□

I – Kashaev's recurrence and the $C_2^{(1)}$ loop model

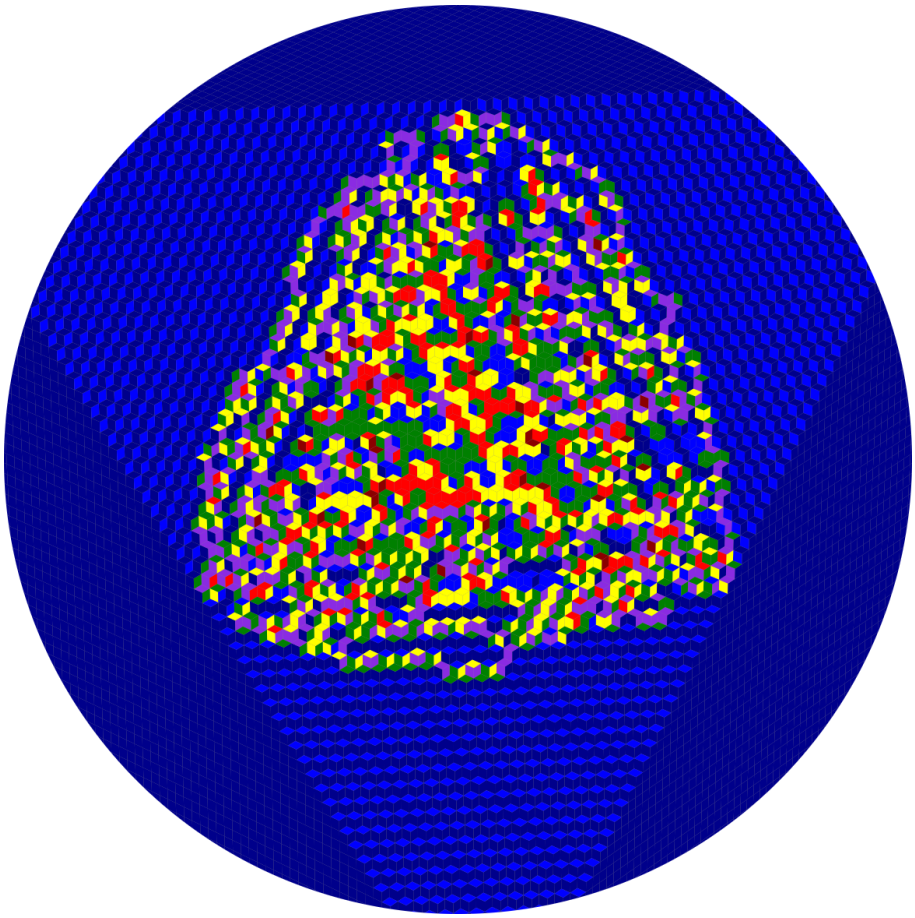

Résumé

Nous étudions un modèle de boucles à deux couleurs, connu sous le nom de modèle $C_2^{(1)}$. Nous définissons un régime de fermions libres pour ce modèle, et nous montrons que dans ce cas le modèle peut être transformé en un couple de modèles de dimères. Nous calculons ensuite l'énergie du modèle de boucles pour des graphes planaires périodiques. Nous étudions les transformations triangle-étoile du modèle, et nous montrons qu'après une reparamétrisation, elles peuvent être résumées en une seule équation connue sous le nom d'équation de Kashaev. Cela permet d'identifier les solutions de la relation de Kashaev avec la fonction de partition du modèle de boucles $C_2^{(1)}$, pour un bon choix de conditions au bord. Cela apporte une solution à un problème ouvert de Kenyon et Pemantle [KP16] sur la combinatoire de la relation de Kashaev.

Abstract

We study a two-color loop model known as the $C_2^{(1)}$ loop model. We define a free-fermionic regime for this model, and show that under this assumption it can be transformed into a double dimer model. We then compute its free energy on periodic planar graphs. We also study the star-triangle relation or Yang-Baxter equations of this model, and show that after a proper parametrization they can be summed up into a single relation known as Kashaev's relation. This is enough to identify the solution of Kashaev's relation as the partition function of a $C_2^{(1)}$ loop model with some boundary conditions. This solves an open question of Kenyon and Pemantle [KP16] about the combinatorics of Kashaev's relation.

I.1 Introduction

In 1996 Kashaev introduced a way to rewrite the star triangle transformation of the Ising model [Kas96]. Specifically, let us take a planar graph $G = (V, E)$ with usual coupling constants for the Ising model $(J_e)_{e\in E}$ on the edges. Let us suppose that there is a set of variables g on the vertices and faces of G such that

$$\sinh^2(J_e) = \frac{g_x g_y}{g_u g_v} \tag{I.1}$$

where x, y are the endpoints of e and u, v are the faces adjacent to e. Then the star-triangle relation, or local Yang-Baxter equation, is equivalent to the variables g satisfying a single polynomial relation:

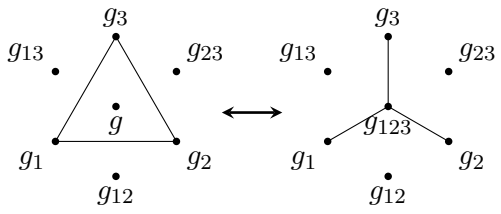

$$\begin{aligned}
&g^2 g_{123}^2 + g_1^2 g_{23}^2 + g_2^2 g_{13}^2 + g_3^2 g_{12}^2 \\
&-2g_2 g_3 g_{13} g_{12} - 2g_1 g_3 g_{23} g_{12} - 2g_1 g_2 g_{23} g_{13} \\
&-2g g_{123}(g_1 g_{23} + g_2 g_{13} + g_3 g_{12}) \\
&-4g g_{12} g_{23} g_{13} - 4g_{123} g_1 g_2 g_3 \\
&=0.
\end{aligned}$$

This relation[1], known as Kashaev's relation, has sparked some interest from the point of view of *spatial recurrences*. It can be embedded in $\mathbb{Z}^3$ by taking $x \in \mathbb{Z}^3$ and denoting $g = g_x$, $g_i = g_{x+e_i}$, $g_{ij} = g_{x+e_i+e_j}$, etc. Then by choosing the greatest root of a degree 2 polynomial we get [KP16]:

$$g_{123} = \frac{2g_1 g_2 g_3 + g(g_1 g_{23} + g_2 g_{13} + g_3 g_{12}) + 2XYZ}{g^2}, \tag{I.2}$$

where $X = \sqrt{g g_{23} + g_2 g_3}$, $Y = \sqrt{g g_{13} + g_1 g_3}$, $Z = \sqrt{g g_{12} + g_1 g_2}$.

This transformation (I.2) is called *Kashaev's recurrence*. It can be iterated to define g on further vertices of $\mathbb{Z}^3$, provided we had a sufficiently large set of initial conditions. A remarkable fact is that it exhibits a *Laurentness* phenomenon: the solution of the recurrence at any point is always a Laurent polynomial in the initial variables. This fact is related to cluster algebras [FZ02a, FZ03], but it also hints at a possible hidden object represented by the solution.

Let us quickly review the current state of spatial recurrences: Speyer related the solution of the octahedron recurrence (which can be traced back to Dodgson [Dod66]) to the partition function of a dimer model [Spe07]; then Carroll and Speyer showed that the cube recurrence (proposed by Propp [Pro01]) corresponds to cube groves [CS04]; more recently Kenyon and Pemantle studied a generalization of Kashaev's relation, known as the hexahedron recurrence, and identified its solution with a double dimer model [KP16]. Unfortunately, when specialized to Kashaev's recurrence, their model does not provide a one-to-one correspondence between configurations and monomials of the Laurent polynomial. In this chapter we

[1] Kashaev's initial equation contained a $+4$ instead of a -4 coefficient for the last terms, but one can easily get from one to another, for instance by multiplying g by -1 at a vertex of the cube and its three neighbors.

provide a model that does give a one-to-one correspondence, known in the physics literature as the $C_2^{(1)}$ loop model.

The $C_2^{(1)}$ loop model was introduced by Warnaar and Nienhuis in [WN93], among other models, as a loop model naturally associated to formal solutions of the Yang-Baxter equation [Baz85, Jim86]. It was also considered, for different reasons, by Jacobsen and Kondev in [JK04] as a generalization of the eight-vertex model, and they conjecture a phase diagram for this model.

It is a dense, two-color loop model where same-colored loops cannot intersect. Let us detail this terminology; see also Figure I.1 for an example.

- *loop model* means that the configurations are unions of simple curves. In our case, these curves use edges of the dual graph of a bipartite quadrangulation G, and are able to turn inside faces of G.
- *two-color* means that each loop is either red or blue.
- *dense* means that every dual edge of G belongs to a loop.
- finally, *same-colored loops cannot intersect* means that the only allowed crossings are between red and blue; see Figure I.2 for all possible local configurations at a face of G.

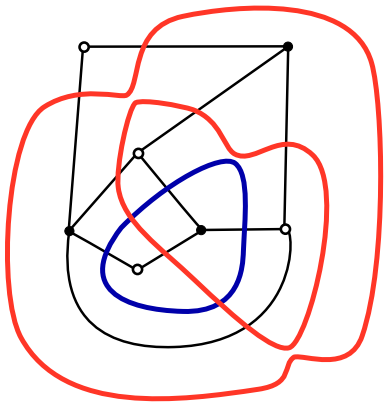

Figure I.1: A quadrangulation G (in black), with a $C_2^{(1)}$ loop configuration.

Equivalently, a $C_2^{(1)}$ loop configuration can be seen as a gluing of quadrangles appearing in Figure I.2, where only same-colored edges can be glued together.

The model is equipped with weights: let n be a positive parameter called *fugacity*, then the weight of a $C_2^{(1)}$ loop configuration σ is

$$w(\sigma) = n^{\#\text{loops in } \sigma} \prod_{f \in F} w_i^f,$$

where F is the set of faces of the quadrangulation and w_i^f is the local weight corresponding to $\sigma|_f$.

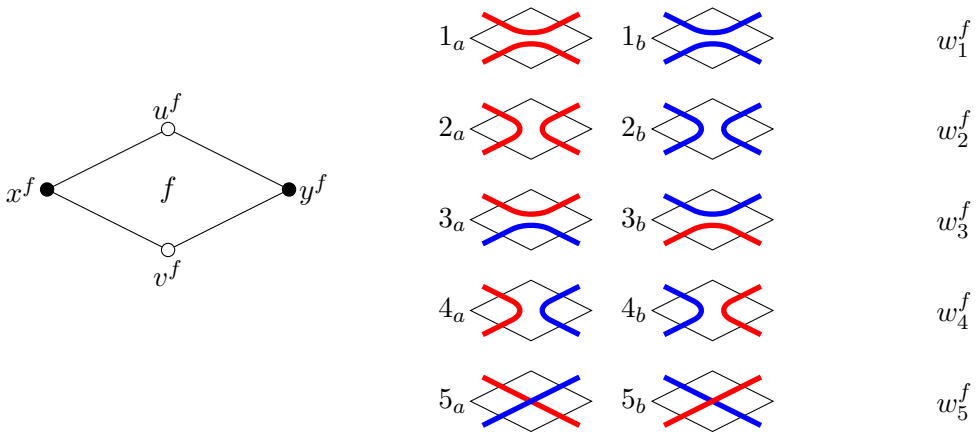

Figure I.2: A face f, the 10 local configurations $1_a, \dots, 5_b$ at f and their local weight w_i^f.

In [WN93] the authors give a two-parameter family of fugacity and weights such that the model is *integrable*, which in their setting means that it satisfies a form of the star-triangle relation:

$$\begin{cases} n = -2\cos 2\lambda \\ w_1 = \frac{\sin(\lambda-u)\sin(3\lambda-u)}{\sin\lambda\sin 3\lambda} \\ w_2 = -\frac{\sin u\sin(2\lambda-u)}{\sin\lambda\sin 3\lambda} \\ w_3 = \frac{\sin(3\lambda-u)}{\sin 3\lambda} \\ w_4 = -\frac{\sin u}{\sin 3\lambda} \\ w_5 = \frac{\sin u\sin(3\lambda-u)}{\sin\lambda\sin 3\lambda} \end{cases} \tag{I.3}$$

In [IC09], Ikhlef and Cardy define a fermionic observable F_s for this model and show that imposing a form of discrete holomorphicity on F_s yields the same integrable weights as in [WN93]; this approach was extended to the case of non-trivial boundary conditions in [dGLR13].

In this chapter we only deal with the $n = 2$ case. We introduce the *free-fermionic* relations (see Section I.2.3 for more details on this terminology):

$$\begin{aligned} w_1^f w_4^f &= w_3^f w_5^f, \\ w_2^f w_3^f &= w_4^f w_5^f, \\ w_5^f(w_1^f + w_2^f) &= w_3^f w_4^f. \end{aligned}$$

For instance, the integrable weights (I.3) at $n = 2$ (*i.e.* $\lambda = \pm\frac{\pi}{2}$) satisfy the free-fermionic relations.

When these relations are satisfied, we show that the $C_2^{(1)}$ loop model can be transformed into a double dimer model. We prove the following; for a precise statement, see Theorem I.4 of Section I.2.

Theorem. *For any free-fermionic $C_2^{(1)}$ loop model, there is a bipartite decorated graph equipped with a dimer model with weights μ, and there are constants $(\lambda_f)_{f\in F}$, such that*

the partition function $\mathcal{Z}^G_{loop}$ is equal to the square of the partition function $\mathcal{Z}_{dim}(\mu)$ of this dimer model, up to multiplicative factors:

$$\mathcal{Z}^G_{loop} = \left(\prod_{f\in F}\lambda_f\right)\left(\mathcal{Z}^G_{dim}(\mu)\right)^2.$$

An application of this result is the computation of the free energy of any free-fermionic $C_2^{(1)}$ loop model on a periodic planar quadrangulation; see Section I.2.4.

Then we define a parametrized free-fermionic $C_2^{(1)}$ loop model, analogous to Kashaev's parametrized Ising model (I.1). Let us suppose that there is a set of variables $(g_v)_{v\in V}$ on the vertices of G such that

$$\begin{cases} w_1^f = g_x g_y \\ w_2^f = g_u g_v \\ w_3^f = \sqrt{g_x g_y}\sqrt{g_x g_y + g_u g_v} \\ w_4^f = \sqrt{g_v g_u}\sqrt{g_x g_y + g_u g_v} \\ w_5^f = \sqrt{g_x g_y g_u g_v}. \end{cases} \tag{I.4}$$

The existence of such a parametrization is discussed in Appendix I.B. In particular, we show that it always exists for a free-fermionic model on a lozenge graph.

In this regime, we show that the Yang-Baxter equations associated to the model (corresponding to a move called *cube flip*, similar to the star/triangle move) are equivalent to g satisfying Kashaev's recurrence (I.2). See Theorem I.12 in Section I.3.

Finally, we get to the solution of Kashaev's recurrence. See Theorems I.18 and I.19 of Section I.4 for a precise statement of the following.

Theorem. *For any solvable initial condition $(g_i)_{i\in I}$ on $I \subset \mathbb{Z}^3_-$, the solution of Kashaev's recurrence at the origin is*

$$g_{0,0,0} = \sum_\sigma \left(2^{\#\text{loops in } \sigma} \prod_f w_i^f \prod_{i\in I} g_i^{-2}\right)$$

where the sum is over taut $C_2^{(1)}$ configurations σ, and the local weights w_i^f are given by (I.4).

Moreover, there is a one-to-one correspondence between such loop configurations and monomials of $g_{0,0,0}$ as a function of the variables $(g_i)_{i\in I}$.

The *taut* configurations are those satisfying some boundary and connectivity conditions; an example is displayed in Figure I.3.

The chapter is organized as follows:

- In Section I.2 we define the models, and show how to get from free-fermionic $C_2^{(1)}$ loops to dimers. We also compute the free energy on periodic planar quadrangulations.
- In Section I.3 we show that for the parametrization (I.4) of the weights, the Yang-Baxter equations of loops are equivalent to Kashaev's recurrence.
- In Section I.4 we define taut configurations, and prove that the solution of Kashaev's recurrence is the partition function of these configurations. We compute some limit shapes of the model by a now standard technique [PS05, DFSG14, KP16, Geo17]. We also show that in characteristic 2 the model reduces to the cube groves of [CS04].

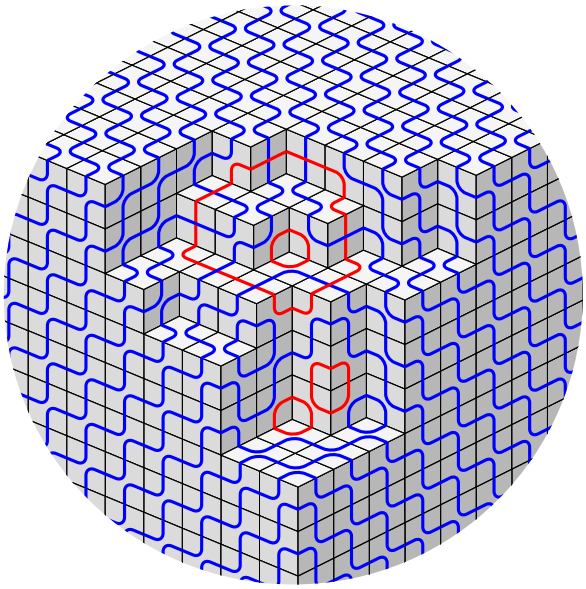

Figure I.3: A taut $C_2^{(1)}$ loop configuration.

Acknowledgments

I am very grateful to my Ph.D. advisors Cédric Boutillier and Béatrice de Tilière for the motivations and questions related to the present work, and for their constant help during the writing of this chapter. I also thank an anonymous referee for pointing at a mistake in the definition of the free-fermionic regime.

I.2 Free-fermionic $C_2^{(1)}$ loops and double dimers

I.2.1 The $C_2^{(1)}$ loop model on a quadrangulation

Definition I.1. Let $\mathcal{S}$ be a connected orientable compact surface without boundary. A *quadrangulation* of $\mathcal{S}$ is a finite connected simple graph $G = (V, E)$ embedded in $\mathcal{S}$ so that edges do not intersect, and so that the *faces* of G (the connected components of the complement of the embedding) are homeomorphic to disks and have degree 4. We denote by F the set of faces.

Definition I.2. Let G be a bipartite quadrangulation of $\mathcal{S}$. For every face $f \in F$, we fix names for the vertices of the boundary of f, in clockwise order, as x^f, u^f, y^f, v^f, with x^f, y^f black vertices and u^f, v^f white vertices like in Figure I.2. Notice that a vertex will have several names, corresponding to all the faces adjacent to it; we only use these labels to make the 10 different configurations of Figure I.2 well defined. When there is no ambiguity, we will also drop the superscript f.

A $C_2^{(1)}$ loop configuration σ on G is the data, for every $f \in F$, of an index $i_k^f \in \{1_a, 1_b, \dots, 5_a, 5_b\}$ (we think of it as $i \in \{1, \dots, 5\}$ and $k \in \{a, b\}$) representing the local configuration $\sigma|_f$, such that glued edges are the same color.

When there is no ambiguity on the face involved, we will often drop the superscript f in i_k^f. Let us denote σ the set $\sigma = \{(f, i_k) \mid f \in F\}$.

Simply stated, a $C_2^{(1)}$ loop configuration on G is an edge-covering set of red or blue loops on the dual graph G^* (which we represent inside a face by turning or crossing when necessary), such that same-colored loops cannot cross.

We equip the faces with a set of positive weights $W = (w_i^f)_{f\in F, i\in\{1,\dots,5\}}$. For a loop configuration σ we let N_σ be the number of loops in σ. The weight of σ is defined as

$$w_{\text{loop}}^G(\sigma) = 2^{N_\sigma} \prod_{(f,i_k)\in\sigma} w_i^f. \tag{I.5}$$

The *partition function* of the model is the weighted sum of loop configurations:

$$\mathcal{Z}_{\text{loop}}^G(W) = \sum_\sigma w_{\text{loop}}^G(\sigma).$$

I.2.2 Dimer model on the quad-graph

Let G^* be the dual graph of G. We consider a decorated graph, denoted G^Q, constructed by expanding every vertex of G^* (which has degree 4) into a small quadrangle called a *city*[2]. Cities are connected by edges called *roads*. Let E^Q be the edges of G^Q.

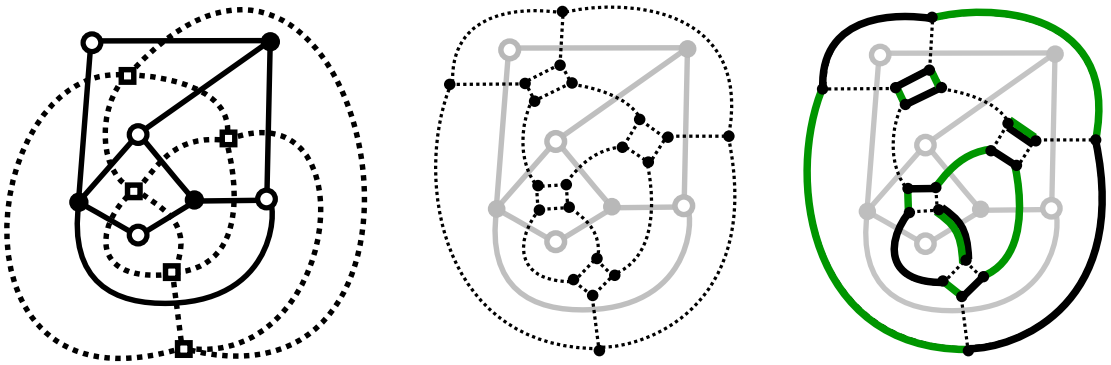

Figure I.4: A quadrangulation G of the sphere with its dual G^* (dotted); the decorated graph G^Q (dotted); a double dimer model (m_A, m_B) on G^Q.

A dimer configuration on G^Q is a subset $m \subset E^Q$ such that every vertex of G^Q belongs to exactly one edge of m. Dimer models on G^Q have appeared several times [WL75, dT07, Dub11a, BdT14] in the study of the 6V model and of the Ising model.

Let $\mu = (\mu_e)_{e\in E^Q}$ be a set of positive real weights on the edges of G^Q. The weight of a dimer configuration is then:

$$w_{\text{dim}}^G(m) = \prod_{e\in m} \mu_e.$$

We similarly define the partition function for dimers:

$$\mathcal{Z}_{\text{dim}}^G(\mu) = \sum_m w_{\text{dim}}^G(m),$$

[2]This terminology is related to the *urban renewal* transformation of the dimer model [KPW00].

where the sum is over all dimer configurations of G^Q.

The aim of this Section is to provide a direct link between the $C_2^{(1)}$ loop model on G in a certain regime and a couple of independent dimer models on G^Q.

I.2.3 Free-fermion regime

Let us make the following assumptions on the $C_2^{(1)}$ loops weights (implicitly evaluated at a face $f \in F$), which we call the *free-fermionic relations*:

$$\begin{aligned} w_1 w_4 &= w_3 w_5, \\ w_2 w_3 &= w_4 w_5, \\ w_5(w_1 + w_2) &= w_3 w_4. \end{aligned} \tag{I.6}$$

Let us make a few remarks on this terminology. We will see that relations (I.6) are sufficient to transform the $C_2^{(1)}$ loop model into dimers. This idea has been used several times in statistical mechanics to get exact solutions for various models, such as the Ising model [Kas63] and various vertex models [FW69, FW70, Ass17]. In the physics literature, this technique is sometimes called the "Pfaffian method", since the dimer model's partition function corresponds to Pfaffians [Kas63]. An alternative representation of Pfaffians is to use Grassman integrals, which are integrals of anti-commuting variables; see for instance [DFMS97], chapter 2.B. These anti-commuting variables are interpreted physically as a system non-interacting fermions [Hur66]. This is why any regime for which there is a transformation to dimers is often called *free-fermionic*.

Lemma I.3. *Let $w_1, w_2, w_3, w_4, w_5 \in (0, \infty)$ be five positive real numbers. Then they satisfy* (I.6) *iff there exists a unique triplet $\lambda, a, b \in (0, \infty)$ such that $a^2 + b^2 = 1$ and*

$$\begin{cases} w_1 = \lambda a^2 \\ w_2 = \lambda b^2 \\ w_3 = \lambda a \\ w_4 = \lambda b \\ w_5 = \lambda ab. \end{cases} \tag{I.7}$$

Proof. Given a set of weights $w_1, w_2, w_3, w_4, w_5 \in (0, \infty)$ that satisfy (I.6), then there is only one candidate for λ, a, b:

$$\begin{aligned} \lambda &= w_1 + w_2, \\ a &= \frac{w_3}{\lambda}, \\ b &= \frac{w_4}{\lambda}. \end{aligned}$$

Then the third equation of (I.6) simplifies into

$$w_5 = \lambda ab$$

and the first two equations become, respectively

$$\begin{aligned} w_1 &= \lambda a^2, \\ w_2 &= \lambda b^2 \end{aligned}$$

and since $\lambda = w_1 + w_2$, we also have $a^2 + b^2 = 1$ so that the parameterization (I.7) is correct. Reciprocally, it is easy to check that (I.7) implies (I.6). □

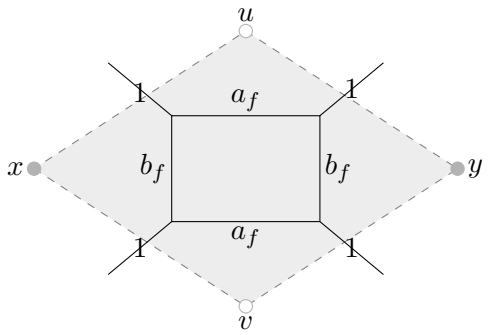

Figure I.5: Edge weights for the dimer model on G^Q at a face $f \in F$.

Theorem I.4. *Let us consider a symmetric $C_2^{(1)}$ loop model such that the free-fermionic relations* (I.6) *are satisfied at each face $f \in F$. Let λ_f, a_f, b_f be the corresponding parameters in representation* (I.7)*.*

Let us consider the dimer model on G^Q with weights $\mu = (\mu_e)_{e \in E^Q}$ given by Figure I.5. Then

$$\mathcal{Z}^G_{loop}(W) = \left(\prod_{f \in F} \lambda_f \right) \left(\mathcal{Z}^G_{dim}(\mu) \right)^2.$$

Proof. **Step 1: double dimers and face weights**

Let us consider a couple of independent dimer configurations m_A and m_B. Dimers A will be colored in black and dimers B in green. Clearly,

$$\left(\mathcal{Z}^G_{\mathrm{dim}}(\mu) \right)^2 = \sum_{m_A, m_B} w^G_{\mathrm{dim}}(m_A) w^G_{\mathrm{dim}}(m_B).$$

Since the roads weights are all equal to 1, the weight of a couple (m_A, m_B) can be seen as a product of "face weight" of the following form; the notation d.dim is a shorthand for "double dimers":

$$w^f_{\mathrm{d.dim}}(m_A, m_B) := \prod_{e \in m_A \text{ in city } f} \mu_e \prod_{e \in m_B \text{ in city } f} \mu_e.$$

Thus,

$$w^G_{\mathrm{dim}}(m_A) w^G_{\mathrm{dim}}(m_B) = \prod_{f \in F} w^f_{\mathrm{d.dim}}(m_A, m_B).$$

In Figure I.6, in the first column, we have listed all local configurations of (m_A, m_B) at a face (up to symmetries).

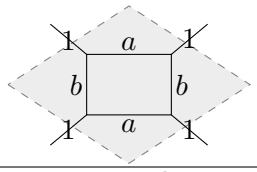

Dimers m_A, m_B	**Fused dimers** $\overline{(m_A, m_B)}$	**Face weight** $\sum w^f_{\text{d.dim}}(m_A, m_B) = w^f_{\text{f.d.dim}}\left(\overline{(m_A, m_B)}\right)$	**Marked loops** σ^{m}	**Face weight** $w^f_{i_{\sigma^{\text{m}}}(f)}$	
		a^2		λa^2	*
		a^2		λa^2	*
		1	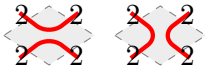	$\lambda a^2 + \lambda b^2 = \lambda$	
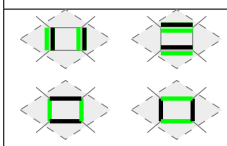		$a^4 + b^4 + 2a^2b^2 = 1$	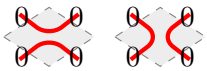	$\lambda a^2 + \lambda b^2 = \lambda$	
		b^2		λb^2	*
		b		λb	*
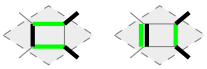		$a^2b + b^3 = b$		λb	*
		ab		λab	*

Figure I.6: Local configurations at a face for double dimers, fused dimers and marked loops. For each row marked with a *, similar rows could be obtained by applying a symmetry or by switching the role of dimers A and B.

Step 2: fused double-dimers

In Figure I.6, the different rows correspond to the possible occupations of roads by double dimers, and how these roads are connected inside the city (up to symmetries). We can group together the local configurations belonging to the same row, to get a *fused* double dimer configuration. More precisely, a fused dimer configuration $\overline{(m_A, m_B)}$ is the equivalence class of the couples of dimer configurations (m_A, m_B) having identical roads, and having the same connections of single-dimered roads.

We can define face weights for fused dimers, simply by summing the double dimers' face weights; they are given in the third column of Figure I.6. We denote these local weights by

$w^f_{\text{f.d.dim}}\left(\overline{(m_A, m_B)}\right)$, and the weight of a fused double dimer configuration is simply

$$w^G_{\text{f.d.dim}}\left(\overline{(m_A, m_B)}\right) = \prod_{f\in F} w^f_{\text{f.d.dim}}\left(\overline{(m_A, m_B)}\right).$$

We thus get a weight-preserving (many-to-one) mapping between a couple of dimer models and a fused dimer model. We represent such a mapping by a diagram:

$$\text{Dimers}_A \times \text{ Dimers}_B \longrightarrow \text{Fused dimers.}$$

Step 3: marked loops

Let us now focus on the $C_2^{(1)}$ loops part. We define a *marked* $C_2^{(1)}$ loop configuration as a $C_2^{(1)}$ loop configuration where every red edge is marked with an index 0 or 2, and every blue edge with an index A or B, so that the index on a path stays constant except when a different-colored path is crossed. When a different-colored path is crossed, the index has to change.

To make this definition well defined, we need the following Lemma:

Lemma I.5. *When G is a connected bipartite quadrangulation on a connected orientable surface, for every $C_2^{(1)}$ loop configuration σ on G, every blue loop of σ crosses red paths an even number of times (and similarly for red loops).*

Proof. Let us color the vertices of G in black and white. Let us consider a blue loop of σ, and let us chose an orientation for that loop. When the loop turns right or left inside a face, the color of the vertex on its left does not change. On the other hand, when the loop goes straight into a face (*i.e.* when it crosses a red loop), this color changes. Since the surface is orientable, when we follow the loop from start to end, we end up with the initial vertex on its left. Therefore it has crossed red paths an even number of times. □

For a marked loop configuration σ^{m}, let σ be its unmarked version. The weight of σ^{m} is defined just as in (I.5), except there is no factor for the number of loops; we use the notation m.loop for marked loops:

$$w^G_{\text{m.loop}}(\sigma^{\text{m}}) = \prod_{(f,i_k)\in\sigma} w_i^f. \tag{I.8}$$

Since there are 2^{N_σ} ways to mark a $C_2^{(1)}$ loop configuration σ, the sum of all possible marked loop weights is equal to the weight of σ. Therefore there is a weight-preserving (2^{N_σ}-to-one) mapping:

$$\text{Marked } C_2^{(1)} \text{ loops} \longrightarrow C_2^{(1)} \text{ loops.}$$

Step 4: marked loops to fused dimers

Let us describe a mapping from marked loops to fused double dimers. Given a marked loop configuration σ^{m}, let us first put dimers on roads: put one A dimer on blue roads marked with an A, one B dimer on blue roads marked with a B, two dimers on red roads marked with a 2, and no dimer on red roads marked with a 0. Then, let us chose the dimers in cities:

when four blue edges come together at a face, chose the city dimers according to the loops connections (see the first row of Figure I.6). Otherwise, there is only one possible fused dimer configuration with roads constructed as before. We thus construct a fused double dimer configuration $\overline{(m_A, m_B)}$. All the cases (up to symmetries) are listed in Figure I.6.

This transformation is several-to-one, indeed, loop configurations having four red loops marked with a 2 (resp. a 0) are mapped onto the same fused dimer configuration. However, up to a global multiplicative factor λ, this transformation is weight-preserving because, after summing over marked loops having the same image, the local weights of both models differ by a same factor λ.

Thus there is a weight-preserving (many-to-one) mapping:

$$\text{marked } C_2^{(1)} \text{ loops} \longrightarrow \text{Fused dimers.}$$

Step 5: conclusion

To sum things up, there is a series of (many-to-one) weight-preserving mappings:

$$\text{Dimers}_A \times \text{ Dimers}_B \longrightarrow \text{Fused dimers} \longleftarrow \text{Marked } C_2^{(1)} \text{ loops} \longrightarrow C_2^{(1)} \text{ loops.}$$

This implies the equality of partition functions, which concludes the proof of Theorem I.4. □

From there, it is natural to ask what information between dimers and loops is kept through these transformations. At the local level, it seems that the best connection we can get is the following:

Given a $C_2^{(1)}$ loop configuration σ, let σ_b be the set of blue paths in σ. If a particular set of blue paths σ_b^0 is fixed, we say that a double dimer configuration (m_A, m_B) has paths σ_b^0 if its set of single-dimer roads is the set of blue edges in σ_b^0, and when the four incoming edges at a city are blue, the dimers in the city are with connection according to σ_b^0. Then we have:

$$\sum_{\substack{\sigma \ C_2^{(1)} \text{ loops conf.} \\ \text{s.t. } \sigma_b = \sigma_b^0}} w_{\text{loop}}^G(\sigma) = \sum_{\substack{(m_A, m_B) \text{ dimers conf.} \\ \text{with paths } \sigma_b^0}} w_{\text{dim}}^G(m_A) w_{\text{dim}}^G(m_B).$$

As a result, all the observables of the $C_2^{(1)}$ loop model related to blue loops and their connectivity correspond to some observable of the double dimer model, which can in turn be computed by determinantal techniques [Ken97]. On the other hand, the connectivity of red loops seems to be lost in translation. Of course, since red and blue loops play a symmetric role, the statistics of red loops connectivities are the same as the blue loops' and can be computed in the same way; what we actually mean is that the joint connectivities of red and blue loops may not be analyzed through the dimer model.

Example I.6. *Probability of a dimer on a road.*

Let $e \in E^Q$ be a road in G^Q. We are interested in the probability p of that road being covered by a dimer in a single dimer model m_A, with our previous dimers weights. So

$$p = \mathbb{P}_{dim}(e \in m_A) = \frac{\sum_{m_A | e \in m_A} w_{dim}^G(m_A)}{\mathcal{Z}_{dim}^G}.$$

When we take two independent dimer models m_A, m_B, the probability of e being covered by a single dimer is then $2p(1-p)$. Because of the relation with loops, this is equal to the probability of e being covered by a blue loop. Since loops are color-symmetric, this is equal to $\frac{1}{2}$, and we deduce that

$$p = \frac{1}{2}.$$

This is true for any dimer model on a G^Q with roads having weight 1 and cities having weights a, b such that $a^2 + b^2 = 1$. This property can be proven straightaway studying this dimer model, but is trivial in loops.

Remark I.7. We have presented the correspondence with dimers on a quadrangulation without boundary, but it is possible to consider, for instance, finite quadrangulations of the plane with a boundary. In that case, there is a number of external dual edges (which we think of as "half-edges", not connected together to the external face), and we have to chose boundary conditions for the $C_2^{(1)}$ loop model. For instance, we could use free boundary conditions by imposing nothing on the red or blue paths that use these external edges; we could also impose the colors of these paths to be fixed; we could even specify how paths starting on external edges are connected inside the graph.

The equivalence with dimers works similarly by defining appropriate boundary conditions for dimers, except if the specification for loops connections concern both blue and red connections, since we cannot keep track of both colors' connections in our mappings.

One example of tractable boundary conditions, where only blue connections are specified, will be studied in Section I.4.

I.2.4 Free energy

In this paragraph, we consider an infinite quadrangulation G of the plane $\mathbb{R}^2$ (so it is necessarily bipartite), that is $\mathbb{Z}^2$-periodic. This means that there is a basis (e_x, e_y) of $\mathbb{R}^2$ such that the translations by e_x and e_y are color-preserving graph isomorphisms.

We define a toroidal exhaustion of G in the following way: for any $n \in \mathbb{N}^*$, G_n is the quotient of G by the lattice $n\mathbb{Z}e_x + n\mathbb{Z}e_y$. We note V_n, E_n, F_n its set of vertices, edges and faces. For each n, G_n is a bipartite quadrangulation on the torus. The graph G_1 is called the *fundamental domain* of our quadrangulation G.

We assume that every face f of G_1 is equipped with a set of weights $w_1^f, \dots, w_5^f$ that satisfy the free-fermion relations (I.6). Then we can define a $C_2^{(1)}$ loop model on G_1 using these weights. We extend those weights periodically to get a similar model on G_n: every face f of G_n has a unique representative f_0 in G_1 and inherits the weights of f_0.

We will use the shorthand notation $\mathcal{Z}_n$ for the partition function $\mathcal{Z}_{\text{loop}}^{G_n}(W)$ of this loop model on G_n. Our goal is to compute the *free energy* of this model, which we define without a minus sign following [CKP01, KOS06]:

$$f = \lim_{n\to\infty} \frac{1}{n^2} \log \mathcal{Z}_n.$$

The fact that this limit exists and its exact value will follow from the correspondence with dimers.

We consider the dimer model of Theorem I.4 for the fundamental domain G_1. It can be extended periodically to get a dimer model on G_n. We simply note μ this set of dimers weights. Then by Theorem I.4,

$$\mathcal{Z}_n = \left(\prod_{f\in F_1} \lambda_f\right)^{n^2} \left(\mathcal{Z}_{\mathrm{dim}}^{G_n}(\mu)\right)^2$$

so that

$$\frac{1}{n^2}\log \mathcal{Z}_n = \sum_{f\in F_1} \log(\lambda_f) + \frac{2}{n^2}\log\left(\mathcal{Z}_{\mathrm{dim}}^{G_n}(\mu)\right). \tag{I.9}$$

The right-hand side of (I.9) contains the free energy of the periodic dimer model on G^Q with weights μ. This quantity can be exactly computed [CKP01, KOS06]. Let us recall how this computation is made.

The graph G_1^Q, is a bipartite graph on the torus. We equip it with a Kasteleyn orientation (*i.e.* an orientation of edges such that every face has an odd number of clockwise edges; there exists such an orientation, see for instance [CR07]). We can split its vertices between black ones B_1^Q and white ones W_1^Q. Then we define its Kasteleyn matrix K_1 as a W_1^Q by B_1^Q weighted adjacency matrix, with entries

$$(K_1)_{w,b} = \begin{cases} \mu(e) & \text{when } \overset{w}{\circ}\!\!\rightarrow\!\!\overset{e}{}\!\!-\!\!\overset{b}{\bullet} \\ -\mu(e) & \text{when } \overset{w}{\circ}\!\!\leftarrow\!\!\overset{e}{}\!\!-\!\!\overset{b}{\bullet} \\ 0 & \text{otherwise.} \end{cases}$$

Let z and w be two complex numbers. We construct a modified matrix $K_1(z,w)$ in the following way. Let γ_x, γ_y be the two oriented cycles on the torus corresponding respectively to e_x, e_y. We multiply the weight of edges crossing γ_x by z when the white vertex is on the left of γ_x, and by z^{-1} when the white vertex is on the right of γ_x; and similarly for γ_y and w. These weights define a Kasteleyn matrix $K_1(z,w)$. The *characteristic polynomial* of G_1 is then:

$$P(z,w) = \det K_1(z,w).$$

The free energy of the dimer model can be expressed using the characteristic polynomial:

Theorem ([CKP01, KOS06])**.** *We have*

$$\lim_{n\to\infty} \frac{1}{n^2}\log\left(\mathcal{Z}_{dim}^{G_n}(\mu)\right) = \frac{1}{(2i\pi)^2}\int_{\mathbb{T}^2} \log|P(z,w)|\frac{dz}{z}\frac{dw}{w}.$$

Therefore, (I.9) gives

$$f = \sum_{f\in F_1}\log(\lambda_f) - \frac{1}{2\pi^2}\int_{\mathbb{T}^2}\log|P(z,w)|\frac{dz}{z}\frac{dw}{w}.$$

Example I.8. *Free energy for integrable weights on $\mathbb{Z}^2$. Let us take for G the quadrangulation $\mathbb{Z}^2$. We equip every face with the positive integrable weights of [WN93, IC09] for the*

fugacity $n = 2$*:*

$$\begin{cases} w_1 = \sin^2(\theta) \\ w_2 = \cos^2(\theta) \\ w_3 = \sin(\theta) \\ w_4 = \cos(\theta) \\ w_5 = \sin(\theta)\cos(\theta) \end{cases}$$

where $\theta \in (0, \frac{\pi}{2})$*. Then for all* $f \in F$*,* $\lambda_f = 1, a_f = \sin(\theta), b_f = \cos(\theta)$*.*

The corresponding weighted graph G_1^Q*, equipped with a Kasteleyn orientation, is represented on the left of Figure I.7. We can perform an urban renewal [KPW00] on this graph to get the graph on the right.*

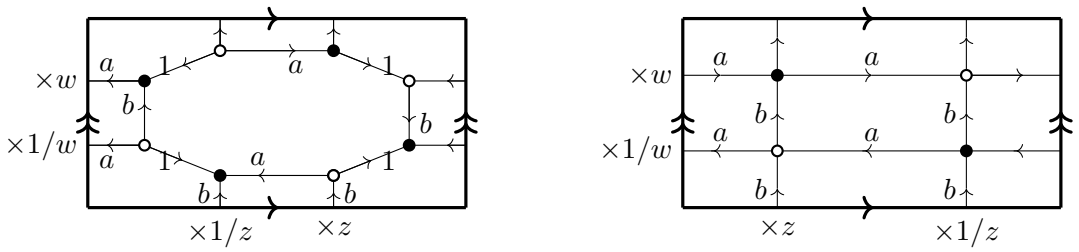

Figure I.7: The dimers' fundamental domain G_1^Q, before (left) and after (right) urban renewal, equipped with a Kasteleyn orientation. Here $a = \sin(\theta)$, $b = \cos(\theta)$.

By using the free energy for dominoes on $\mathbb{Z}^2$ *[Fis61] with horizontal weight* $\sin(\theta)$ *and vertical weight* $\cos(\theta)$*, we get*

$$f = -\frac{1}{2\pi^2} \int_{\mathbb{T}^2} \log \left| -2 + \cos^2(\theta) \left(z + \frac{1}{z} \right) + \sin^2(\theta) \left(w + \frac{1}{w} \right) \right| \frac{dz}{z} \frac{dw}{w}.$$

Several other expressions can be given for this quantity, for instance following [Ken02]:

$$f = \frac{2}{\pi} L(\theta) + \frac{2}{\pi} L\left(\frac{\pi}{2} - \theta \right) + \frac{2\theta}{\pi} \ln(\tan(\theta)) + \ln(2\cos(\theta))$$

where L *is the Lobachevsky function.*

I.3 Cube flip and Kashaev's recurrence

From now on, G might be a planar quadrangulation in the sense of Definition I.1, or a finite planar quadrangulation with a boundary, in the following sense:

Definition I.9. A quadrangulation with a boundary is a finite simple graph $G = (V, E)$, properly embedded in the plane, such that all *internal* (bounded) faces have degree 4.

In this case, we define a $C_2^{(1)}$ loop model on G by specifying a boundary condition in any way discussed in Remark I.7 – since the correspondence with dimers won't be used, both blue and red connections can be specified.

We start by proving a few identities on Kashaev's relation, then we relate the star-triangle relation for loops to Kashaev's relation.

I.3.1 Kashaev's recurrence

Kashaev's relation reads:

$$\begin{aligned} & g^2 g_{123}^2 + g_1^2 g_{23}^2 + g_2^2 g_{13}^2 + g_3^2 g_{12}^2 \\ & \quad - 2g_2 g_3 g_{13} g_{12} - 2g_1 g_3 g_{23} g_{12} - 2g_1 g_2 g_{23} g_{13} \\ & \quad - 2g g_{123}(g_1 g_{23} + g_2 g_{13} + g_3 g_{12}) \\ & \quad - 4g g_{12} g_{23} g_{13} - 4 g_{123} g_1 g_2 g_3 = 0. \end{aligned} \tag{I.10}$$

If seven of the g variables are positive real numbers, then the eighth one can be deduced from (I.10), up to the choice of the square root of a quadratic polynomial. The choice of the greatest root guarantees that the g variables stay positive. In this case, the recurrence can be explicitly written, see Proposition I.10.

We define six other variables X, Y, Z, X_1, Y_2, Z_3 by

$$\begin{aligned} X &= \sqrt{g g_{23} + g_2 g_3}, \\ Y &= \sqrt{g g_{13} + g_1 g_3}, \\ Z &= \sqrt{g g_{12} + g_1 g_2}, \\ X_1 &= \sqrt{g_1 g_{123} + g_{12} g_{13}}, \\ Y_2 &= \sqrt{g_2 g_{123} + g_{12} g_{23}}, \\ Z_3 &= \sqrt{g_3 g_{123} + g_{13} g_{23}}. \end{aligned}$$

All of these quantities can be nicely represented on the vertices and faces of a cube, see Figure I.8.

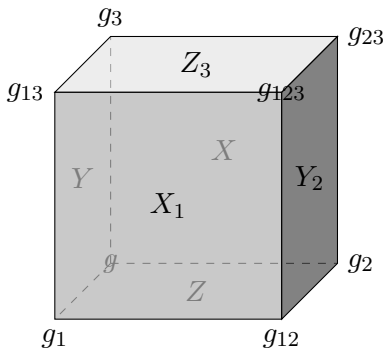

Figure I.8: The g, X, Y and Z variables, implicitly taken at $x \in \mathbb{Z}^3$.

The following relations can be obtained by simple calculations:

Proposition I.10 (Kashaev's recurrence)**.** *When Kashaev's relation* (I.10) *is satisfied, the value of* g_{123} *obtained by taking the greatest root reads*

1. $g_{123} = \frac{2g_1 g_2 g_3 + g(g_1 g_{23} + g_2 g_{13} + g_3 g_{12}) + 2XYZ}{g^2}$.

Furthermore,

2. $X_1 = \frac{g_1 X + YZ}{g}$,

3. $Y_2 = \frac{g_2 Y + XZ}{g}$,

4. $Z_3 = \frac{g_3 Z + XY}{g}$,

5. $\frac{X_1 Y_2 Z_3 + g_{12} g_{13} g_{23}}{g_{123}} = \frac{XYZ + g_1 g_2 g_3}{g}$.

The first 4 relations are a particular case of the *hexahedron recurrence* [KP16].

Kashaev's relation (I.10) has the same symmetries as the cube. In particular, by considering the central symmetry relative to the center of the cube, we get that the previous transformation is self-dual, in the following sense:

Proposition I.11. *Let g_{123} be defined in terms of $g, g_1, g_2, g_3, g_{12}, g_{13}, g_{23}$ as in Item 1 of Proposition I.10. Then the transformation:*

$$\begin{pmatrix} g \\ g_1 \\ g_2 \\ g_3 \\ g_{23} \\ g_{13} \\ g_{12} \end{pmatrix} \mapsto \begin{pmatrix} g_{123} \\ g_{23} \\ g_{13} \\ g_{12} \\ g_1 \\ g_2 \\ g_3 \end{pmatrix}.$$

is an involution.

Also note that this involution exchanges X and X_1, Y and Y_2, Z and Z_3.

I.3.2 Parametrization of a free-fermionic $C_2^{(1)}$ loop model

Let us suppose that there is a set of positive real values on the vertices V of G, denoted $g = (g_x)_{x \in V}$, such that the local loop weights take the following form at a face $f = \begin{smallmatrix} & u & \\ x & \diamond & y \\ & v & \end{smallmatrix}$:

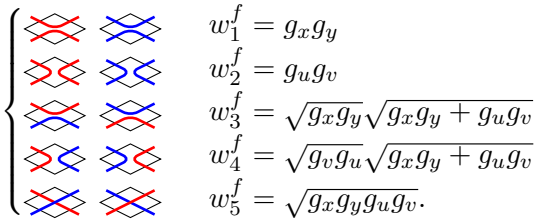

$$\begin{aligned} w_1^f &= g_x g_y \\ w_2^f &= g_u g_v \\ w_3^f &= \sqrt{g_x g_y}\sqrt{g_x g_y + g_u g_v} \\ w_4^f &= \sqrt{g_v g_u}\sqrt{g_x g_y + g_u g_v} \\ w_5^f &= \sqrt{g_x g_y g_u g_v}. \end{aligned} \tag{I.11}$$

Notice that these weights satisfy the free-fermionic relations (I.6). In fact, on a class of planar quadrangulations that includes finite lozenge graphs (embedded graphs whose internal faces are non-degenerate rhombi with same edge length), every free-fermionic $C_2^{(1)}$ loop model can be parametrized in this way. This is proved in Appendix I.B.

Notice also that the bipartite coloring of G is no longer important to define the weights. We will no longer show this coloring.

We can define a marked model with these weights using the weights of equation (I.8). We will show that the Yang-Baxter equations for this marked loop model are equivalent to g satisfying Kashaev's relation. This implies a similar statement for non-marked loops as well as for the double dimer model. However, since the indices on loops don't affect the

weight, the proof for marked loops will not be any more difficult that what it would be for non-marked loops.

We now denote by $\mathcal{Z}^G_{\text{m.loop}}(g)$ the partition function of marked loops on G:

$$\mathcal{Z}^G_{\text{m.loop}}(g) = \sum_\sigma w^G_{\text{m.loop}}(\sigma)$$

where σ runs over all marked $C_2^{(1)}$ loop configurations on G, and $w^G_{\text{m.loop}}(\sigma)$ is the same as (I.8) with the local weights defined by (I.11).

I.3.3 Cube flip

Let us suppose that G contains a vertex $x \in V$ of degree 3, such that the graph around x looks like the left-hand side of Figure I.9. We can perform a "cube flip" at x by changing the edges around this vertex. It gives a new graph G', on the right-hand side of Figure I.9. This is a form of star-triangle (or $Y - \Delta$) move.

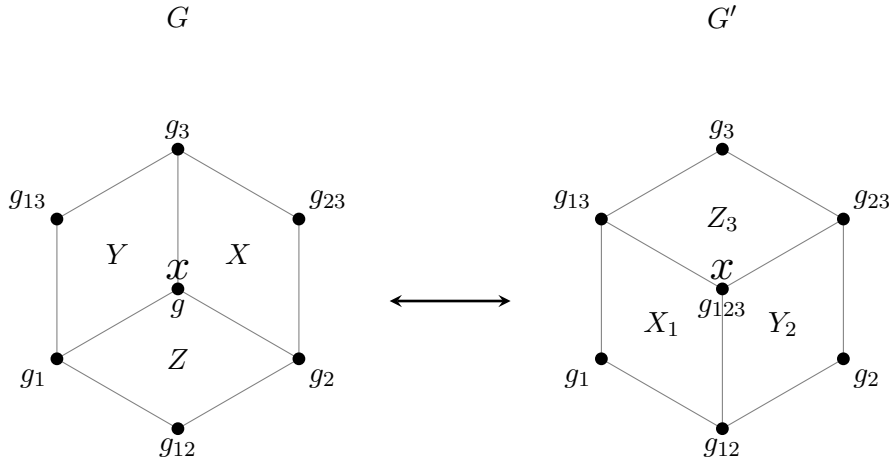

Figure I.9: Cube flip at x.

When such a move is performed, we allow g_x to change into a new value g'_x; let g' be the set of variables equal to g everywhere except at x where it is g'_x.

By labeling the g variables around x as in Figure I.9, we say that g *satisfies Kashaev's recurrence* at x when $g, g_1, \ldots, g_{123}$ satisfy (I.2). Note that performing cube flips at x twice with g satisfying Kashaev's recurrence would bring back the original graph and constants, because of Proposition I.11.

Theorem I.12. *When g satisfies Kashaev's recurrence at x,*

$$\frac{1}{g_x^2}\mathcal{Z}^G_{m.loop}(g) = \frac{1}{(g'_x)^2}\mathcal{Z}^{G'}_{m.loop}(g').$$

Another way to phrase this is to say that the Yang-Baxter equations for the $C_2^{(1)}$ loop model, as defined in [WN93], taken in our parametrization, become equivalent to Kashaev's recurrence.

Proof. There are six dual edges incoming in the region at x. We call *connection pattern* any way to color, label and connect these six incoming edges. For example, in the first row of Figure I.10, the connection pattern is the following: all edges are all colored in blue; the west and northwest edges are labeled k and connected; the east and northeast edges are labeled l and connected; the southeast and southwest edges are labeled m and connected.

We want to construct a coupling between marked $C_2^{(1)}$ loops on G and on G' so that they agree everywhere except inside the changed region around x, and such that the connection pattern doesn't change. Thus we want to group the marked loop configurations on G and on G' according to their connection pattern. All possible cases are listed in Figure I.10; indices on loops are arbitrary and we used the notation $\hat{k}$ for the index different from k (so $\hat{A} = B$, $\hat{B} = A$, $\hat{0} = 2$, $\hat{2} = 0$). We omitted a few cases: first, the ones that can be derived from represented ones by a simple rotation, symmetry or color swap; secondly, for any row $i \in \{1, \dots, 7\}$, there is a dual row obtained by taking the right-hand side configurations of i, turning them upside-down and drawing them on the left - and similarly for the other side (notice that rows $2, 6, 7$ are self-dual).

Note that connection patterns are the same for G and G'. Let m be the total number of connection patterns, and let $\{1, \dots, m\}$ be a set of indices representing them. For any $j \in \{1, \dots, m\}$, let Σ_j be the set of marked $C_2^{(1)}$ loop configurations on G having that connection pattern. Then $\Sigma_1, \dots, \Sigma_m$ are a partition of the set of all marked configurations on G. Thus in terms of partition functions we have

$$\mathcal{Z}^G_{\text{m.loop}}(g) = \sum_{j=1}^{m} \mathcal{Z}_j$$

where $\mathcal{Z}_j = \sum_{\sigma \in \Sigma_j} w^G_{\text{m.loop}}(\sigma)$. Similarly,

$$\mathcal{Z}^{G'}_{\text{m.loop}}(g) = \sum_{j=1}^{m} \mathcal{Z}'_j$$

where $\mathcal{Z}'_j = \sum_{\sigma \in \Sigma'_j} w^{G'}_{\text{m.loop}}(\sigma)$, and Σ'_j being the set of marked $C_2^{(1)}$ loop configurations on G' having connection pattern j.

If $\sigma \in \Sigma_j$, then its total weight can be written as

$$w^G_{\text{m.loop}}(\sigma) = a(\sigma) w_{\text{loc.}}(\sigma)$$

where $w_{\text{loc.}}(\sigma) = w^X_{i_1} w^Y_{i_2} w^Z_{i_2}$, with $(X, i_1), (Y, i_2), (Z, i_3) \in \sigma$; this is the local weight coming from the faces around x, and $a(\sigma)$ doesn't depend on the local configuration around x. Actually, if two local configurations have the same connection pattern, the possible ways to extend them to construct a loop configuration are the same, so the possible values of $a(\sigma)$ for these configurations are the same. This shows that $\mathcal{Z}_j$ can be factored into:

$$\mathcal{Z}_j = A_j \left(\sum_{\sigma \in L_j} w_{\text{loc.}}(\sigma) \right),$$

where A_j is the sum of weight of all possible $a(\sigma)$ for any $\sigma \in \Sigma_j$, and L_j is the set of all local configurations around x in G that have connection pattern j.

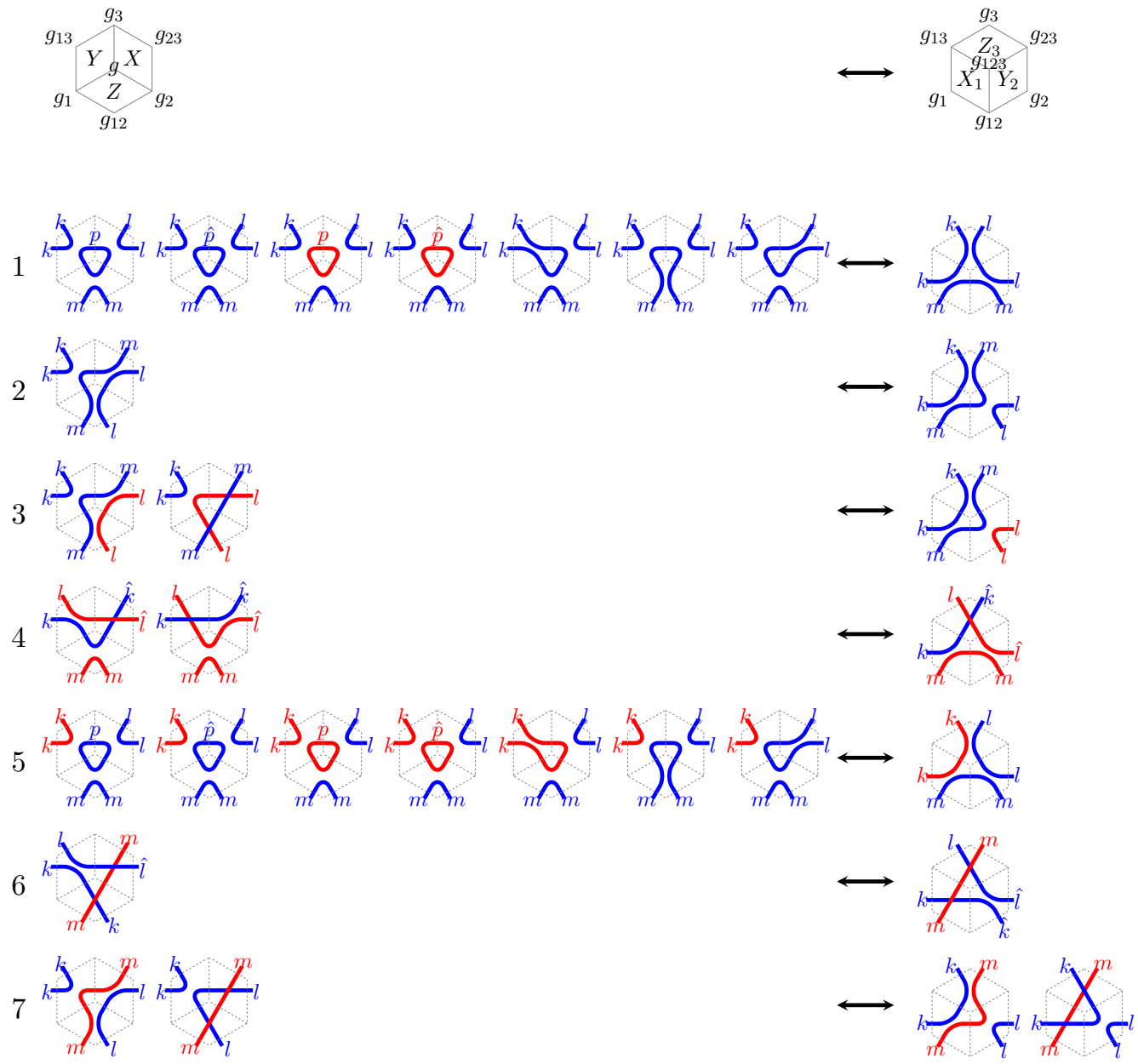

Figure I.10: Correspondence between marked loops on G (left) and G' (right) having the same connection pattern.

Similarly, $\mathcal{Z}'_j$ takes the form

$$\mathcal{Z}'_j = A_j \left(\sum_{\sigma \in L'_j} w_{\text{loc.}}(\sigma) \right).$$

Notice that the part A_j is the same for $\mathcal{Z}_j$ and $\mathcal{Z}'_j$: indeed, G and G' are the same outside of the region around x; given a local configuration in that region, the list of possible

extensions into a global loop configuration only depends on its connection pattern.

As a result, the following lemma is sufficient to conclude the proof.

Lemma I.13. *For any row $i \in \{1, \dots, 7\}$ in Figure I.10, let L_i (resp. L'_i) be the list of local configurations in row i on G (resp. G'). If g satisfies Kashaev's recurrence, then*

$$\frac{1}{g_x^2} \sum_{\sigma \in L_i} w_{loc.}(\sigma) = \frac{1}{(g'_x)^2} \sum_{\sigma \in L'_i} w_{loc.}(\sigma).$$

Proof. For $i = 1$, L_1 contains 7 configurations, and the sum of their local weights is, in the same order as in Figure I.10 (using the notation $g, g_1, \dots, g_{123}$ like in Figure I.9),

$$\begin{aligned} \frac{1}{g_x^2} \sum_{\sigma \in L_1} w_{\mathrm{loc.}}(\sigma) &= \frac{2g_1^2 g_2^2 g_3^2}{g^2} + \frac{2g_1 g_2 g_3 XYZ}{g^2} + \frac{g_1 g_2^2 g_3 g_{13}}{g} + \frac{g_1 g_2 g_3^2 g_{12}}{g} + \frac{g_1^2 g_2 g_3 g_{23}}{g} \\ &= g_1 g_2 g_3 \left(\frac{2g_1 g_2 g_3 + g(g_1 g_{23} + g_2 g_{13} + g_3 g_{12}) + 2XYZ}{g^2} \right). \end{aligned} \tag{I.12}$$

There is only one configuration in L'_1 which has local weight:

$$\frac{1}{(g'_x)^2} \sum_{\sigma \in L'_1} w_{\mathrm{loc.}}(\sigma) = g_1 g_2 g_3 g_{123}. \tag{I.13}$$

The equality of (I.13) and (I.12) is given by Item 1 in Proposition I.10.

The other cases are similar, using the various relations of Proposition I.10. This is done in Appendix I.A. □

Because of the self-duality property (Proposition I.11) and the symmetries of the model, Lemma I.13 is also true for any represented or non-represented row. Since connection patterns of configurations on G and G' are the same, the boundary conditions (if any) are preserved by this coupling. This concludes the proof of Theorem I.12 □

Remark I.14. Based on Theorem I.12, it is natural to define a renormalized partition function

$$\mathcal{Y}^G_{\mathrm{m.loop}}(g) = \left(\prod_{x \in V} \frac{1}{g_x^2} \right) \mathcal{Z}^G_{\mathrm{m.loop}}(g).$$

We can also go back to unmarked loops, weighted by a factor 2^{N_σ} (I.5), so that

$$\mathcal{Y}^G_{\mathrm{loop}}(g) = \mathcal{Y}^{G'}_{\mathrm{loop}}(g').$$

This quantity will appear again as the combinatorial object representing the solution of Kashaev's recurrence on a stepped surface.

Remark I.15. In the language of statistical physics, Theorem I.12 is a case of Z-invariance. Since marked loops generalize unmarked loops as well as dimers, Z-invariance for marked loops under Kashaev's recurrence implies Z-invariance for unmarked loops, and (when the boundary conditions, if any, don't involve red connections) for the double dimer model of Theorem I.4 for parametrized weights (I.11).

This particular dimer model is represented in Figure I.11. After performing gauge transformations (by multiplying weights by $\frac{1}{\sqrt{g_x g_u}}$ around any vertex of G^Q that is closest to the edge $\{xu\}$ of G), we get the weights on the right of Figure I.11. This is the dimer model of [KP16] in the particular case of Kashaev's relation; we get an alternative proof of its Z-invariance.

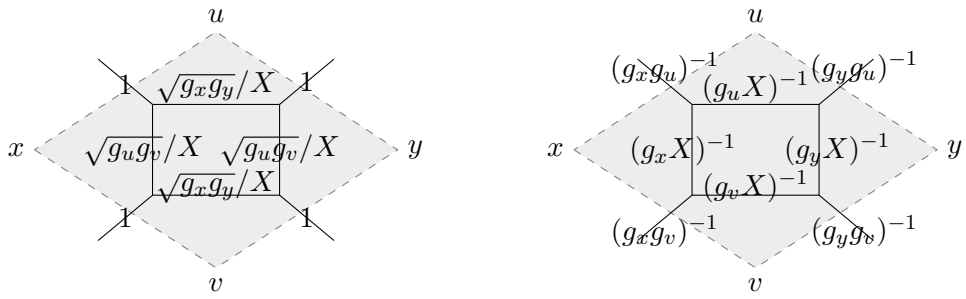

Figure I.11: The dimer model's weights before (left) and after (right) gauge transformations. Here we have set $X = \sqrt{g_x g_y + g_u g_v}$.

Interestingly enough, if one starts from Kashaev's parametrized Ising model (I.1), and applies the procedure transforming Ising models into dimers on G^Q [Dub11a, BdT14], one gets the same dimer model as in Figure I.11. However, the transformation between Ising model and dimers is not a direct mapping, so it is not completely clear in that setting why the Yang-Baxter equations for the Ising model translate into the same equations for dimers.

I.4 Taut configurations on stepped surfaces

We now turn to the study of *taut* configurations, which will be the appropriate objects counted by the solution of Kashaev's recurrence for arbitrary initial conditions.

I.4.1 Stepped surfaces

We denote by (e_1, e_2, e_3) the canonical basis of $\mathbb{R}^3$. For $x = (i, j, k) \in \mathbb{Z}^3$, let $C_x \subset \mathbb{R}^3$ be the unit cube $[i, i+1] \times [j, j+1] \times [k, k+1]$.

We call *stepped solid* a union of such unit cubes. A stepped solid U is said to be *monotone* if, for every $C_{(i,j,k)} \subset U$, and for every $i' \leq i, j' \leq j, k' \leq k$, $C_{(i',j',k')} \subset U$.

In this section, we always assume that U is a monotone stepped solid. In that case, the topological boundary ∂U is a union of squares of the form $(x, x + e_i, x + e_i + e_j, x + e_j)$ where $x \in \mathbb{Z}^3$ and $1 \leq i < j \leq 3$; it is called a *stepped surface*. This boundary naturally corresponds to an infinite planar quadrangulation $G(U)$, formally defined by the following sets of vertices and edges:

$$\begin{aligned} V(U) =& \{x \in U \cap \mathbb{Z}^3 \mid x + e_1 + e_2 + e_3 \notin U\}, \\ E(U) =& \{\{x, y\} \mid x, y \in V,\ x - y \in \{\pm e_1, \pm e_2, \pm e_3\}\}. \end{aligned}$$

We will also denote $F(U)$ the set of faces of $G(U)$.

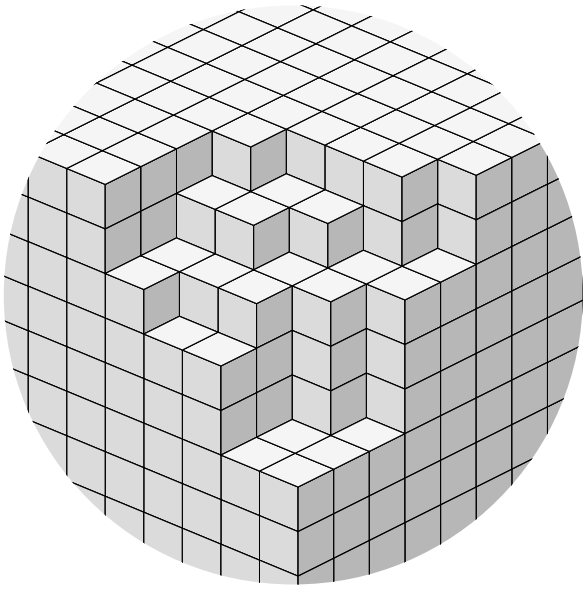

Figure I.12: A portion of a stepped solid U.

I.4.2 Boundary conditions

To define a loop model on $G(U)$ we need some extra boundary conditions. Consider the negative corner $U_0 = \mathbb{R}_- \times \mathbb{R}_- \times \mathbb{R}_-$. We require that $U \subset U_0$ and that $U_0 \setminus U$ be composed of finitely many cubes. In this case, we say that U is *regular* (see Figure I.12 for example). The infinite graph $G(U)$ is then equal to $G(U_0)$ outside of a sufficiently big ball for the euclidean distance centered at the origin. Let $B(O, R_U)$ be such a ball.

If U is a regular stepped solid, and $(g_x)_{x\in V(U)}$ is a collection of variables on the vertices of $G(U)$, then Kashaev's recurrence (I.2) is enough to recursively define g on $\mathbb{Z}^3_- \setminus U$. Then, the value at the origin $g_{(0,0,0)}$ is called the *solution of Kashaev's recurrence* with initial conditions $(g_x)_{x\in V(U)}$.

On $G(U_0)$ let σ_0 be the configuration given in Figure I.13. Following the terminology of [KP16], we say that a $C_2^{(1)}$ loop configuration σ on $G(U)$ is *taut* when it has the same connectivity as σ_0 on a neighborhood of infinity – meaning that outside of a ball of radius $R_\sigma \geq R_U$, σ has to be equal to σ_0, and σ has to contain paths connecting the edges of $U \cap B(O, R_\sigma)$ that are connected in σ_0. This is the case in Figure I.3 for example.

Let $\Sigma(U)$ be the set of taut $C_2^{(1)}$ loop configuration on $G(U)$.

The following lemmas are direct adaptations of Carroll and Speyer's arguments on cube groves [CS04].

Lemma I.16. *$\Sigma(U_0)$ only contains σ_0.*

Proof. Let σ be a taut configuration on $G(U_0)$. Suppose that it is different from σ_0. Without loss of generality, we can assume that there is a face f of the form $\{x, x+e_1, x+e_1+e_2, x+e_2\}$ that differs from σ_0. Take such a face with $x = (i, j, 0)$ and $i + j$ minimal; this is possible because σ is equal to σ_0 for all faces far enough from the origin. Then the faces $f - e_1$ and $f - e_2$ have to be the same for σ and σ_0, which implies that the dual edges of $\{x, x + e_1\}$ and

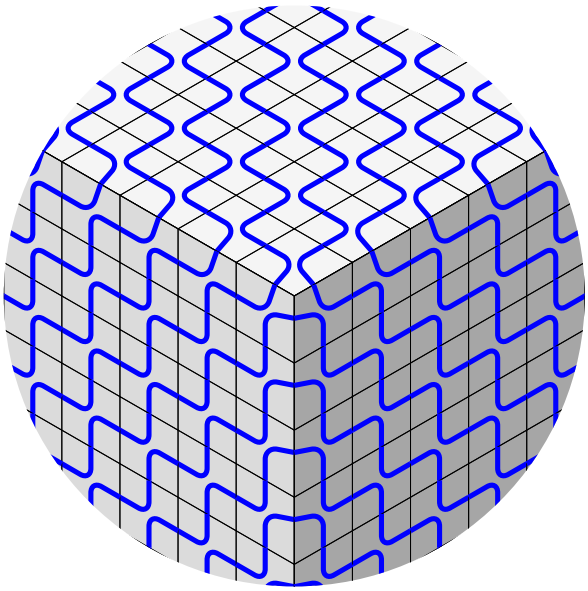

Figure I.13: The initial stepped solid U_0 and initial configuration σ_0.

$\{x, x+e_2\}$ are blue. Now since σ differs from σ_0 on f, the only possible local configurations connect these two blue edges inside of f. This implies that the connectivity of σ differs from the one in σ_0, which contradicts the definition of a taut configuration. □

Note that a configuration σ contains two types of paths: infinite simple paths, and finite closed simple loops. In the rest of the chapter, the latter will simply be called "loops".

Lemma I.17. *For a regular stepped solid U, $\Sigma(U)$ is finite. Moreover, a taut $C_2^{(1)}$ loop configuration on U has a finite number of loops.*

Proof. Let $\sigma \in \Sigma(U)$. We know that σ has the same connectivity as σ_0 and is equal to σ_0 outside of $B(O, R_\sigma)$. By the same argument described in the proof of Lemma I.16, σ actually has to be equal to σ_0 outside of $B(O, R_U)$. For a fixed U, there is only a finite number of such σ, and their loops have to be in $B(O, R_U)$ so there is a finite number of them. □

I.4.3 Weights

Let U be a regular stepped solid, and let $(g_x)_{x\in V(U)}$ be a collection of variables on the vertices of $G(U)$ that can be thought of as positive real numbers. For a taut $C_2^{(1)}$ loop configuration $\sigma \in \Sigma(U)$, we still denote N_σ its number of loops. Let us consider the weight:

$$w^U_{\text{taut}}(\sigma) = 2^{N_\sigma} \left(\prod_{(f,i_k)\in\sigma} w_i^f \right) \left(\prod_{x\in V(U)} \frac{1}{g_x^2} \right), \tag{I.14}$$

where the local weights w_i^f are defined using parametrization (I.11). This expression makes sense because N_σ is finite (Lemma I.17) and $\prod w_i^f$ formally makes g_x appear with exponent 2 for every x in the "flat" region where $\sigma = \sigma_0$, so the two products cancel out for all but a finite number of terms. For example, $w^{U_0}_{\text{taut}}(\sigma_0) = g_{(0,0,0)}$.

Since the number of taut configurations is finite (Lemma I.17), we can define the renormalized partition function:

$$\mathcal{Y}^U_{\text{taut}}(g) = \sum_{\sigma \in \Sigma(U)} w^U_{\text{taut}}(\sigma).$$

Formally, $\mathcal{Y}^U_{\text{taut}}(g)$ is simply a Laurent polynomial in the g variables and in the $\sqrt{g_x g_y + g_u g_v}$ variables, for any face bordered by x, u, y, v; we call these *face variables*.

Theorem I.18. *Let U be a regular stepped solid, and $(g_x)_{x \in V(U)}$ be a collection of variables on the vertices of $G(U)$. Then the solution of Kashaev's recurrence at the origin with initial condition $(g_x)_{x \in V(U)}$ is*

$$g_{(0,0,0)} = \mathcal{Y}^U_{taut}(g).$$

Proof. Let g be the solution of Kashaev's recurrence with initial conditions on $V(U)$ (so that g is also defined on $\mathbb{Z}^3_- \setminus U$).

The results of Section I.3 imply that the renormalized partition function $\mathcal{Y}^U_{\text{taut}}(g)$ doesn't change when a cube is added to, or removed from, U in such a way that it remains a stepped solid - as long as we keep using the g variables. Indeed, the boundary conditions are unchanged when a cube flip is performed so all the computations stay the same for taut configurations.

By repeatedly removing cubes starting from U_0 to get to U, this implies

$$\mathcal{Y}^U_{\text{taut}}(g) = \mathcal{Y}^{U_0}_{\text{taut}}(g).$$

But $\Sigma(U_0)$ only contains σ_0 (Lemma I.16), and $w^{U_0}_{\text{taut}}(\sigma_0) = g_{(0,0,0)}$, so that $\mathcal{Y}^{U_0}_{\text{taut}}(g) = g_{(0,0,0)}$. □

I.4.4 Algebraic consequences

We have seen that the solution of Kashaev's recurrence is equal to the partition function $\mathcal{Y}^U_{\text{taut}}(g)$. However, several taut $C_2^{(1)}$ loop configurations on $G(U)$ might correspond to the same monomial in $\mathcal{Y}^U_{\text{taut}}(g)$. The following Theorem states that it is not the case, and gives consequences on the exponents and coefficients appearing in the Laurent polynomial. The first and third points were already obtained in [KP16] (Theorem 7.8) by an indirect method.

Theorem I.19. *For any formal initial condition $(g_x)_{x \in V(U)}$ where U is a regular stepped solid, let $g_{(0,0,0)}$ be the solution at the origin of Kashaev's recurrence. Then:*

1. *$g_{(0,0,0)}$ is a Laurent polynomial in the $(g_x)_{x \in V(U)}$ vertex variables and in the face variables defined on the faces of $G(U)$;*
2. *The monomials are in one-to-one correspondence with taut $C_2^{(1)}$ loop configurations on U;*
3. *The g variables appear with exponent in $\{-2, \dots, 4\}$. The face variables appear with exponent in $\{0, 1\}$;*
4. *The coefficients in front of monomials are powers of 2.*

Proof. For any $\sigma \in \Sigma(U)$ and $x \in V(U)$, the g_x variable appears with an integer exponent in $w_U(\sigma)$. Indeed, it gets an exponent $\frac{1}{2}$ when, and only when, the color of the loops change around x (see the weights (I.11) and (I.14)), and this happens an even number of times. The first point is thus a direct consequence of Theorem I.18.

The third point comes from the observation that any vertex belongs to at most 6 faces of $G(U)$, so its exponent is between $0-2$ and $6-2$. The face variables can only appear once and with exponent 1.

The last point is a direct consequence of the second point, so all that remains to be proved is the following statement:

Let $\sigma, \sigma' \in \Sigma(U)$ be two taut $C_2^{(1)}$ loop configurations on $G(U)$. If the following expressions in the formal g variables are equal:

$$\left(\prod_{(f,i_k)\in\sigma} w_i^f\right)\left(\prod_{x\in V(U)} \frac{1}{g_x^2}\right) = \left(\prod_{(f,i_k)\in\sigma'} w_i^f\right)\left(\prod_{x\in V(U)} \frac{1}{g_x^2}\right) \tag{I.15}$$

then $\sigma = \sigma'$.

To prove this, we give a procedure to reconstruct σ from the monomial in the left-hand side of (I.15).

Suppose that there is a vertex $x \in \mathbb{Z}^3$ so that σ is already known on every face around x except for one, which we call f. We claim that we can find $\sigma|_f$. To do so, first we look whether the face variable associated to f is present in the monomial. If it is present, then the local configuration of σ at f belongs to the third or fourth row of (I.11); otherwise it belongs to the first, second or fifth row. Then we look at the exponent of g_x that doesn't come from already known faces: in the first case it can be $\frac{1}{2}$ (third row) or 0 (fourth row). In the second case it can be 1 (first row), 0 (second row) or $\frac{1}{2}$ (fifth row), so now we know which row $\sigma|_f$ belongs to. There are two local configurations in this row. To know which one it is, just look at the color of an incoming edge that is already known.

Since σ is taut, we already know it outside of a sufficiently big ball centered at the origin. We want to use the previous argument to successively discover new faces, until σ is known everywhere. To do so, we need to show that there is always an x that satisfies the first statement of the previous paragraph. Any x having degree 2 on the boundary of the graph formed by currently unknown faces would do the trick.

We prove that such an x always exists by showing a slightly more general result on *lozenge graphs*. A lozenge graph is a finite planar quadrangulation such that all internal faces are non-degenerate rhombi with same edge length. We call *outer boundary* of a lozenge graph the set of edges separating a face from the infinite connected component of the complement of the graph in the plane.

Lemma I.20. *Any non-empty lozenge graph has at least three vertices of degree* 2 *on its outer boundary.*

Proof. Let G be a lozenge graph. By restricting ourselves to a connected component, we can assume that G is connected. Let x_1 be a vertex on the boundary of G. We orient the boundary clockwise, meaning that we orient each of its edges so that the infinite connected component is on the left, see Figure I.14. Starting from x_1, we follow the boundary by taking the leftmost edge when several outgoing edges are present. We denote $(x_1, \dots, x_p, x_1)$ this

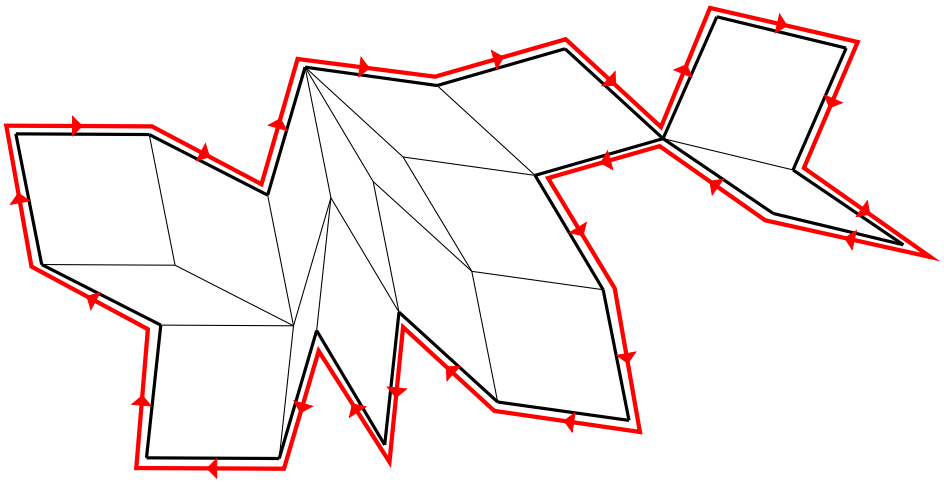

Figure I.14: A connected lozenge graph and its oriented outer boundary.

closed path, which is a single oriented curve around G, with possible pinches (some of the x_i vertices may be equal). We also take $x_0 := x_p$.

For any $i \in \{1, \dots, p\}$, the edge $\{x_{i-1}, x_i\}$ belongs to exactly one rhombus (otherwise it would not be on the boundary). Let u_i be the vertex of that lozenge that is diagonally opposite to x_{i-1}. Similarly, let v_i be the vertex that is diagonally opposite to x_{i+1} in the rhombus that contains the edge $\{x_i, x_{i+1}\}$; see Figure I.15.

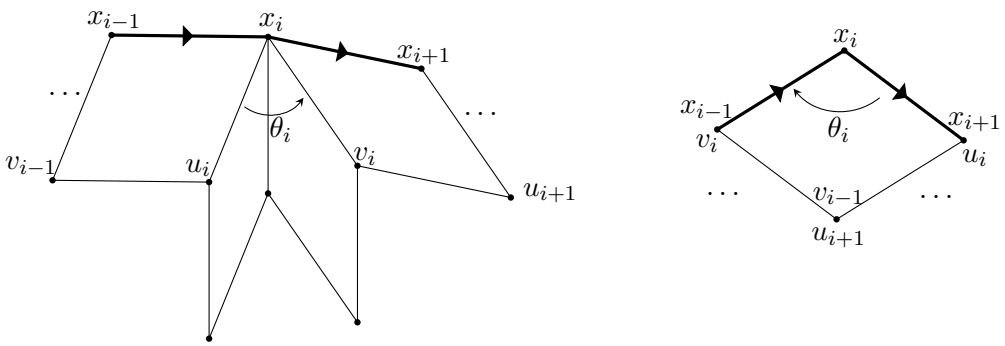

Figure I.15: The u_i, v_i vertices and θ_i angle when x_i has degree > 2 (left) or 2 (right).

Let θ_i be

$$\theta_i = \angle(\overrightarrow{x_i x_{i-1}}, \overrightarrow{x_i x_{i+1}}) - \angle(\overrightarrow{x_i x_{i-1}}, \overrightarrow{x_i u_i}) - \angle(\overrightarrow{x_i v_i}, \overrightarrow{x_i x_{i+1}}),$$

where the three angles are taken in $]0, 2\pi[$. Clearly, θ_i is equal to $\angle(\overrightarrow{x_i u_i}, \overrightarrow{x_i v_i})$ modulo 2π. By checking all possible cases like in Figure I.15, we can be more precise:

- when x_i does not have degree 2 in G, $\theta_i \in]0, 2\pi[$,

- otherwise, $\theta_i \in]-\pi, 0[$.

Our goal is to show that the sum of these angles is -2π, so that at least three of them have to be negative, and we can conclude.

Notice that $\overrightarrow{x_i v_i} = \overrightarrow{x_{i+1} u_{i+1}}$. By using this fact and reorganizing the sums we get:

$$\begin{aligned}\sum_{i=1}^{p} \theta_i &= \sum_{i=1}^{p} \angle(\overrightarrow{x_i x_{i-1}}, \overrightarrow{x_i x_{i+1}}) \; - \sum_{i=1}^{p} \angle(\overrightarrow{x_i x_{i-1}}, \overrightarrow{x_i u_i}) \; - \sum_{i=1}^{p} \angle(\overrightarrow{x_{i+1} u_{i+1}}, \overrightarrow{x_i x_{i+1}}) \\ &= \sum_{i=1}^{p} \angle(\overrightarrow{x_i x_{i-1}}, \overrightarrow{x_i x_{i+1}}) \; - \sum_{i=1}^{p} \left(\angle(\overrightarrow{x_i x_{i-1}}, \overrightarrow{x_i u_i}) + \angle(\overrightarrow{x_i u_i}, \overrightarrow{x_{i-1} x_i})\right).\end{aligned}$$

By the choice of angles, $\angle(\overrightarrow{x_i x_{i-1}}, \overrightarrow{x_i u_i}) + \angle(\overrightarrow{x_i u_i}, \overrightarrow{x_{i-1} x_i})$ is equal to π, so we have:

$$\sum_{i=1}^{p} \theta_i = \sum_{i=1}^{p} \left(\angle(\overrightarrow{x_i x_{i-1}}, \overrightarrow{x_i x_{i+1}}) - \pi\right).$$

Now the angles $\angle(\overrightarrow{x_i x_{i-1}}, \overrightarrow{x_i x_{i+1}}) - \pi$ are the oriented angles $\angle(\overrightarrow{x_{i-1} x_i}, \overrightarrow{x_i x_{i+1}})$ taken in $]-\pi, \pi[$. Since the boundary $(x_1, \dots, x_p, x_1)$ is a clockwise oriented closed curve, they sum up to -2π, so that

$$\sum_{i=1}^{p} \theta_i = -2\pi$$

as claimed. □

This concludes the proof of Theorem I.19. □

I.4.5 Limit shapes

The existence of limit shapes is shown exactly as in [KP16]. We just do the computations here to show how it fits into our particular framework. See also [PS05, DFSG14, Geo17] for similar proofs in the case of the octahedron and cube recurrences.

For $v = (i, j, k) \in \mathbb{Z}^3$, we define its *height* as $h(v) = i + j + k$.

For $N \in \mathbb{Z}^+$, let U_N be the following regular stepped solid:

$$U_N = \{C_v \mid v \in (\mathbb{Z}^-)^3, h(v) \leq -N\}.$$

We put a periodic g function on the vertices $V(U_N)$ that only depends on the height of vertices (see Figure I.16). The values of g in the flat regions don't appear in the weight of a taut configuration so they may be chosen arbitrarily. Our aim is to describe the shape of a random taut loop configuration on $G(U_N)$ sampled proportionally to its weight, when N is large.

Instead of letting N change, it will be convenient to consider instead the infinite stepped solid

$$U = \{C_v \mid h(v) \leq 2\},$$

represented in Figure I.17, and to see it from some $x \in \mathbb{Z}^3$ of positive height, and to let x change. Thus for any $x \in \mathbb{Z}^3$, we consider the "regular" stepped solid

$$U_x = U \cap (x + U_0).$$

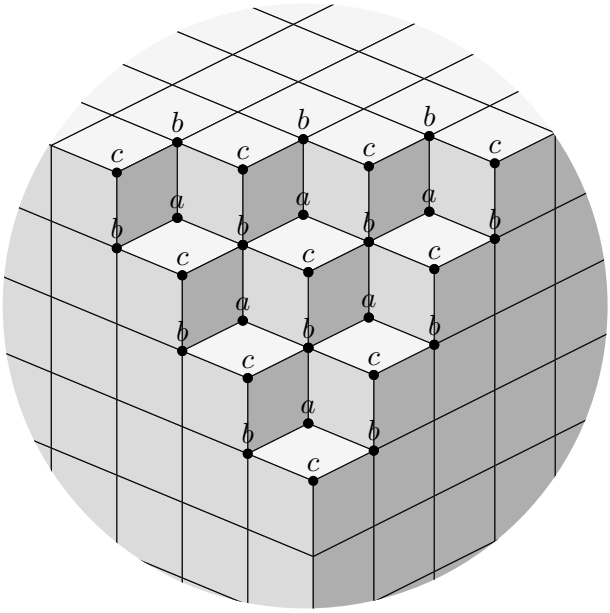

Figure I.16: The stepped solid U_3 and periodic weights on the vertices.

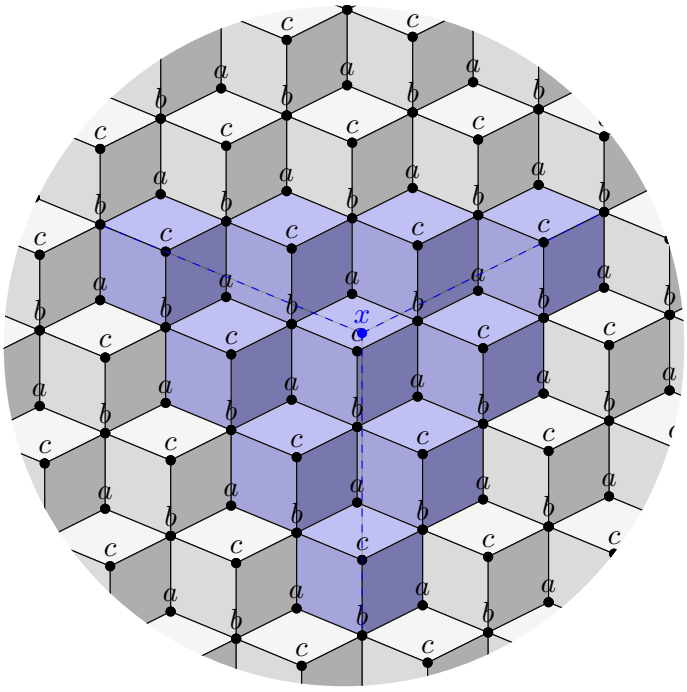

Figure I.17: The infinite stepped solid U with vertex weights $g^{a,b,c}$, an x of height 5 and the associated U_x (in blue). The origin $(0,0,0)$ is one of the a variables.

Up to a translation of vector $-x$, U_x is a regular stepped solid, similar to U_N where $N = h(x) - 2$ for $h(x) \geq 3$.

Let $g^{a,b,c}$ denote the set of initial conditions of Figure I.17:

$$g^{a,b,c}(x) = \begin{cases} a & \text{if } h(x) = 0, \\ b & \text{if } h(x) = 1, \\ c & \text{if } h(x) = 2. \end{cases}$$

Using these weights, we can define a partition function of loops on U_x:

$$Y_x = \mathcal{Y}_{\text{taut}}^{U_x}(g^{a,b,c}).$$

Of course Y_x depends only on the height of x. If $h(x) = N$, we simply denote $Y_N = Y_x$. We also define $X_N = \sqrt{Y_N Y_{N+2} + Y_{N+1}^2}$. These quantity can be exactly computed using Kashaev's relation for a function depending only on height, see [KP16], Section 7.5. The result is the following.

Let $R = \frac{ac}{b^2}$ and $S = \frac{bd}{c^2}$, where $d = \frac{2b^3+3abc+2(ac+b^2)^{\frac{3}{2}}}{a^2}$. As a side note, S and R can be deduced from one another as the greatest root of the intrinsic relation

$$R^2S^2 - 6RS - 4R - 4S - 3 = 0.$$

We have:

$$\begin{aligned} Y_{2n} &= a^{1-2n} b^{2n} R^{n^2} S^{n^2-n}, \\ Y_{2n+1} &= a^{-2n} b^{2n+1} R^{n^2+n} S^{n^2}, \\ X_{2n} &= \sqrt{1+R}\, Y_{2n+1}, \\ X_{2n+1} &= \sqrt{1+S}\, Y_{2n+2}. \end{aligned}$$

We are interested in the quantity

$$\rho(x) = \left(g_{(0,0,0)} \frac{\partial \log\left(\mathcal{Y}_{\text{taut}}^{U_x}(g)\right)}{\partial g_{(0,0,0)}} \right)\Bigg|_{g=g^{a,b,c}}. \tag{I.16}$$

This quantity has a probabilistic meaning. If σ is a random taut loop configuration on $G(U_x)$ chosen proportionally to its weight $w_{\text{taut}}^{U_x}(\sigma)$ for the initial conditions $g^{a,b,c}$, let n_0 be the power of $g_{(0,0,0)}$ appearing in the formal weight of σ. For a face f, let $\epsilon_f(\sigma)$ be 1 if $\sigma|_f$ is in the third or fourth row in Figure I.2, and 0 otherwise. Then

$$\rho(x) = \mathbb{E}\left[n_0 + \frac{1}{2(1+R)} \sum_{f \in F \text{ around } (0,0,0)} \epsilon_f(\sigma) \right]. \tag{I.17}$$

If we looked instead at U_N for $N = h(x) - 2$, by a simple symmetry, this quantity would be equal to the same expectation on the vertex $-x$ instead of 0 (and this vertex would have to be of type a in U_N). By defining the same partial derivative as in (I.16) with respect to $g_{(1,0,0)}$ or $g_{(1,1,0)}$, we could keep track of similar observables for vertices of type b and c. We will not make use of the exact formula of that observable, we just use it to show that the behavior of loops changes depending on the vertex of U_N.

The observable ρ is defined as some logarithmic derivative of the partition function $\mathcal{Y}_{\text{taut}}^{U_x}$. By taking the logarithmic derivative of Kashaev's relation (I.10), which is satisfied by $\mathcal{Y}_{\text{taut}}^{U_x}$, and evaluating at the initial condition $g^{a,b,c}$, we get linear relations on ρ:

$$\begin{aligned}\text{if } h(x) \text{ is even, } \rho(x+e_1+e_2+e_3) =&\alpha\rho(x) + \beta\left(\rho(x+e_1)+\rho(x+e_2)+\rho(x+e_3)\right)\\ &+\gamma\left(\rho(x+e_1+e_2)+\rho(x+e_1+e_3)+\rho(x+e_2+e_3)\right),\end{aligned} \tag{I.18}$$

$$\begin{aligned}\text{if } h(x) \text{ is odd, } \rho(x+e_1+e_2+e_3) =&\alpha'\rho(x) + \beta'\left(\rho(x+e_1)+\rho(x+e_2)+\rho(x+e_3)\right)\\ &+\gamma'\left(\rho(x+e_1+e_2)+\rho(x+e_1+e_3)+\rho(x+e_2+e_3)\right),\end{aligned} \tag{I.19}$$

where

$$\begin{aligned}\alpha &= \frac{3+3\sqrt{1+R}-2RS}{RS}, & \beta &= \frac{2+2\sqrt{1+R}+R}{R^2S}, & \gamma &= \frac{1+\sqrt{1+R}}{RS},\\ \alpha' &= \frac{3+3\sqrt{1+S}-2RS}{RS}, & \beta' &= \frac{2+2\sqrt{1+S}+R}{RS^2}, & \gamma' &= \frac{1+\sqrt{1+S}}{RS}.\end{aligned}$$

Let us define the generating function:

$$F(x,y,z) = \sum_{(i,j,k)\in\mathbb{Z}^3, h(i,j,k)\geq 0} \rho(i,j,k)x^iy^jz^k.$$

Using (I.18) (I.19), it is straightforward to compute F. It is a rational function of the form

$$F(x,y,z) = \frac{P(x,y,z)}{H(x,y,z)}$$

where P is some polynomial and

$$\begin{aligned}H(x,y,z) =& \left(\alpha xyz + \gamma(x+y+z)\right)\left(\alpha' xyz + \gamma'(x+y+z)\right)\\ &-\left(1-\beta(xy+xz+yz)\right)\left(1-\beta'(xy+yz+xz)\right).\end{aligned}$$

The coefficients $\alpha, \beta, \gamma, \alpha', \beta', \gamma'$ can all be defined using R so they are all dependent. Actually, by defining $\theta = \gamma\gamma'$, H takes the form:

$$H(x,y,z) = \theta(x^2-1)(y^2-1)(z^2-1) + (1-\theta)(xy-1)(xz-1)(yz-1).$$

At that point, we have recovered the denominator studied in [KP16]. The asymptotic behavior of the observables $\rho(i,j,k)$ can be obtained from the analysis of their generating function F at the singularity $(1,1,1)$ (Theorem 5.7 of [KP16], which is a corollary of various results of [PW13, BP11]). Around that point, the leading homogeneous part of $H(1+X, 1+Y, 1+Z)$ is

$$\bar{H}(X,Y,Z) = 2(1+3\theta)XYZ + (1-\theta)(X^2Y + XY^2 + X^2Z + XZ^2 + Y^2Z + YZ^2).$$

Thus the limit shape of the model can be computed as the dual of the curve

$$X^2Y + XY^2 + X^2Z + XZ^2 + Y^2Z + YZ^2 + \lambda XYZ$$

where $\lambda = \frac{2(1+3\theta)}{1-\theta}$. See [KP16] for the computation of this dual, its shape, and the behavior of ρ depending on its position relatively to the limit shape. The dual is a projective curve in $P\mathbb{R}^3$, in the following figures we represent it in $\mathbb{R}^3$ intersected with the plane $x+y+z=-1$.

We note that the limit shape only depends on R, and there is an extra symmetry: when R and S are exchanged, λ remains the same so the limit shape is the same. In general, $\lambda \in (2,3]$. When $\lambda \neq 3$, the limit shape looks like a rounded triangle tangent to the borders of the carved section of U_N, with an internal facet; see Figure I.18. The point $\lambda = 3$ is somehow critical and corresponds to $R = S = 3$. At that point, the limit shape becomes a circle and the central facet is reduced to a point.

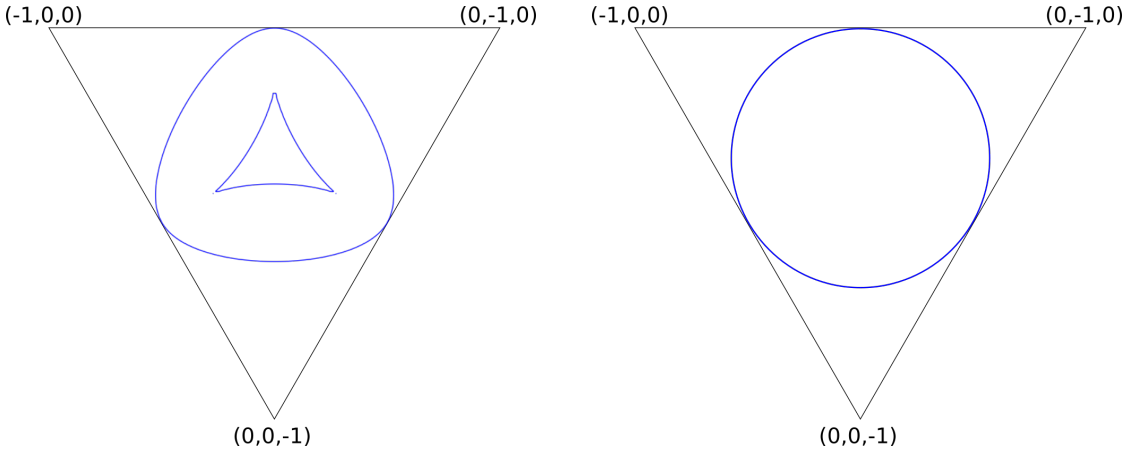

Figure I.18: Limit shapes for $R = 0.2$ (left) and $R = 3$ (right).

We computed simulations of the model for different values of R in Figure I.19. In the three corner regions ρ decays to 0 exponentially fast in N, which corresponds to the "frozen phase" where only infinite blue paths appear in the densest possible packing; it is possible to convince oneself that this is indeed the behavior implied by (I.17) being close to 0. The annular region around the facet corresponds to a "liquid phase" where ρ tends to 0 polynomially fast. It seems that this region's interface with the central facet is delimited by the infinite blue paths closest to the center. In the central facet there is a "gaseous phase" where ρ tends to $\frac{1}{3}$, and the boundary conditions don't appear any more.

I.4.6 Cube groves

Cube groves were introduced by Carroll and Speyer in [CS04]. They are essential spanning forests, often represented with their dual forest, on the graph consisting of the even vertices of $G(U)$ with edges on diagonals of the faces of the cubes. One example is displayed in black lines in Figure I.21.

Let $\Sigma_0(U)$ be the subset of $\Sigma(U)$ containing all taut $C_2^{(1)}$ loop configurations $\sigma \in \Sigma(U)$ such that $N_\sigma = 0$, *i.e.* σ has no finite loop. Such a configuration cannot contain any red edge, since all red paths are finite loops. Thus σ can be represented by a subset of the diagonals of the faces of the cubes, as in Figure I.20.

It is easy to check that this set of diagonals is necessarily a cube grove, and conversely, any cube grove corresponds to such a loop configuration (which is in fact the classical interface between the spanning forest and its dual). The transformation is thus a bijection between

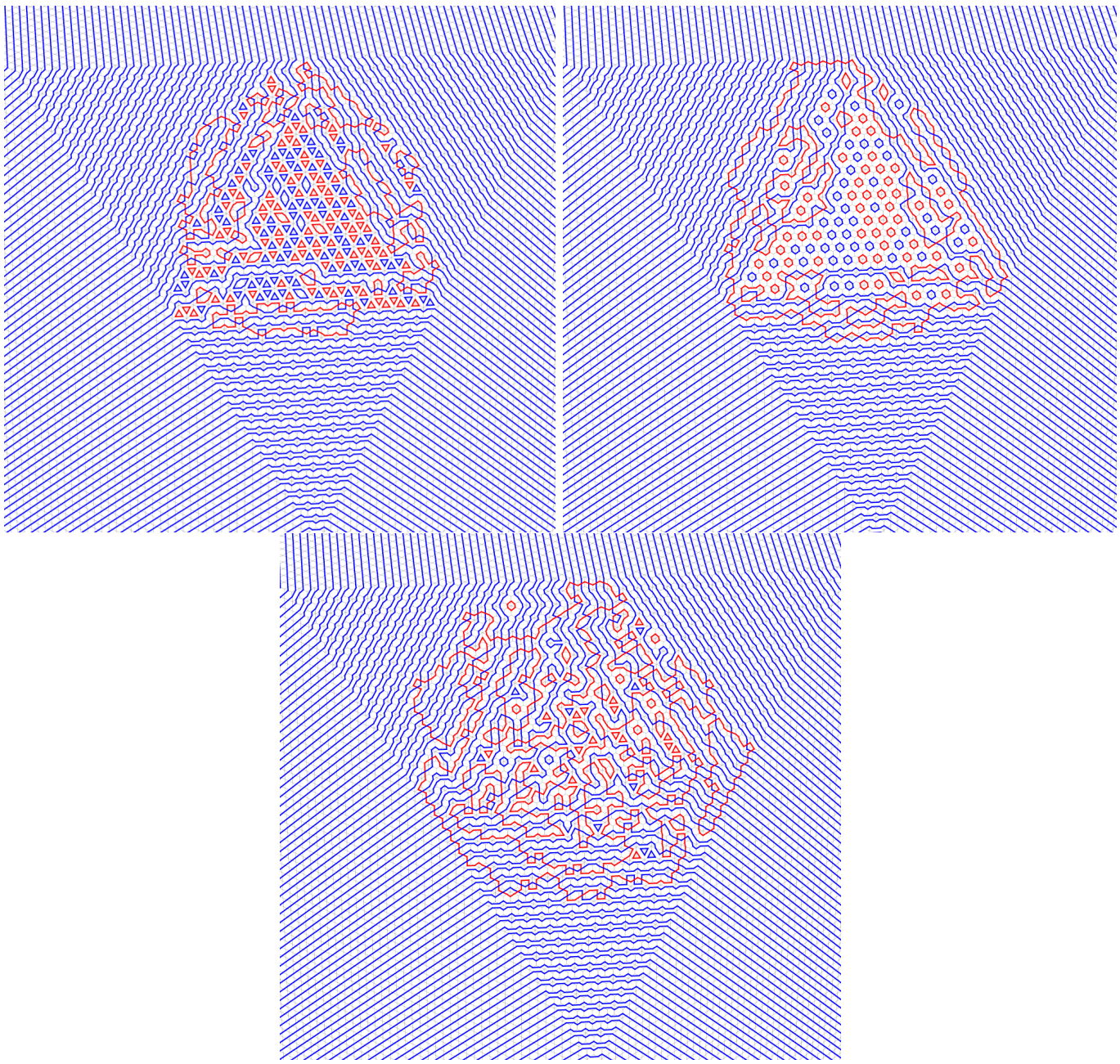

Figure I.19: Simulations for $N = 40$, and $R = 0.2$ (top left), $R \simeq 130.7$ ($S = 0.2$) (top right), $R = 3$ (bottom). The first two simulations correspond to the same limit shape.

$\Sigma_0(U)$ and cubes groves on U. Moreover, this bijection is weight-preserving, in the sense that the weight of $\sigma \in \Sigma_0(U)$ is equal to the weight of its associated cube grove as defined by Carroll and Speyer (using the vertices variables g^2 and setting face variables are set to be equal to 1).

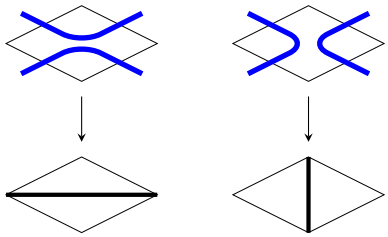

Figure I.20: Local transformation from $\Sigma_0(U)$ to cube groves

As a result, the partition function truncated to $\Sigma_0(U)$,

$$\mathcal{Y}^U_{0\,\mathrm{taut}}(g) = \sum_{\sigma\in\Sigma_0(U)} w^U_{\mathrm{taut}}(\sigma),$$

is formally equal to the solution of the cube recurrence with initial conditions g^2 on U. This is not such a surprise: on a field of characteristic 2, Kashaev's relation (I.10) reduces to

$$g^2 g^2_{123} + g^2_1 g^2_{23} + g^2_2 g^2_{13} + g^2_3 g^2_{12} = 0,$$

which is exactly the cube recurrence in characteristic 2 for the variables g^2, while $\mathcal{Y}^U_{\mathrm{taut}}(g)$ reduces to $\mathcal{Y}^U_{0\,\mathrm{taut}}(g)$.

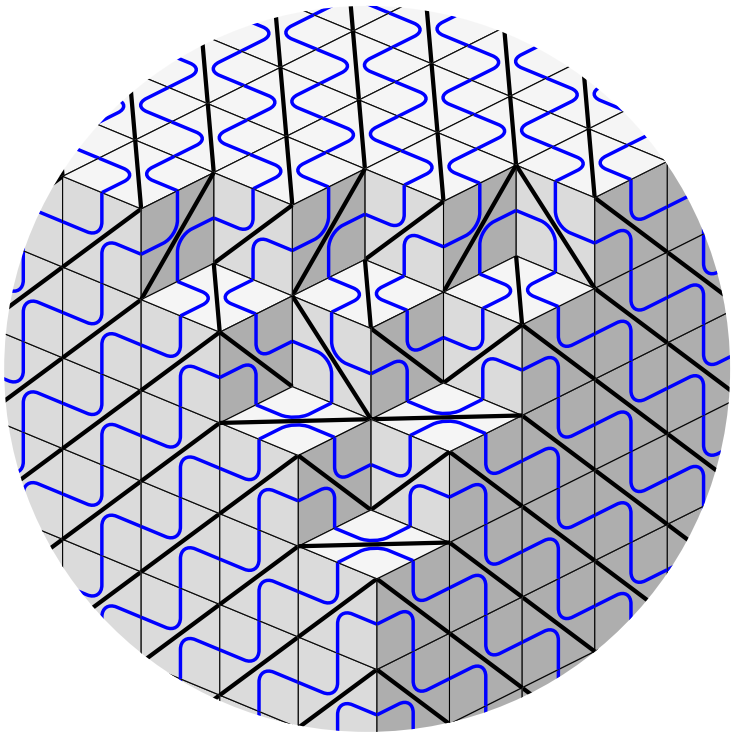

Figure I.21: A configuration $\sigma \in \Sigma_0(U)$ and the corresponding cube grove.

I.A Calculations for Lemma I.13

- $i = 2$:

$$\frac{1}{g_x^2}\sum_{\sigma\in L_2} w_{\mathrm{loc}}(\sigma) = g_1 g_3 g_{12} g_{23},$$
$$\frac{1}{(g'_x)^2}\sum_{\sigma\in L'_2} w_{\mathrm{loc}}(\sigma) = g_1 g_3 g_{12} g_{23}.$$

- $i = 3$:

$$\begin{aligned}\frac{1}{g_x^2}\sum_{\sigma\in L_3} w_{\mathrm{loc}}(\sigma) &= g^{-1} g_1 g_3 g_{12}^{\frac{1}{2}} g_{23}^{\frac{1}{2}} XZ \;+\; g^{-1} g_1 g_2 g_3 g_{12}^{\frac{1}{2}} g_{23}^{\frac{1}{2}} Y\\ &= g_1 g_3 g_{12}^{\frac{1}{2}} g_{23}^{\frac{1}{2}} \left(\frac{XZ + g_2 Y}{g}\right),\\ \frac{1}{(g'_x)^2}\sum_{\sigma\in L'_3} w_{\mathrm{loc}}(\sigma) &= g_1 g_3 g_{12}^{\frac{1}{2}} g_{23}^{\frac{1}{2}} Y_2.\end{aligned}$$

  The equality of $\frac{1}{(g'_x)^2}\sum_{\sigma\in L'_2} w_{\mathrm{loc}}(\sigma)$ and $\frac{1}{g_x^2}\sum_{\sigma\in L_2} w_{\mathrm{loc}}(\sigma)$ is equivalent to Item 3 of Proposition I.10.

- $i = 4$:

$$\begin{aligned}\frac{1}{g_x^2}\sum_{\sigma\in L_4} w_{\mathrm{loc}}(\sigma) &= g^{-1} g_1^{\frac{1}{2}} g_2 g_3^{\frac{1}{2}} g_{13}^{\frac{1}{2}} g_{23}^{\frac{1}{2}} YZ \;+\; g^{-1} g_1^{\frac{3}{2}} g_2 g_3^{\frac{1}{2}} g_{13}^{\frac{1}{2}} g_{23}^{\frac{1}{2}} X\\ &= g_1^{\frac{1}{2}} g_2 g_3^{\frac{1}{2}} g_{13}^{\frac{1}{2}} g_{23}^{\frac{1}{2}} \left(\frac{YZ + g_1 X}{g}\right),\\ \frac{1}{(g'_x)^2}\sum_{\sigma\in L'_4} w_{\mathrm{loc}}(\sigma) &= g_1^{\frac{1}{2}} g_2 g_3^{\frac{1}{2}} g_{13}^{\frac{1}{2}} g_{23}^{\frac{1}{2}} X_1.\end{aligned}$$

  The equality is equivalent to Item 2 of Proposition I.10.

- $i = 5$:

$$\begin{aligned}\frac{1}{g_x^2}\sum_{\sigma\in L_5} w_{\mathrm{loc}}(\sigma) &= 2g^{-2} g_1^{\frac{3}{2}} g_2^2 g_3^{\frac{3}{2}} Y \;+\; 2g^{-2} g_1^{\frac{3}{2}} g_2 g_3^{\frac{3}{2}} XZ \;+\; g^{-1} g_1^{\frac{1}{2}} g_2 g_3^{\frac{1}{2}} g_{13} XZ\\ &\quad + g^{-1} g_1^{\frac{3}{2}} g_2 g_3^{\frac{1}{2}} g_{23} Y + g^{-1} g_1^{\frac{1}{2}} g_2 g_3^{\frac{3}{2}} g_{12} Y\\ &= g_1^{\frac{1}{2}} g_2 g_3^{\frac{1}{2}} \left(\frac{2g_1 g_2 g_3 Y}{g^2} + \frac{2g_1 g_3 XZ}{g^2} + \frac{g_{13} XZ}{g} + \frac{g_1 g_{23} Y}{g} + \frac{g_3 g_{12} Y}{g}\right),\\ \frac{1}{(g'_x)^2}\sum_{\sigma\in L'_5} w_{\mathrm{loc}}(\sigma) &= g_1^{\frac{1}{2}} g_2 g_3^{\frac{1}{2}} X_1 Z_3.\end{aligned}$$

Using Items 2 and 4 of Proposition I.10, we get

$$\begin{aligned} X_1Z_3 &= \left(\frac{g_1X+YZ}{g}\right)\left(\frac{g_3Z+XY}{g}\right) \\ &= \frac{g_1g_3XZ + g_1X^2Y + g_3YZ^2 + XY^2Z}{g^2} \\ &= \frac{g_1g_3XZ + g_1(gg_{23}+g_2g_3)Y + g_3(gg_{12}+g_1\ g_2)Y + (gg_{13}+g_1g_3)XZ}{g^2} \\ &= \frac{2g_1g_2g_3Y}{g^2} + \frac{2g_1g_3XZ}{g^2} + \frac{g_{13}XZ}{g} + \frac{g_1g_{23}Y}{g} + \frac{g_3g_{12}Y}{g} \end{aligned}$$

and the equality follows.

- $i = 6$:

$$\begin{aligned} \frac{1}{g_x^2}\sum_{\sigma\in L_6} w_{\mathrm{loc}}(\sigma) &= g_1^{\frac12}g_2g_3^{\frac12}g_{12}^{\frac12}g_{13}g_{23}^{\frac12}, \\ \frac{1}{(g'_x)^2}\sum_{\sigma\in L'_6} w_{\mathrm{loc}}(\sigma) &= g_1^{\frac12}g_2g_3^{\frac12}g_{12}^{\frac12}g_{13}g_{23}^{\frac12}. \end{aligned}$$

- $i = 7$:

$$\begin{aligned} \frac{1}{g_x^2}\sum_{\sigma\in L_7} w_{\mathrm{loc}}(\sigma) &= g^{-1}g_1^{\frac12}g_3^{\frac12}g_{12}^{\frac12}g_{23}^{\frac12}XYZ \ + \ g^{-1}g_1^{\frac32}g_2g_3^{\frac32}g_{12}^{\frac12}g_{23}^{\frac12} \\ &= g_1^{\frac12}g_3^{\frac12}g_{12}^{\frac12}g_{23}^{\frac12}\left(\frac{XYZ+g_1g_2g_3}{g}\right), \\ \frac{1}{(g'_x)^2}\sum_{\sigma\in L'_7} w_{\mathrm{loc}}(\sigma) &= g_1^{\frac12}g_3^{\frac12}g_{12}^{\frac12}g_{23}^{\frac12}g_{123}^{-1}X_1Y_2Z_3 \ + \ g_1^{\frac12}g_3^{\frac12}g_{12}^{\frac32}g_{13}g_{23}^{\frac32}g_{123}^{-1} \\ &= g_1^{\frac12}g_3^{\frac12}g_{12}^{\frac12}g_{23}^{\frac12}\left(\frac{X_1Y_2Z_3+g_{12}g_{13}g_{23}}{g_{123}}\right). \end{aligned}$$

The equality is equivalent to Item 5 of Proposition I.10.

I.B Full Kashaev parametrization of free-fermionic $C_2^{(1)}$ loops

Let G be a planar quadrangulation with a boundary, V its set of vertices, F its set of internal faces. Then G is necessarily bipartite; we fix a bipartite coloring of V into black and white vertices.

A *train track* of G is a path on the dual graph G^* (defined with "half-edges" on the boundary of G, *i.e.* not connected at the external face), such that whenever it enters a face it exits on the opposite edge of that face; see Figure I.22. Let T be the set of all train tracks of G.

It is a theorem of Kenyon and Schlenker [KS05] that a quadrangulation is a lozenge graph *iff* no train track $t \in T$ is a loop or crosses itself, and two distinct train tracks $t, t' \in T$ cross at most once. For instance the quadrangulation of Figure I.22 cannot be made of non-degenerate rhombi.

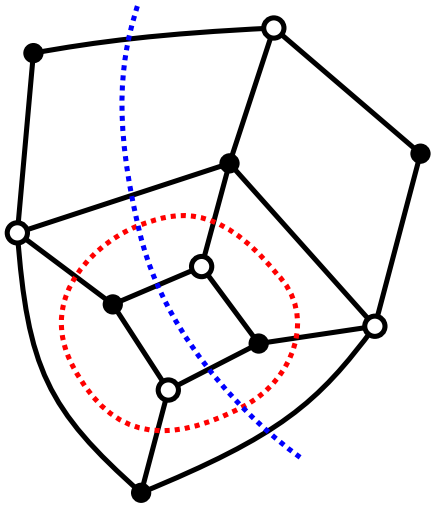

Figure I.22: A planar finite quadrangulation with a boundary, and two train tracks.

Here we show that on a slightly more general class of quadrangulations, an application is surjective. This linear application will be needed to construct a parametrization such as (I.11).

Lemma I.21. *If G is a connected planar finite quadrangulation with a boundary, such that no train track is a loop, then the mapping*

$$\begin{aligned}\Phi : \ \mathbb{R}^V &\to \mathbb{R}^F \\ (h_v)_{v\in V} &\mapsto (h_x + h_y - h_u - h_v)_{f\in F,\ f=\ x \overset{u}{\underset{v}{\diamond}} y}\end{aligned}$$

is surjective.

Proof. Because of the rank-nullity theorem, it is sufficient to prove that the dimension of $\ker(\Phi)$ is $|V| - |F|$.

Let h be a vector in $\ker\Phi$, and let $t \in T$. We chose an orientation of t. Whenever t crosses a face $f = x \overset{u}{\underset{v}{\diamond}} y$, for instance with x, u on its left and y, v on its right, we have $h_x - h_v = h_u - h_y$. This means that the quantity given by the value of h on the right minus its value on the left of an edge crossed by t is constant along t. Let $\alpha_t(h)$ be this value.

If we fix an orientation of every train track and a base vertex x_0, we thus get a linear transformation from $\ker(\Phi)$ to $\mathbb{C}^{|T|+1}$ by associating $(h_{x_0}, (\alpha_t(h))_{t\in T})$ to h. It is easy to see that this transformation is injective: if the family is null then $h_{x_0} = 0$ and similarly for its neighbors using the train tracks adjacent to x_0, etc.

Conversely, if we fix values $(\alpha_t)_{t\in T}$ and a h_{x_0}, we can to reconstruct a vector h in the kernel of Φ associated to these values: starting from x_0, define h on its neighbors using the values α_t associated to train tracks adjacent to x_0, then on their neighbors, etc. The orientation of train tracks guaranties that these choices are coherent, and the fact that α_t is constant along t is equivalent to $\Phi(h)$ being 0 on every face crossed by t.

Thus $\ker(\Phi)$ has dimension $|T|+1$.

Let E_{ext} be the set of edges adjacent to the external face, and $E_{\text{int}} = E \setminus E_{\text{ext}}$. Since the train tracks never loop, the set of train tracks define a coupling of external edges so

$$2|T| = |E_{\text{ext}}|. \tag{I.20}$$

Since every internal face is a quadrangle, we have

$$4|F| = 2|E_{\text{int}}| + |E_{\text{ext}}|. \tag{I.21}$$

Finally we have Euler's formula:

$$|V| - |E| + |F| = 1. \tag{I.22}$$

Combining (I.20), (I.21), (I.22) and $|E| = |E_{\text{int}}| + |E_{\text{ext}}|$ easily gives

$$|T| + 1 = |V| - |F|$$

so $\dim(\ker \Phi) = |V| - |F|$ as needed. □

Now we can go back to the proof that parametrization (I.11) exists for any free-fermionic loop model on a graph G that satisfies the assumption of Lemma I.21.

On every face f we have a set of positive weights $w_1^f, \dots, w_5^f$ that satisfy (I.6). Let us define $\kappa_f = w_5^f$ and $R_f = \left(\frac{w_1^f}{\kappa_f}\right)^2$. We get:

$$\begin{cases} w_1^f = \kappa_f \sqrt{R_f} \\ w_2^f = \kappa_f \sqrt{\frac{1}{R_f}} \\ w_3^f = \kappa_f \sqrt{1+R_f} \\ w_4^f = \kappa_f \sqrt{1+\frac{1}{R_f}} \\ w_5^f = \kappa_f. \end{cases} \tag{I.23}$$

By Lemma I.21, there is a function $h : V \to \mathbb{R}$ such that on every face $f =$,

$$\log(R_f) = h_x + h_y - h_u - h_v.$$

If we set $g_x = e^{h_x}$, we get

$$R_f = \frac{g_x g_y}{g_u g_v}$$

and (I.23) becomes

$$\begin{cases} w_1^f = \kappa_f \sqrt{\frac{g_x g_y}{g_u g_v}} \\ w_2^f = \kappa_f \sqrt{\frac{g_u g_v}{g_x g_y}} \\ w_3^f = \kappa_f \sqrt{\frac{g_x g_y + g_u g_v}{g_u g_v}} \\ w_4^f = \kappa_f \sqrt{\frac{g_x g_y + g_u g_v}{g_x g_y}} \\ w_5^f = \kappa_f. \end{cases}$$

Multiplying all weights at a face by a same constant doesn't change the relative weights of loop configurations. Here, if we multiply all weights by $\frac{\sqrt{g_x g_y g_u g_v}}{\kappa_f}$, we get the parametrization (I.11).

Remark I.22. One can prove in exactly the same way that Kashaev's parametrization of the Ising model [Kas96] is possible whenever the underlying quadrangulation satisfies the assumption of Lemma I.21. For instance, the Ising model on any finite isoradial graph admits a Kashaev parametrization.

II – Free-fermion eight-vertex models on a quadrangulation

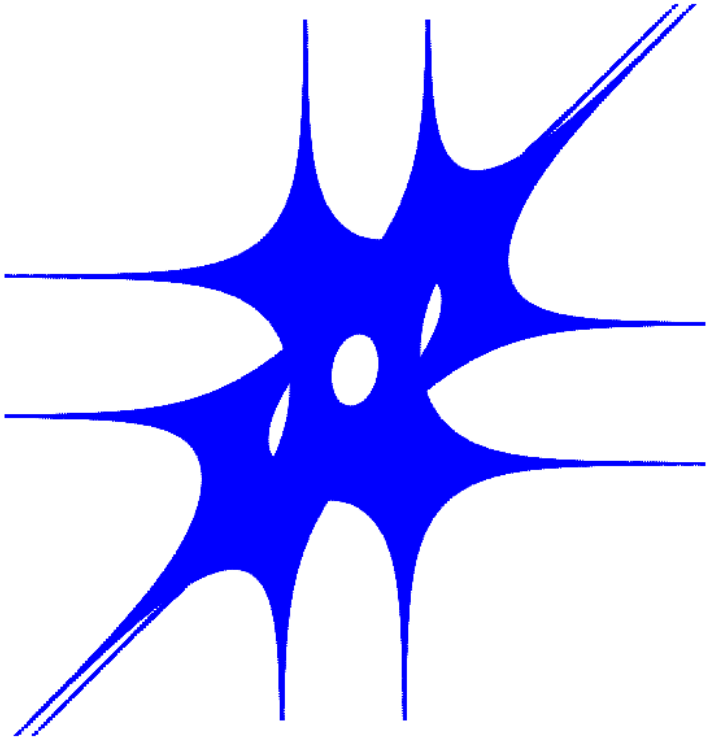

Résumé

Nous étudions le modèle “à huit sommets” dans le régime des fermions libres. Nous exprimons une nouvelle symétrie “d’échange” pour ce modèle, de plusieurs façons différentes : fonctions de partition, variables d’ordre et de désordre, couplages, matrices de Kasteleyn. Cette symétrie peut être utilisée pour relier le modèle à huit sommets en régime fermions libres avec des modèles à six sommets, ou des dimères sur des graphes bipartis. Nous définissons également des nouvelles solutions aux équations de Yang-Baxter dans un cadre “d’échiquier”, et un régime Z-invariant correspondant. En utilisant les dimères bipartis définis par Boutillier, de Tilière et Raschel [BdTR18], nous donnons des formules exactes et locales pour les corrélations entre arêtes du modèle à huit sommets Z-invariant en régime de fermions libres sur un graphe de losanges, et en déduisons la construction d’une mesure de Gibbs ergodique.

Abstract

We study the eight-vertex model at its free-fermion point. We express a new “switching” symmetry of the model in several forms: partition functions, order-disorder variables, couplings, Kasteleyn matrices. This symmetry can be used to relate free-fermion 8V-models to free-fermion 6V-models, or bipartite dimers. We also define new solution of the Yang-Baxter equations in a “checkerboard” setting, and a corresponding Z-invariant model. Using the bipartite dimers of Boutillier, de Tilière and Raschel [BdTR18], we give exact local formulas for edge correlations in the Z-invariant free-fermion 8V-model on rhombic graphs, and we deduce the construction of an ergodic Gibbs measure.

II.1 Introduction

The eight-vertex model, or 8V-model for short, was introduced by Sutherland [Sut70] and Fan and Wu [FW69] as a generalization of the 6V, or ice model [Sla41, Lie67]. The configurations are orientations of the edges of $\mathbb{Z}^2$ such that every vertex has an even number of incoming edges, like in Figure II.1. Equivalently, it can be represented as a polygon, by choosing a checkerboard coloring of the faces of $\mathbb{Z}^2$ and drawing in bold the edges oriented with, say, a white face on their left. The interactions live on vertices and depend on the eight possible local configurations, hence the name. These notions can naturally be extended to graphs that are dual of a planar quadrangulation $\mathcal{Q}$; an example is displayed in Figure II.5.

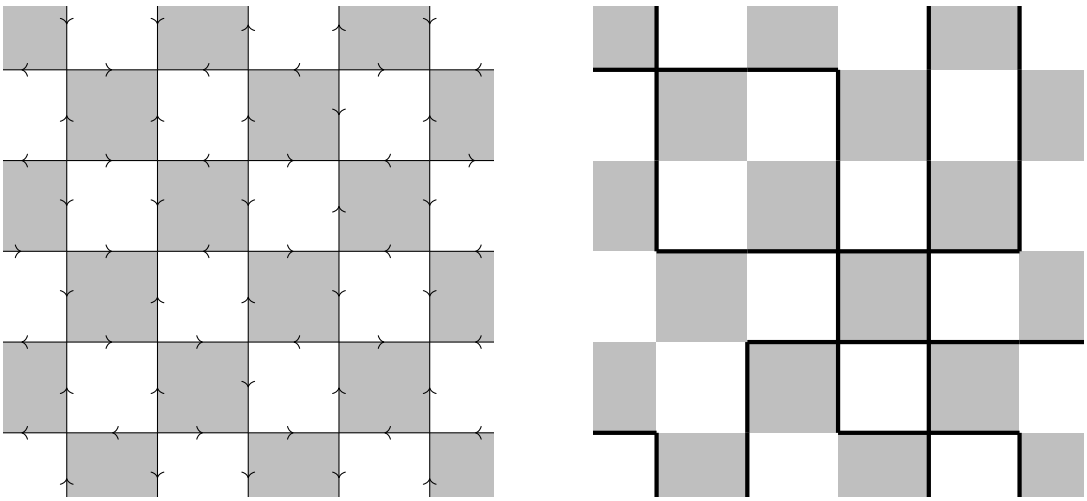

Figure II.1: Two equivalent representations of an eight-vertex configuration on $\mathbb{Z}^2$.

More precisely, the Boltzmann weight of a configuration is the product of local weights associated to local configurations at a face f of the quadrangulation $\mathcal{Q}$, as in Figure II.4, that are denoted $A(f), B(f), C(f), D(f)$. The case of a 6V-model corresponds to $D(f) = 0$ at every face. Notice that complementary configurations have the same weight, which means that we are in a "zero field" case. To make these weights well-defined, notice also that we fixed a bipartite coloring of $\mathcal{Q}$. This is sometimes referred to as a *checkerboard model* [Bax86, BPAY88], or a *staggered* model on the square lattice [HLW75]. Checkerboard (or alternating, or staggered) 8V models have attracted some attention, in particular for their relation with the Ashkin-Teller model [Weg72, Bax82], but little is known about them in general. In this chapter we investigate checkerboard 8V-models that satisfy the *free-fermion* condition defined below; we do so on general quadrangulations, in the hope that it lets us capture properties that are intrinsic to the model.

The 8V-model with constant weights has been famously solved on the square lattice and a few other regular lattices using transfer matrices methods, see [Bax82] and references therein. In particular, the free energy and the different phases of the model are described. At the special *free-fermion* point

$$A^2 + B^2 = C^2 + D^2 \tag{II.1}$$

there exists a different method using a correspondence with non-bipartite dimers, leading

to the computation of Pfaffians [LW77, FW69, HLW75, Lin76, Lin84]. It is also possible to adapt the theory of transfer matrices to the free-fermion case, which makes computation easier than for the complete 8V-model [BS85a, BS85b, BS85c, Fel73c, Fel73a, Fel73b]. The current chapter is based on a "switching" result, that we now explain.

If we multiply all weights $A(f), B(f), C(f), D(f)$ at a face f by the same constant, the relative weight of different 8V-configurations are unchanged; this is known as a *gauge transformation*. Thus an 8V model with weights satisfying the free-fermion condition (II.1) can be effectively represented by two free parameters per face, say $\alpha(f), \beta(f) \in \mathbb{R}/2\pi\mathbb{Z}$; see (II.8) for the exact parametrization. Our parametrization is such that when $\alpha = \beta$, the model becomes a 6V one. We denote by $X_{\alpha,\beta}$ the whole set of weights corresponding to α, β, and by $\mathcal{Z}_{8V}(\mathcal{Q}, X_{\alpha,\beta})$ the partition function; when $\alpha = \beta$, we denote it by $\mathcal{Z}_{6V}(\mathcal{Q}, X_{\alpha,\alpha})$ to emphasize that it becomes a 6V-model. The choice of parameters α, β is such that we have the following "switching" relation, see Theorem II.13 for a precise statement and (II.18) for the value of the constant $c_{\alpha,\beta}$:

Theorem II.1. *Let $\mathcal{Q}$ be a quadrangulation of the sphere. For any $\alpha, \beta, \alpha', \beta'$ satisfying natural hypothesis,*

$$\frac{\mathcal{Z}_{8V}(\mathcal{Q}, X_{\alpha,\beta})}{\sqrt{c_{\alpha,\beta}}} \frac{\mathcal{Z}_{8V}(\mathcal{Q}, X_{\alpha',\beta'})}{\sqrt{c_{\alpha',\beta'}}} = \frac{\mathcal{Z}_{8V}(\mathcal{Q}, X_{\alpha,\beta'})}{\sqrt{c_{\alpha,\beta'}}} \frac{\mathcal{Z}_{8V}(\mathcal{Q}, X_{\alpha',\beta})}{\sqrt{c_{\alpha',\beta}}}.$$

In particular, for $(\alpha', \beta') = (\beta, \alpha)$, this gives

$$(\mathcal{Z}_{8V}(\mathcal{Q}, X_{\alpha,\beta}))^2 = \frac{c_{\alpha,\beta}}{\sqrt{c_{\alpha,\alpha} c_{\beta,\beta}}} \mathcal{Z}_{6V}(\mathcal{Q}, X_{\alpha,\alpha}) \mathcal{Z}_{6V}(\mathcal{Q}, X_{\beta,\beta})$$

which is a new relation between free-fermion 8V-models and 6V ones. The identity of Theorem II.1 is central to this chapter. It suggests that other hidden features of free-fermion 8V-models might exist. We identify several of them.

First, it hints at a possible coupling of pairs of 8V-configurations. If τ, τ' are two 8V-configurations, seen as subsets of the dual edges of $\mathcal{Q}$, their XOR (or symmetric difference) is still an 8V-configuration; we denote it by $\tau \oplus \tau'$. We prove the following, see Theorem II.15 for a precise statement.

Theorem II.2. *Let $\mathcal{Q}$ be a quadrangulation of the sphere. For any standard $\alpha, \beta, \alpha', \beta'$, let $\tau_{\alpha,\beta}, \tau_{\alpha',\beta'}, \tau_{\alpha,\beta'}, \tau_{\alpha',\beta}$ be independent 8V-configurations distributed with the corresponding Boltzmann weights. Then the configurations $\tau_{\alpha,\beta} \oplus \tau_{\alpha',\beta'}$ and $\tau_{\alpha,\beta'} \oplus \tau_{\alpha',\beta}$ are equal in distribution.*

This theorem is proved via the formalism of order-disorder variables [KC71, Dub11a], see Theorem II.13. We also illustrate in Appendix II.A how discrete Fourier theory is a useful object to deduce such statistical results from order-disorder variables.

For $(\alpha', \beta') = (\beta, \alpha)$, Theorem II.2 implies that the XOR of two independent 8V-configurations (with the same distribution) is distributed as the XOR of two independent 6V-configurations (with different distributions). Although being unexpected, this is reminiscent of the coupling identities of [BdT14, Dub11a] on the Ising model. However these previous identities involved two independent Ising models, while our results are naturally associated with four Ising models (see Corollary II.12) and do not seem to be easy consequences of their work.

Second, it is natural to wonder what happens if $\mathcal{Q}$ is a quadrangulation of the torus. This is useful in particular to understand periodic boundary conditions and construct infinite measures on the full plane, as we explain later. In the toric case, the 8V-weights $X_{\alpha,\beta}$ are naturally associated with a characteristic (Laurent) polynomial of two complex variables, denoted $P^{8V}_{\alpha,\beta}(z,w)$, and defined in (II.21) just like in the case of the dimer model [KOS06]. The analogous statement of Theorem II.1 is that (see Theorem II.26 for the precise statement):

Theorem II.3. *Let $\mathcal{Q}$ be a quadrangulation of the torus. For any standard $\alpha,\beta,\alpha',\beta'$,*

$$c_{\alpha,\beta}c_{\alpha',\beta'}\ \ P^{8V}_{\alpha,\beta}(z,w)P^{8V}_{\alpha',\beta'}(z,w) \ = \ c_{\alpha,\beta'}c_{\alpha',\beta}\ \ P^{8V}_{\alpha,\beta'}(z,w)P^{8V}_{\alpha',\beta}(z,w).$$

In particular (see Corollary II.28),

$$P^{8V}_{\alpha,\beta}(z,w) = \tilde{c}\ P^{6V}_{\alpha}(z,w)P^{6V}_{\beta}(z,w).$$

The polynomials P^{6V}_{α} and P^{6V}_{β} correspond to bipartite dimers [WL75, Nie84, Dub11a, BdT14]. The curves defined by their zero locus in $\mathbb{C}^2$ are Harnack curves [KOS06]. Thus the zero locus of $P^{8V}_{\alpha,\beta}$ is the union of two Harnack curves. This can be observed in the amoebae of Figure II.2, where the *amoeba* is the image of the zero locus under the map $(z,w)\mapsto(\log|z|,\log|w|)$.

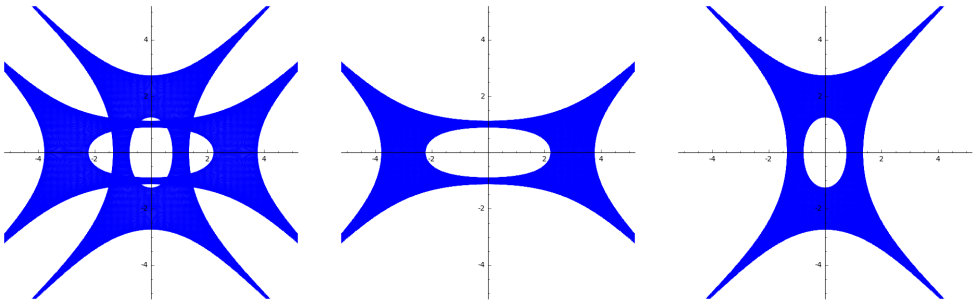

Figure II.2: Amoebae of the curves defined by $P^{8V}_{\alpha,\beta}$, P^{6V}_{α} and P^{6V}_{β} for the square lattice.

Third, the 8V-models at the free-fermion point corresponds to non-bipartite dimers, for which we can define a version of a Kasteleyn matrix $K_{\alpha,\beta}$, see Section II.4.3. The elements of the inverse of $K_{\alpha,\beta}$ are related to the correlations of the 8V-model (see Proposition II.21). It is possible to get a relation between those inverse matrices; precise statements are given in Theorem II.22 on the sphere and in Theorem II.25 on the torus, and the matrix T is defined by (II.28).

Theorem II.4.

$$K^{-1}_{\alpha,\beta} = \frac{1}{2}\left((I+T)K^{-1}_{\alpha,\beta'} + (I-T)K^{-1}_{\alpha',\beta}\right).$$

This has the remarkable property of holding for all α',β', even though this is not apparent in the right-hand-side. Again we can set $(\alpha',\beta')=(\beta,\alpha)$, so that this formula relates 8V-correlations to 6V ones, *i.e.* to bipartite dimers [WL75, Nie84, Dub11a, BdT14]. This is an

important property, as a powerful theory exists to study bipartite dimers [CKP01, KOS06] which is mostly unavailable for non-bipartite dimers. We give several consequences of this identity with the solution of the 8V-model in the Z-invariant regime on lozenge graphs.

A model is said to be *Z-invariant* when it satisfies a form of the Yang-Baxter equations, or a star-triangle transformation (see Figure II.15). In the approach via transfer matrices, this property is often seen as a sufficient condition for the commutativity of transfer matrices [Bax82], see also [Bel79, Dut80]. However it has also been shown by Baxter that the star-triangle move is enough information to guess the behavior of the model on very generic lattices [Bax78], without requiring transfer matrices. In particular, it should imply a form of *locality* for the model, which means that the two-point correlations depend only on a path (any path) between the two points. This property is surprising, since in general correlations are expected to depend on the geometry of the whole graph.

One way to interpret Z-invariance geometrically is to use *isoradial* graphs. For these graphs, the faces of the quadrangulation $\mathcal{Q}$ are supposed to be rhombi with the same edge-length (we call $\mathcal{Q}$ a *lozenge graph*), and the weights $A(f), B(f), C(f), D(f)$ at a face f are supposed to depend on the half-angle θ of the rhombus f at the black vertices. The angles θ satisfy some relations under star-triangle transformation (see Figure II.3), and the goal is to define Boltzmann weights in terms of θ so as to transform these relations into the Yang-Baxter equations. Several Z-invariant models have been studied on lozenge graphs, including the bipartite dimer model [Ken02], Ising model [BdT11, BdTR18], Laplacian (or spanning forest model) [Ken02, BdTR17], random cluster model [DCLM18], etc. The results of [KS05] also imply that we do not lose anything by considering the Yang-Baxter equations on a lozenge graph rather than on a pseudoline arrangement, like that of [Bax78].

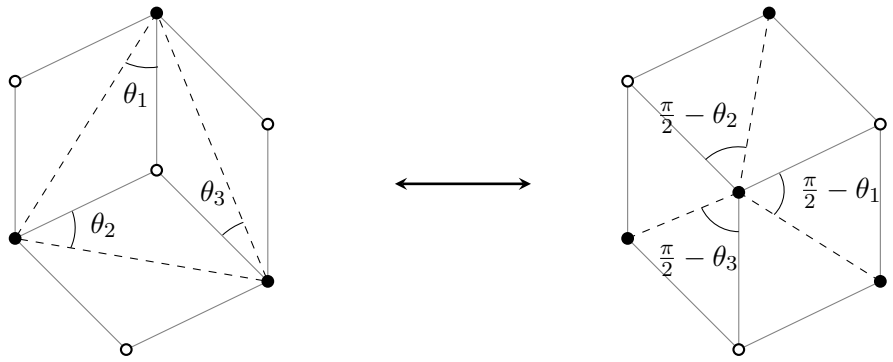

Figure II.3: Star-triangle move on a lozenge graph. The angles satisfy $\theta_1 + \theta_2 + \theta_3 = \frac{\pi}{2}$.

The Z-invariant weights of the 8V model in the non-checkerboard case have been parameterized by Baxter [Bax72, Bax78, Bax82] and Zamolodchikov [Zam79]. Other techniques have appeared since to classify these solutions [SUAW82, GM02, KS13, Vie18]. By considering checkerboard Yang-Baxter equations, more solutions can appear, as noted for instance in [PAY06]. Here we introduce what seems to be the first set of checkerboard Z-invariant weights for the 8V model, but only in the free-fermion case.

Let k, l be complex numbers such that $k^2, l^2 \in (-\infty, 1)$. For any real number x let $x_k = \frac{2\mathrm{K}(k)}{\pi} x$, where $\mathrm{K}(k)$ is the complete elliptic integral of the first kind, and similarly for x_l. Then the following 8V-weights of lozenge graphs, expressed in terms of Jacobi's

elliptic functions (see [AS64, Law89]) at a face f with half-angle θ, satisfy the Yang-Baxter equations:

$$\begin{aligned} A(f) &= \operatorname{sn}(\theta_k|k) + \operatorname{sn}(\theta_l|l) \\ B(f) &= \operatorname{cn}(\theta_k|k) + \operatorname{cn}(\theta_l|l) \\ C(f) &= 1 + \operatorname{sn}(\theta_k|k)\operatorname{sn}(\theta_l|l) + \operatorname{cn}(\theta_k|k)\operatorname{cn}(\theta_l|l) \\ D(f) &= \operatorname{cn}(\theta_k|k)\operatorname{sn}(\theta_l|l) - \operatorname{sn}(\theta_k|k)\operatorname{cn}(\theta_l|l) \end{aligned}. \tag{II.2}$$

We prove this in Proposition II.30. When $(1-k^2)(1-l^2) = 1$ (or $k^* = l$ in the notation of [BdTR18]) the weights no longer depend on the bipartite coloring of $\mathcal{Q}$ (*i.e* if a face f has a half-angle θ and g has a half-angle $\frac{\pi}{2} - \theta$, then $A(f) = B(g)$, etc.), and we recover Baxter's solution in the free-fermion case. When $k = l$ we get a Z-invariant 6V model whose corresponding dimer model can be found in [BdTR18]. At this point we do not know if such parameterizations of the checkerboard Yang-Baxter equations exist outside of the free-fermion manifold.

Using Theorem II.4, we are able to relate the correlations for the Z-invariant weights (II.2) to the bipartite dimers of [BdTR18]. In [BdTR18] the authors give explicit, local formulas for the correlations and deduce the construction of an ergodic Gibbs measure on any lozenge graphs of the whole plane. Consequently, we get the same kind of results for our Z-invariant 8V-model, confirming in that case the prediction of Baxter that correlations are given by local formulas.

We can also deduce the asymptotics of coefficients from [BdTR18]: under some technical hypothesis, we show that when $0 < k < l < 1$ the coefficients of the inverse Kasteleyn matrix between points at distance r decays as $r^{-\frac{1}{2}} e^{-r/\zeta_k}$ (see Corollary II.36). Notice that the effect of l vanishes in the asymptotics. When $k = 0$ the decay is polynomial, corresponding to a critical model. When $k \to 0$, we prove that the quantity ζ_k is a $\Theta(k^{-2})$ in Proposition II.37. As k^2 plays the role of $(\beta - \beta_c)$ in usual statistical mechanics terms, this critical exponent is compatible with that of the correlation length, $\nu = 1$, in the universality class of the Ising model (see Section 7.12 of [Bax82]).

Finally, the exact computation of correlations allows for the construction of an ergodic Gibbs measure in the full plane, using the procedure of [KOS06].

Outline of the chapter

In Section II.2 we properly define the 8V, Ising and dimer models in spherical, toric and planar settings. We also introduce the formalism of order-disorder correlators.

In Section II.3 we restrict ourselves to the spherical case. We compute the correlators of free-fermion 8V models and relate them to Ising ones, generalizing results of [Dub11a], see Corollary II.12. We prove the coupling result of Theorem II.2, first in correlators terms (Theorem II.13), then in probabilistic terms (Theorem II.15). The latter is deduced from the former by using a discrete Fourier transformation described in Appendix II.A. The results of Section II.3 imply Theorem II.1. Sections II.4 and II.5 are independent of Section II.3.

In Section II.4 we define the dimer model associated to the 8V-model, and appropriate versions of Kasteleyn matrices, one being skew-symmetric and the other being skew-hermitian; they are related by a diagonal conjugation, see Lemma II.19. We show that the

edge correlations can be expressed as minors of the inverse Kasteleyn matrices, see Proposition II.21. We prove the relation of inverses of Theorem II.4. This gives an alternative proof of Theorem II.1, as well as its toric counterpart, Theorem II.3.

In Section II.5 we prove that the weights (II.2) satisfy the Yang-Baxter equations. Using the relation to 6V models coming from Section II.4, we give a local formula for the inverse Kasteleyn matrix in the full plane in Section II.5.3. We prove the mentioned asymptotics and critical exponent in Corollary II.36 and Proposition II.37. Finally we construct an ergodic Gibbs measure in the Z-invariant case in Section II.5.4.

Acknowledgements

I am very grateful to Cédric Boutillier and Béatrice de Tilière for the motivation of this chapter, as well as their help and supervision. I also thank Béatrice de Tilière for her critical help in proving Theorem II.26. I am grateful to Yacine Ikhlef for useful discussions.

II.2 Definitions

Let $\mathcal{Q}$ be a *quadrangulation* of a surface $\mathcal{S}$, that is a finite connected graph $\mathcal{Q} = (\mathcal{V}, \mathcal{E})$, without multi-edges and self-loops, embedded on $\mathcal{S}$ so that edges do not intersect, and so that the *faces* of $\mathcal{Q}$ are homeomorphic to disks and have degree 4. We denote by $\mathcal{F}$ its set of faces. We will focus on three cases:

- *the spherical case* where $\mathcal{S}$ is the two-dimensional sphere and $\mathcal{Q}$ is finite;
- *the planar case* where $\mathcal{S}$ is $\mathbb{R}^2$ and $\mathcal{Q}$ is infinite and covers the whole plane;
- *the toric case* where $\mathcal{S}$ is the two-dimensional torus and $\mathcal{Q}$ is finite and bipartite.

Since $\mathcal{Q}$ is bipartite in all these cases, we can fix a partition of $\mathcal{V}$ into a set of black vertices $\mathcal{B}$ and white vertices $\mathcal{W}$, such that edges only connect black and white vertices together. We also set $G^{\mathcal{B}}$ (resp. $G^{\mathcal{W}}$) to be the graph formed by black (resp. white) vertices, joined *iff* they form the diagonal of a face of $\mathcal{Q}$. Finally, in the toric case, we suppose that there are two simple cycles $\gamma_x^{\mathcal{B}}$ and $\gamma_y^{\mathcal{B}}$ on $G^{\mathcal{B}}$ that wind once, respectively horizontally and vertically on the torus; see Figure II.12.

The dual of $\mathcal{Q}$, denoted by $\mathcal{Q}^*$, is the embedded graph whose set of vertices is $\mathcal{F}$ and which has edges connecting elements of $\mathcal{F}$ that are adjacent in $\mathcal{Q}$. We denote by $\mathcal{E}^*$ the set of edges of $\mathcal{Q}^*$; for an edge $e \in \mathcal{E}$, we denote by e^* its corresponding dual edge.

II.2.1 Eight-vertex-model

An 8V-configuration is a subset $\tau \subset \mathcal{E}^*$ such that, at each face $f \in \mathcal{F}$, an even number of dual edges that belong to τ meet at f. Thus at any face $f \in \mathcal{F}$, τ has to be one of the eight types shown in Figure II.4. Let $\Omega(\mathcal{Q})$ be the set of all 8V-configurations on $\mathcal{Q}$.

Let A, B, C, D be four functions from $\mathcal{F}$ to $\mathbb{R}$. We associate to f a local weight function w_f, such that $w_f(\tau)$ is either $A(f), B(f), C(f)$ or $D(f)$ depending on the local configuration, as in Figure II.4. In the spherical and toric cases, the global weight of τ is defined as

$$w_{8V}(\tau) = \prod_{f \in \mathcal{F}} w_f(\tau). \tag{II.3}$$

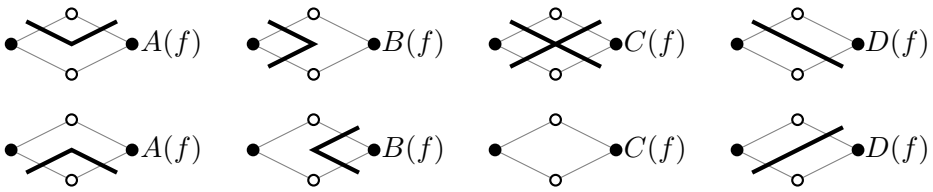

Figure II.4: The eight possible configurations for τ at a face $f \in \mathcal{F}$ and their local weight $w_f(\tau)$.

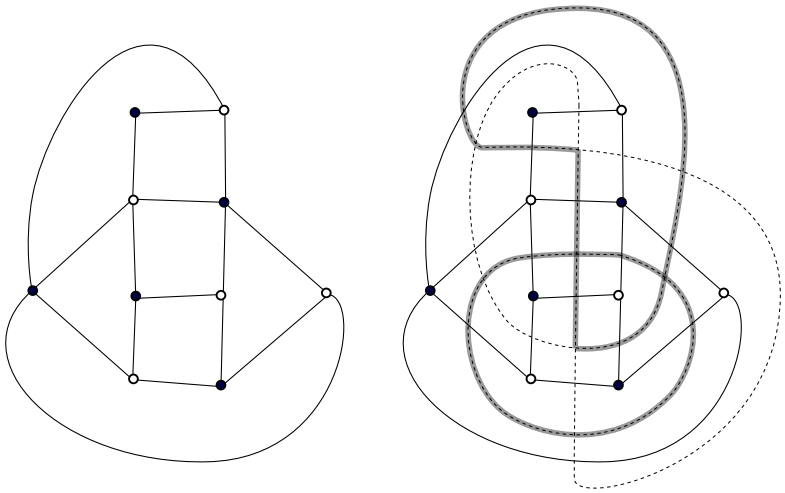

Figure II.5: Left: a quadrangulation $\mathcal{Q}$ in the spherical case. Right: the same quadrangulation with its dual $\mathcal{Q}^*$ (dashed) and an eight-vertex configuration.

It is more difficult to make sense of formula (II.3) in the planar case, where the product becomes infinite, requiring the construction of an appropriate Gibbs measure. We discuss this construction in the case of a Z-invariant, free-fermion model in Section II.5.4.

For the remainder of this section, we only deal with the spherical and toric cases. Let $X = (A, B, C, D)$ denote the whole set of weights. The partition function of the model is

$$\mathcal{Z}_{8V} = \mathcal{Z}_{8V}(\mathcal{Q}, X) = \sum_{\tau \in \Omega(\mathcal{Q})} w_{8V}(\tau).$$

When the weights X take values in positive real numbers, the Boltzmann measure associated to X is the probability measure on $\Omega(\mathcal{Q})$ defined by

$$\mathbb{P}_{8V}(\tau) = \frac{w(\tau)}{\mathcal{Z}_{8V}}. \tag{II.4}$$

Even if we are only interested in the positive real values *in fine*, it is convenient to let the weights X take any real values. In this case, $w(\tau)$ and $\mathcal{Z}_{8V}$ are still well-defined but (II.4) does not define a probability measure.

A *gauge transformation* at some face $f \in \mathcal{F}$ consists in multiplying the weights $A(f), B(f), C(f), D(f)$ by the same constant $\lambda \neq 0$. This has the effect of multiplying all weights $w_{8V}(\tau)$ by λ, and $\mathcal{Z}_{8V}$ is also multiplied by λ. Thus the Boltzmann measure is unchanged.

The weights $X = (A, B, C, D)$ are said to be *free-fermion* if

$$\forall f \in \mathcal{F},\ A(f)^2 + B(f)^2 = C(f)^2 + D(f)^2.$$

They are said to be *standard* if

$$\forall f \in \mathcal{F},\ C(f) \neq 0.$$

Lemma II.5. *Let a, b, c, d be real numbers such that $c \neq 0$ and*

$$a^2 + b^2 = c^2 + d^2. \tag{II.5}$$

Then there exists a couple $(\alpha, \beta) \in (\mathbb{R}/2\pi\mathbb{Z})^2$ such that in homogeneous coordinates,

$$\Big[a : b : c : d\Big] = \begin{bmatrix} \sin\alpha + \sin\beta : \\ \cos\alpha + \cos\beta : \\ 1 + \sin\alpha\sin\beta + \cos\alpha\cos\beta : \\ \cos\alpha\sin\beta - \sin\alpha\cos\beta \end{bmatrix} \tag{II.6}$$

$$= \left[\sin\left(\tfrac{\alpha+\beta}{2}\right) : \cos\left(\tfrac{\alpha+\beta}{2}\right) : \cos\left(\tfrac{\alpha-\beta}{2}\right) : \sin\left(\tfrac{-\alpha+\beta}{2}\right)\right]. \tag{II.7}$$

Proof. We can rewrite (II.5) as

$$\left(\frac{a}{\lambda}\right)^2 + \left(\frac{b}{\lambda}\right)^2 = \left(\frac{c}{\lambda}\right)^2 + \left(\frac{d}{\lambda}\right)^2 = 1$$

for some constant $\lambda > 0$. Thus there exists $u, v \in \mathbb{R}/2\pi\mathbb{Z}$ such that

$$[a : b : c : d] = [\sin u : \cos u : \cos v : -\sin v].$$

Then we define $\alpha = u + v, \beta = u - v$, which gives the form (II.7) of the homogeneous coordinates. The form (II.6) is obtained by multiplying all weights of (II.7) by $2\cos\left(\frac{\alpha-\beta}{2}\right)$, which is non zero because $c \neq 0$, and performing simple trigonometric computations. □

For that reason, we fix two functions $\alpha, \beta : \mathcal{F} \to \mathbb{R}/2\pi\mathbb{Z}$ and we define the associated free-fermion weights by the following formula, implicitly evaluated at any $f \in \mathcal{F}$:

$$X_{\alpha,\beta} = \begin{pmatrix} A_{\alpha,\beta} \\ B_{\alpha,\beta} \\ C_{\alpha,\beta} \\ D_{\alpha,\beta} \end{pmatrix} = \begin{pmatrix} \sin\alpha + \sin\beta \\ \cos\alpha + \cos\beta \\ 1 + \sin\alpha\sin\beta + \cos\alpha\cos\beta \\ \cos\alpha\sin\beta - \sin\alpha\cos\beta \end{pmatrix}. \tag{II.8}$$

By Lemma II.5, any standard free-fermion 8V-model can be written in this way, after proper gauge transformations.

Remark II.6.

- The weights $X_{\alpha,\beta}$ satisfy

$$2C_{\alpha,\beta} = A_{\alpha,\beta}^2 + B_{\alpha,\beta}^2 = C_{\alpha,\beta}^2 + D_{\alpha,\beta}^2. \tag{II.9}$$

  As a result, given standard free-fermion 8V-weights $X = (A, B, C, D)$, one gets to the weights $X_{\alpha,\beta}$ by applying gauge transformations at each face with parameter $\lambda(f) = \frac{2C(f)}{A(f)^2+B(f)^2}$.

- The weight $X_{\alpha,\beta}$ are standard *iff*

$$\forall f \in \mathcal{F},\ \alpha(f) - \beta(f) \neq \pi[2\pi]. \tag{II.10}$$

We also say that α, β are *standard* when (II.10) is satisfied. Note that if this is not the case at some face $f \in \mathcal{F}$, then all the weights $A(f), B(f), C(f), D(f)$ vanish.

- If α, β lie in the range

$$\forall f \in \mathcal{F},\ 0 < \alpha(f) \leq \beta(f) < \frac{\pi}{2} \tag{II.11}$$

then the weights $A_{\alpha,\beta}, B_{\alpha,\beta}, C_{\alpha,\beta}$ are positive and $D_{\alpha,\beta}$ is non-negative. As a result, the Boltzmann measure is a probability measure.

- If $\alpha = \beta$, then the weights $D_{\alpha,\beta}$ vanish and we are left with a 6V model. We simply denote X_α the weights in that case, and $\mathcal{Z}_{6V}(\mathcal{Q}, X_\alpha)$ for the partition function. We have

$$[A_\alpha : B_\alpha : C_\alpha] = [\sin\alpha : \cos\alpha : 1].$$

- Switching α and β has the effect of multiplying the weights D by -1. Since any 8V-configuration contains an even number of D faces (see [Dub11a]), in both the spherical and toric cases,

$$\mathcal{Z}_{8V}(\mathcal{Q}, X_{\alpha,\beta}) = \mathcal{Z}_{8V}(\mathcal{Q}, X_{\beta,\alpha}). \tag{II.12}$$

II.2.2 Ising model

Let $\alpha, \beta : \mathcal{F} \to (0, \frac{\pi}{2})$. Let $J^\alpha_{\mathcal{B}}, J^\beta_{\mathcal{W}} : \mathcal{F} \to \mathbb{R}$ be the following *coupling constants*:

$$\forall f \in \mathcal{F}, \quad J^\alpha_{\mathcal{B}}(f) = \frac{1}{2}\ln\left(\frac{1+\sin\alpha(f)}{\cos\alpha(f)}\right), \qquad J^\beta_{\mathcal{W}}(f) = \frac{1}{2}\ln\left(\frac{1+\cos\beta(f)}{\sin\beta(f)}\right).$$

An *spin configuration* on $G^{\mathcal{B}}$ (resp. $G^{\mathcal{W}}$) is an application from $\mathcal{B}$ (resp. $\mathcal{W}$) to $\{\pm 1\}$. The weight of such a configuration $\sigma_{\mathcal{B}}$ (resp. $\sigma_{\mathcal{W}}$) is defined as

$$w_{\mathcal{B}}(\sigma_{\mathcal{B}}) = \prod_{f\in\mathcal{F}} e^{J^\alpha_{\mathcal{B}}(f)\ \sigma_u\sigma_v}, \qquad w_{\mathcal{W}}(\sigma_{\mathcal{W}}) = \prod_{f\in\mathcal{F}} e^{J^\beta_{\mathcal{W}}(f)\ \sigma_x\sigma_y},$$

where u, v are the black vertices of f, and x, y its white vertices.

The partition functions are:

$$\mathcal{Z}^{\mathcal{B}}_{\text{Ising}} = \mathcal{Z}^{\mathcal{B}}_{\text{Ising}}(J^\alpha_{\mathcal{B}}) = \sum_{\sigma_{\mathcal{B}}} w_{\mathcal{B}}(\sigma_{\mathcal{B}}), \qquad \mathcal{Z}^{\mathcal{W}}_{\text{Ising}} = \mathcal{Z}^{\mathcal{W}}_{\text{Ising}}(J^\beta_{\mathcal{W}}) = \sum_{\sigma_{\mathcal{W}}} w_{\mathcal{W}}(\sigma_{\mathcal{W}}),$$

where the sums are over spin configurations. Again, the associated Boltzmann measure is

$$\mathbb{P}^{\mathcal{B}}_{\text{Ising}}(\sigma_{\mathcal{B}}) = \frac{w_{\mathcal{B}}(\sigma_{\mathcal{B}})}{\mathcal{Z}^{\mathcal{B}}_{\text{Ising}}}, \qquad \mathbb{P}^{\mathcal{W}}_{\text{Ising}}(\sigma_{\mathcal{W}}) = \frac{w_{\mathcal{W}}(\sigma_{\mathcal{W}})}{\mathcal{Z}^{\mathcal{W}}_{\text{Ising}}}.$$

II.2.3 Dimer model

Let $G = (V, E)$ be a finite graph, equipped with real weights on the edges $(\nu_e)_{e\in E}$. A *dimer configuration*, or *perfect matching*, is a subset of edges $m \subset E$ such that every vertex of G is adjacent to exactly one edge of m. We denote by $\mathcal{M}(G)$ the set of all dimer configurations on G.

The Boltzmann measure on $\mathcal{M}(G)$ is defined by

$$\mathbb{P}_{\mathrm{dim}}(m) = \frac{\prod_{e\in m} \nu_e}{\mathcal{Z}_{\mathrm{dim}}(G, \nu)}$$

where $\mathcal{Z}_{\mathrm{dim}}(G, \nu)$ is the partition function:

$$\mathcal{Z}_{\mathrm{dim}}(G, \nu) = \sum_{m\in\mathcal{M}(G)} \prod_{e\in m} \nu_e.$$

II.2.4 Order and disorder variables

The notions of order and disorder variables were defined by Kadanoff and Ceva for the Ising model [KC71] and play a central role in the study of spinor and fermionic observables; see for instance [CCK17] for a unifying review. The definition for the Ising model is classical; for the 8V model, we adapt definitions of Dubédat [Dub11a].

For these definitions $\mathcal{Q}$ can be a quadrangulation in the spherical or toric case.

a) Ising correlators

Let $B_0 \subset \mathcal{B}$ and $W_1 \subset \mathcal{W}$ be two subset of black and white vertices of $\mathcal{Q}$, of even cardinality. Let γ_{B_0} be the union of disjoint simple paths on $G^{\mathcal{B}}$ that connect the vertices of B_0 pairwise (these are called *order lines*); γ_{B_0} can be alternatively seen as a subset of $\mathcal{F}$. We similarly define γ_{W_1} as a union of disjoint simple paths on $G^{\mathcal{W}}$ that connect the W_1 pairwise (also called *disorder lines*).

Let $\alpha : \mathcal{F} \to (0, \frac{\pi}{2})$. We modify the coupling constants $J^{\alpha}_{\mathcal{B}}$ by adding $i\frac{\pi}{2}$ to the coupling constant at f when $f \in \gamma_{B_0}$, and afterwards multiplying the coupling constant by -1 when $f \in \gamma_{W_1}$ (the order is important). Let J' be these new coupling constants. Then the *mixed correlator* of Kadanoff and Ceva is defined as

$$\left\langle \prod_{b\in B_0} \sigma_b \prod_{w\in W_1} \mu_w \right\rangle^{\mathrm{Ising}\mathcal{B}}_{\alpha,\gamma_{B_0},\gamma_{W_1}} = \langle \sigma(B_0)\mu(W_1)\rangle^{\mathrm{Ising}\mathcal{B}}_{\alpha,\gamma_{B_0},\gamma_{W_1}} := \mathcal{Z}^{\mathcal{B}}_{\mathrm{Ising}}(J').$$

This depends on the choice of paths and the order of operations on the coupling constants, but only up to a global sign. The *order* variables are simply the spins σ_b, with $\langle\cdot\rangle$ representing an unnormalized expectation under the Boltzmann measure. The *disorder* variables μ_w represent defects in the configuration, and are conjugated with order variables under Kramers-Wannier duality [KW41]. Again we refer to [KC71].

Similarly for the Ising model on $G^{\mathcal{W}}$, if $W_0 \subset \mathcal{W}$ and $B_1 \subset \mathcal{B}$ are even subsets, we chose paths $\gamma_{W_0}, \gamma_{B_1}$. Then for $\beta : \mathcal{F} \to (0, \frac{\pi}{2})$, we add $i\frac{\pi}{2}$ to the constants $J^{\mathcal{W}}_{\beta}$ on γ_{W_0}, then multiply the constants by -1 on γ_{B_1}, and we name the new constants J''. The mixed

correlator is

$$\left\langle \prod_{w\in W_0}\sigma_w \prod_{b\in B_1}\mu_b \right\rangle^{\mathrm{Ising}\mathcal{W}}_{\beta,\gamma_{W_0},\gamma_{B_1}} = \langle\sigma(W_0)\mu(B_1)\rangle^{\mathrm{Ising}\mathcal{W}}_{\beta,\gamma_{W_0},\gamma_{B_1}} := \mathcal{Z}^{\mathcal{W}}_{\mathrm{Ising}}(J'').$$

b) 8V correlators

Order and disorder variables for the 8V-model are defined in [Dub11a]. The following definition is original but it is easy to check that it is equivalent to that of [Dub11a]. In the 8V case, order and disorder variables can be located on either black or white vertices of $\mathcal{Q}$.

Definition II.7. Let $\mathcal{Q}$ be a quadrangulation in the spherical case. Let $X = (A, B, C, D) : \mathcal{F} \to \mathbb{R}^4$ be a family of weights. For every $f \in \mathcal{F}$, we define operators $\nu^{\mathcal{B}}_f, \nu^{\mathcal{W}}_f, \xi^{\mathcal{B}}_f, \xi^{\mathcal{W}}_f$ that act on X by transforming $X(f)$ in the following way:

$$\nu^{\mathcal{B}}_f : \begin{pmatrix} A(f)\\ B(f)\\ C(f)\\ D(f)\end{pmatrix} \mapsto \begin{pmatrix} A(f)\\ -B(f)\\ C(f)\\ -D(f)\end{pmatrix} \qquad \nu^{\mathcal{W}}_f : \begin{pmatrix} A(f)\\ B(f)\\ C(f)\\ D(f)\end{pmatrix} \mapsto \begin{pmatrix} -A(f)\\ B(f)\\ C(f)\\ -D(f)\end{pmatrix}$$

$$\xi^{\mathcal{B}}_f : \begin{pmatrix} A(f)\\ B(f)\\ C(f)\\ D(f)\end{pmatrix} \mapsto \begin{pmatrix} C(f)\\ D(f)\\ A(f)\\ B(f)\end{pmatrix} \qquad \xi^{\mathcal{W}}_f : \begin{pmatrix} A(f)\\ B(f)\\ C(f)\\ D(f)\end{pmatrix} \mapsto \begin{pmatrix} D(f)\\ C(f)\\ B(f)\\ A(f)\end{pmatrix}$$

Let $B_0, B_1 \subset \mathcal{B}$ (resp. $W_0, W_1 \subset \mathcal{W}$) be two even subsets of black (resp. white) vertices, with simple paths $\gamma_{B_0}, \gamma_{B_1}$ (resp. $\gamma_{W_0}, \gamma_{W_1}$) joining them pairwise. As these paths use black (resp. white) diagonals of faces, we can identify them with subsets of $\mathcal{F}$. Let $\gamma = (\gamma_B, \gamma_W, \gamma_{B'}, \gamma_{W'})$. We define modified weights X'_γ obtained by the following composition of operators:

$$X'_\gamma = \left(\prod_{f\in\gamma_{B_1}} \xi^{\mathcal{B}}_f \prod_{f\in\gamma_{W_1}} \xi^{\mathcal{W}}_f \prod_{f\in\gamma_{B_0}} \nu^{\mathcal{B}}_f \prod_{f\in\gamma_{W_0}} \nu^{\mathcal{W}}_f \right) X. \tag{II.13}$$

We define the *mixed correlator* as:

$$\left\langle \prod_{b\in B_0}\sigma_b \prod_{w\in W_0}\sigma_w \prod_{b\in B_1}\mu_b \prod_{w\in W_1}\mu_w \right\rangle^{8V}_{X,\gamma} := \mathcal{Z}_{8V}(X'_\gamma).$$

We will also use the shorthand notation $\langle\sigma(B_0)\sigma(W_0)\mu(B_1)\mu(W_1)\rangle^{8V}_{X,\gamma}$.

Remark II.8.

- Mixed correlators may depend on the set of paths γ, but only up to a global sign [Dub11a]. Also note that in (II.13) we always apply order operators before disorder ones. This is important because these operators do not always commute. The only cases were they do not commute are

$$\nu^{\mathcal{B}}_f \xi^{\mathcal{W}}_f = -\xi^{\mathcal{W}}_f \nu^{\mathcal{B}}_f,$$
$$\nu^{\mathcal{W}}_f \xi^{\mathcal{B}}_f = -\xi^{\mathcal{B}}_f \nu^{\mathcal{W}}_f,$$

but like for path dependence, changing the order might only multiply the correlator by a factor -1.

- Again these correlators can be interpreted as unnormalized expectations under the Boltzmann measure. If $b, b' \in B_0$, then the couple of order variables $\sigma_b \sigma_{b'}$ represents the random variable $(-1)^n$ where n is the number of edges in the 8V configuration on any path on $\mathcal{Q}$ between b and b'.

  The disorder variables are equivalent to modifying every eight-vertex configuration by applying a XOR with the configuration of "half edges" shown in Figure II.6. The resulting "configuration" is no longer a subset of edges of $\mathcal{Q}$, but we could still define its weight as in (II.3). The advantage of modifying weights with the operators of Definition II.7 is that we never actually have to work with these *disordered* configurations.

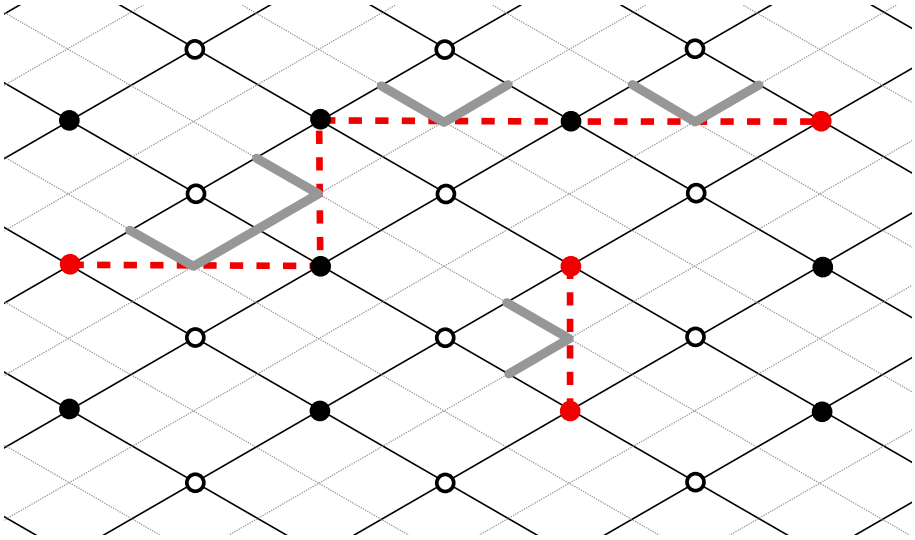

Figure II.6: A piece of a quadrangulation, a subset $B_1 \subset \mathcal{B}$ with paths γ_{B_1} joining them pairwise (dashed), and a partial configuration (bold grey)

II.3 Couplings of 8V-models

We review classical results on the Ising-8V correspondence [Bax78], on the 8V duality [Wu69], in terms of order and disorder variables [Dub11a]. We then apply them to prove couplings results for different free-fermion 8V-models.

II.3.1 Spin-vertex correspondence

The spin-vertex correspondence comes from the following simple remark, that seems to be due to Baxter [Bax78]. If we superimpose two spin configurations, one on $G^{\mathcal{B}}$ and one on $G^{\mathcal{W}}$, and we draw the interfaces between $+1$ and -1 spins, we get an 8V-configuration. This transformation is two-to-one, and can be made weight-preserving by choosing the appropriate 8V weights.

Proposition II.9 ([Bax78, Dub11a])**.** *Let $\mathcal{Q}$ be a quadrangulation in the spherical case, and $\alpha, \beta : \mathcal{F} \to (0, \frac{\pi}{2})$. Consider the 8V-weights $X : \mathcal{F} \to \mathbb{R}^4$ given by*

$$X = \begin{pmatrix} e^{J^\alpha_{\mathcal{B}} - J^\beta_{\mathcal{W}}} \\ e^{-J^\alpha_{\mathcal{B}} + J^\beta_{\mathcal{W}}} \\ e^{J^\alpha_{\mathcal{B}} + J^\beta_{\mathcal{W}}} \\ e^{-J^\alpha_{\mathcal{B}} - J^\beta_{\mathcal{W}}} \end{pmatrix}. \tag{II.14}$$

Then for any B_0, B_1, W_0, W_1 and paths γ as in Definition II.7,

$$2\,\langle \sigma(B_0)\sigma(W_0)\mu(B_1)\mu(W_1)\rangle^{8V}_{X,\gamma} = \langle \sigma(B_0)\mu(W_1)\rangle^{Ising\mathcal{B}}_{\alpha,\gamma_{B_0},\gamma_{W_1}} \ \langle \sigma(W_0)\mu(B_1)\rangle^{Ising\mathcal{W}}_{\beta,\gamma_{W_0},\gamma_{B_1}}.$$

In particular,

$$2\mathcal{Z}_{8V}(\mathcal{Q}, X) = \mathcal{Z}^{\mathcal{B}}_{Ising}\,(J^\alpha_{\mathcal{B}}) \times \mathcal{Z}^{\mathcal{W}}_{Ising}(J^\beta_{\mathcal{W}}).$$

II.3.2 Modifications of weights

One key feature of the 8V-model is its duality relation. This is an instance of Kramers-Wannier duality [KW41], and in the case of the eight-vertex model it was discovered by Wu [Wu69] using high-temperature expansion techniques. The formulation for correlators comes from Dubédat [Dub11a], and means that duality exchanges order and disorder. We give an interpretation in terms of discrete Fourier transform in Appendix II.A.

Proposition II.10 ([Wu69, Dub11a])**.** *Let $\mathcal{Q}$ be a quadrangulation in the spherical case, and let $X = (A, B, C, D) : \mathcal{F} \to \mathbb{R}^4$ be any 8V-weights. Let $\hat{X} = (\hat{A}, \hat{B}, \hat{C}, \hat{D})$ be defined by*

$$\forall f \in \mathcal{F},\ \begin{pmatrix} \hat{A}(f) \\ \hat{B}(f) \\ \hat{C}(f) \\ \hat{D}(f) \end{pmatrix} = \frac{1}{2} \begin{pmatrix} 1 & -1 & 1 & -1 \\ -1 & 1 & 1 & -1 \\ 1 & 1 & 1 & 1 \\ -1 & -1 & 1 & 1 \end{pmatrix} \begin{pmatrix} A(f) \\ B(f) \\ C(f) \\ D(f) \end{pmatrix}. \tag{II.15}$$

Then for any B_0, B_1, W_0, W_1 and paths γ as in Definition II.7, let $\hat{\gamma} = (\gamma_{B_1}, \gamma_{W_1}, \gamma_{B_0}, \gamma_{W_0})$; we have

$$\langle \sigma(B_0)\sigma(W_0)\mu(B_1)\mu(W_1)\rangle^{8V}_{X,\gamma} = \langle \sigma(B_1)\sigma(W_1)\mu(B_0)\mu(W_0)\rangle^{8V}_{\hat{X},\hat{\gamma}}.$$

In particular,

$$\mathcal{Z}_{8V}(\mathcal{Q}, X) = \mathcal{Z}_{8V}(\mathcal{Q}, \hat{X}). \tag{II.16}$$

Another transformation of weights consists in multiplying all weights $D(f)$ by -1. As any 8V-configuration contains an even number of faces of type D, this does not change its global weight. However, in correlators containing disorder operators, the effect is non trivial; a result of [Dub11a] is that μ variables become $\sigma\mu$, while σ variables are unchanged, we rephrase it here using symmetric differences $\triangle$.

Proposition II.11 ([Dub11a])**.** *Let $\mathcal{Q}$ be a quadrangulation in the spherical case, and let $X = (A, B, C, D) : \mathcal{F} \to \mathbb{R}^4$ be any 8V-weights. Let $X' = (A, B, C, -D)$.*

Then for any B_0, B_1, W_0, W_1 and paths γ as in Definition II.7, let $\gamma' = (\gamma_{B_0} \triangle \gamma_{B_1}, \gamma_{W_0} \triangle \gamma_{W_1}, \gamma_{B_1}, \gamma_{W_1})$; we have

$$\langle \sigma(B_0)\sigma(W_0)\mu(B_1)\mu(W_1)\rangle^{8V}_{X,\gamma} = \langle \sigma(B_0 \triangle B_1)\sigma(W_0 \triangle W_1)\mu(B_1)\mu(W_1)\rangle^{8V}_{X',\gamma'}.$$

In particular,

$$\mathcal{Z}_{8V}(\mathcal{Q}, X) = \mathcal{Z}_{8V}(\mathcal{Q}, X').$$

II.3.3 Free-fermion 8V correlators

By combining the previous results, we can relate free-fermion 8V correlations with Ising ones. This has been done in [Dub11a] when the Ising models are dual of each other (which in our case corresponds to $\alpha = \beta$), but the proof works identically when this is not the case.

Corollary II.12. *Let $\mathcal{Q}$ be a quadrangulation in the spherical case, and let $\alpha, \beta : \mathcal{F} \to (0, \frac{\pi}{2})$.*

For any B_0, B_1, W_0, W_1 and paths γ as in Definition II.7, let $\gamma_{\mathcal{B}} = (\gamma_{B_0}, \gamma_{W_0} \triangle \gamma_{W_1})$ and $\gamma_{\mathcal{W}} = (\gamma_{W_0}, \gamma_{B_0} \triangle \gamma_{B_1})$. Then

$$\langle \sigma(B_0)\sigma(W_0)\mu(B_1)\mu(W_1)\rangle^{8V}_{X_{\alpha,\beta},\gamma} = \; c_0 \; \langle \sigma(B_0)\mu(W_0 \triangle W_1)\rangle^{Ising\mathcal{B}}_{\alpha,\gamma_{\mathcal{B}}} \; \langle \sigma(W_0)\mu(B_0 \triangle B_1)\rangle^{Ising\mathcal{W}}_{\beta,\gamma_{\mathcal{W}}} \tag{II.17}$$

where

$$c_0 = \frac{1}{2} \prod_{f \in \mathcal{F}} \sqrt{\cos\alpha(f) \sin\beta(f) C_{\alpha,\beta}(f)}.$$

In particular,

$$\mathcal{Z}_{8V}(\mathcal{Q}, X_{\alpha,\beta}) = c_0 \; \mathcal{Z}^{\mathcal{B}}_{Ising}(J^{\alpha}_{\mathcal{B}}) \; \mathcal{Z}^{\mathcal{W}}_{Ising}(J^{\beta}_{\mathcal{W}}).$$

Proof. From Proposition II.9, the product of Ising correlators on the right-hand side of (II.17) is equal to

$$2\,\langle \sigma(B_0)\sigma(W_0)\mu(B_0 \triangle B_1)\mu(W_0 \triangle W_1)\rangle^{8V}_{X,(\gamma_{\mathcal{B}},\gamma_{\mathcal{W}})}$$

for the weights $X = (A, B, C, D)$ given by

$$\begin{cases} A = e^{J^{\alpha}_{\mathcal{B}} - J^{\beta}_{\mathcal{W}}} = \sqrt{\frac{1+\sin\alpha}{\cos\alpha}\frac{\sin\beta}{1+\cos\beta}}, \\ B = e^{-J^{\alpha}_{\mathcal{B}} + J^{\beta}_{\mathcal{W}}} = \sqrt{\frac{\cos\alpha}{1+\sin\alpha}\frac{1+\cos\beta}{\sin\beta}}, \\ C = e^{J^{\alpha}_{\mathcal{B}} + J^{\beta}_{\mathcal{W}}} = \sqrt{\frac{1+\sin\alpha}{\cos\alpha}\frac{1+\cos\beta}{\sin\beta}}, \\ D = e^{-J^{\alpha}_{\mathcal{B}} - J^{\beta}_{\mathcal{W}}} = \sqrt{\frac{\cos\alpha}{1+\sin\alpha}\frac{\sin\beta}{1+\cos\beta}}. \end{cases}$$

On these weights, we perform the transformation of Proposition II.11, then of Proposition II.10, and again of Proposition II.11. This amounts to defining $\tilde{X} = (\tilde{A}, \tilde{B}, \tilde{C}, \tilde{D})$ by

$$\begin{pmatrix} \tilde{A} \\ \tilde{B} \\ \tilde{C} \\ \tilde{D} \end{pmatrix} = \frac{1}{2} \begin{pmatrix} 1 & -1 & 1 & 1 \\ -1 & 1 & 1 & 1 \\ 1 & 1 & 1 & -1 \\ 1 & 1 & -1 & 1 \end{pmatrix} \begin{pmatrix} A \\ B \\ C \\ D \end{pmatrix}.$$

Following the transformations in the Propositions, we get that the Ising correlators are equal to

$$2\,\langle \sigma(B_0)\sigma(W_0)\mu(B_1)\mu(W_1)\rangle^{8V}_{\tilde{X},\gamma}.$$

Trigonometric computations show that (implicitly at any $f \in \mathcal{F}$):

$$\begin{pmatrix} \tilde{A} \\ \tilde{B} \\ \tilde{C} \\ \tilde{D} \end{pmatrix} = \frac{1}{\sqrt{\cos\alpha \sin\beta\,(1+\cos(\alpha-\beta))}} \begin{pmatrix} A_{\alpha,\beta} \\ B_{\alpha,\beta} \\ C_{\alpha,\beta} \\ D_{\alpha,\beta} \end{pmatrix}$$

and using the definition of correlators as partition function, we see that these gauge transformations multiply the correlator by the same factor. □

II.3.4 Coupling of free-fermion 8V-models

With Corollary II.12, we are able to factor correlators for the weights $X_{\alpha,\beta}$ into a part that depends on α and a part that depends on β. By doing the same for $X_{\alpha',\beta'}$ and rearranging the Ising correlators, we can get the correlators of $X_{\alpha,\beta'}$ and $X_{\alpha',\beta}$. This is expressed in the following "switching" result. The constants can be defined in terms of

$$c_{\alpha,\beta} = \prod_{f\in\mathcal{F}} C_{\alpha,\beta}(f) = \prod_{f\in\mathcal{F}} \frac{A^2_{\alpha,\beta}(f) + B^2_{\alpha,\beta}(f)}{2}. \tag{II.18}$$

Theorem II.13. *Let $\mathcal{Q}$ be a quadrangulation in the spherical case, and let $\alpha, \beta, \alpha', \beta' : \mathcal{F} \to (0, \frac{\pi}{2})$. Let $B_0, B_1, W_0, W_1, \gamma$ (resp. $B'_0, B'_1, W'_0, W'_1, \gamma'$) be as in Definition II.7. Then*

$$\begin{aligned} &\langle\sigma(B_0)\sigma(W_0)\mu(B_1)\mu(W_1)\rangle^{8V}_{X_{\alpha,\beta},\gamma} \quad \langle\sigma(B'_0)\sigma(W'_0)\mu(B'_1)\mu(W'_1)\rangle^{8V}_{X_{\alpha',\beta'},\gamma'} \\ =&c_1 \langle\sigma(B''_0)\sigma(W''_0)\mu(B''_1)\mu(W''_1)\rangle^{8V}_{X_{\alpha,\beta'},\gamma''} \langle\sigma(B'''_0)\sigma(W'''_0)\mu(B'''_1)\mu(W'''_1)\rangle^{8V}_{X_{\alpha',\beta},\gamma'''} \end{aligned} \tag{II.19}$$

where

$$\begin{pmatrix} B''_0 \\ W''_0 \\ B''_1 \\ W''_1 \end{pmatrix} = \begin{pmatrix} B_0 \\ W'_0 \\ B_0 \triangle B'_0 \triangle B'_1 \\ W_0 \triangle W'_0 \triangle W_1 \end{pmatrix}, \quad \begin{pmatrix} B'''_0 \\ W'''_0 \\ B'''_1 \\ W'''_1 \end{pmatrix} = \begin{pmatrix} B'_0 \\ W_0 \\ B_0 \triangle B'_0 \triangle B_1 \\ W_0 \triangle W'_0 \triangle W'_1 \end{pmatrix},$$

with the same formulas for the paths in γ'', γ''', and

$$c_1 = \sqrt{\frac{c_{\alpha,\beta} c_{\alpha',\beta'}}{c_{\alpha,\beta'} c_{\alpha',\beta}}}.$$

In particular,

$$\mathcal{Z}_{8V}(\mathcal{Q}, X_{\alpha,\beta})\ \mathcal{Z}_{8V}(\mathcal{Q}, X_{\alpha',\beta'}) = \ c_1\ \mathcal{Z}_{8V}(\mathcal{Q}, X_{\alpha,\beta'})\ \mathcal{Z}_{8V}(\mathcal{Q}, X_{\alpha',\beta}). \tag{II.20}$$

Proof. This immediately comes from writing both the left-hand side and the right-hand side in terms of Ising correlators using Corollary II.12, and checking that they are the same. □

Example II.14. *By taking $B_0 = B'_0 = B$ and $W_0 = W'_0 = W$ (i.e. the initial order variables being the same), we get the simpler formula*

$$\begin{aligned} &\langle\sigma(B)\sigma(W)\mu(B_1)\mu(W_1)\rangle^{8V}_{X_{\alpha,\beta},\gamma}\ \ \langle\sigma(B)\sigma(W)\mu(B'_1)\mu(W'_1)\rangle^{8V}_{X_{\alpha',\beta'},\gamma'} \\ =&c_1 \langle\sigma(B)\sigma(W)\mu(B'_1)\mu(W_1)\rangle^{8V}_{X_{\alpha,\beta'},\gamma''} \langle\sigma(B)\sigma(W)\mu(B_1)\mu(W'_1)\rangle^{8V}_{X_{\alpha',\beta},\gamma'''} \end{aligned}$$

This nontrivial equality of correlators (and of partition functions) suggests that there exists a coupling between pairs of 8V-configurations. Specifically, when (α, β) and (α', β') satisfy (II.11), then the 8V-weights define a Boltzmann probability; if $\tau_{\alpha,\beta}, \tau_{\alpha',\beta'}$ are independent and Boltzmann distributed, we want to couple them with $\tau_{\alpha,\beta'}, \tau_{\alpha',\beta}$, while keeping as much information as possible. The following Theorem means that it is possible to do so while keeping the XOR of configurations equal (*i.e.* the XOR of the corresponding sets of dual edges of $\mathcal{Q}$, which is still an 8V-configuration). This is a consequence of Theorem II.13, but our proof requires the introduction of a discrete Fourier transform on the space of 8V-configurations and is postponed to the end of Appendix II.A. An extended statement can be formulated for the XOR of configurations with disorder, see Remark II.43.

Theorem II.15. *Let $\mathcal{Q}$ be a quadrangulation in the spherical case, and let $\alpha, \beta, \alpha', \beta' : \mathcal{F} \to (0, \frac{\pi}{2})$ be such that $(\alpha, \beta), (\alpha', \beta'), (\alpha, \beta'), (\alpha', \beta)$ all satisfy* (II.11)*. Let $\tau_{\alpha,\beta}, \tau_{\alpha',\beta'}, \tau_{\alpha,\beta'}, \tau_{\alpha',\beta}$ be independent 8V-configurations with the corresponding Boltzmann distributions. Then $\tau_{\alpha,\beta} \oplus \tau_{\alpha',\beta'}$ and $\tau_{\alpha,\beta'} \oplus \tau_{\alpha',\beta}$ are equal in distribution.*

II.4 Kasteleyn matrices

We review the transformation of free-fermion 8V-configurations into vdimers, and we compute special relations for the corresponding (inverse) Kasteleyn matrices.

II.4.1 Free-fermion 8V to dimers

In the case of the square lattice, it has been shown by Fan and Wu that the 8V-model at its free-fermion point can be transformed into a dimer model on a planar decorated graph [FW69]. Their arguments work identically on any quadrangulation. The corresponding decorated graph is represented in Figure II.7.

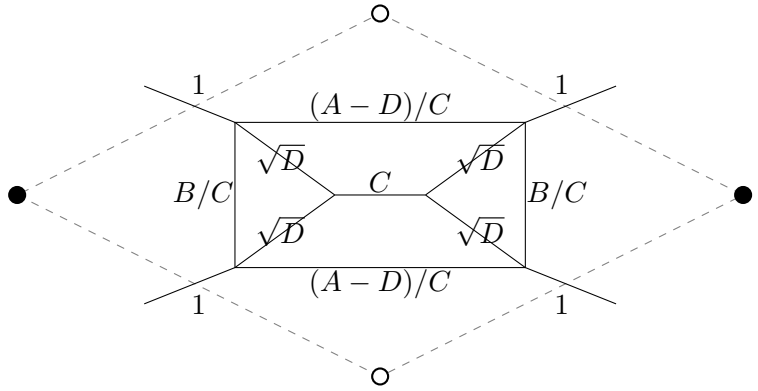

Figure II.7: The quadrangulation $\mathcal{Q}$ (dashed) at a face f and the decorated graph of Fan and Wu [FW69] (solid lines) with its dimer weights. The functions A, B, C, D are implicitly evaluated at f.

In the more special case of a free-fermionic 6V model, the graph becomes bipartite and the dimer model can be studied in more details [WL75, Dub11a, BdT14]. No such bipartite dimer decoration is known for the 8V-model, and the techniques of bipartite dimers are unavailable as such.

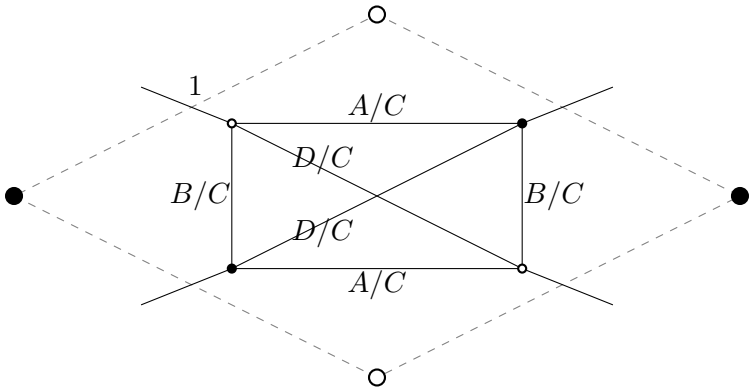

Figure II.8: The decorated graph G^T of Hsue, Lin and Wu [HLW75] with its dimer weights.

In our setting we will make use of another decorated graph due to Hsue, Lin and Wu [HLW75], see Figure II.8. This graph is more symmetric but non planar, which makes the usual theory of dimers as Pfaffians not available, but an adapted theory has been developed by Kasteleyn [Kas63, Kas67].

More precisely, let $G^T = (V^T, E^T)$ be a decorated version of $\mathcal{Q}^*$ obtained by drawing small complete graphs K_4 inside faces of $\mathcal{Q}$ and joining them by "legs" that cross the edges of $\mathcal{Q}$, as represented in Figure II.8. Even if this graph is not bipartite, we still decompose V^T into a subset of black vertices B^T and white vertices W^T, such that the black (resp. white) vertices lie on the left (resp. right) of an edge of $\mathcal{Q}$ oriented from black to white. For every edge $\mathrm{e} \in E^T$, we define ν_e as in Figure II.8. We will need a nonstandard weight for $m \in \mathcal{M}(G^T)$, defined as

$$\tilde{w}(m) = (-1)^{N(m)} \prod_{\mathrm{e} \in m} \nu_\mathrm{e}$$

where $N(m)$ is the number of pairs of intersecting edges in m. The corresponding partition function is

$$\tilde{\mathcal{Z}}_{\mathrm{dim}}(G^T, \nu) = \sum_{m \in \mathcal{M}(G^T)} \tilde{w}(m).$$

Note that at the boundary of every face $f \in \mathcal{F}$, m uses an even number of legs. As a result, if we only keep the occupied legs of m, we get an 8V-configuration $\tau \in \Omega(\mathcal{Q})$. We denote this by $m \mapsto \tau$. This mapping is weight-preserving in the following sense; this was noted when $\mathcal{Q}$ is the square lattice by Hsue, Lin and Wu [HLW75] but works in the exact same way for any quadrangulation:

Theorem II.16 ([HLW75])**.** *Let $\mathcal{Q}$ be a quadrangulation in the spherical or toric case, and X a set of standard free-fermionic 8V-weights on $\mathcal{Q}$. Then for every $\tau \in \Omega(\mathcal{Q})$,*

$$w_{8V}(\tau) = \left(\prod_{f \in \mathcal{F}} C(f) \right) \sum_{\substack{m \in \mathcal{M}(G^T) \\ s.t.\ m \mapsto \tau}} \tilde{w}(m).$$

In particular,

$$\mathcal{Z}_{8V}(\mathcal{Q}, X) = \left(\prod_{f \in \mathcal{F}} C(f) \right) \tilde{\mathcal{Z}}_{dim}(G^T, \nu).$$

We now describe how to compute $\tilde{\mathcal{Z}}_{\mathrm{dim}}(G^T, \nu)$ using an adapted version of Kasteleyn matrices.

II.4.2 Skew-symmetric real matrix

A *Kasteleyn orientation* of a planar or toric graph is an orientation of the edges such that every face is clockwise-odd, meaning that it has an odd number of clockwise-oriented edges; by the planarity condition, such an orientation can always be constructed, and may be used to identify the partition function of dimers with the Pfaffian of the corresponding skew-symmetric, weighted adjacency matrix [Kas61, TF61]. Since G^T is non-planar, there might not exist a usual Kasteleyn orientation, but there still exists an *admissible* orientation so that the Pfaffian is equal to $\tilde{\mathcal{Z}}_{\mathrm{dim}}(G^T, \nu)$ [Kas63, Kas67], which we describe now.

If we remove all edges of G^T that join black vertices (the *black diagonals* of decorations), we get a planar (or toric) graph G^T_B. Similarly, removing the *white diagonals* gives a graph G^T_W. An orientation of G^T is said to be *admissible* if its restriction to G^T_B and G^T_W are both Kasteleyn orientation. The existence of such an orientation is established in Section F of [Kas67].

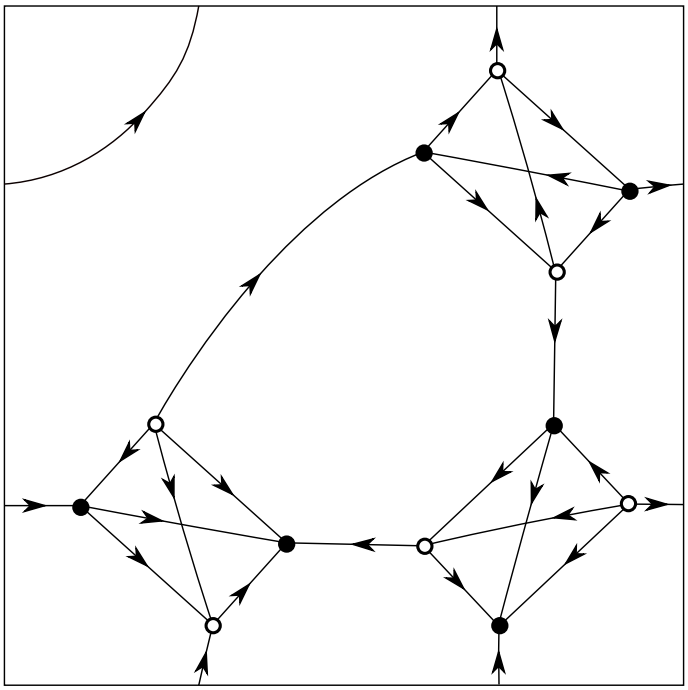

Figure II.9: An admissible orientation of G^T in the toric case.

To define a Kasteleyn matrix, we first fix an admissible orientation of G^T. For any standard $\alpha, \beta : \mathcal{F} \to \mathbb{R}/2\pi\mathbb{Z}$, the 8V-weights $X_{\alpha,\beta}$ are standard. Thus we can define dimer weights $\nu_{\alpha,\beta}$ as in Figure II.8. Let $\tilde{K}_{\alpha,\beta}$ be the weighted, skew-symmetric adjacency matrix associated to the oriented weighted graph G^T.

In the spherical case, the arguments leading to equation (79) in [Kas67] imply the following.

Proposition II.17 ([Kas63, Kas67])**.** *In the spherical case, for any quadrangulation $\mathcal{Q}$ and any standard $\alpha, \beta : \mathcal{F} \to \mathbb{R}/2\pi\mathbb{Z}$,*

$$\tilde{\mathcal{Z}}_{dim}(G^T, \nu_{\alpha,\beta}) = \operatorname{Pf} \tilde{K}_{\alpha,\beta}.$$

In the toric case, there also exists an admissible orientation, but its Pfaffian is no longer equal to $\tilde{\mathcal{Z}}_{\dim}(G^T, \nu_{\alpha,\beta})$. We recall here the standard way of dealing with this problem; the idea was suggested but not proved by Kasteleyn [Kas61, Kas63] and was then proved in various forms of generality in the works of Dolbilin et al. [DMS+96], Galluccio and Loebl [GL99], Tesler [Tes00], Cimasoni and Reshetikhin [CR07].

Let m_0 be the dimer configuration consisting of all dimers in the decorations that are parallel to the edges of $G^{\mathcal{B}}$; see the darker configuration of Figure II.12. For any dimer configuration m on G^T, the superimposition of m and m_0 is the disjoint union of alternating loops covering all the vertices. This union of curves has a well defined homology in $H_1(\mathbb{T}^2, \mathbb{Z}/2\mathbb{Z})$, which we denote $(h_x^m, h_y^m) \in (\mathbb{Z}/2\mathbb{Z})^2$. For any $\theta, \tau \in \{0, 1\}$, let $\tilde{K}^{\theta,\tau}_{\alpha,\beta}$ be the Kasteleyn matrix where the weights of edges of G^T crossing $\gamma_x^{\mathcal{B}}$ (resp. $\gamma_y^{\mathcal{B}}$) have been multiplied by $(-1)^\theta$ (resp. $(-1)^\tau$). Then there exists an admissible orientation such that we have the following.

Proposition II.18 ([Kas61, Kas63, DMS+96, GL99, Tes00, CR07])**.** *In the toric case, for any quadrangulation $\mathcal{Q}$ and any standard $\alpha, \beta : \mathcal{F} \to \mathbb{R}/2\pi\mathbb{Z}$, for any $\theta, \tau \in \{0, 1\}$,*

$$\operatorname{Pf} \tilde{K}^{\theta,\tau}_{\alpha,\beta} = \sum_{m \in \mathcal{M}(G^T)} (-1)^{h_x^m h_y^m + h_y^m + h_y^m + \theta h_x^m + \tau h_y^m} \tilde{w}(m).$$

Consequently,

$$\tilde{\mathcal{Z}}_{dim}(G^T, \nu_{\alpha,\beta}) = \frac{1}{2}\left(-\operatorname{Pf} \tilde{K}^{0,0}_{\alpha,\beta} + \operatorname{Pf} \tilde{K}^{0,1}_{\alpha,\beta} + \operatorname{Pf} \tilde{K}^{1,0}_{\alpha,\beta} + \operatorname{Pf} \tilde{K}^{1,1}_{\alpha,\beta}\right). \tag{II.21}$$

For any $(z, w) \in (\mathbb{C}^*)^2$, consider the modified matrix $\tilde{K}_{\alpha,\beta}(z, w)$, obtained by multiplying the coefficients $\tilde{K}_{\alpha,\beta}[\mathrm{u}, \mathrm{v}]$ by z (resp z^{-1}) when the edge uv crosses $\gamma_x^{\mathcal{B}}$ from left to right (resp. right to left), and similarly for w and $\gamma_y^{\mathcal{B}}$. This leads to the definition of the *characteristic polynomial* of the eight-vertex as the Laurent polynomial

$$P^{8V}_{\alpha,\beta}(z, w) = \det \tilde{K}_{\alpha,\beta}(z, w).$$

When $(z, w) \notin \{\pm 1\}^2$, this quantity has no reason to factor as a square product.

We conclude this part with a few remarks on the planar case. Then $\tilde{K}_{\alpha,\beta}$ is an infinite matrix, or equivalently can be seen as an operator on $\mathbb{C}^{V^T}$:

$$\forall f \in \mathbb{C}^{V^T},\ (\tilde{K}_{\alpha,\beta} f)[\mathrm{x}] = \sum_{\mathrm{y} \in V^T} K_{\alpha,\beta}[\mathrm{x}, \mathrm{y}] f[\mathrm{y}].$$

This is well defined because for all $\mathrm{x} \in V^T$, $\tilde{K}_{\alpha,\beta}[\mathrm{x}, \mathrm{y}]$ is zero for all but a finite number of y's.

An *inverse* of $\tilde{K}_{\alpha,\beta}$ is an infinite matrix $\tilde{K}^{-1}_{\alpha,\beta}$ such that $\tilde{K}_{\alpha,\beta}\tilde{K}^{-1}_{\alpha,\beta} = \mathrm{Id}$ as a matrix product. This is well defined by the previous remark.

When the graph is $\mathbb{Z}^2$-periodic, let $G_1^T = G^T/\mathbb{Z}^2$ be the *fundamental graph*. Note that G_1^T corresponds to the toric case. For any $(z, w) \in \mathbb{C}^2$ the subspace $V^T_{(z,w)}$ of (z, w)-quasiperiodic functions f:

$$\forall \mathrm{x} \in V_1^T,\ \forall (m, n) \in \mathbb{Z}^2,\ f(\mathrm{x} + (m, n)) = z^{-m} w^{-n} f(\mathrm{x})$$

is fixed by $\tilde{K}_{\alpha,\beta}$. The restriction of $\tilde{K}_{\alpha,\beta}$ to this finite-dimensional subspace is equal to the matrix $\tilde{K}_{\alpha,\beta}(z, w)$ defined in the toric case for G_1^T, via the identification of $\mathrm{x} \in V_1^T$ with the only (z, w)-quasiperiodic function $\delta_{\mathrm{x}}(z, w)$ that takes value 1 at x and 0 at the other vertices V_1^T of the fundamental domain.

II.4.3 Skew-hermitian complex matrix

There is another way to define Kasteleyn matrices that is more intrinsic and does not require fixing an orientation, by using instead complex arguments on the edges. Let $K_{\alpha,\beta}$ be the matrix whose entries are indexed by vertices V^T and defined by Figure II.10 and by the skew-hermitian condition:

$$K_{\alpha,\beta}[\mathrm{u}, \mathrm{v}] = -\overline{K_{\alpha,\beta}[\mathrm{v}, \mathrm{u}]}.$$

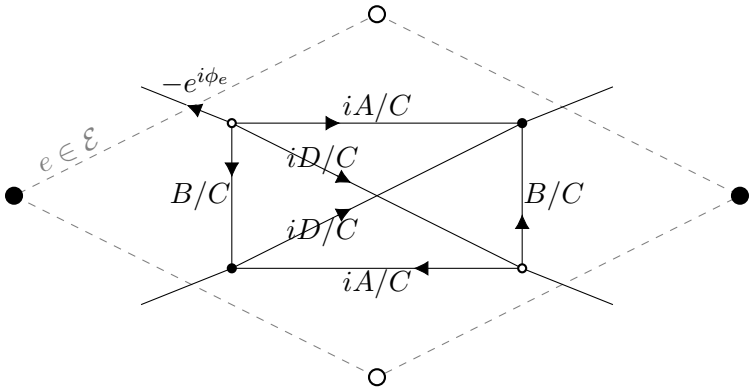

Figure II.10: The skew-hermitian Kasteleyn matrix $K_{\alpha,\beta}$ on G^T.

The arguments of the entries are inspired by the relation with the Kac-Ward matrix [KW52, CDC13, CCK17]. The "angles" $(\phi_e)_{e\in\mathcal{E}}$ are defined in the following way:

- In the spherical and planar cases, we embed the graph $G^{\mathcal{B}}$ properly in the plane, with straight edges. Then the white vertices of $\mathcal{Q}$, $\mathcal{W}$, are in bijection with faces of $G^{\mathcal{B}}$, and the edges $\mathcal{E}$ of $\mathcal{Q}$ are in bijection with the *corners* of $G^{\mathcal{B}}$. For every $e \in \mathcal{E}$, we set $2\phi_e$ to be the direct angle at the corner corresponding to e, taken in $[0, 2\pi)$. See Figure II.11.

- In the toric case, we lift $\mathcal{Q}$ to a bipartite periodic quadrangulation of the plane, and we proceed as in the planar case. This yields a periodic choice of angles ϕ, which can be mapped again to the torus.

In the toric case, we also define $K_{\alpha,\beta}(z, w)$ just as before.

The following result relates the matrices $\tilde{K}_{\alpha,\beta}$ and $K_{\alpha,\beta}$ by "gauge equivalence". In particular, it shows that all their principal minors are equal.

Lemma II.19. *In the spherical and toric cases, there exists a diagonal unitary matrix $\mathcal{D}$, that depends only on the chosen admissible orientation of G^T, such that*

$$K_{\alpha,\beta} = \mathcal{D}^{-1}\tilde{K}_{\alpha,\beta}\mathcal{D} \tag{II.22}$$

Proof. We use Theorem 2.1 of [SS78]; see also Appendix A of [dT18]. The existence of such a diagonal (not necessarily unitary) matrix is equivalent to having, for every cycle $\mathcal{C} = (\mathrm{x}_1, \ldots, \mathrm{x}_p, \mathrm{x}_{p+1} = \mathrm{x}_1)$ of adjacent vertices on G^T,

$$\prod_{i=1}^{p} K_{\alpha,\beta}[\mathrm{x}_i, \mathrm{x}_{i+1}] = \prod_{i=1}^{p} \tilde{K}_{\alpha,\beta}[\mathrm{x}_i, \mathrm{x}_{i+1}]. \tag{II.23}$$

Since the complex moduli of the entries of $K_{\alpha,\beta}$ and $\tilde{K}_{\alpha,\beta}$ are equal, it is sufficient to show that the complex arguments in (II.23) are the same. Notice that for the simple cycles $(\mathrm{x}, \mathrm{y}, \mathrm{x})$, by the skew-symmetric and skew-hermitian properties,

$$\arg(K_{\alpha,\beta}[\mathrm{x},\mathrm{y}]K_{\alpha,\beta}[\mathrm{y},\mathrm{x}]) = \pi = \arg(\tilde{K}_{\alpha,\beta}[\mathrm{x},\mathrm{y}]\tilde{K}_{\alpha,\beta}[\mathrm{y},\mathrm{x}]).$$

Moreover, if we show that the right-hand side of (II.23) is real (*i.e.* the argument is $0[\pi]$), then we only have to check one direction for any cycle.

All in all, by decomposing cycles, it suffices to check that the complex arguments in (II.23) are equal and real for the following cycles:

1. the cycles that winds once in the counter-clockwise direction around a vertex of $\mathcal{B}$, or of $\mathcal{W}$;

2. the counter-clockwise 3-cycles inside decorations that use two sides and a diagonal;

3. in the torus case, two fixed cycles that wind once vertically (resp. horizontally) around the torus.

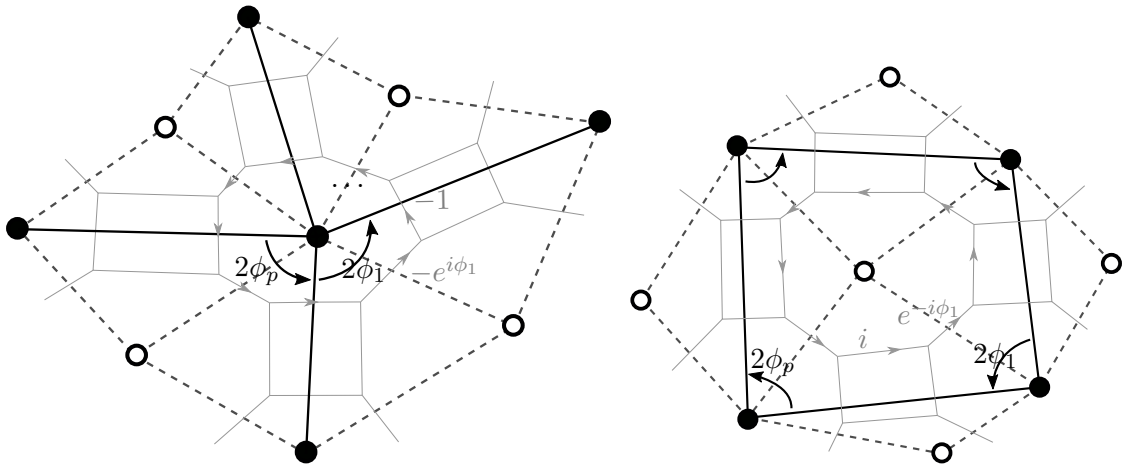

Figure II.11: Embedded graph $G^{\mathcal{B}}$ and unitary part of the entries of $K_{\alpha,\beta}$ on simple cycles around black and white vertices

Case 1: let $\mathcal{C}$ be such a cycle corresponding to a black vertex $b \in \mathcal{B}$. Let $\phi_1, \dots, \phi_p$ be the successive angles around b as in Figure II.11. By grouping together the successive steps of $\mathcal{C}$ on legs and inside decorations, the argument of the left-hand side of (II.23) is

$$\sum_{i=1}^{p} \phi_i = \pi. \tag{II.24}$$

On the right-hand side, as the cycle is even, the product is also a negative real number for an admissible orientation.

If $\mathcal{C}$ corresponds to a white vertex $w \in \mathcal{W}$, we also set $\phi_1, \dots, \phi_p$ to be the successive angles around w as in Figure II.11. Then

$$\sum_{i=1}^{p} 2\phi_i = (p \pm 2)\pi, \tag{II.25}$$

with a $-$ sign when w corresponds to an interior face of $G^{\mathcal{B}}$ when embedded in the plane, and a $+$ sign for the exterior face. Again by grouping the steps, the argument for the product of the left-hand side of (II.23) is $\sum_{i=1}^{p} \left(\frac{\pi}{2} - \phi_i\right) = \pi[2\pi]$, and we conclude similarly.

Case 2: In Figure II.10 we easily check that for any of these 3-cycles, the argument of the product of the elements of $K_{\alpha,\beta}$ is $\pi[2\pi]$. By the construction of admissible orientations, these are also clockwise-odd so the product for $\tilde{K}_{\alpha,\beta}$ is also a negative real number.

Case 3: We show this for a cycle that winds once vertically around the torus, the horizontal case being identical. We chose the alternating cycle $\mathcal{C}_y$ represented in Figure II.12. This cycle is obtained by superimposing the dimer configuration m_0 with a configuration m_y that uses the legs that cross edges of $\mathcal{Q}$ that touch $\gamma_y^{\mathcal{B}}$ on the right, edges parallel to the white diagonal in the decorations of faces containing two such edges of $\mathcal{Q}$, and is equal to m_0 otherwise.

Again by decomposing the path, one easily checks that the argument on the left-hand side of (II.23) is

$$\sum_{i=1}^{p} \left(\psi_i - \frac{\pi}{2}\right) = 0. \tag{II.26}$$

For the right-hand side, we know that m_0 has homology $(0,0)$ while m_y has homology $(0,1)$, so that by Proposition II.18 the term in $\det \tilde{K}_{\alpha,\beta}$ corresponding to the superimposition of m_0 and m_y must appear with a minus sign. All the double dimers in this superimposition give a $+$ sign, because the $-$ sign of the product of opposite matrix elements is compensated by the signature of a 2-cycle. Following this reasoning, the product corresponding to the alternating cycle C_y must be positive, since the signature of the corresponding cycle of the permutation is -1. This proves that the arguments match.

The fact that $\mathcal{D}$ does not depend on α, β is a consequence of the explicit form given in [dT18]. Finally, to show that the matrix $\mathcal{D}$ can be taken to be unitary, we just have to show that its diagonal elements have the same modulus, since multiplying it by a constant leaves relation (II.22) unchanged. For any two adjacent vertices $\mathrm{x}, \mathrm{y} \in V^T$,

$$K_{\alpha,\beta}[\mathrm{x},\mathrm{y}] = \frac{\mathcal{D}[\mathrm{y},\mathrm{y}]}{\mathcal{D}[\mathrm{x},\mathrm{x}]} \tilde{K}_{\alpha,\beta}[\mathrm{x},\mathrm{y}]$$

so that $|\mathcal{D}[\mathrm{x},\mathrm{x}]| = |\mathcal{D}[\mathrm{y},\mathrm{y}]|$. Since the graph is connected, all these moduli are equal. □

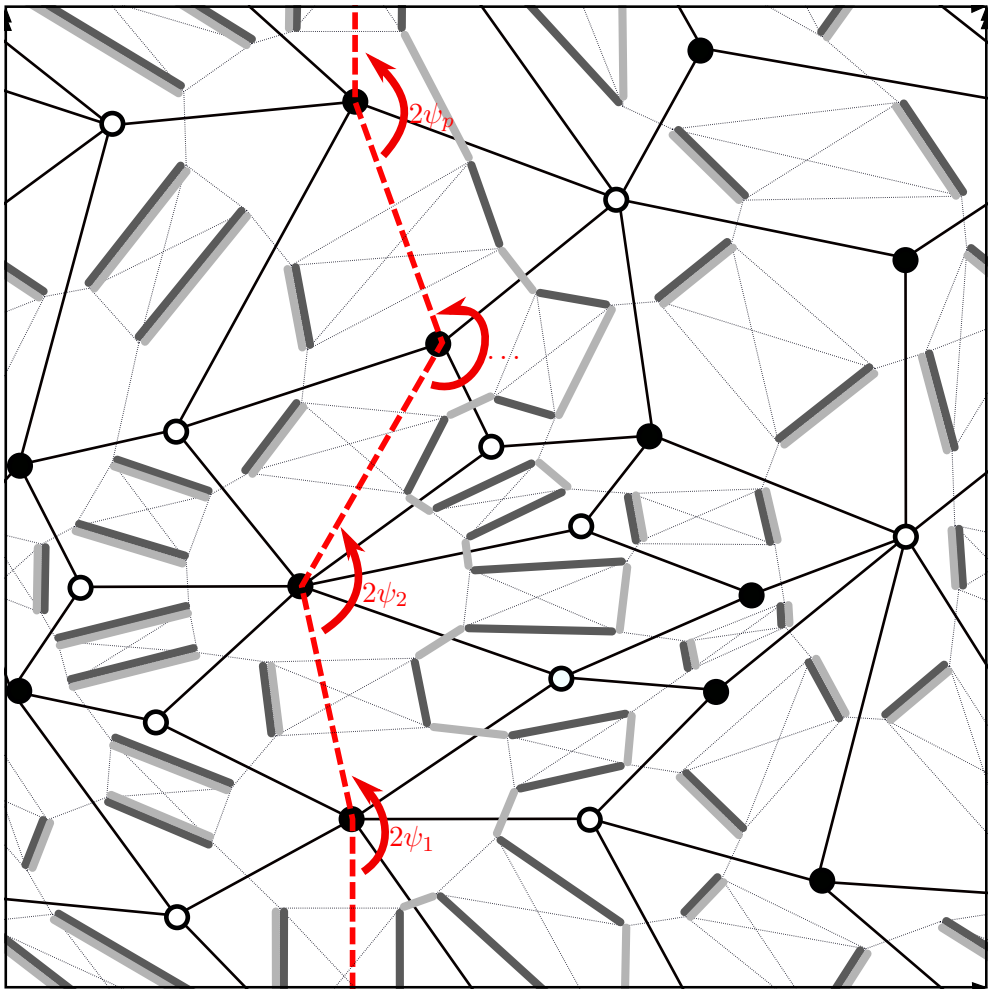

Figure II.12: A quadrangulation of the torus with the path $\gamma_y^{\mathcal{B}}$ (dashed); the graph G^T equipped with two dimer configurations, m_0 (dark grey) and m_y (light grey).

II.4.4 Eight-vertex partition function and correlations

By injecting the result of Theorem II.16 into Propositions II.17 and II.18, and using Lemma II.19 to transform the determinant of $\tilde{K}_{\alpha,\beta}$ into that of $K_{\alpha,\beta}$ (we cannot do the same for Pfaffian, since the latter is only defined for skew-symmetric matrices *a priori*) we get

Corollary II.20. *Let $\mathcal{Q}$ be a quadrangulation and $\alpha, \beta : \mathcal{F} \to \mathbb{R}/2\pi\mathbb{Z}$ be standard. In the spherical case,*

$$(\mathcal{Z}_{8V}(\mathcal{Q}, X_{\alpha,\beta}))^2 = \left(\prod_{f\in\mathcal{F}} C_{\alpha,\beta}(f)\right)^2 \det K_{\alpha,\beta}.$$

In the toric case,

$$\mathcal{Z}_{8V}(\mathcal{Q}, X_{\alpha,\beta}) = \frac{\prod_{f\in\mathcal{F}} C_{\alpha,\beta}(f)}{2}\left(-\operatorname{Pf}\tilde{K}^{0,0}_{\alpha,\beta} + \operatorname{Pf}\tilde{K}^{0,1}_{\alpha,\beta} + \operatorname{Pf}\tilde{K}^{1,0}_{\alpha,\beta} + \operatorname{Pf}\tilde{K}^{1,1}_{\alpha,\beta}\right).$$

Another standard result is the computation of dimer statistics in terms of minors of the inverse Kasteleyn matrix; see [Ken97, Ken05]. If we adapt this to the 8V statistics, where we are only interested in the statistics of the legs dimers, *i.e.* dimers that have weight 1, we obtain:

Proposition II.21 ([Ken97])**.** *Let $\mathcal{Q}$ be a quadrangulation in the spherical or toric case. Let $e_1, \dots, e_p \in \mathcal{E}$, each e_i corresponding to a leg of G^T, whose endpoints we denote $\mathrm{b}_i \in B^T$ and $\mathrm{w}_i \in W^T$. Let $\mathrm{V} = \{\mathrm{b}_1, \mathrm{w}_1, \dots, \mathrm{b}_p, \mathrm{w}_p\}$.*

Let $\alpha, \beta : \mathcal{F} \to \mathbb{R}/2\pi\mathbb{Z}$ satisfy (II.11)*. Let τ be a random 8V-configuration with Boltzmann distribution $\mathbb{P}_{8V}$. Then in the spherical case,*

$$\left(\mathbb{P}_{8V}\left(\{e_1, \dots, e_p\} \subset \tau\right)\right)^2 = \det\left[\left(K^{-1}_{\alpha,\beta}\right)_{\mathrm{V}}\right]$$

where the matrix on the right-hand side is the submatrix of $K^{-1}_{\alpha,\beta}$ with rows and columns indexed by V*.*

In the toric case,

$$\begin{aligned}&\mathbb{P}_{8V}\left(\{e_1, \dots, e_p\} \subset \tau\right) = \\ &\frac{\prod_{f\in\mathcal{F}} C_{\alpha,\beta}(f)}{2\mathcal{Z}_{8V}(\mathcal{Q}, X_{\alpha,\beta})}\left(-\operatorname{Pf}\left(\tilde{K}^{0,0}_{\alpha,\beta}\right)_{\mathrm{V}^c} + \operatorname{Pf}\left(\tilde{K}^{0,1}_{\alpha,\beta}\right)_{\mathrm{V}^c} + \operatorname{Pf}\left(\tilde{K}^{1,0}_{\alpha,\beta}\right)_{\mathrm{V}^c} + \operatorname{Pf}\left(\tilde{K}^{1,1}_{\alpha,\beta}\right)_{\mathrm{V}^c}\right).\end{aligned} \tag{II.27}$$

II.4.5 Relations between matrices $K^{-1}_{\alpha,\beta}$

We now exhibit a symmetry in the 8V-model in the form of a relation between inverse matrices for different values of α, β.

a) Spherical and planar cases

Let us define the matrix T with entries indexed by the vertices V^T of the dimer graph G^T, in the following way: if $\mathrm{w} \in W^T$, then there is a unique "leg" adjacent to w. Let us denote $\hat{\mathrm{w}} \in B^T$ the other endpoint of this leg. Let $e \in \mathcal{E}$ be the edge of $\mathcal{Q}$ crossed by $\{\mathrm{w}\hat{\mathrm{w}}\}$. We define

$$\begin{aligned}T(\mathrm{w}, \hat{\mathrm{w}}) &= -e^{i\phi_e}, \\ T(\hat{\mathrm{w}}, \mathrm{w}) &= -e^{-i\phi_e},\end{aligned} \tag{II.28}$$

and all the other entries of T are zero. Thus T is a weighted permutation matrix between vertices x and their associated neighbor, which we still denote $\hat{\mathrm{x}}$, x being black or white.

Theorem II.22. *In the spherical case or planar case, let (α, β) and (α', β') be standard elements of $\left([0, 2\pi)^{\mathcal{F}}\right)^2$. If the matrices $K^{-1}_{\alpha,\beta'}, K^{-1}_{\alpha',\beta}$ are inverses of $K_{\alpha,\beta'}, K_{\alpha',\beta}$, then the following are inverses of $K_{\alpha,\beta}, K_{\alpha',\beta'}$:*

$$\begin{aligned}K^{-1}_{\alpha,\beta} &= \frac{1}{2}\left((I+T)K^{-1}_{\alpha,\beta'} + (I-T)K^{-1}_{\alpha',\beta}\right), \\ K^{-1}_{\alpha',\beta'} &= \frac{1}{2}\left((I-T)K^{-1}_{\alpha,\beta'} + (I+T)K^{-1}_{\alpha',\beta}\right).\end{aligned} \tag{II.29}$$

Proof. To simplify notation, we will denote

- (A, B, C, D) the weights $X_{\alpha,\beta}$;
- (A', B', C', D') the weights $X_{\alpha',\beta'}$;
- (a, b, c, d) the weights $X_{\alpha,\beta'}$, and $K^{-1}_{\alpha,\beta'} = (u_{\mathrm{x,y}})_{\mathrm{x,y}\in V^T}$;
- (a', b', c', d') the weights $X_{\alpha',\beta}$, and $K^{-1}_{\alpha',\beta} = \left(u'_{\mathrm{x,y}}\right)_{\mathrm{x,y}\in V^T}$.

Lemma II.23. *The following relations, implicitly evaluated at any $f \in \mathcal{F}$, hold:*

$$\begin{aligned} cA + dB - aC - bD &= 0, & c'A - d'B - a'C + b'D &= 0,\\ dA - cB + bC - aD &= 0, & d'A + c'B - b'C - a'D &= 0,\\ aA + bB - cC - dD &= 0, & a'A + b'B - c'C - d'D &= 0,\\ bA - aB + dC - cD &= 0, & b'A - a'B - d'C + c'D &= 0. \end{aligned}$$

Proof of Lemma II.23. This is done by direct computations, which are made easier by the use of the alternative form of weights (II.7). □

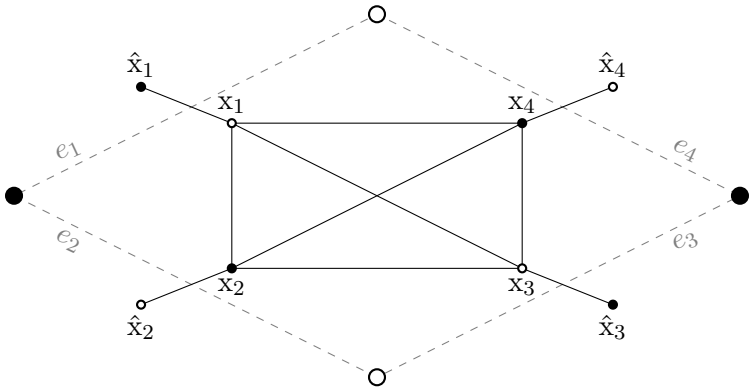

Figure II.13: Notation for G^T around $\mathrm{x}_1 \in W^T$.

Let $\mathrm{x}_1 \in W^T$. Its neighbors are denoted $\hat{\mathrm{x}}_1, \mathrm{x}_2, \mathrm{x}_3, \mathrm{x}_4$ as in Figure II.13. For any $\mathrm{y} \in V^T$ and $i \in \{1, \dots, 4\}$ we have $\left(K_{\alpha,\beta'} K^{-1}_{\alpha,\beta'}\right)[\mathrm{x}_i, \mathrm{y}] = \delta_{\mathrm{x}_i,\mathrm{y}}$, which reads:

$$\begin{aligned} -e^{i\phi_{e_1}} u_{\hat{\mathrm{x}}_1,\mathrm{y}} + \frac{b}{c} u_{\mathrm{x}_2,\mathrm{y}} + i\frac{d}{c} u_{\mathrm{x}_3,\mathrm{y}} + i\frac{a}{c} u_{\mathrm{x}_4,\mathrm{y}} &= \delta_{\mathrm{x}_1,\mathrm{y}}\\ -\frac{b}{c} u_{\mathrm{x}_1,\mathrm{y}} + e^{-i\phi_{e_2}} u_{\hat{\mathrm{x}}_2,\mathrm{y}} + i\frac{a}{c} u_{\mathrm{x}_3,\mathrm{y}} + i\frac{d}{c} u_{\mathrm{x}_4,\mathrm{y}} &= \delta_{\mathrm{x}_2,\mathrm{y}}\\ i\frac{d}{c} u_{\mathrm{x}_1,\mathrm{y}} + i\frac{a}{c} u_{\mathrm{x}_2,\mathrm{y}} - e^{i\phi_{e_3}} u_{\hat{\mathrm{x}}_3,\mathrm{y}} + \frac{b}{c} u_{\mathrm{x}_4,\mathrm{y}} &= \delta_{\mathrm{x}_3,\mathrm{y}}\\ i\frac{a}{c} u_{\mathrm{x}_1,\mathrm{y}} + i\frac{d}{c} u_{\mathrm{x}_2,\mathrm{y}} - \frac{b}{c} u_{\mathrm{x}_3,\mathrm{y}} + e^{-i\phi_{e_4}} u_{\hat{\mathrm{x}}_4,\mathrm{y}} &= \delta_{\mathrm{x}_4,\mathrm{y}} \end{aligned}$$

By writing the same equations for $K_{\alpha',\beta}$, we get the same relations where $u_{\mathrm{x,y}}$ is changed into $u'_{\mathrm{x,y}}$ and (a, b, c, d) are changed into (a', b', c', d'). We denote these four new equations by $(E'_1), (E'_2), (E'_3), (E'_4)$.

Now we compute

$$\begin{aligned} &C(E_1) - B(E_2) + iD(E_3) - iA(E_4) \\ &+C(E_1') + B(E_2') - iD(E_3') + iA(E_4'). \end{aligned}$$

On the right-hand side, this is $2C\delta_{\mathrm{x}_1,\mathrm{y}}$. On the left-hand side, we can group the terms corresponding to the same $u_{\mathrm{x},\mathrm{y}}$ (or $u'_{\mathrm{x},\mathrm{y}}$). For instance, $u_{\mathrm{x}_1,\mathrm{y}}$ will appear with coefficient

$$\frac{b}{c}B - \frac{d}{c}D + \frac{a}{c}A$$

which is equal to C according to Lemma II.23. All in all, using all relations of Lemma II.23, this yields

$$\begin{aligned} &-Ce^{i\phi_{e_1}} \left(u_{\hat{\mathrm{x}}_1,\mathrm{y}} + u'_{\hat{\mathrm{x}}_1,\mathrm{y}} - e^{-i\phi_{e_1}} \left(u_{\mathrm{x}_1,y} - u'_{\mathrm{x}_1,y}\right)\right) \\ &+B \left(u_{\mathrm{x}_2,\mathrm{y}} + u'_{\mathrm{x}_2,\mathrm{y}} - e^{-i\phi_{e_2}} \left(u_{\hat{\mathrm{x}}_2,y} - u'_{\hat{\mathrm{x}}_2,y}\right)\right) \\ &+iD \left(u_{\mathrm{x}_3,\mathrm{y}} + u'_{\mathrm{x}_3,\mathrm{y}} - e^{i\phi_{e_3}} \left(u_{\hat{\mathrm{x}}_3,y} - u'_{\hat{\mathrm{x}}_3,y}\right)\right) \\ &+iA \left(u_{\mathrm{x}_4,\mathrm{y}} + u'_{\mathrm{x}_4,\mathrm{y}} - e^{-i\phi_{e_4}} \left(u_{\hat{\mathrm{x}}_4,y} - u'_{\hat{\mathrm{x}}_4,y}\right)\right) = 2C\delta_{\mathrm{x}1,\mathrm{y}}. \end{aligned} \tag{II.34}$$

For $\mathrm{x},\mathrm{y} \in V^T$, let $e_{\mathrm{x}} \in \mathcal{E}$ be the edge of the quadrangulation closest to x, and let $M_{\mathrm{x},\mathrm{y}}$ be

$$\begin{aligned} &\text{if } \mathrm{x} \in W^T, \quad M_{\mathrm{x},\mathrm{y}} = \frac{1}{2}\left(u_{\mathrm{x},\mathrm{y}} + u'_{\mathrm{x},\mathrm{y}} - e^{i\phi_{e_{\mathrm{x}}}} \left(u_{\hat{\mathrm{x}},\mathrm{y}} - u'_{\hat{\mathrm{x}},\mathrm{y}}\right)\right), \\ &\text{if } \mathrm{x} \in B^T, \quad M_{\mathrm{x},\mathrm{y}} = \frac{1}{2}\left(u_{\mathrm{x},\mathrm{y}} + u'_{\mathrm{x},\mathrm{y}} - e^{-i\phi_{e_{\mathrm{x}}}} \left(u_{\hat{\mathrm{x}},\mathrm{y}} - u'_{\hat{\mathrm{x}},\mathrm{y}}\right)\right). \end{aligned} \tag{II.35}$$

Then Equation (II.34) exactly means that the matrix $M = (M_{\mathrm{x},\mathrm{y}})_{\mathrm{x},\mathrm{y}\in V^T}$ satisfies

$$(K_{\alpha,\beta}M)\,[\mathrm{x}_1,\mathrm{y}] = \delta_{\mathrm{x}_1,\mathrm{y}} \tag{II.36}$$

when $\mathrm{x}_1 \in W^T$. A similar computation shows that (II.36) also holds when $\mathrm{x}_1 \in B^T$. As a result, M is an inverse of $K_{\alpha,\beta}$, and (II.35) is equivalent to

$$M = \frac{1}{2}\left[(I+T)K^{-1}_{\alpha,\beta'} + (I-T)K^{-1}_{\alpha',\beta}\right].$$

The second matrix relation in (II.29) is obtained by switching $(\alpha,\beta) \leftrightarrow (\alpha',\beta')$. □

Remark II.24. Theorem II.22 can be used to give an alternative proof of the relation of partition functions (II.20). This works exactly as in the forthcoming proof of the analogous statement for toric quadrangulations, see Theorem II.26.

b) Toric case

Theorem II.25. *Let $\mathcal{Q}$ be a quadrangulation in the toric case. Let (α,β) and (α',β') be two standard elements of $\left([0,2\pi)^{\mathcal{F}}\right)^2$.*

Let $(z,w) \in (\mathbb{C}^*)^2$ be such that $K_{\alpha,\beta'}(z,w)$ and $K_{\alpha',\beta}(z,w)$ are invertible. Then $K_{\alpha,\beta}(z,w)$ and $K_{\alpha',\beta'}(z,w)$ are invertible and their inverses are given by

$$\begin{aligned} K^{-1}_{\alpha,\beta}(z,w) &= \frac{1}{2}\left[(I+T)K^{-1}_{\alpha,\beta'}(z,w) + (I-T)K^{-1}_{\alpha',\beta}(z,w)\right], \\ K^{-1}_{\alpha',\beta'}(z,w) &= \frac{1}{2}\left[(I-T)K^{-1}_{\alpha,\beta'}(z,w) + (I+T)K^{-1}_{\alpha',\beta}(z,w)\right]. \end{aligned}$$

Proof. The proof, being based on a local computation of matrix products, is identical to that of Theorem II.22. One simply has to take into account the possible multiplication by $z^{\pm 1}$ and $w^{\pm 1}$ in the weights when the face considered is crossed by $\gamma_x^{\mathcal{B}}, \gamma_y^{\mathcal{W}}$, or both. For instance, if it is crossed by $\gamma_x^{\mathcal{B}}$, in the notation of the proof of Theorem II.22, one has to compute

$$\begin{aligned} &C(E_1) - zB(E_2) + izD(E_3) - iA(E_4) \\ &+C(E_1') + zB(E_2') - izD(E_3') + iA(E_4'). \end{aligned}$$

to get the correct matrix relation. The other cases are similar. □

Theorem II.26. *Let $\mathcal{Q}$ be a quadrangulation in the toric case. Let (α, β) and (α', β') be two standard elements of $\left([0, 2\pi)^{\mathcal{F}}\right)^2$. Then the characteristic polynomials satisfy*

$$P^{8V}_{\alpha,\beta} P^{8V}_{\alpha',\beta'} = c_2 P^{8V}_{\alpha,\beta'} P^{8V}_{\alpha',\beta}$$

where

$$c_2 = \frac{c_{\alpha,\beta'} c_{\alpha',\beta}}{c_{\alpha,\beta} c_{\alpha',\beta'}} = \prod_{f \in \mathcal{F}} \frac{C_{\alpha,\beta'}(f) C_{\alpha',\beta}(f)}{C_{\alpha,\beta}(f) C_{\alpha',\beta'}(f)}.$$

To prove Theorem II.26, we also need the following diagonal matrix D, whose rows and columns are indexed by the vertices of G^T:

$$D_{\mathrm{xx}} = \begin{cases} -1 & \text{if } \mathrm{x} \in W^T, \\ 1 & \text{if } \mathrm{x} \in B^T. \end{cases}$$

Lemma II.27. *Let $\mathcal{Q}$ be a quadrangulation in the toric case, and let $\alpha, \beta : \mathcal{F} \to [0, 2\pi[$ be standard, and $(z, w) \in (\mathbb{C}^*)^2$. The commutator of $K_{\alpha,\beta}(z, w)$ with T is*

$$[K_{\alpha,\beta}(z, w), T] = -K_{\alpha,\beta}(z, w) D K_{\alpha,\beta}(z, w). \tag{II.37}$$

If $P_{\alpha,\beta}(z, w) \neq 0$, the commutator of $K^{-1}_{\alpha,\beta}(z, w)$ with T is

$$\left[K^{-1}_{\alpha,\beta}(z, w), T\right] = D. \tag{II.38}$$

Proof. Equality (II.37) can be verified by a straightforward computation of the matrix elements. For instance, in the notation of Figure II.13 (we drop the (z, w) in the computation to simplify notation) the matrix element $[\mathrm{x}_1, \hat{\mathrm{x}}_2]$ are

$$\begin{aligned} \left(K_{\alpha,\beta} T\right)[\mathrm{x}_1, \hat{\mathrm{x}}_2] - \left(T K_{\alpha,\beta}\right)[\mathrm{x}_1, \hat{\mathrm{x}}_2] &= K_{\alpha,\beta}[\mathrm{x}_1, \mathrm{x}_2] T[\mathrm{x}_2, \hat{\mathrm{x}}_2] - 0 \\ &= \frac{B}{C}\left(-e^{-i\phi_{e_2}}\right); \\ -\left(K_{\alpha,\beta} D K_{\alpha,\beta}\right)[\mathrm{x}_1, \hat{\mathrm{x}}_2] &= -K_{\alpha,\beta}[\mathrm{x}_1, \mathrm{x}_2] D[\mathrm{x}_2, \mathrm{x}_2] K_{\alpha,\beta}[\mathrm{x}_2, \hat{\mathrm{x}}_2] \\ &= -\frac{B}{C}\left(e^{-i\phi_{e_2}}\right). \end{aligned}$$

Another important case is the matrix element $[\mathrm{x}_1, \mathrm{x}_1]$:

$$\begin{aligned}
(K_{\alpha,\beta}T)[\mathrm{x}_1,\mathrm{x}_1] - (TK_{\alpha,\beta})[\mathrm{x}_1,\mathrm{x}_1] =& K_{\alpha,\beta}[\mathrm{x}_1,\hat{\mathrm{x}_1}]T[\hat{\mathrm{x}_1},\mathrm{x}_1] - T[\mathrm{x}_1,\hat{\mathrm{x}_1}]K_{\alpha,\beta}[\hat{\mathrm{x}_1},\mathrm{x}_1]\\
=& \left(-e^{i\phi_{e_1}}\right)\left(-e^{-i\phi_{e_1}}\right) - \left(-e^{i\phi_{e_1}}\right)e^{-i\phi_{e_1}};\\
=& 2;\\
-(K_{\alpha,\beta}DK_{\alpha,\beta})[\mathrm{x}_1,\hat{\mathrm{x}}_2] =& -\left(\left(-e^{i\phi_{e_1}}\right)e^{-i\phi_{e_1}} + \frac{B}{C}\left(-\frac{B}{C}\right) + i\frac{D}{C}(-1)i\frac{D}{C} + i\frac{A}{C}i\frac{A}{C}\right)\\
=& -\left(-1 + \frac{-B^2-A^2+D^2}{C^2}\right)\\
=& 2.
\end{aligned}$$

All other cases are similar.

For the second point, $P(z,w) = \det\left(\tilde{K}_{\alpha,\beta}(z,w)\right) = \det\left(K_{\alpha,\beta}(z,w)\right)$ Lemma II.19, so the matrix $K_{\alpha,\beta}(z,w)$ is invertible. Then (II.38) is simply obtained by multiplying (II.37) by $K^{-1}_{\alpha,\beta}(z,w)$ on both sides. □

Proof of Theorem II.26. We prove the polynomials relation for (z,w) such that none of the four polynomials is zero at (z,w) (*i.e.* the four Kasteleyn matrices are invertible); the relation is then obtained by analytic continuation. By noting that $T^2 = I$, we can rewrite Theorem II.25 as a block-matrix relation:

$$\begin{pmatrix} I & I \\ I & -I \end{pmatrix}\begin{pmatrix} K^{-1}_{\alpha,\beta}(z,w) & 0 \\ K^{-1}_{\alpha',\beta'}(z,w) & K^{-1}_{\alpha',\beta'}(z,w)\end{pmatrix} = \begin{pmatrix} I & I \\ T & -T \end{pmatrix}\begin{pmatrix} K^{-1}_{\alpha,\beta'}(z,w) & \frac{1}{2}(I-T)K^{-1}_{\alpha,\beta'}(z,w) \\ K^{-1}_{\alpha',\beta}(z,w) & \frac{1}{2}(I+T)K^{-1}_{\alpha',\beta}(z,w)\end{pmatrix} \tag{II.39}$$

We take the determinant of these. The matrices $\begin{pmatrix} I & I \\ I & -I \end{pmatrix}$ and $\begin{pmatrix} I & I \\ T & -T \end{pmatrix}$ can be written in block-diagonal form, with blocks corresponding to the two copies of the pair $(\mathrm{x},\hat{\mathrm{x}})$ for $\mathrm{x} \in W^T$. For the two matrices, the blocks have determinant 4 and there are $2\mathcal{F}$ blocks, so both their determinants are equal to $2^{4\mathcal{F}}$.

The determinant of both sides of (II.39) can now be computed; we successively use the formula for determinants of block matrices, Lemma II.27 to exchange T and the matrices $K^{-1}_{\cdot,\cdot}(z,w)$, and $\det(D) = (-1)^{2\mathcal{F}} = 1$; we drop the (z,w) in the notation to make the computation clearer:

$$\begin{aligned}
\left|K^{-1}_{\alpha,\beta}\right|\left|K^{-1}_{\alpha',\beta'}\right| &= \left|K^{-1}_{\alpha',\beta}\right|\left|\frac{1}{2}(I-T)K^{-1}_{\alpha,\beta'} - K^{-1}_{\alpha,\beta'}K_{\alpha',\beta}\frac{1}{2}(I+T)K^{-1}_{\alpha',\beta}\right|\\
&= \left|K^{-1}_{\alpha',\beta}\right|\left|K^{-1}_{\alpha,\beta'}\right|\left|-\frac{1}{2}\left(K_{\alpha,\beta'}TK^{-1}_{\alpha,\beta'} + K_{\alpha',\beta}TK^{-1}_{\alpha',\beta}\right)\right|\\
&= \left|K^{-1}_{\alpha',\beta}\right|\left|K^{-1}_{\alpha,\beta'}\right|\left|-T + \frac{1}{2}\left(K_{\alpha,\beta'} + K_{\alpha',\beta}\right)D\right|\\
&= \left|K^{-1}_{\alpha',\beta}\right|\left|K^{-1}_{\alpha,\beta'}\right|\left|-TD + \frac{1}{2}\left(K_{\alpha,\beta'} + K_{\alpha',\beta}\right)\right|.
\end{aligned} \tag{II.40}$$

Notice that TD is exactly equal the part of $K_{\alpha,\beta}$ that corresponds to legs of G^T. Thus $-TD + \frac{1}{2}\left(K_{\alpha,\beta'} + K_{\alpha',\beta}\right)$ is a block-diagonal matrix, where blocks correspond to decorations

inside of the faces $\mathcal{F}$ of $\mathcal{Q}$. When the face is not crossed by $\gamma_x^{\mathcal{B}}$ nor $\gamma_y^{\mathcal{B}}$, the block we get is represented in Figure II.14, where (in the notation of the proof of Theorem II.22):

$$\tilde{a} = \frac{1}{2}\left(\frac{a}{c} + \frac{a'}{c'}\right)$$
$$\tilde{b} = \frac{1}{2}\left(\frac{b}{c} + \frac{b'}{c'}\right)$$
$$\tilde{d} = \frac{1}{2}\left(\frac{d}{c} + \frac{d'}{c'}\right)$$

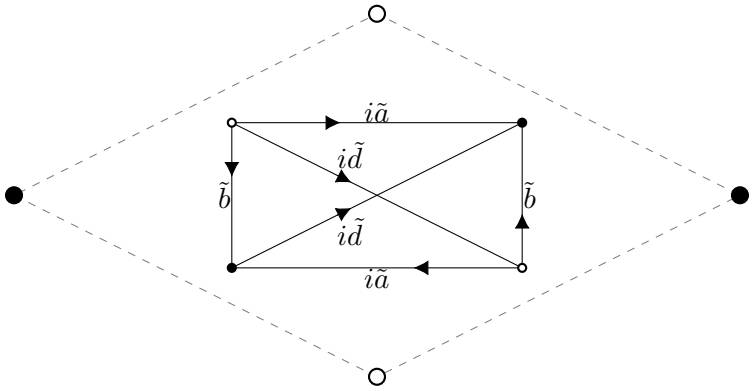

Figure II.14: Coefficients of the matrix $-TD + \frac{1}{2}\left(K_{\alpha,\beta'} + K_{\alpha',\beta}\right)$ at a face.

The determinant of this block can be easily computed using (II.7), giving

$$\left(\tilde{a}^2 + \tilde{b}^2 - \tilde{d}^2\right)^2 = \frac{1}{4}\left(1 + \frac{a}{c}\frac{a'}{c'} + \frac{b}{c}\frac{b'}{c'} - \frac{d}{c}\frac{d'}{c'}\right)^2$$
$$= \frac{\frac{a^2+b^2}{c^2}\frac{a'^2+b'^2}{c'^2}}{\frac{A^2+B^2}{C^2}\frac{A'^2+B'^2}{C'^2}}$$

When the face is crossed by $\gamma_x^{\mathcal{B}}$ or $\gamma_y^{\mathcal{B}}$, some weights are multiplied by $z^{\pm 1}, w^{\pm 1}$ but the determinant is the same.

All in all, (II.40) becomes

$$\left(\prod_{f\in\mathcal{F}} \frac{A(f)^2 + B(f)^2}{C(f)^2}\frac{A'(f)^2 + B'(f)^2}{C'(f)^2}\right)\left|K^{-1}_{\alpha,\beta}(z,w)\right|\left|K^{-1}_{\alpha',\beta'}(z,w)\right|$$
$$= \left(\prod_{f\in\mathcal{F}} \frac{a(f)^2 + b(f)^2}{c(f)^2}\frac{a'(f)^2 + b'(f)^2}{c'(f)^2}\right)\left|K^{-1}_{\alpha,\beta'}(z,w)\right|\left|K^{-1}_{\alpha',\beta}(z,w)\right|.$$

Using relation (II.9) finishes the proof. □

An important case appears when we set $\alpha = \beta'$ and $\beta = \alpha'$. The model with weights $X_{\alpha,\alpha}$ is actually a 6V model, and the weights of diagonals in G^T become null. This gives the bipartite decorated graph of Wu and Lin [WL75], see also [Dub11a, BdT14] which we denote $G^{\mathcal{Q}}$.

More precisely, our Kasteleyn skew-hermitian matrix $K_{\alpha,\alpha}(z,w)$ can be related to Boutillier, de Tilière and Raschel's $\mathcal{K}$ matrix from Section 5 of [BdTR18] - whose rows are indexed by white vertices and columns by black vertices of $G^{\mathcal{Q}}$ - via

$$K_{\alpha,\alpha}(z,w) = i\begin{pmatrix} & W^T & B^T \\ W^T & 0 & \overline{\mathcal{K}}_\alpha(z,w) \\ B^T & {}^t\mathcal{K}_\alpha(z^{-1},w^{-1}) & 0 \end{pmatrix}. \tag{II.41}$$

The determinant of $\mathcal{K}(z,w)$ is the characteristic polynomial of a bipartite dimer model; we denote it by $P^{6V}_\alpha(z,w)$. Thus $P^{6V}_\alpha(z,w)$ is the determinant of a matrix twice as small as $K_{\alpha,\beta}(z,w)$.

Corollary II.28. *Let $\mathcal{Q}$ be a quadrangulation in the toric case. Let (α,β) and (α',β') be two standard elements of $\left([0,2\pi)^{\mathcal{F}}\right)^2$. Then the characteristic polynomial of the 8V-model satisfies*

$$P^{8V}_{\alpha,\beta} = \tilde{c} P^{6V}_\alpha P^{6V}_\beta$$

for some constant $\tilde{c}$ satisfying

$$|\tilde{c}| = \prod_{f\in\mathcal{F}} \frac{2}{|C_{\alpha,\beta}(f)|}.$$

Proof. Equation (II.41) yields

$$P^{8V}_{\alpha,\alpha}(z,w) = \overline{P^{6V}_\alpha}(z,w)\ P^{6V}_\alpha(z^{-1},w^{-1}). \tag{II.42}$$

However, P^{6V}_α has extra symmetries. First, as it is the characteristic polynomial of a (bipartite) dimer model, up to a global factor its entries are real (see for instance Proposition 3.1 in [KOS06]), so that $\overline{P^{6V}_\alpha} = c_3 P^{6V}_\alpha$ for some constant $c_3 \in S^1$. It also corresponds to the dimer model on the decorated graph $G^{\mathcal{Q}}$, and the characteristic polynomial in that case is proportional to that of Fisher's decorated graph [Fis66] (see Section 4 of [Dub11a]). By Corollary 16 of [BdTR18],the characteristic polynomial on Fisher's graph has a symmetry $(z,w)\leftrightarrow(z^{-1},w^{-1})$. This gives $P^{6V}_\alpha(z,w) = P^{6V}_\alpha(z^{-1},w^{-1})$. As a result (II.42) becomes

$$P^{8V}_{\alpha,\alpha} = c_3 \left(P^{6V}_\alpha\right)^2$$

We can now apply Theorem II.26 with $\alpha=\beta'$ and $\beta=\alpha'$. By the same argument as for (II.12), $P^{8V}_{\alpha,\beta} = P^{8V}_{\beta,\alpha}$. Thus Theorem II.26 becomes

$$\left(P^{8V}_{\alpha,\beta}\right)^2 = c_2 c_3^2 \left(P^{6V}_\alpha P^{6V}_\beta\right)^2.$$

By analytic continuation and by computing the constant we get the desired relation. □

II.5 Z-invariant regime

In this section we restrict to the planar case. The graph may be periodic (in which case we will still make use of the toric case) or not. We study the Z-invariant regime of the model, which is a regime where the star-triangle relations are satisfied.

II.5.1 Checkerboard Yang-Baxter equations

Here we generalize Baxter's star-triangle relations [Bax78, Bax82] in our "checkerboard" setting, and we find free-fermion solutions.

Let us suppose that the quadrangulation $\mathcal{Q}$ contains three adjacent faces in the configuration on the left of Figure II.15. Then we can transform it locally into the configuration on the right. We need to update the weights of the eight-vertex model at the same time. This can be done in such a way that there exists a coupling of the configurations on the right and of the left quadrangulations, such that they agree everywhere except at the central dashed "triangles".

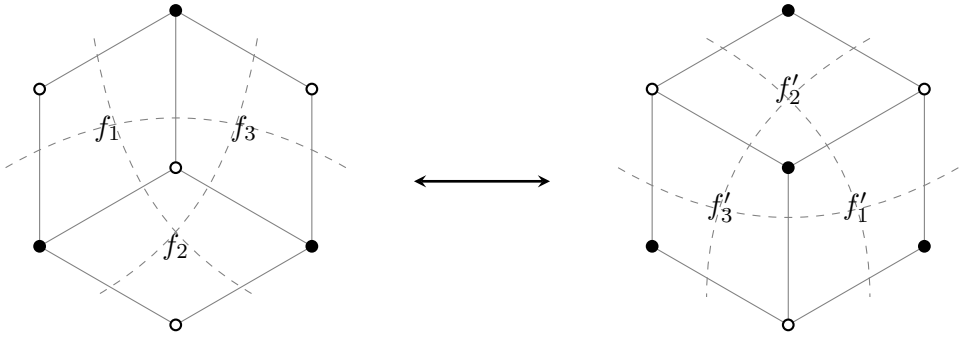

Figure II.15: "Star-triangle" move on the quadrangulation (solid lines) and its dual on which the 8V-configurations are defined (dashed lines).

Specifically, let us denote (a_i, b_i, c_i, d_i) the 8V-weights at f_i, and (a'_i, b'_i, c'_i, d'_i) those at f'_i. By conditioning on every possible boundary condition, we get the following equations for the existence of a coupling: for every i, j, k with $\{i, j, k\} = \{1, 2, 3\}$,

$$\begin{aligned}
c_i c_j c_k + a_i a_j a_k &\propto c'_i c'_j c'_k + b'_i b'_j b'_k \\
a_i c_j c_k + c_i a_j a_k &\propto c'_i a'_j a'_k + b'_i d'_j d'_k \\
c_i b_j b_k + a_i d_j d_k &\propto b'_i c'_j c'_k + c'_i b'_j b'_k \\
c_i d_j d_k + a_i b_j b_k &\propto c'_i d'_j d'_k + b'_i a'_j a'_k \\
c_i b_j d_k + a_i d_j b_k &\propto d'_i a'_j c'_k + a'_i d'_j b'_k
\end{aligned} \tag{II.43}$$

where the proportionality constants are all the same. We call equations (II.43) the *Yang-Baxter equations* of our model.

Remark II.29.

- Most of the equations (all but the last one) are invariant under some nontrivial subgroup of the permutation of indices $\{i, j, k\}$. All in all (II.43) contains 16 distinct equations.

- We presented the "star-triangle" move as going from the left configuration to the right one, but it can of course be done in both ways, giving the same set of equations.

Equations (II.43) are often written in matrix form. For the checkerboard setting, we define R and $\bar{R}$ matrices containing the weights at every face, with the indexing of Figure II.16:

$$R(f) = \begin{array}{c} \\ \\ \\ \\ \end{array} \begin{array}{c} \begin{array}{cccc} \diagup\diagdown & \diagdown\diagdown & \diagup\diagup & \diagdown\diagup \end{array} \\ \begin{pmatrix} C(f) & 0 & 0 & A(f) \\ 0 & D(f) & B(f) & 0 \\ 0 & B(f) & D(f) & 0 \\ A(f) & 0 & 0 & C(f) \end{pmatrix} \end{array},$$

$$\bar{R}(f) = \begin{array}{c} \\ \\ \\ \\ \end{array} \begin{array}{c} \begin{array}{cccc} \diagup\diagup & \diagup\diagup & \diagup\diagup & \diagup\diagup \end{array} \\ \begin{pmatrix} C(f) & 0 & 0 & B(f) \\ 0 & D(f) & A(f) & 0 \\ 0 & A(f) & D(f) & 0 \\ B(f) & 0 & 0 & C(f) \end{pmatrix} \end{array}.$$

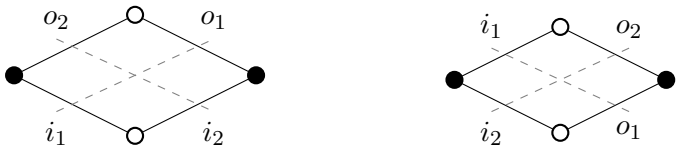

Figure II.16: Entries of $R(f)$ (left) and $\bar{R}(f)$ (right) are indexed by the occupation state of (i_1, i_2) and (o_1, o_2), in the order (absent, absent), (absent, present), (present, absent), (present, present).

These matrices are elements of $\mathrm{End}(V \otimes V)$, where V is a complex vector space of dimension 2. For $i, j \in \{1, 2, 3\}$, $i < j$, we define $\mathcal{R}_{i,j}(f) \in \mathrm{End}(V \otimes V \otimes V)$ that acts as $R(f)$ on the components i and j, and as the identity on the other component. We similarly define $\bar{\mathcal{R}}_{i,j}(f)$. Then equations (II.43) are equivalent to (see for instance [PAY06])

$$\mathcal{R}_{1,2}(f_1)\bar{\mathcal{R}}_{1,3}(f_2)\mathcal{R}_{2,3}(f_3) \propto \bar{\mathcal{R}}_{2,3}(f_3')\mathcal{R}_{1,3}(f_2')\bar{\mathcal{R}}_{1,2}(f_1').$$

II.5.2 Lozenge graphs

One way to make sure that (II.43) always hold is to make the 8V weights depend on the geometry of the embedding. This has been done for several models on special embedded graphs called *isoradial*; see for instance [Ken02]. In our context it is more natural to talk only about lozenge graphs.

We say that the planar quadrangulation $\mathcal{Q}$ is a *lozenge graph* if it is embedded in such a way that all faces are nondegenerate rhombi, with edge length equal to 1. Then for every $f \in \mathcal{F}$, there is a natural parameter $\theta(f) \in (0, \pi/2)$, which is the half-angle of the black corners of the rhombus. For a vertex $\mathrm{x} \in V^T$, we also denote $\theta(\mathrm{x}) = \theta(f)$ where f is the face containing x.

A lozenge graph $\mathcal{Q}$ is said to be *quasicrystalline* if the number l of possible directions $\pm e^{i\alpha}$ of the edges of the rhombi is finite. In that case there exists an $\epsilon > 0$ such that for all faces f, $\theta(f) \in (\epsilon, \frac{\pi}{2} - \epsilon)$.

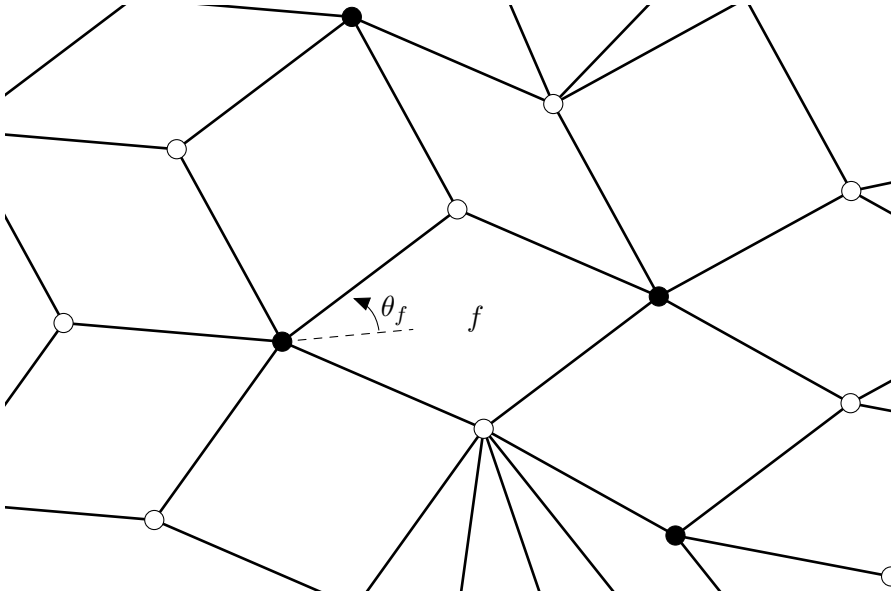

Figure II.17: A portion of a lozenge graph.

Let k be a complex number such that $k^2 \in (-\infty, 1)$, which will serve as an *elliptic modulus*. We denote by $\mathrm{K}(k)$ (or simply K) the complete elliptic integral of the first kind associated to k. We denote by $\mathrm{am}(\cdot|k)$ the Jacobi amplitude with modulus k. For every complex number $\theta \in \mathbb{C}$, we define θ_k as

$$\theta_k = \frac{2\mathrm{K}(k)}{\pi}\theta.$$

Proposition II.30. *Let $\mathcal{Q}$ be a lozenge graph. Let k, l be two elliptic moduli, with $k^2 \leq l^2$. For every $f \in \mathcal{F}$, let*

$$\begin{aligned} \alpha(f) &= \mathrm{am}\left(\theta(f)_k \middle| k\right), \\ \beta(f) &= \mathrm{am}\left(\theta(f)_l \middle| l\right). \end{aligned} \tag{II.44}$$

Then α, β satisfy (II.11)*, and the weights $X_{\alpha,\beta}$ satisfy the Yang-Baxter equations* (II.43)*.*

Proof. The rhombi are supposed to be nondegenerate so that $\theta_f \in (0, \frac{\pi}{2})$, and for $u \in (0, \mathrm{K}(k))$ one has $\mathrm{am}(u|k) \in (0, \frac{\pi}{2})$ (see for instance [AS64]). To show that (II.11) holds, it suffices to show that for all $\lambda \in (0, 1)$,

$$f_\lambda(k) = \mathrm{am}\left(\lambda \mathrm{K}(k) | k\right)$$

is an increasing function of $k^2 \in (-\infty, 1)$. This has been shown in [Jor55] (see also [CT83] for a reference in English) on the domain $k^2 \in [0, 1)$, but the proof works identically for $k^2 \in (-\infty, 1)$.

We now prove (II.43). It is easy to check that these equations are unchanged if we multiply the weights d at every face by -1. Simple but lengthy computations also show that they are still satisfied if we apply the duality of Proposition II.10 at every face. As a result,

we just have to check equations II.43 for the weights (II.14) (we show how these weights can be transformed into $X_{\alpha,\beta}$ in the proof of Corollary II.12). This holds *iff* the Ising models defined by α and β of (II.44) satisfy the star-triangle relations on lozenge graphs, which is the case as shown in [BdT10]. □

Remark II.31. The weights of this Z-invariant 8V model are

$$\begin{aligned}
A(f) &= \mathrm{sn}(\theta(f)_k|k) + \mathrm{sn}(\theta(f)_l|l)\\
B(f) &= \mathrm{cn}(\theta(f)_k|k) + \mathrm{cn}(\theta(f)_l|l)\\
C(f) &= 1 + \mathrm{sn}(\theta(f)_k|k)\,\mathrm{sn}(\theta(f)_l|l) + \mathrm{cn}(\theta(f)_k|k)\,\mathrm{cn}(\theta(f)_l|l)\\
D(f) &= \mathrm{cn}(\theta(f)_k|k)\,\mathrm{sn}(\theta(f)_l|l) - \mathrm{sn}(\theta(f)_k|k)\,\mathrm{cn}(\theta(f)_l|l)
\end{aligned}$$

The *dual* modulus of k is defined as $k' = \sqrt{1-k^2}$. When $k' = \frac{1}{l'}$, (or $l = k^*$ in the notation of [BdTR18]), the bipartite coloring no longer matters and we recover the Z-invariant weights of Baxter [Bax78, Bax82] at the free-fermion point.

When $k = l$, we get a Z-invariant 6V model whose corresponding bipartite dimer model has been studied in [BdTR18].

From now on, we suppose that $\mathcal{Q}$ is a lozenge graph, and that two elliptic moduli $k^2 \leq l^2$ are chosen. *We replace the indices α, β by k, l*, meaning that they correspond to the α, β of (II.44). We also slightly modify our Kasteleyn matrices by setting $\phi_e = \theta_e$ in the notation of Figure II.10. These angles also satisfy (II.24), (II.25), (II.26) so the results of Section II.4 still hold.

II.5.3 Local expression for $K_{k,l}^{-1}$

In the case where $k = l$, we have $\alpha = \beta$ and we already know that this corresponds to a free-fermionic *six*-vertex model – or equivalently to dimers on a bipartite decorated graph $G^{\mathcal{Q}}$. The operator $K_{k,k}$ can be written as

$$K_{k,k} = i\begin{array}{c} \begin{matrix} W^{\mathcal{Q}} & B^{\mathcal{Q}} \end{matrix} \\ \begin{pmatrix} 0 & \overline{\mathcal{K}_k} \\ {}^t\mathcal{K}_k & 0 \end{pmatrix} \end{array} \begin{matrix} W^{\mathcal{Q}} \\ B^{\mathcal{Q}} \end{matrix} \tag{II.45}$$

where $\mathcal{K}_k$ is the operator from black to white vertices, associated to the elliptic modulus k, defined in Section 5 of [BdTR18]; we only change notation slightly to emphasize the dependence on k. In the following subsection we recall the tools of [BdTR17, BdTR18] that are required to compute a local formula for $\mathcal{K}_k^{-1}$. Our definitions differ from those of [BdTR17, BdTR18] by the multiplication of the arguments by a factor $\frac{\pi}{2\mathrm{K}(k)}$, which is aimed at making the dependence in k more apparent.

a) Inverse of $\mathcal{K}_k$

Let $b \in B^T$ and $w \in W^T$. We chose a path on $\mathcal{Q}$ going from the half-edge closest to b to the half-edge closest to w, which we denote $\frac{1}{2}e^{i\alpha_1}, e^{i\alpha_2}, \ldots, e^{i\alpha_{n-1}}, \frac{1}{2}e^{i\alpha_n}$. We also set $a_1, \ldots, a_{n-1}$ to be the successive vertices of $\mathcal{Q}$ in that path. See Figure II.18. The following definitions do not depend on the choice of this path.

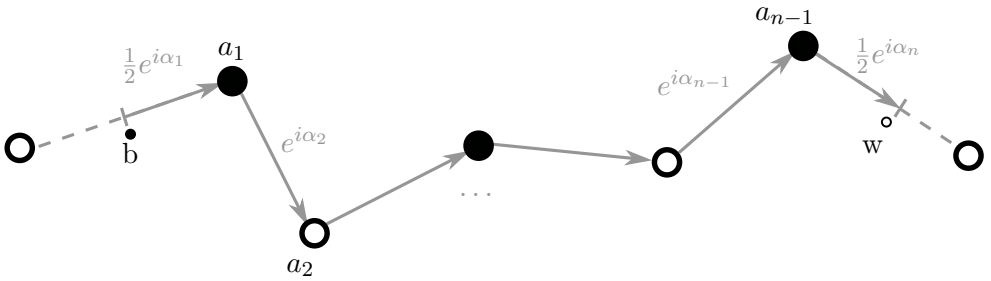

Figure II.18: A path on $\mathcal{Q}$ from b to w.

The *discrete k-massive exponential function* is defined in [BdTR17] as

$$\mathrm{e}_{a_1,a_{n-1}}(u|k) = \prod_{j=2}^{n-1} i\sqrt{k'}\ \mathrm{sc}\left(\left(\frac{u-\alpha_j}{2}\right)_k \middle| k\right).$$

This is a well-defined function of the complex argument u. It is moreover 2π-periodic, and $2i\pi\frac{\mathrm{K}'}{\mathrm{K}}$-periodic when a_1 and a_{n-1} are the same color (*i.e.* the product contains an even number of terms), $2i\pi\frac{\mathrm{K}'}{\mathrm{K}}$-antiperiodic otherwise.

Let also

$$h(u \mid k) = \begin{cases} \mathrm{nc}\left(\left(\frac{u-\alpha_1}{2}\right)_k \middle| k\right)\ \mathrm{nc}\left(\left(\frac{u-\alpha_n}{2}\right)_k \middle| k\right)\ (-k') & \text{if } a_1 \in \mathcal{B}, a_{n-1} \in \mathcal{B} \\ \mathrm{nc}\left(\left(\frac{u-\alpha_1}{2}\right)_k \middle| k\right)\ \mathrm{dc}\left(\left(\frac{u-\alpha_n}{2}\right)_k \middle| k\right)\ (-\sqrt{k'}) & \text{if } a_1 \in \mathcal{B}, a_{n-1} \in \mathcal{W} \\ \mathrm{dc}\left(\left(\frac{u-\alpha_1}{2}\right)_k \middle| k\right)\ \mathrm{nc}\left(\left(\frac{u-\alpha_n}{2}\right)_k \middle| k\right)\ \sqrt{k'} & \text{if } a_1 \in \mathcal{W}, a_{n-1} \in \mathcal{B} \\ \mathrm{dc}\left(\left(\frac{u-\alpha_1}{2}\right)_k \middle| k\right)\ \mathrm{dc}\left(\left(\frac{u-\alpha_n}{2}\right)_k \middle| k\right) & \text{if } a_1 \in \mathcal{W}, a_{n-1} \in \mathcal{W}. \end{cases}$$

Then the function $e^{-\frac{i}{2}(\alpha_n-\alpha_1)}h(u|k)$ is well defined and has the same (anti)periodicity as $e_{a_1,a_{n-1}}(u|k)$. As a result the following function is meromorphic on the torus $\mathbb{T}(k) = \mathbb{C}/\left(2\pi\mathbb{Z} + 2i\pi\frac{\mathrm{K}'}{\mathrm{K}}\mathbb{Z}\right)$:

$$f_{\mathrm{b,w}}(u|k) = e^{i\theta(\mathrm{w})}e^{-\frac{i}{2}(\alpha_n-\alpha_1)}\ h(u|k)\ e_{a_1,a_{n-1}}(u|k).$$

Its only possible poles are the $\alpha_i + \pi$. On can chose the paths joining b and w such that the angles α_i all lie in an open interval of length π. Let $\Gamma_{\mathrm{b,w}|k}$ be a vertical contour on $\mathbb{T}(k)$ avoiding this sector.

Theorem ([BdTR18], Theorem 37)**.** *For* $\mathrm{b} \in B^T, \mathrm{w} \in W^T$*, let*

$$\mathcal{K}_k^{-1}[\mathrm{b},\mathrm{w}] = \frac{\mathrm{K}(k)}{2i\pi^2}\int_{\Gamma_{\mathrm{b,w}|k}} f_{\mathrm{b,w}|k}(u)\ \mathrm{d}u. \tag{II.46}$$

Then $\mathcal{K}_k^{-1}$ *is an inverse of the operator* $\mathcal{K}_k$*. For* $k \neq 0$*, it is the only inverse with bounded coefficients.*

b) Inverse of $K_{k,l}$

By (II.45), the following are inverses of $K_{k,k}$ and $K_{l,l}$:

$$K_{k,k}^{-1} = -i\begin{pmatrix} & \begin{matrix} W^T & B^T \end{matrix} \\ \begin{matrix} W^T \\ B^T \end{matrix} & \begin{pmatrix} 0 & {}^t\mathcal{K}_k^{-1} \\ \mathcal{K}_k^{-1} & 0 \end{pmatrix} \end{pmatrix}, \quad K_{l,l}^{-1} = -i\begin{pmatrix} & \begin{matrix} W^T & B^T \end{matrix} \\ \begin{matrix} W^T \\ B^T \end{matrix} & \begin{pmatrix} 0 & {}^t\mathcal{K}_l^{-1} \\ \mathcal{K}_l^{-1} & 0 \end{pmatrix} \end{pmatrix}.$$

Corollary II.32. *The operator*

$$K_{k,l}^{-1} = \frac{1}{2}\left((I+T)K_{k,k}^{-1} + (I-T)K_{l,l}^{-1}\right)$$

is an inverse of $K_{k,l}$. It is the only inverse with bounded coefficients.

Its coefficients read, for $\mathrm{w}, \mathrm{w}' \in W^T, \mathrm{b}, \mathrm{b}' \in B^T$,

$$\begin{aligned}
K_{k,l}^{-1}[\mathrm{w},\mathrm{b}] &= \frac{-i}{2}\left(\mathcal{K}_k^{-1}[\mathrm{b},\mathrm{w}] + \mathcal{K}_l^{-1}[\mathrm{b},\mathrm{w}]\right), \\
K_{k,l}^{-1}[\mathrm{b},\mathrm{w}] &= \frac{-i}{2}\left(\overline{\mathcal{K}_k^{-1}[\mathrm{b},\mathrm{w}]} + \overline{\mathcal{K}_l^{-1}[\mathrm{b},\mathrm{w}]}\right), \\
K_{k,l}^{-1}[\mathrm{w},\mathrm{w}'] &= \frac{ie^{i\theta(\mathrm{w})}}{2}\left(\overline{\mathcal{K}_k^{-1}[\hat{\mathrm{w}},\mathrm{w}']} - \overline{\mathcal{K}_l^{-1}[\hat{\mathrm{w}},\mathrm{w}']}\right), \\
K_{k,l}^{-1}[\mathrm{b},\mathrm{b}'] &= \frac{ie^{-i\theta(\mathrm{b})}}{2}\left(\mathcal{K}_k^{-1}[\mathrm{b}',\hat{\mathrm{b}}] - \mathcal{K}_l^{-1}[\mathrm{b}',\hat{\mathrm{b}}]\right).
\end{aligned}$$

Proof. This is a direct consequence of (II.45), (II.46) and Theorem II.22. □

c) Asymptotics of coefficients

The asymptotics of the coefficients of $\mathcal{K}^{-1}$ for points b and w far away is also computed in [BdTR18]. To state the result, using the notation of Section a), we also introduce the following real function:

$$\chi(u,k) = \frac{1}{|a_1 - a_{n-1}|}\log\left[\mathrm{e}_{a_1,a_{n-1}}\left(u + i\pi\frac{\mathrm{K}'}{\mathrm{K}}\middle|\, k\right)\right].$$

As stated before, the α_i can be taken in an interval of length π; let α be the center of this interval. According to [BdTR17], for any $k \in (0,1)$ the equation $\frac{\partial\chi}{\partial u}(u,k) = 0$ has a unique solution in $\alpha + (-\frac{\pi}{2}, \frac{\pi}{2})$. Let $u_0(k)$ be this solution, then $u_0(k)$ corresponds to a local minimum of $\chi(\cdot|k)$, and $\chi(u_0(k),k) < 0$.

Theorem II.33 ([BdTR18], Theorem 38)**.** *Let $\mathcal{Q}$ be a quasicrystalline planar lozenge graph, and $k \in (0,1)$. Then when $|\mathrm{b} - \mathrm{w}| \to \infty$,*

$$\mathcal{K}_k^{-1}[\mathrm{b},\mathrm{w}] = \frac{\mathrm{K}(k)\ e^{i\theta(\mathrm{w})}e^{-\frac{i}{2}(\alpha_n-\alpha_1)}\ h\left(u_0(k) + i\pi\frac{\mathrm{K}'}{\mathrm{K}}\middle|\, k\right) + o(1)}{\sqrt{2\pi^2|a_1 - a_{n-1}|\frac{\partial^2\chi}{\partial u^2}(u_0(k),k)}}e^{|a_1-a_{n-1}|\chi(u_0(k),k)}.$$

The case $k = 0$ can be deduced from Theorem 4.3 of [Ken02] and corresponds to a polynomial decay of the coefficients of the inverse matrix.

To get precise asymptotics for $K^{-1}_{k,l}$, we need to compare two terms coming from $\mathcal{K}^{-1}_k$ and $\mathcal{K}^{-1}_l$. The following Lemma lets us compare the main term, $e^{|a_1-a_{n-1}|\chi(u_0(k),k)}$. The conclusion is natural, since the case $k = 0$ corresponds to critical models (where the decay of correlations is polynomial), while as k gets bigger the decay is exponential and should have a faster rate. Thus for $0 < k < l < 1$, only the term corresponding to k remains in the asymptotics.

Lemma II.34. *The function $k \mapsto |\chi(u_0(k), k)|$ is increasing in $(0, 1)$.*

The proof can be found in Appendix II.B.

Remark II.35. In the case of the Z-invariant elliptic Laplacian [BdTR17], Ising or free-fermion 6V model [BdTR18], the characteristic polynomial defines a Harnack curve of genus 1; in fact every Harnack curve of genus 1 with a central symmetry can be obtained in this way. This means that its amoeba's complement has only one bounded component, or "oval" (see Figure II.2). The boundary of this convex oval is parametrized by functions $\chi(\cdot, k)$ for appropriate paths, and the value of $\chi(u_0(k), k)$ corresponds to the position of an extremal point of the oval in the path direction. Thus Lemma II.34 shows that as k goes from 0 to 1, these ovals are actually included into each other. In [BdTR17] the authors show that the area of the oval grows from 0 to ∞, but the monotonic inclusion is new.

We can now deduce the asymptotics of coefficients for $K^{-1}_{k,l}$. There is a technical difficulty due to the fact that the prefactor $h\left(u_0(k) + i\pi\frac{\mathrm{K}'}{\mathrm{K}}\middle| k\right)$ in Theorem II.33 can be zero. This may happen when $u_0(k)$ is equal to α_1 or to α_n, in the notation of Figure II.18. We do not expect this to happen except for a finite number of moduli k, but we could not get rid of this hypothesis.

Corollary II.36. *Let $\mathcal{Q}$ be a quasicrystalline planar lozenge graph, and $0 \leq k < 1$. We let $|\mathrm{b} - \mathrm{w}| \to \infty$; suppose that there is an $\epsilon > 0$ such that $|u_0(k) - \alpha_1| > \epsilon, |u_0(k) - \alpha_n| > \epsilon$ for all b, w. Then*

$$K^{-1}_{k,l}[\mathrm{w}, \mathrm{b}] = \frac{-i\mathrm{K}(k)\ e^{i\theta(\mathrm{w})}e^{-\frac{i}{2}(\alpha_n-\alpha_1)}\ h\left(u_0(k) + i\pi\frac{\mathrm{K}'}{\mathrm{K}}\middle| k\right) + o(1)}{2\sqrt{2\pi^2|a_1 - a_{n-1}|\frac{\partial^2\chi}{\partial u^2}(u_0(k), k)}} e^{|a_1-a_{n-1}|\chi(u_0(k),k)}.$$

Proof. This comes immediately from Corollary II.32, Theorem II.33 and Lemma II.34. The fact that h is bounded away from zero is a consequence of the technical hypothesis, and the fact that $\frac{\partial^2\chi}{\partial u^2}(u_0(k), k)$ is bounded and bounded away from zero is proven in [BdTR17]. □

The other coefficients of $K^{-1}_{k,l}$ can be computed in a similar way using Corollary II.32, giving the same exponential behavior. When $k = 0 < l < 1$, the decay is polynomial, so that all these models can be considered as "critical".

We conclude this part on asymptotics with the computation of a critical parameter.

Proposition II.37. *Let $\mathcal{Q}$ be a quasicrystalline planar lozenge graph. For any b, w, as $k \to 0$, there exists positive constants $c, C > 0$ such that the exponential rate of decay $\chi(u_0(k), k)$ satisfies*

$$-Ck^2 \leq \chi(u_0(k), k) \leq -ck^2.$$

Proof. In the notation of Appendix II.B, we showed that the minimum of g is $\frac{1}{2}\log(k')$, so that

$$\chi\left(u_0(k),k\right) \geq \frac{n-2}{2r}\log(k') = \frac{n-2}{2r}\log\left((1-k^2)^{1/2}\right) \sim -\frac{n-2}{4r}k^2.$$

On the other hand, by Lemma 16 of [BdTR17], there exists an $\epsilon > 0$ such that $\chi\left(u_0(k),k\right) < \log(\sqrt{k'}\,\mathrm{nd}\,(\epsilon|k))$. As $\mathrm{nd}\,(\epsilon|k) \to 1$ when $k \to 0$, this is equivalent to $-\frac{1}{4}k^2$. □

II.5.4 Free energy and Gibbs measure

A Gibbs measure can be constructed by taking the limit of Boltzmann measures on toric graphs, *i.e.* to consider periodic boundary conditions. When $\mathcal{Q}$ is a $\mathbb{Z}^2$-periodic quadrangulation, we can define a toric exhaustion by $\mathcal{Q}_n = \mathcal{Q}/n\mathbb{Z}^2$.

Theorem II.38. *Let $\mathcal{Q}$ be a planar lozenge graph. For any $0 \leq k < l < 1$, there exists a unique probability measure $\mathcal{P}_{8V}$ on the space of 8V-configurations equipped with the σ-field generated by cylinders, such that for any $e_1,\dots,e_p \in \mathcal{E}$, each e_i corresponding to a "leg" of G^T whose endpoints we denote $\mathrm{b}_i \in B^T$ and $\mathrm{w}_i \in W^T$, if we set $\mathrm{V} = \{\mathrm{b}_1,\mathrm{w}_1,\dots,\mathrm{b}_p,\mathrm{w}_p\}$,*

$$\mathcal{P}_{8V}(e_1,\dots,e_m \in \tau) = \sqrt{\det\left[\left(K^{-1}_{k,l}\right)_V\right]}. \tag{II.47}$$

Moreover, $\mathcal{P}$ is a translation invariant ergodic Gibbs measure.

Proof of Theorem II.38. The proof follows closely from the arguments of [CKP01], see also Theorem 6 of [BdT10]. We sketch the main steps here.

First consider the case where $\mathcal{Q}$ is $\mathbb{Z}^2$-periodic. We denote $\mathbb{P}^n_{8V}$ the Boltzmann probability on $\mathcal{Q}_n$. We use Kolmogorov's extension theorem; to do so, it is sufficient to show that the right-hand side of (II.47) is the limit as $n \to \infty$ of the probability that $e_1,\dots,e_m \in \tau$ in the toric graph $\mathcal{Q}_n$. This probability is given by (II.27). Thus we want to compute the limit of $\mathrm{Pf}\left(\tilde{K}^{s,t}_{n;k,l}\right)_{V^c}$ (where the n means that the matrix is defined on $\mathcal{Q}_n$) for any $s,t \in \{0,1\}$. When $k \neq 0$ or $(s,t) \neq (0,0)$, the matrix $\tilde{K}^{s,t}_{n;k,l}$ is invertible and by Jacobi's identity,

$$\mathrm{Pf}\left(\tilde{K}^{s,t}_{n;k,l}\right)_{V^c} = \mathrm{Pf}\left[\left(\tilde{K}^{s,t}_{n;k,l}\right)^{-1}\right]_V \mathrm{Pf}\left(\tilde{K}^{s,t}_{n;k,l}\right). \tag{II.48}$$

By Lemma II.19 and Theorem II.25,

$$\left(\tilde{K}^{s,t}_{n;k,l}\right)^{-1} = \mathcal{D}^{-1}\frac{1}{2}\left[(I+T)\left(K^{s,t}_{n;k,k}\right)^{-1} + (I-T)\left(K^{s,t}_{n;l,l}\right)^{-1}\right]\mathcal{D}.$$

As $n \to \infty$, the coefficients of $\left(K^{s,t}_{n;k,k}\right)^{-1}$ tend to that of the infinite matrix $K^{-1}_{k,k}$ by the 6V case [BdTR18]. Using Corollary II.32 we get that the coefficients of $\left(\tilde{K}^{s,t}_{n;k,l}\right)^{-1}$ converge to that of the infinite matrix $\tilde{K}^{-1}_{k,l}$ (where the orientation of the infinite graph is obtained by periodizing the orientation of $\mathcal{Q}_1$).

As a result, (II.48) implies that for $(s,t) \neq (0,0)$ or $k \neq 0$,

$$\mathrm{Pf}\left(\tilde{K}^{s,t}_{n;k,l}\right)_{V^c} \sim_{n\to\infty} \mathrm{Pf}\left[\tilde{K}^{-1}_{k,l}\right]_V \mathrm{Pf}\left(\tilde{K}^{s,t}_{n;k,l}\right).$$

When $k = 0$ and $(s,t) = (0,0)$, the generic arguments in [BdT10] imply that

$$\frac{\mathrm{Pf}\left(\tilde{K}^{0,0}_{n;0,l}\right)_{V^c}}{\mathcal{Z}_{8V}(\mathcal{Q}_n, X_{0,l})} = O\left(\frac{1}{n}\right).$$

Using these estimates, Proposition II.21 implies

$$\mathbb{P}^n_{8V}(e_1,\dots,e_m \in \tau) \sim \mathrm{Pf}\left[\tilde{K}^{-1}_{k,l}\right]_V \left(\frac{\prod_{f\in\mathcal{F}_n} C_{k,l}(f)}{2\mathcal{Z}_{8V}(\mathcal{Q}_n, X_{k,l})} \sum_{s,t} \epsilon_{s,t}\, \mathrm{Pf}\left(\tilde{K}^{s,t}_{n;k,l}\right)\right)$$

where $\epsilon_{0,0} = -1$ and the others are 1. By Corollary II.20, the right-hand side is simply $\mathrm{Pf}\left[\tilde{K}^{-1}_{k,l}\right]_V = \sqrt{\det\left[\left(K^{-1}_{k,l}\right)_V\right]}$.

The non-periodic case can be deduced from the periodic case by the generic arguments of [dT07]. It comes from the uniqueness of an inverse of the infinite Kasteleyn matrix with bounded coefficients and the locality property of Corollary II.32. □

When $\mathcal{Q}$ is $\mathbb{Z}^2$-periodic, the *free energy* is defined as

$$F^{k,l}_{8V} = -\lim_{n\to\infty} \frac{1}{n^2} \log \mathcal{Z}_{8V}(\mathcal{Q}_n, X_{k,l}).$$

Its existence and exact value can be deduced from that of dimers [CKP01, KOS06], giving the following:

Proposition II.39. *Let $\mathcal{Q}$ be a periodic lozenge graph, and $0 \le k < l < 1$. Let $P^{8V}_{k,l}$ be the characteristic polynomial of the 8V-model on the toric graph $\mathcal{Q}_1$. Then*

$$F^{k,l}_{8V} = -\sum_{f\in\mathcal{F}_1} \log C_{k,l}(f) \; - \frac{1}{2}\iint_{\mathbb{T}^2} \left|\log P^{8V}_{k,l}(z,w)\right| \frac{\mathrm{d}z}{2i\pi z}\frac{\mathrm{d}w}{2i\pi w}.$$

II.A 8V-configurations as 1-forms

This section aims at providing a simple algebraic framework to understand 8V duality and order-disorder variables. Specifically, we write configurations as elements of certain $\mathbb{Z}_2$-modules, so we use additive notation; similar definitions can be found for various models, in multiplicative notation, in [Dub11b]. We do this for a quadrangulation $\mathcal{Q}$ only in the spherical case.

II.A.1 Setup

A spin configuration on the vertices $\mathcal{V}$ of $\mathcal{Q}$ can be seen as an element $\boldsymbol{\sigma} \in \mathbb{Z}_2^{\mathcal{V}}$ (we will use a bold notation to represent objects defined in $\mathbb{Z}_2$-modules). Then the spin-vertex correspondence sketched at the beginning of Section II.3.1 can be seen as a linear map $\boldsymbol{\Phi} : \mathbb{Z}_2^{\mathcal{V}} \to (\mathbb{Z}_2^2)^{\mathcal{F}}$, such that for a spin configuration $\boldsymbol{\sigma} = (\boldsymbol{\sigma}_v)_{v\in\mathcal{V}}$ and a face $f \in \mathcal{F}$ with boundary vertices $b, b' \in \mathcal{B}$ and $w, w' \in \mathcal{W}$,

$$\boldsymbol{\Phi}(\boldsymbol{\sigma})_f = (\boldsymbol{\sigma}_b + \boldsymbol{\sigma}_{b'}, \boldsymbol{\sigma}_w + \boldsymbol{\sigma}_{w'}).$$

Thus an 8V-configuration can be represented as an element $\boldsymbol{\tau} = (\boldsymbol{\alpha}_f, \boldsymbol{\beta}_f)_{f\in\mathcal{F}} \in \left(\mathbb{Z}_2^2\right)^{\mathcal{F}}$, with $\boldsymbol{\alpha}_f$ taking the value $\mathbf{0}$ when $\boldsymbol{\tau}_f$ is of type A or C (*i.e.* the black spins are equal) and $\mathbf{1}$ when it is of type B or D, and similarly for $\boldsymbol{\beta}_f$ and white spins. Note that this characterizes the 8V configuration up to global complement, so that this setup is only relevant in the zero field case.

Thus we define the set of 8V-configurations as $\boldsymbol{H} = \operatorname{Im} \boldsymbol{\Phi}$, which is a strict subset of $\left(\mathbb{Z}_2^2\right)^{\mathcal{F}}$. Also note that if $\boldsymbol{\tau} = (\boldsymbol{\alpha}_f, \boldsymbol{\beta}_f)_{f\in\mathcal{F}} \in \boldsymbol{H}$, then for any $b \in \mathcal{B}$, $\sum_{f\sim b} \boldsymbol{\beta}_f = \mathbf{0}$ where the sum is over all faces adjacent to b. Similarly, if $w \in \mathcal{W}$, $\sum_{f\sim w} \boldsymbol{\alpha}_f = \mathbf{0}$. This motivates the definition of $\boldsymbol{\Psi} : \left(\mathbb{Z}_2^2\right)^{\mathcal{F}} \to \mathbb{Z}_2^{\mathcal{V}}$, such that if $\boldsymbol{\tau} = (\boldsymbol{\alpha}_f, \boldsymbol{\beta}_f)_{f\in\mathcal{F}} \in \left(\mathbb{Z}_2^2\right)^{\mathcal{F}}$,

$$\boldsymbol{\Psi}(\boldsymbol{\tau})_x = \begin{cases} \sum_{f\sim x} \boldsymbol{\beta}_f & \text{if } x \in \mathcal{B}, \\ \sum_{f\sim x} \boldsymbol{\alpha}_f & \text{if } x \in \mathcal{W}. \end{cases}$$

The applications $\boldsymbol{\Phi}$ and $\boldsymbol{\Psi}$ can be considered as dual of each other. To do so, we equip $\left(\mathbb{Z}_2^2\right)^{\mathcal{F}}$ with the symplectic form $\langle\cdot|\cdot\rangle$

$$\langle \boldsymbol{\tau} | \boldsymbol{\tau}' \rangle = \sum_{f\in F} \boldsymbol{\alpha}_f \boldsymbol{\beta}'_f + \boldsymbol{\alpha}'_f \boldsymbol{\beta}_f,$$

and $\mathbb{Z}_2^{\mathcal{V}}$ with the canonical bilinear symmetric form $(\cdot,\cdot)$

$$(\boldsymbol{\sigma}, \boldsymbol{\sigma}') = \sum_{v\in V} \boldsymbol{\sigma}_v \boldsymbol{\sigma}'_v.$$

Proposition II.40.

1. *The applications $\boldsymbol{\Psi}$ and $\boldsymbol{\Phi}$ are dual of each other, meaning that for any $\boldsymbol{\sigma} \in \mathbb{Z}_2^{\mathcal{V}}$ and $\boldsymbol{\tau} \in \left(\mathbb{Z}_2^2\right)^{\mathcal{F}}$,*
$$\langle \boldsymbol{\Phi}\boldsymbol{\sigma} | \boldsymbol{\tau} \rangle = (\boldsymbol{\sigma}, \boldsymbol{\Psi}\boldsymbol{\tau}). \tag{II.49}$$
2. *$\boldsymbol{H} = \operatorname{Im} \boldsymbol{\Phi} = \ker \boldsymbol{\Psi}$. In other words, the following sequence is exact*
$$\mathbb{Z}_2^{\mathcal{V}} \xrightarrow{\boldsymbol{\Phi}} \left(\mathbb{Z}_2^2\right)^{\mathcal{F}} \xrightarrow{\boldsymbol{\Psi}} \mathbb{Z}_2^{\mathcal{V}}. \tag{II.50}$$
3. *$\boldsymbol{H} = \boldsymbol{H}^{\perp}$.*

Proof. Let $\boldsymbol{\sigma} = (\boldsymbol{\sigma}_v)_{v\in\mathcal{V}}$ and $\boldsymbol{\tau} = (\boldsymbol{\alpha}_f, \boldsymbol{\beta}_f)_{f\in\mathcal{F}}$. By linearity, it is enough to prove (II.49) when $\boldsymbol{\sigma}, \boldsymbol{\tau}$ are elements of the canonical basis, *i.e.* when $\boldsymbol{\sigma}_v$ is $\mathbf{0}$ for all vertices but one, and $\boldsymbol{\alpha}_f, \boldsymbol{\beta}_f$ are all $\mathbf{0}$ except one.

If $\boldsymbol{\sigma}_b$ is $\mathbf{1}$ for one black vertex $b \in \mathcal{B}$ and $\mathbf{0}$ for all other vertices, then $\boldsymbol{\Phi}\boldsymbol{\sigma}$ is $(\mathbf{1}, \mathbf{0})$ on faces adjacent to b and $(\mathbf{0}, \mathbf{0})$ otherwise. Two cases may appear:

- if $\boldsymbol{\alpha}_f = \mathbf{1}$ at some face f and all the other components of $\boldsymbol{\tau}$ are $\mathbf{0}$, then $\boldsymbol{\Psi}\boldsymbol{\tau}$ is $\mathbf{1}$ on the white vertices of f and $\mathbf{0}$ everywhere else, and we have
$$\langle \boldsymbol{\Phi}\boldsymbol{\sigma} | \boldsymbol{\tau} \rangle = (\boldsymbol{\sigma}, \boldsymbol{\Psi}\boldsymbol{\tau}) = \mathbf{0}.$$
- if $\boldsymbol{\beta}_f = \mathbf{1}$ at some face f and all the other components of $\boldsymbol{\tau}$ are $\mathbf{0}$, then $\boldsymbol{\Psi}\boldsymbol{\tau}$ is $\mathbf{1}$ on the black vertices of f and $\mathbf{0}$ everywhere else, and we have
$$\langle \boldsymbol{\Phi}\boldsymbol{\sigma} | \boldsymbol{\tau} \rangle = (\boldsymbol{\sigma}, \boldsymbol{\Psi}\boldsymbol{\tau}) = \begin{cases} \mathbf{1} & \text{if } u \text{ is a vertex of } f, \\ \mathbf{0} & \text{otherwise.} \end{cases}$$

The case where $\boldsymbol{\sigma}_w$ is $\mathbf{1}$ at a white vertex $w \in W$ and $\mathbf{0}$ elsewhere is similar. This proves *1.*

We now prove *2.* We already know that Im $\boldsymbol{\Phi} \subset \ker \boldsymbol{\Psi}$. Let us show that they have the same dimension.

- The kernel of $\boldsymbol{\Phi}$ is clearly composed of elements of $\mathbb{Z}_2^{\mathcal{V}}$ constant on $\mathcal{B}$ and constant on $\mathcal{W}$, so it has dimension 2. By the rank-nullity theorem, Im $\boldsymbol{\Phi}$ has dimension $|\mathcal{V}| - 2$.
- The applications $\boldsymbol{\Phi}$ and $\boldsymbol{\Psi}$ are dual of each other so they have the same rank. By the rank-nullity theorem, $\ker \boldsymbol{\Psi}$ has dimension $2|\mathcal{F}| - |\mathcal{V}| + 2$.
- We have Euler's formula $|\mathcal{V}| - |\mathcal{E}| + |\mathcal{F}| = 2$, and the graph is a quadrangulation so $4|\mathcal{F}| = 2|\mathcal{E}|$. Combining these gives $|\mathcal{V}| - 2 = 2|\mathcal{F}| - |\mathcal{V}| + 2$ as needed.

Since $\boldsymbol{\Phi}$ and $\boldsymbol{\Psi}$ are dual of each other, Im $\boldsymbol{\Phi} = (\ker \boldsymbol{\Psi})^{\perp}$ and *3* is obvious from *2.* □

Remark II.41.

- It is clear now that we are working with an avatar of discrete Hodge theory. The applications $\boldsymbol{\Phi}$ and $\boldsymbol{\Psi}$ are in fact the d applications defined by Mercat for the *double* of a chain complex [Mer01]. For that reason, we will now simply denote the sequence (II.50) as
$$\mathbb{Z}_2^{\mathcal{V}} \xrightarrow{\boldsymbol{d}} \left(\mathbb{Z}_2^2\right)^{\mathcal{F}} \xrightarrow{\boldsymbol{d}} \mathbb{Z}_2^{\mathcal{V}}$$
so, for instance, an 8V configuration is a closed 1-form (i.e. a $\boldsymbol{\tau} \in \left(\mathbb{Z}_2^2\right)^{\mathcal{F}}$ s.t. $\boldsymbol{d\tau} = \mathbf{0}$).
- The elements of $\left(\mathbb{Z}_2^2\right)^{\mathcal{F}} \setminus \boldsymbol{H}$ do not correspond to 8V-configurations, but can be thought of as configurations with defects. More precisely, if $\boldsymbol{d\tau} = \mathbf{1}_{B_1 \cup W_1}$, with $B_1 \subset \mathcal{B}$ and $W_1 \subset \mathcal{W}$, then B_1 and W_1 have to be of even cardinality, and $\boldsymbol{\tau}$ corresponds to the disordered configurations of [Dub11a] mentioned in b). We will alternatively denote $\boldsymbol{d\tau} = B_1 \cup W_1$.
- Properties similar to Proposition II.40 might hold when $\mathcal{Q}$ is not a quadrangulation of the sphere but of the torus, or other surfaces. These are beyond the scope of the present chapter.

II.A.2 Fourier transform

Let $g : \left(\mathbb{Z}_2^2\right)^{\mathcal{F}} \to \mathbb{C}$. We define its Fourier transform $\hat{g} : \left(\mathbb{Z}_2^2\right)^{\mathcal{F}} \to \mathbb{C}$ by

$$\hat{g}(\boldsymbol{\tau}) = 2^{-|\mathcal{F}|} \sum_{\boldsymbol{\tau}' \in \left(\mathbb{Z}_2^2\right)^{\mathcal{F}}} (-1)^{\langle \boldsymbol{\tau} | \boldsymbol{\tau}' \rangle} g(\boldsymbol{\tau}').$$

The normalization is such that we have the Inverse Fourier transform formula is $\hat{\hat{g}} = g$.

Another important formula is Poisson's summation identity. For any subspace $\boldsymbol{F} \subset \left(\mathbb{Z}_2^2\right)^{\mathcal{F}}$,

$$\sum_{\boldsymbol{\tau} \in \boldsymbol{F}} g(\boldsymbol{\tau}) = \sum_{\boldsymbol{\tau} \in \boldsymbol{F}^{\perp}} \hat{g}(\boldsymbol{\tau}).$$

Example II.42. *For 8V weights $X : \mathcal{F} \to \mathbb{R}^4$, the weight function w_{8V} that we defined for 8V-configuration* (II.3) *can be extended to a function on $(\mathbb{Z}_2^2)^{\mathcal{F}}$. Then it is easy to check that its Fourier transform is actually the weight function for the dual weights $\hat{X}$* (II.15)*. Then Poisson's summation identity applied to $\boldsymbol{H}$, given that $\boldsymbol{H} = \boldsymbol{H}^\perp$, becomes*

$$\sum_{\boldsymbol{\tau} \in \boldsymbol{H}} w_{8V}(\boldsymbol{\tau}) = \sum_{\boldsymbol{\tau} \in \boldsymbol{H}} \hat{w}_{8V}(\boldsymbol{\tau})$$

which is the duality relation for partition functions (II.16)*.*

II.A.3 Correlators

We now describe how correlators of Definition II.7 fit into this description. In the absence of disorder, the order variables $\sigma(B_0)\sigma(W_0)$ correspond to a random variable taking value 1 (resp. -1) when there is an even (resp. odd) number of edges in $\boldsymbol{\tau}$ between the B_0, W_0 joined pairwise. If we fix paths $\gamma_{B_0}, \gamma_{W_0}$, and if $\boldsymbol{\tau} = (\boldsymbol{\alpha}_f, \boldsymbol{\beta}_f)_{f \in \mathcal{F}}$, this is equivalent to considering

$$\prod_{f \in \gamma_{B_0}} (-1)^{\boldsymbol{\alpha}_f} \prod_{f \in \gamma_{W_0}} (-1)^{\boldsymbol{\beta}_f}.$$

If we define $\boldsymbol{\tau}_\gamma = (\mathbf{1}_{\gamma_{W_0}}, \mathbf{1}_{\gamma_{B_0}})$ (where the paths are identified with subsets of $\mathcal{F}$), then this quantity is exactly $(-1)^{\langle \boldsymbol{\tau}_\gamma | \boldsymbol{\tau} \rangle}$. On the other hand, disorder variables at B_1, W_1 correspond to configurations $\boldsymbol{\tau}$ with $\boldsymbol{d\tau} = B_1 \cup W_1$. Thus we have:

$$\langle \sigma(B_0)\sigma(W_0)\mu(B_1)\mu(W_1) \rangle_{X,\gamma}^{8V} = 2 \sum_{\substack{\boldsymbol{\tau} \text{ s.t.} \\ \boldsymbol{d\tau} = B_1 \cup W_1}} (-1)^{\langle \boldsymbol{\tau}_\gamma | \boldsymbol{\tau} \rangle} w_{8V}(\boldsymbol{\tau}).$$

The factor 2 comes from the fact that the representation of 8V-configurations in $(\mathbb{Z}_2^2)^{\mathcal{F}}$ is two-to-one.

Proof of Theorem II.15. Our goal is to prove that for any 8V-configuration $\tau \in \Omega(\mathcal{Q})$,

$$\mathbb{P}_{8V}\left(\tau_{\alpha,\beta} \oplus \tau_{\alpha',\beta'} = \tau\right) = \mathbb{P}_{8V}\left(\tau_{\alpha,\beta'} \oplus \tau_{\alpha',\beta} = \tau\right).$$

By definition of Boltzmann probabilities, this is equivalent to (we indicate the dependence of w_{8V} in the α, β variables):

$$\sum_{\substack{\tau_{\alpha,\beta}, \tau_{\alpha',\beta'} \text{ s.t.} \\ \tau_{\alpha,\beta} \oplus \tau_{\alpha',\beta'} = \tau}} \frac{w_{8V}^{\alpha,\beta}(\tau_{\alpha,\beta})}{\mathcal{Z}_{8V}(\mathcal{Q}, X_{\alpha,\beta})} \frac{w_{8V}^{\alpha',\beta'}(\tau_{\alpha',\beta'})}{\mathcal{Z}_{8V}(\mathcal{Q}, X_{\alpha',\beta'})} = \sum_{\substack{\tau_{\alpha,\beta'}, \tau_{\alpha',\beta} \text{ s.t.} \\ \tau_{\alpha,\beta'} \oplus \tau_{\alpha',\beta} = \tau}} \frac{w_{8V}^{\alpha,\beta'}(\tau_{\alpha,\beta'})}{\mathcal{Z}_{8V}(\mathcal{Q}, X_{\alpha,\beta'})} \frac{w_{8V}^{\alpha',\beta}(\tau_{\alpha',\beta})}{\mathcal{Z}_{8V}(\mathcal{Q}, X_{\alpha',\beta})}.$$

We already know that the product of partition functions are proportional with a factor c_1 (II.20), so we just have to show that

$$\sum_{\substack{\tau_{\alpha,\beta}, \tau_{\alpha',\beta'} \text{ s.t.} \\ \tau_{\alpha,\beta} \oplus \tau_{\alpha',\beta'} = \tau}} w_{8V}^{\alpha,\beta}(\tau_{\alpha,\beta}) w_{8V}^{\alpha',\beta'}(\tau_{\alpha',\beta'}) = c_1 \sum_{\substack{\tau_{\alpha,\beta'}, \tau_{\alpha',\beta} \text{ s.t.} \\ \tau_{\alpha,\beta'} \oplus \tau_{\alpha',\beta} = \tau}} w_{8V}^{\alpha,\beta'}(\tau_{\alpha,\beta'}) w_{8V}^{\alpha',\beta}(\tau_{\alpha',\beta}). \tag{II.51}$$

To prove (II.51), we first rewrite the correlators of Theorem II.13 in the formalism of 1-forms. In the particular case $B = B_0 = B_0'$, $W = W_0 = W_0'$ and $B_1 = B_1' = W_1 = W_1' = \emptyset$, let $\boldsymbol{\tau}_\gamma = (\mathbf{1}_{\gamma_W}, \mathbf{1}_{\gamma_B})$, then (II.19) reads

$$\sum_{\boldsymbol{\tau}',\boldsymbol{\tau}''\in\boldsymbol{H}} (-1)^{\langle \boldsymbol{\tau}'+\boldsymbol{\tau}''|\boldsymbol{\tau}_\gamma\rangle} w_{8V}^{\alpha,\beta}(\boldsymbol{\tau}') w_{8V}^{\alpha',\beta'}(\boldsymbol{\tau}'') = c_1 \sum_{\boldsymbol{\tau}',\boldsymbol{\tau}''\in\boldsymbol{H}} (-1)^{\langle \boldsymbol{\tau}'+\boldsymbol{\tau}''|\boldsymbol{\tau}_\gamma\rangle} w_{8V}^{\alpha,\beta'}(\boldsymbol{\tau}') \boldsymbol{w}_{8V}^{\alpha',\beta}(\boldsymbol{\tau}'').$$

Reordering these sums according to $\boldsymbol{\tau} = \boldsymbol{\tau}' + \boldsymbol{\tau}''$ gives

$$\sum_{\boldsymbol{\tau}\in\left(\mathbb{Z}_2^2\right)^{\mathcal{F}}} (-1)^{\langle \boldsymbol{\tau}|\boldsymbol{\tau}_\gamma\rangle} \sum_{\substack{\boldsymbol{\tau}',\boldsymbol{\tau}''\in\boldsymbol{H}\ s.t \\ \boldsymbol{\tau}'+\boldsymbol{\tau}''=\boldsymbol{\tau}}} w_{8V}^{\alpha,\beta}(\boldsymbol{\tau}') \boldsymbol{w}_{8V}^{\alpha',\beta'}(\boldsymbol{\tau}'') = c_1 \sum_{\boldsymbol{\tau}\in\left(\mathbb{Z}_2^2\right)^{\mathcal{F}}} (-1)^{\langle \boldsymbol{\tau}|\boldsymbol{\tau}_\gamma\rangle} \sum_{\substack{\boldsymbol{\tau}',\boldsymbol{\tau}''\in\boldsymbol{H}\ s.t \\ \boldsymbol{\tau}'+\boldsymbol{\tau}''=\boldsymbol{\tau}}} w_{8V}^{\alpha,\beta'}(\boldsymbol{\tau}') \boldsymbol{w}_{8V}^{\alpha',\beta}(\boldsymbol{\tau}'').$$

Note that we always have $\boldsymbol{\tau} = \boldsymbol{\tau}' + \boldsymbol{\tau}'' \in \boldsymbol{H}$, so when $\boldsymbol{\tau} \notin \boldsymbol{H}$ the inner sum is empty. We rewrite this as

$$\sum_{\boldsymbol{\tau}\in\left(\mathbb{Z}_2^2\right)^{\mathcal{F}}} (-1)^{\langle \boldsymbol{\tau}|\boldsymbol{\tau}_\gamma\rangle} f(\boldsymbol{\tau}) = 0$$

where

$$f(\boldsymbol{\tau}) = \sum_{\substack{\boldsymbol{\tau}',\boldsymbol{\tau}''\in\boldsymbol{H}\ s.t \\ \boldsymbol{\tau}'+\boldsymbol{\tau}''=\boldsymbol{\tau}}} w_{8V}^{\alpha,\beta}(\boldsymbol{\tau}') w_{8V}^{\alpha',\beta'}(\boldsymbol{\tau}'') \ - c_1 \sum_{\substack{\boldsymbol{\tau}',\boldsymbol{\tau}''\in\boldsymbol{H}\ s.t \\ \boldsymbol{\tau}'+\boldsymbol{\tau}''=\boldsymbol{\tau}}} w_{8V}^{\alpha,\beta'}(\boldsymbol{\tau}') w_{8V}^{\alpha',\beta}(\boldsymbol{\tau}'').$$

In other words, we have $\hat{f}(\boldsymbol{\tau}_\gamma) = 0$. This is true for any B, W and paths γ joining them pairwise. Conversely, any element $\boldsymbol{\tau} \in \left(\mathbb{Z}_2^2\right)^{\mathcal{F}}$ can be considered as such a $\boldsymbol{\tau}_\gamma$ – namely, if $\boldsymbol{d\tau} = B \cup W$, then $\boldsymbol{\tau} = (\mathbf{1}_{\gamma_W}, \mathbf{1}_{\gamma_B})$ for some paths γ_B, γ_W that satisfy the hypothesis of Theorem II.13. This means that $\hat{f}$ is actually the null function, and by injectivity of the Fourier transform, so is f. This proves (II.51). □

Remark II.43. In the previous proof, if we let B_1, B_1', W_1, W_1' be any even subsets of black and white vertices of $\mathcal{Q}$, we get

$$\sum_{\substack{\boldsymbol{\tau}',\boldsymbol{\tau}''\in\left(\mathbb{Z}_2^2\right)^{\mathcal{F}}\ s.t \\ \boldsymbol{\tau}'+\boldsymbol{\tau}''=\boldsymbol{\tau} \\ \boldsymbol{d\tau}'=B_1\cup W_1 \\ \boldsymbol{d\tau}''=B_1'\cup W_1'}} \frac{w_{8V}^{\alpha,\beta}(\boldsymbol{\tau}')}{\mathcal{Z}_{8V}(\mathcal{Q}, X_{\alpha,\beta})} \frac{w_{8V}^{\alpha',\beta'}(\boldsymbol{\tau}'')}{\mathcal{Z}_{8V}(\mathcal{Q}, X_{\alpha',\beta'})} = \sum_{\substack{\boldsymbol{\tau}',\boldsymbol{\tau}''\in\left(\mathbb{Z}_2^2\right)^{\mathcal{F}}\ s.t \\ \boldsymbol{\tau}'+\boldsymbol{\tau}''=\boldsymbol{\tau} \\ \boldsymbol{d\tau}'=B_1'\cup W_1 \\ \boldsymbol{d\tau}''=B_1\cup W_1'}} \frac{w_{8V}^{\alpha,\beta'}(\boldsymbol{\tau}')}{\mathcal{Z}_{8V}(\mathcal{Q}, X_{\alpha,\beta'})} \frac{w_{8V}^{\alpha',\beta}(\boldsymbol{\tau}'')}{\mathcal{Z}_{8V}(\mathcal{Q}, X_{\alpha',\beta})}$$

which expresses a coupling for the XOR of 8V-configurations *with disorder*.

II.B Proof of Lemma II.34

By rotating the graph, we can suppose that $\alpha = 0$, *i.e.* the angles α_i and $u_0(k)$ all lie in $(-\frac{\pi}{2}, \frac{\pi}{2})$. We also fix a $k \in (0,1)$ and suppose that $u_0(k) \geq 0$, the other case being symmetric.

Using the chain rule we have

$$\frac{\mathrm{d}}{\mathrm{d}k}\chi(u_0(k), k) = \frac{\mathrm{d}}{\mathrm{d}k}u_0(k)\frac{\partial\chi}{\partial u}(u_0(k), k) + \frac{\partial\chi}{\partial k}(u_0(k), k).$$

By definition of $u_0(k)$ the first term of the sum is null so we just have to show that $\frac{\partial \chi}{\partial k}$ is negative at $(u_0(k), k)$.

We denote $r = |a_1 - a_{n-1}|$; this does not depend on k. By using the change of arguments in Jacobi elliptic functions (see Table 16.8 in [AS64]),

$$\chi(u,k) = \frac{1}{r}\sum_{j=2}^{n-1} \log\left[\sqrt{k'}\,\mathrm{nd}\left(\left(\frac{u-\alpha_j}{2}\right)_k \middle| k\right)\right]. \tag{II.52}$$

Let

$$g(u,k) = \log\left[\sqrt{k'}\,\mathrm{nd}\left(\left(\frac{u}{2}\right)_k \middle| k\right)\right].$$

By the properties of the function $\mathrm{nd}(\cdot,k)$ (see 16.2 in [AS64]), for any $k \in (0,1)$, $g(\cdot,k)$ is decreasing on $[-\pi,0]$ and increasing on $[0,\pi]$. Its minimum is $g(0,k) = \frac{1}{2}\log(k') < 0$. As a result, if all the angles α_j are equal, then $u_0(k)$ has the same value and $\chi(u_0(k),k) = \frac{n-2}{2r}\log(k')$, which is indeed a decreasing function of k. We now suppose that the α_j are not all equal. We need some extra properties on g.

Lemma II.44. *For all $k \in (0,1)$,*

1. *$g(-u,k) = g(u,k)$ and $g(\pi-u,k) = -g(u,k)$.*
2. *$\frac{\partial g}{\partial k}(u,k)$ is a strictly decreasing function of u on $[-\pi,0]$, and strictly increasing on $[0,\pi]$. It is zero at $u = \pm\frac{\pi}{2}$.*

Lemma II.45. *We have the following inequality of cardinals:*

$$\#\left\{j \in [2,n-1] \mid \alpha_j < u_0(k) - \frac{\pi}{2}\right\} < \#\left\{j \in [2,n-1] \mid \alpha_j > u_0(k)\right\}.$$

We prove these two Lemmas later, and first show how they imply Lemma II.34. By differentiation of (II.52), for $u \in [0, \frac{\pi}{2})$ we have (using Lemma II.44 to remove possible terms equal to zero):

$$\begin{aligned} r\,\frac{\partial \chi}{\partial k}(u,k) &= \sum_{j=2}^{n-1} \frac{\partial g}{\partial k}(u-\alpha_j,k) \\ &= \sum_{j|\alpha_j<u-\frac{\pi}{2}} \frac{\partial g}{\partial k}(u-\alpha_j,k) \;+ \sum_{j|u-\frac{\pi}{2}<\alpha_j\le u} \frac{\partial g}{\partial k}(u-\alpha_j,k) \;+ \sum_{j|u<\alpha_j} \frac{\partial g}{\partial k}(u-\alpha_j,k) \end{aligned} \tag{II.53}$$

By Lemma II.44, the terms in the first sum are positive while those in the second an third sums are negative. We show that for $u = u_0(k)$, the first sum is, in absolute value, smaller than the third one, which is enough to conclude.

For the first sum, if $-\frac{\pi}{2} < \alpha_j < u - \frac{\pi}{2}$ then $\frac{\pi}{2} < u - \alpha_j < u + \frac{\pi}{2}$ and by Lemma II.44,

$$0 < \frac{\partial g}{\partial k}(u-\alpha_j,k) < \frac{\partial g}{\partial k}\left(u+\frac{\pi}{2},k\right).$$

Thus the first sum S_1 in (II.53) satisfies

$$0 \leq S_1 \leq \left(\frac{\partial g}{\partial k}\left(u+\frac{\pi}{2},k\right)\right) \ \#\left\{j \in [2,n-1] \mid \alpha_j < u-\frac{\pi}{2}\right\}. \tag{II.54}$$

Similarly, for the third sum S_3, we have

$$S_3 \leq \left(\frac{\partial g}{\partial k}\left(u-\frac{\pi}{2},k\right)\right) \ \#\left\{j \in [2,n-1] \mid \alpha_j > u\right\} < 0. \tag{II.55}$$

By Lemma II.44, $g\left(u+\frac{\pi}{2},k\right) = -g\left(u-\frac{\pi}{2},k\right) > 0$, and by differentiating the same symmetry holds for $\frac{\partial g}{\partial k}$. Hence (II.55) becomes

$$|S_3| \geq \left(\frac{\partial g}{\partial k}\left(u+\frac{\pi}{2},k\right)\right) \ \#\left\{j \in [2,n-1] \mid \alpha_j > u\right\}. \tag{II.56}$$

Using (II.56), (II.54) and Lemma II.45 we see that for $u = u_0(k)$, $|S_3| > S_1$ as needed. □

Proof of Lemma II.44. The first point is a direct consequence of the change of arguments in elliptic functions, see Table 16.8 in [AS64].

For the second point, first notice that for all k, using Table 16.5 in [AS64], $g\left(\frac{\pi}{2},k\right) = 1$ so $\frac{\partial g}{\partial k}\left(\frac{\pi}{2},k\right) = 0$. Using the symmetries of the first point of the Lemma, it remains to check that $\frac{\partial g}{\partial k}(u,k)$ is a strictly increasing function of u on $\left[0,\frac{\pi}{2}\right]$.

Using the derivatives of elliptic functions with respect to u and k (see Sections 2.5 and 3.10 in [Law89]), and setting $v = \left(\frac{u}{2}\right)_k$, we get

$$\frac{\partial g}{\partial k}(u,k) = -\frac{k}{2k'^2} + \frac{k}{k'^2}\left(\frac{v}{\mathrm{K}(k)}\mathrm{E}(k) - \mathrm{E}(v,k) + \frac{\mathrm{sn}\,\mathrm{dn}}{\mathrm{cn}}(v|k)\right)\frac{\mathrm{sn}\,\mathrm{cn}}{\mathrm{dn}}(v|k) \tag{II.57}$$

where E is the elliptic integral of the second kind:

$$\mathrm{E}(v,k) = \int_0^v \mathrm{dn}^2(t|k)\mathrm{d}t,$$
$$\mathrm{E}(k) = \mathrm{E}(\mathrm{K}(k),k).$$

As $v = \frac{\mathrm{K}(k)}{\pi}u$, it is sufficient to prove that the right-hand side of (II.57) is a strictly increasing function of v on $\left[0,\frac{\mathrm{K}(k)}{2}\right]$. On that interval,

- $v \mapsto \frac{v}{\mathrm{K}(k)}\mathrm{E}(k) - \mathrm{E}(v,k) + \frac{\mathrm{sn}\,\mathrm{dn}}{\mathrm{cn}}(v|k)$ is strictly increasing because its derivative in v is (using Section 2.5 in [Law89])

$$\frac{\mathrm{E}(k)}{\mathrm{K}(k)} + k'^2\mathrm{sc}(v|k) > 0$$

- $v \mapsto \frac{\mathrm{sn}\,\mathrm{cn}}{\mathrm{dn}}(v|k)$ is strictly increasing because, using the ascending Landen transform $\tilde{k} = \frac{1-k'}{1+k'}$ (see 16.14.1 in [AS64]), this is equal to

$$\frac{1+\tilde{k}}{2}\,\mathrm{sn}\left(2\frac{\mathrm{K}(\tilde{k})}{\mathrm{K}(k)}v\middle|\tilde{k}\right)$$

and $\mathrm{sn}(\cdot|\tilde{k})$ is strictly increasing on $[0,\mathrm{K}(\tilde{k})]$.

As a result, (II.57) is a strictly increasing function of v on $\left[0, \frac{\mathrm{K}(k)}{2}\right]$. □

Proof of Lemma II.45. We take again $\tilde{k} = \frac{1-k'}{1+k'}$. By equation (26) in [BdTR17], $u_0(k)$ is also the unique element of $(-\frac{\pi}{2}, \frac{\pi}{2})$ such that

$$\sum_{j=2}^{n-1} \mathrm{sn}\left((u_0(k) - \alpha_j)_{\tilde{k}} \middle| \tilde{k} \right) = 0. \tag{II.58}$$

Let $s_j = \mathrm{sn}\left((u_0(k) - \alpha_j)_{\tilde{k}} \middle| \tilde{k} \right)$. We fix an $\epsilon > 0$ such that the angles α_i and $u_0(k)$ all lie in $(-\frac{\pi}{2} + \epsilon, \frac{\pi}{2} - \epsilon)$. Since we supposed that $u_0(k) \geq 0$, we have $u_0(k) - \alpha_j \in \left[-\frac{\pi}{2} + \epsilon, \pi - \epsilon\right]$. As a result, $(u_0(k) - \alpha_j)_{\tilde{k}} \in \left[-\mathrm{K}(\tilde{k}) + \epsilon_{\tilde{k}}, 2\mathrm{K}(\tilde{k}) - \epsilon_{\tilde{k}}\right]$. By the properties of the sn function, this implies that $s_j < 0$ when $\alpha_j > u_0(k)$, that $s_j > 0$ when $\alpha_j < u_0(k)$, and that $s_j = 0$ when $\alpha_j = u_0(k)$. As a result,

$$\sum_{j|\alpha_j < u_0(k)} s_j = \sum_{j|\alpha_j > u_0(k)} (-s_j)$$

where all the terms in the sums are positive. In particular,

$$\sum_{j|\alpha_j < u_0(k) - \frac{\pi}{2}} s_j \leq \sum_{j|\alpha_j > u_0(k)} (-s_j).$$

When $\alpha_j < u_0(k) - \frac{\pi}{2}$, then $(u_0(k) - \alpha_j)_{\tilde{k}} \in \left[\mathrm{K}(\tilde{k}), \mathrm{K}(\tilde{k}) + (u_0(k) - \epsilon)_{\tilde{k}}\right)$. Since $\mathrm{sn}(\cdot, \tilde{k})$ is decreasing on $[\mathrm{K}(\tilde{k}), 2\mathrm{K}(\tilde{k})]$, in that case

$$0 < \mathrm{sn}\left(\mathrm{K}(\tilde{k}) + (u_0(k) - \epsilon)_{\tilde{k}} \middle| \tilde{k} \right) < s_j \leq 1.$$

When $\alpha_j > u_0(k)$, then $(u_0(k) - \alpha_j)_{\tilde{k}} \in \left(-\mathrm{K}(\tilde{k}) + (u_0(k) + \epsilon)_{\tilde{k}}, 0\right)$. Since $\mathrm{sn}(\cdot, \tilde{k})$ is increasing on $[-\mathrm{K}(\tilde{k}), 0]$ and odd, in that case

$$0 < -s_j < \mathrm{sn}\left(\mathrm{K}(\tilde{k}) - (u_0(k) + \epsilon)_{\tilde{k}} \middle| \tilde{k} \right).$$

Moreover, using again the symmetry and monotonicity of the sn function,

$$\begin{aligned}
\mathrm{sn}\left(\mathrm{K}(\tilde{k}) - (u_0(k) + \epsilon)_{\tilde{k}} \middle| \tilde{k} \right) &= \mathrm{sn}\left(2\mathrm{K}(\tilde{k}) - \left(\mathrm{K}(\tilde{k}) - (u_0(k) + \epsilon)_{\tilde{k}} \right) \middle| \tilde{k} \right) \\
&= \mathrm{sn}\left(\mathrm{K}(\tilde{k}) + (u_0(k) + \epsilon)_{\tilde{k}} \middle| \tilde{k} \right) \\
&< \mathrm{sn}\left(\mathrm{K}(\tilde{k}) + (u_0(k) - \epsilon)_{\tilde{k}} \middle| \tilde{k} \right).
\end{aligned}$$

As a result, we get the following inequalities:

$$\begin{aligned}
&\mathrm{sn}\left(\mathrm{K}(\tilde{k}) + (u_0(k) - \epsilon)_{\tilde{k}} \middle| \tilde{k} \right) \quad \# \left\{ j \in [2, n-1] \mid \alpha_j < u_0(k) - \frac{\pi}{2} \right\} \\
\leq &\sum_{j|\alpha_j < u_0(k) - \frac{\pi}{2}} s_j \\
\leq &\sum_{j|\alpha_j > u_0(k)} (-s_j) \\
\leq &\mathrm{sn}\left(\mathrm{K}(\tilde{k}) - (u_0(k) + \epsilon)_{\tilde{k}} \middle| \tilde{k} \right) \quad \# \left\{ j \in [2, n-1] \mid \alpha_j > u_0(k) \right) \\
< &\mathrm{sn}\left(\mathrm{K}(\tilde{k}) + (u_0(k) - \epsilon)_{\tilde{k}} \middle| \tilde{k} \right) \quad \# \left\{ j \in [2, n-1] \mid \alpha_j > u_0(k) \right).
\end{aligned}$$

In the last inequality, we used the fact that the cardinal is not zero since these j are exactly those that give a negative term in in (II.58); those negative terms have to exist because the α_j are not all equal. Dividing by $\mathrm{sn}\left(\mathrm{K}(\tilde{k}) + (u_0(k) - \epsilon)_{\tilde{k}} \middle| \tilde{k}\right) > 0$, we get the claim of Lemma II.45.

□

III – Star-triangle transformation on canonical embeddings

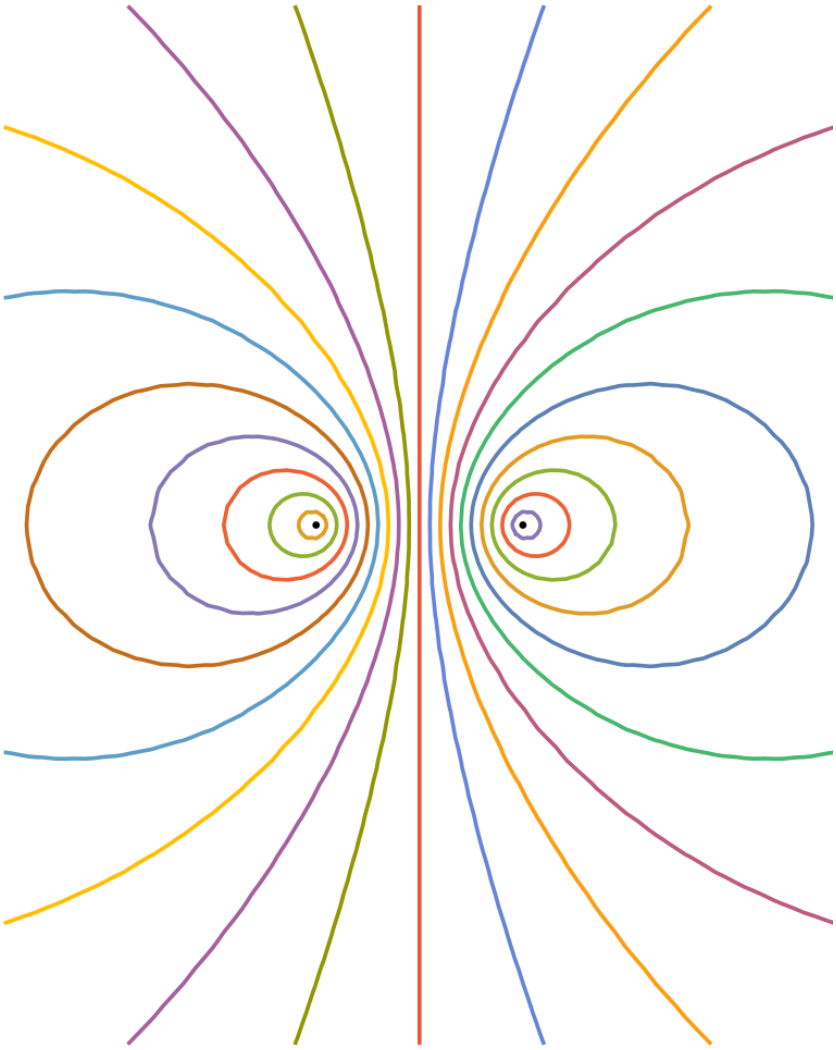

Picture by Sanjay Ramassamy

Résumé

Pour f une fonction de deux variables homogène et symétrique, nous définissons un f-quad comme un quadrilatère de côtés successifs a, b, c, d tels que $f(a, c) = f(b, d)$. Nous étudions notamment le cas où $f(x, y) = x^\alpha + y^\alpha$ pour un certain réel α, et nous donnons des caractérisations géométriques des quadrilatères associés. Nous montrons dans des cas particuliers que les plongements de graphes en f-quads sont intégrables, au sens où ils vérifient une forme de transformation triangle-étoile locale.

Abstract

Let f be a homogeneous symmetric function in two variables. We define an f-quad as a quadrilateral whose successive sides a, b, c, d satisfy $f(a, c) = f(b, d)$. We study in particular the case where $f(x, y) = x^\alpha + y^\alpha$ for some real number α, and we give properties and geometric characterizations of such quadrilaterals. We show in a few particular cases that embeddings of graphs into f-quads are integrable, meaning that they satisfy a form of local star-triangle transformation.

III.1 Introduction

In this chapter, we are investigate families of quadrilaterals defined as follows.

Definition III.1. Let $f : (\mathbb{R}_+)^2 \to \mathbb{R}$ be a symmetric function of two variables. The function f is said to be *homogeneous* if there exists $u \in \mathbb{R}$ such that for any $\lambda, x, y > 0$, we have $f(\lambda x, \lambda y) = \lambda^u f(x, y)$.

Definition III.2. Let $f : (\mathbb{R}_+)^2 \to \mathbb{R}$ be a non-constant homogeneous symmetric function of two variables. A quadrilateral $ABCD$ is called an *f-quad* if

$$f(AB, CD) = f(BC, AD).$$

Note that multiplying f by a non-zero scalar does not change the class of f-quads; in fact, post-composing f with a bijection produces the same class of quads.

We will consider in particular the families of quads associated to functions $f(x, y) = x^\alpha + y^\alpha$ for $\alpha \in \mathbb{R}^*$, and in appropriate limits for $\alpha = 0$ and $\pm\infty$. We denote by $\overline{\mathbb{R}}$ the set $\mathbb{R} \cup \{-\infty, +\infty\}$ of extended real numbers.

Definition III.3. Let $\alpha \in \mathbb{R}^*$. A quadrilateral $ABCD$ is called an *α-quad* if it is an f-quad for

$$f(x, y) = x^\alpha + y^\alpha.$$

It is called a 0-quad if it is an f-quad for

$$f(x, y) = xy. \tag{III.1}$$

It is called a $+\infty$-quad if it is an f-quad for

$$f(x, y) = \max(x, y)$$

and a $-\infty$-quad for

$$f(x, y) = \min(x, y).$$

Let $\beta \in \mathbb{R}$. A quadrilateral $ABCD$ is called a β-quadri if it is an f-quad for

$$f(x, y) = x^2 + y^2 + \beta xy.$$

Of particular interest are the following families:

- α-quads with $\alpha = 1$ (or β-quadris with $\beta = 2$) correspond to *tangential quads*, *i.e.* quads such that there is a circle tangential to their four sides. Embeddings of graphs into tangential quads are called s-embeddings, as introduced by Chelkak for the Ising model [Che17].
- α-quads with $\alpha = 2$ (or β-quadris with $\beta = 0$) correspond to *orthodiagonal quads*, i.e. quads whose diagonals are perpendicular. Embeddings of graphs into orthodiagonal quads correspond to *harmonic* embeddings (where the dual graph is also embedded and each dual edge is orthogonal to the corresponding primal edge) defined by Tutte [Tut63b, KLRR18]

- The class of 0-quads contains a known class of quads: harmonic quads are defined as the cyclic quads satisfying (III.1). According to [Jos11], 0-quads are known under the name of *balanced quads*.

There exists other interesting families of f-quads, such as $f(x,y) = \min(x/y, y/x)$. That latter function gives the class of quads such that $BA.BC = DA.DC$ (up to symmetries). Then, given three points A, B, C, the possible locus for the fourth point D is a Cassini oval. We will thus dub them "Cassini quads". Note that the function $\max(x/y, y/x)$ produces the same class of quads as $f(x,y) = \min(x/y, y/x)$.

As a first attempt to classify these families, let u be the homogeneity weight of f and the function $h : [0, \pi/4] \to \mathbb{R}$ by

$$h(\theta) = f(\cos\theta, \sin\theta)$$

for any $\theta \in [0, \pi/4]$. Then f is uniquely determined by the pair (h, u). Indeed, if u is an arbitrary real number and h is an arbitrary function from $[0, \pi/4]$ to $\mathbb{R}$, then one recovers a function f producing the pair (h, u) as follows. If $x < y$ are two positive real numbers, write $x + iy = re^{i\theta}$ and set

$$f(x,y) = \begin{cases} r^u h(\theta) & \text{if } x \geq y \\ r^u h(\frac{\pi}{2} - \theta) & \text{if } x < y. \end{cases}$$

Nice classes of quads correspond to nice functions h, as one can see in the table below.

$h(\theta)$	u	$f(x,y)$	name of the class
1	2	$x^2 + y^2$	orthodiagonal quads
$\cos\left(\theta - \frac{\pi}{4}\right)$	1	$\frac{x+y}{\sqrt{2}}$	tangential quads
$\sin 2\theta$	2	$2xy$	balanced quads
$\cos\theta$	1	$\max(x,y)$	$+\infty$-quads
$\sin\theta$	1	$\min(x,y)$	$-\infty$-quads
$\tan\theta$	0	$\min(\frac{x}{y}, \frac{y}{x})$	Cassini quads
$(\cos\theta)^\alpha + (\sin\theta)^\alpha$	α	$x^\alpha + y^\alpha$	α-quads
$1 + \beta \sin 2\theta$	2	$x^2 + y^2 + 2\beta xy$	β-quadris

Let $\mathscr{G}$ be a planar graph, finite or infinite. We consider its *diamond* graph $\mathscr{G}^\diamond$, which is the bipartite graph whose black (resp. white) vertices are the vertices of $\mathscr{G}$ (resp. $\mathscr{G}^*$) and where an edge connects a black vertex to a white vertex whenever a vertex of $\mathscr{G}$ lies on the face associated with the corresponding vertex of $\mathscr{G}^*$. All the faces of $\mathscr{G}^\diamond$ are quadrilaterals.

Definition III.4. An *f-embedding* of $\mathscr{G}$ is defined to be an embedding of $\mathscr{G}^\diamond$ in the plane such that every face of $\mathscr{G}^\diamond$ is an f-quad.

Our goal is to investigate the *integrability* of such embeddings, in terms of a possible star-triangle transformation that they may satisfy. This is represented in Figure III.1, and we give a more precise definition of its meaning hereafter.

Definition III.5. A set of points $A_0, A_1, \ldots, A_6$ in the plane is said to be a *proper embedding* of left-hand side of Figure III.1 if it has the following properties:

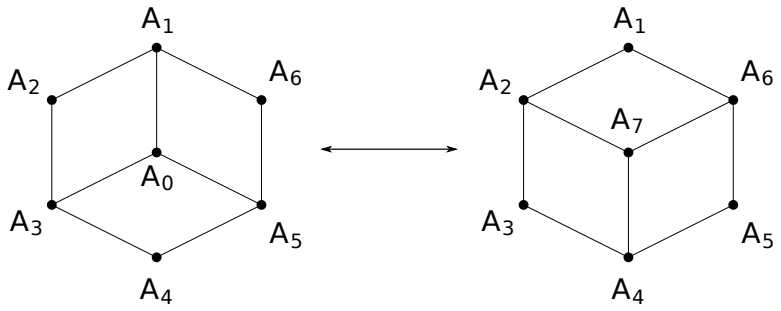

Figure III.1: The combinatorics of a star-triangle move.

1. The seven points are distinct;
2. Among the points $A_1, \ldots, A_6$, no three points are in a line;
3. Edges represented in Figure III.1 do not intersect each other;
4. Each of the three quadrilaterals $A_0A_1A_2A_3$, $A_0A_3A_4A_5$ and $A_0A_5A_6A_1$ is *proper*, meaning that it has a nonempty interior and the vertices of its boundary are oriented in the same order as in Figure III.1.

A proper embedding of the right-hand side of Figure III.1 $A_1, A_2, \ldots, A_7$ is defined similarly.

Definition III.6. A homogeneous symmetric function f is said to satisfy the *flip property* if it has the property that for any six distinct points $A_1, A_2, \ldots, A_6$, the following are equivalent:

- There exists a point A_0 such that $A_0, A_1, \ldots, A_6$ is a proper embedding of the left-hand side of Figure III.1, and the three quadrilaterals $A_0A_1A_2A_3$, $A_0A_3A_4A_5$ and $A_0A_5A_6A_1$ are f-quads;
- There exists a point A_7 such that $A_1, \ldots, A_7$ is a proper embedding of the right-hand side of Figure III.1, and the three quadrilaterals $A_7A_6A_1A_2$, $A_7A_2A_3A_4$ and $A_7A_4A_5A_6$ are f-quads.

The function f is said to satisfy the *unique flip property* if it satisfies the flip property and, when the point A_0 (resp. A_7) exists, it is unique.

The function $f(x, y) = x^2 + y^2$ satisfies the unique flip property; this can be proved using a Theorem of Steiner, see [Ako11, KLRR18]. We prove:

Theorem III.7. *The function $f(x, y) = x + y$ satisfies the unique flip property.*

However, we suspect that a much wider result might hold, although we do not conjecture uniqueness in that generality:

Conjecture III.8. *Any continuous, symmetric, homogeneous function f satisfies the flip property.*

The rest of this chapter is organised as follows: in Section III.2 we give a few geometric results about the space of α-quads. In Section III.3 we prove Theorem III.7, by first showing uniqueness using purely geometric tools, and then proving existence using the formalism of s-embeddings defined by Chelkak [Che17]. In Section III.4 we give partial results towards Conjecture III.8 for α-quads, *i.e.* for $f(x,y) = x^\alpha + y^\alpha$.

Acknowledgements

We are grateful to Dmitry Chelkak, Marianna Russkikh and Andrea Sportiello for numerous fruitful discussions. We also thank Thomas Blomme and Othmane Safsafi for discussions leading to the proof of Propositions III.12 and III.13.

III.2 The space of α-quads

Definition III.9. A pair of opposite sides of a quadrilateral is called an *extremal pair* if these two sides achieve both the maximum and the minimum side-lengths.

Definition III.10. A quadrilateral $ABCD$ is a *kite* if its sides satisfy $\{AB, CD\} = \{AD, BC\}$.

Proposition III.11. *A quadrilateral is an α-quad for some $\alpha \in \overline{\mathbb{R}}$ if and only if it has an extremal pair.*

Proof. Let Q be a quadrilateral with side-lengths denoted by l_1, l_2, l_3, l_4 in cyclic order. Assume that Q has no extremal pair. Without loss of generality, one may assume that l_1 is the maximal length and l_4 the minimal length, and they are distinct. Since (l_1, l_3) is not an extremal pair, l_3 does not achieve the minimum, thus $l_3 > l_4$ and Q is not a $-\infty$-quad. Similarly, l_2 does not achieve the maximum so $l_2 < l_1$ and Q is not a $+\infty$-quad. By the previous inequalities, $l_1^\alpha + l_3^\alpha > l_2^\alpha + l_4^\alpha$ if $\alpha > 0$ and $l_1^\alpha + l_3^\alpha < l_2^\alpha + l_4^\alpha$ if $\alpha < 0$. Also $l_1 l_3 > l_2 l_4$ (case $\alpha = 0$). Hence Q is not an α-quad for any $\alpha \in \overline{\mathbb{R}}$.

Conversely, suppose that Q has an extremal pair. We can assume that l_1 is the maximal length, l_3 is the minimal length, and $l_2 \leq l_4$ (up to a possible mirror symmetry). If $l_2 = l_3$ or if $l_4 = l_1$ then Q is, respectively, a $-\infty$-quad or a $+\infty$-quad, so we can assume that $l_3 < l_2 \leq l_4 < l_1$. Then consider the function

$$f(\alpha) = \frac{l_1^\alpha + l_3^\alpha - l_2^\alpha - l_4^\alpha}{\alpha}.$$

It can be extended to a continuous function on $\mathbb{R}$ by setting $f(0) = \ln\left(\frac{l_1 l_3}{l_2 l_4}\right)$. By the previous inequalities, for $\alpha \to -\infty$, $f(\alpha) \sim \frac{l_3^\alpha}{\alpha} < 0$ and for $\alpha \to +\infty$, $f(\alpha) \sim \frac{l_1^\alpha}{\alpha} > 0$, hence by the intermediate value theorem there is an $\alpha \in \mathbb{R}$ such that $f(\alpha) = 0$ and Q is an α-quad. □

Proposition III.12. *Let Q be a quadrilateral which is an α-quad and an α'-quad for two values $\alpha \neq \alpha' \in \overline{\mathbb{R}}$. Then Q is a kite.*

Proof. Denote by l_1, l_2, l_3, l_4 the side-lengths of Q in cyclic order. Assume first that neither α nor α' take the values $-\infty, \infty$ or 0. Then up to replacing l_i by $l_i^{\alpha'}$, one may assume that

$\alpha' = 1$. Write $s = l_1 + l_3$ and $t = l_1^\alpha + l_3^\alpha$. Since Q is a 1-quad, we have $l_4 = s - l_2$. Since Q is also an α-quad, we have

$$l_2^\alpha + (s - l_2)^\alpha = t, \tag{III.2}$$

and $0 \leq l_2 \leq s$. The function $x \mapsto x^\alpha + (s-x)^\alpha$ is strictly monotonous on $[0, s/2]$ symmetric with respect to $x = s/2$, so that the only solutions of equation (III.2) are $l_2 = l_1$ and $l_2 = l_3$. Hence $\{l_1, l_3\} = \{l_2, l_4\}$, i.e. Q is a kite. If $\alpha = 0$, and α' is finite, one may again assume that $\alpha' = 1$, in which case the sums and products of each pair $\{l_1, l_3\}$ and $\{l_2, l_4\}$ are equal, thus Q is again a kite. If $\alpha \in \{-\infty, \infty\}$ and α' is finite non-zero, one may again assume that $\alpha' = 1$ and the conclusion follows easily. The case when $\alpha \in \{-\infty, \infty\}$ and $\alpha' = 0$ is similar. Finally the case when $\{\alpha, \alpha'\} = \{-\infty, \infty\}$ is also easy. □

This generalizes a result of [Jos11] which claims that a quad which is both a 0-quad and a 1-quad is a kite. We conclude this part with another geometric property, that generalizes a result known for 1-quads and 2-quads [Jos12].

Proposition III.13. *Let $ABCD$ be a quad with P denoting the intersection point of its diagonals, and suppose that P is distinct from A, B, C, D. We denote the circumradii of the triangles ABP, BCP, CDP, DAP by R_1, R_2, R_3, R_4. Let $f : (\mathbb{R}_+)^2 \to \mathbb{R}$ be a symmetric homogeneous function. The following are equivalent:*

1. *$ABCD$ is an f-quad ;*
2. *$f(R_1, R_3) = f(R_2, R_4)$.*

Proof. We denote the center of the circumcircles of ABP, BCP, CDP, DAP by, respectively, O_1, O_2, O_3, O_4. Since AO_1B is isosceles in O_1, we have

$$AB = 2R_1 \sin \frac{\widehat{AO_1B}}{2}.$$

Since P lies on the circle centered at O_1 and going through A and B, we have that

$$\frac{\widehat{AO_1B}}{2} \in \left\{\widehat{APB}, \pi - \widehat{APB}\right\},$$

hence

$$AB = 2R_1 \sin \widehat{APB}.$$

Similarly we have

$$BC = 2R_2 \sin \widehat{BPC}$$
$$CD = 2R_3 \sin \widehat{CPD}$$
$$DA = 2R_4 \sin \widehat{DPA}$$

Observing that $\widehat{APB} = \widehat{CPD} = \pi - \widehat{BPC} = \pi - \widehat{DPA}$, we deduce that the quadruples (AB, BC, CD, DA) and (R_1, R_2, R_3, R_4) are proportional. Since f is homogeneous, $f(AB, CD) = f(BC, DA)$ if and only if $f(R_1, R_3) = f(R_2, R_4)$, which concludes the proof. □

III.3 The star-triangle move for tangential quads

This section is devoted to the proof of Theorem III.7.

III.3.1 Uniqueness

We first aim at proving the following:

Proposition III.14. *For any proper hexagon $A_1, A_2, \dots, A_6$, there is at most one point A_0 so that $A_0, A_1, \dots, A_6$ is a proper embedding of the left-hand side of Figure III.1.*

First we need some information on the geometric properties of 1-quads. Notice that if three distinct point A, B, C are fixed, then the set of all points D such as $ABCD$ is a 1-quad is defined by

$$AD - CD = AB - BC$$

hence it is a hyperbola branch with foci A, C (with possible degenerate cases being the perpendicular bisector of $[AC]$, and half-lines $A + t(A - C)$ or $C + t(C - A)$ for $t \geq 0$). We put all these cases under the same name:

Definition III.15. Let A, C be two distinct points in the plane. For any $\lambda \in \mathbb{R}$, the set of points D in the plane such that

$$AD - CD = \lambda \tag{III.3}$$

is called a *generalised hyperbola branch* with foci A, C.

The following Lemma already implies that there are at most two admissible points A_0.

Lemma III.16. *Assume that two generalised hyperbola branches have exactly one common focus, then they have at most two intersection points.*

This result appears in [LSFW08, XSR08]. Although this result has a very classical flavor, we could not find any older reference. We give an elementary, self-contained proof below.

Proof. When one of the generalised branches is a line or a half-line, the result comes easily from the fact that a hyperbola and a line have at most two points of intersection; we now suppose that it is not the case.

Let $\mathcal{B}$ be a hyperbola branch, we call the focus of $\mathcal{B}$ which belongs to (resp. does not belong to) the convex hull $\mathcal{B}$ the *interior* (resp. *exterior*) focus of $\mathcal{B}$. Assume that $\mathcal{B}_1$ is a hyperbola branch with foci A and C and $\mathcal{B}_2$ is a hyperbola branch with foci A and E, with A, C, E distinct. Then any intersection point of $\mathcal{B}_1$ and $\mathcal{B}_2$ lies on a hyperbola branch $\mathcal{B}_3$ with foci C and E (this can be seen by subtracting the equations (III.3) for $\mathcal{B}_1$ and $\mathcal{B}_2$), and we can also suppose that $\mathcal{B}_3$ is not a line or a half-line. Then there is at least one of the three points A, C or E which is the interior focus of one branch and the exterior focus of another branch. Without loss of generality, we assume that A is the interior focus of $\mathcal{B}_1$ and the exterior focus of $\mathcal{B}_2$, and we will show that these two branches intersect in at most two points.

Suppose that $\mathcal{B}_1, \mathcal{B}_2$ intersect at three distinct points S, T, U; as they belong to a non-degenerate hyperbola branch, they are not in a line. The lines $(ST), (TU), (SU)$ delimit seven open regions in the plane, three of which touching the triangle STU only at one vertex; we call these three regions the *corner chambers* of S, T, U.

Lemma III.17. *Let S, T, U be three distinct points on a hyperbola branch $\mathcal{B}$. Then the exterior focus of $\mathcal{B}$ belongs to a corner chamber of S, T, U, and the interior focus does not.*

Before proving this Lemma, notice that it is enough to conclude the proof of Lemma III.16, as A should be both in a corner chamber of S, T, U (because A is the exterior focus of $\mathcal{B}_2$) and not in one (because A is the interior focus of $\mathcal{B}_1$).

□

Proof of Lemma III.17. For any two distinct points A, B on $\mathcal{B}$, the line (AB) cuts the interior of $\mathcal{B}$ into a finite part and an infinite part. The half-plane delimited by (AB) that contains the finite part is called the *exterior half-plane* of A, B. It is easy to see that the exterior focus belongs to the exterior half-plane of A, B, for instance by noting that this property is invariant by affine transformations of the plane, and is straightforward to prove for the special branch $\{(x, y) \in (0, \infty)^2 \mid xy = 1\}$.

Suppose that S, T, U are met in that order when following the branch $\mathcal{B}$. Then, applying the previous property to (S, T) and (T, U), we get that the exterior focus has to belong to the corner chamber that touches T.

As for the interior focus, by convexity of $\mathcal{B}$, the corner chambers are disjoint from the interior of the convex hull of $\mathcal{B}$. □

Proof of Proposition III.14. Suppose that there exists such a point A_0. As the hexagon is made of three 1-quads, we have

$$A_1A_2 + A_3A_4 + A_5A_6 = A_2A_3 + A_4A_5 + A_6A_1. \tag{III.4}$$

The admissible point A_0 has to be at the intersection of the three generalised hyperbola branches associated to the three 1-quads (those going through A_{i+1} with foci A_i, A_{i+2}, for $i \in \{1, 3, 5\}$). Notice that $A_1A_2 < A_2A_3$ *iff* A_1 is the interior focus of the hyperbola branch with foci A_1, A_3 going through A_2. Using this and relation (III.4), we see that one of the points A_1, A_3, A_5 must be the interior focus of both the hyperbola branches associated to it (otherwise every term on the left would be smaller than a term on the right, or the converse). Suppose that it is A_1. As A_0 has to be at the intersection of the three branches, by Lemma III.16 there is at most one other possible point A_0'.

The situation is shown in Figure III.2. For $A_1A_2A_3A_0$ to be a proper quadrilateral oriented as in Figure III.1, and this holding for both the possible positions of A_0, A_2 can only belong to the red part of the hyperbola. Similarly, A_6 can only belong to the blue part of the second hyperbola. But then it is impossible to have the segments $[A_2A_3], [A_1A_6]$ not intersecting, and at the same time the segments $[A_5A_6], [A_1A_2]$ not intersecting.

This Figure corresponds to the case where the triangle $A_1A_3A_5$ is oriented in that order counterclockwise; the other situation is almost identical, but one has to consider the intersection of $[A_2, A_3]$ and $[A_5, A_6]$ to conclude. □

III.3.2 Existence

It remains to prove that if we start with a proper embedding $A_0, A_1, \ldots, A_6$ of the left-hand side of Figure III.1, then there actually exists a point A_7 as in the right-hand side. To prove this, we transform the problem into a linear one by using the *propagation equations* and *s-embeddings* defined by Chelkak [Che17]. We first sum up this construction, then give a

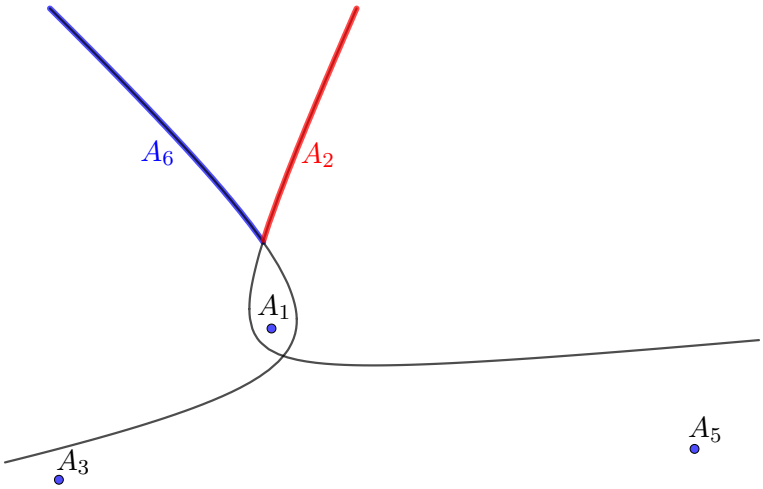

Figure III.2: The case of two intersections of the branches.

few extra property concerning the ordering of the vertices of the quads it gives, and finally apply it to our setting.

a) Ising model, propagation equation and s-embeddings

Suppose that $\mathscr{G}$ is equipped with Ising model coupling constants on the edges, $(J_e)_{e\in\mathscr{E}}$, taken in $(0,\infty)$. For every $e \in \mathscr{E}$ there is a unique $\theta_e \in (0, \frac{\pi}{2})$ such that

$$J_e = \frac{1}{2}\ln\left(\frac{1+\sin\theta_e}{\cos\theta_e}\right).$$

We also set

$$x_e = \tanh J_e = \tan\frac{\theta_e}{2} \in (0,1).$$

Let $\mathscr{G}^c$ be the graph with vertices in bijection with the *corners* of the faces of $\mathscr{G}$, linked *iff* they lie around the same edge of e, and weighted like in Figure III.3. There exists a double-cover $\Upsilon^\times$ of $\mathscr{G}^c$ that branches around every edge, vertex and face of $\mathscr{G}$, graphically represented around an edge in Figure III.4, see also Figure III.9. It inherits the edge weights of $\mathscr{G}^c$.

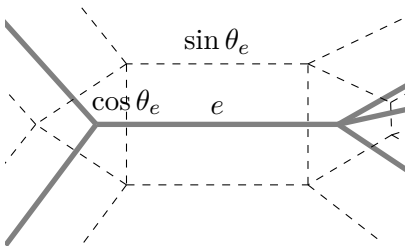

Figure III.3: The corner graph $\mathscr{G}^c$ (dashed) around an edge e of $\mathscr{G}$ (solid).

Let $\mathscr{V}^\times$ be the vertices of $\Upsilon^\times$. We say that a function $X : \mathscr{V}^\times \to \mathbb{C}$ satisfies the *propagation equation* if, for every $v \in \mathscr{V}^\times$ with neighbours $v', v'' \in \mathscr{V}^\times$ around an edge e like

in Figure III.4,

$$X_v = \sin\theta_e X_{v'} + \cos\theta_e X_{v''}.$$

It is easy to check that if X satisfies the propagation equation, its value is multiplied by -1 whenever we change sheet above a vertex of $\mathscr{G}^c$.

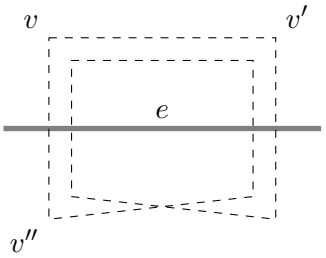

Figure III.4: The double cover $\Upsilon^\times$ around the edge e of $\mathscr{G}$.

If X is a solution to the propagation equations, then one can construct a *s-embedding* $\mathcal{S} : \mathscr{G}^\diamond \to \mathbb{C}$ in the following way. Fix the image $\mathcal{S}(u_0)$ of a base vertex u_0 of $\mathscr{G}$ in the plane. Then define $\mathcal{S}$ such that for every vertex u of $\mathscr{G}$ and every face f adjacent to it, and if c is the corner between u and f,

$$\mathcal{S}(f) - \mathcal{S}(u) = X_c^2$$

where X_c is any of the two values of X above the corner c. See Figure III.6.

Proposition III.18 ([Che17])**.** *For any solution X of the propagation equation such that $\mathrm{Re}(X), \mathrm{Im}(X)$ are two free vectors over $\mathbb{R}$, the associated s-embedding is well-defined, and is such that every face of $\mathscr{G}^\diamond$ is sent to a 1-quad in the complex plane.*

Conversely, for any f-embedding $\mathcal{T}$ of $\mathscr{G}$ with $f(x,y) = x + y$, for any edge $e \in \mathscr{E}$ let θ_e be the unique angle in $\left(0, \frac{\pi}{2}\right)$ such that, in the notation of Figure III.5,

$$\tan^2\theta_e = \frac{\operatorname{cotan}\delta + \operatorname{cotan}\beta}{\operatorname{cotan}\alpha + \operatorname{cotan}\gamma}.$$

Then $\mathcal{T}$ is an s-embedding associated to a solution to the propagation equations on $\mathscr{G}$ with parameters $(\theta_e)_{e\in\mathscr{E}}$.

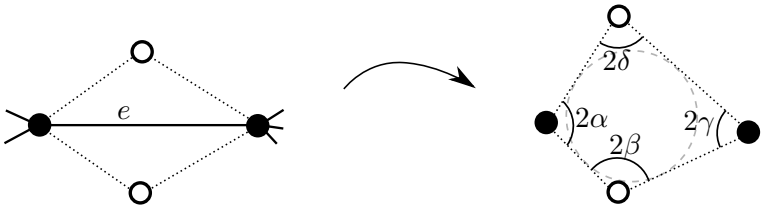

Figure III.5: A piece of an f-embedding for $f(x,y) = x + y$.

The plan of our proof of the flip property is therefore to translate the initial configuration into a solution of the propagation equations, then show that one can apply a star-triangle transformation on these solution, and finally to go back to embeddings. However, we want a bit more information than is contained in Proposition III.18, as we want to keep track of the orientation of quadrilaterals. This is the aim of the following part.

b) Orientation of quads in s-embeddings

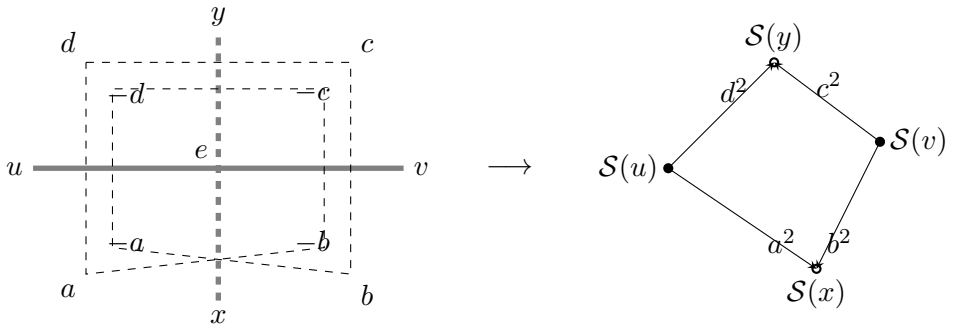

Figure III.6: An edge $e \in \mathscr{E}$ with vertices u, v and adjacent faces x, y, with a solution of its propagation equation, and the corresponding s-embedding.

Lemma III.19. *Let $a, b, c, d \in \mathbb{C}^*$ be a solution to the propagation equation at an edge $e \in \mathscr{E}$ with parameter $\theta \in (0, \frac{\pi}{2})$, set around e as in Figure III.6. Suppose that $b/a \notin \mathbb{R}$. Then the following are equivalent:*

(i) The 1-quad $\mathcal{S}(u)\mathcal{S}(x)\mathcal{S}(v)\mathcal{S}(y)$ is oriented counterclockwise in that order;

(ii) $\mathrm{Im}(b/a) > 0$*;*

(iii) The arguments of $\pm a, \pm b, \pm c, \pm d$ are in the cyclic order $(a, d, c, b, -a, -d, -c, -b)$ around the circle (as in Figure III.7).

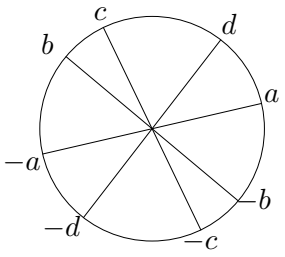

Figure III.7: Cyclic order of the arguments of the complex numbers a, b, c, d.

Proof. All the propositions are unaltered if we multiply all the complex numbers a, b, c, d by the same nonzero complex number, hence we can suppose $a = 1$.

- $(ii) \Rightarrow (iii)$: Suppose that $\mathrm{Im}(b) > 0$. Solving the propagation equation gives

$$c = \frac{b}{\cos\theta} + \tan\theta,$$
$$d = \frac{1}{\cos\theta} + b\tan\theta.$$

Thus c and d are positive combinations of 1 and b, so their complex arguments lie between 0 and that of b. Moreover, by a computation,

$$\operatorname{Im}\left(\frac{c}{d}\right) = \frac{1}{\left|\frac{1}{\cos\theta} + b\tan\theta\right|^2}\left[(1+|b|^2)\frac{\sin\theta}{\cos^2\theta} + \frac{1}{\cos^2\theta}\operatorname{Im}(b+\bar{b}\sin^2\theta)\right]$$

and it is easy to check that $\operatorname{Im}(b+\bar{b}\sin^2\theta) \geq 0$. Thus $\operatorname{Im}\left(\frac{c}{d}\right) > 0$ and we deduce the full Figure III.7.

- $(iii) \Rightarrow (ii)$: Clear.
- $(i) \Rightarrow (iii)$: Suppose that the quad is oriented in the order of (i), then the sum of its internal angles is 2π. These internal angles can be written as the oriented angles of vectors $(\widehat{a^2, d^2}), (\widehat{b^2, a^2}), (\widehat{c^2, b^2}), (\widehat{d^2, c^2})$ taken in $(0, 2\pi)$. In the case of (iii), the arguments of a^2, d^2, c^2, b^2 are in that order around the circle and it is easy to check that the angles sum up to 2π. On the other hand, when (iii) is not verified, we have $\operatorname{Im}(b) < 0$ and we can apply the previous result to $\bar{b}, \bar{c}, \bar{d}$ (which is still a solution to the propagation equation); thus in that case the order is completely opposite, and the angles sum up to 6π. Hence by contraposition $(i) \Rightarrow (iii)$.
- $(iii) \Rightarrow (i)$: By Proposition III.18, the embedding $\mathcal{S}(u)\mathcal{S}(x)\mathcal{S}(v)\mathcal{S}(y)$ is a tangential quad, hence it is not crossed. Consequently, it is correctly oriented *iff* the sum of the expected internal angles is 2π, and we already noted that it is the case under (iii).

□

c) Star-triangle transformation on propagation equations

We rephrase Baxter's results on the star-triangle transformation of the Ising model; see Section 6.4 of [Bax82].

Let us suppose that the graph $\mathscr{G}$ contains a triangle, as in the left-hand side of Figure III.8. We label the edges with the θ_i parameters, and we define as well x_i, J_i. It is possible to transform the triangle into the star displayed on the right-hand side, while finding parameters such that both Ising models are coupled and agree everywhere except at A_7. We call this the *star-triangle transformation.*

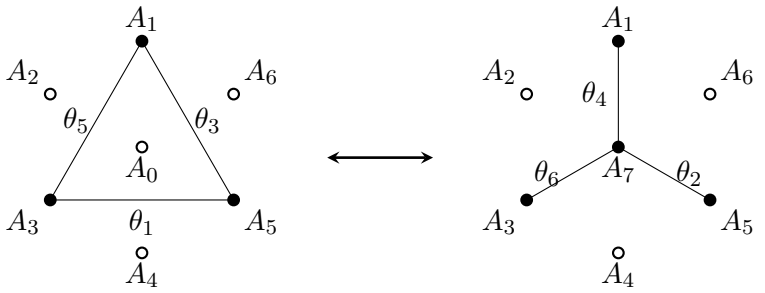

Figure III.8: star-triangle transformation on $\mathscr{G}$ (black vertices)

Proposition III.20 ([Bax82])**.** *Let $k' \in (0,\infty)$ be defined as*

$$k' = \frac{(1-x_1^2)(1-x_3^2)(1-x_5^2)}{4\sqrt{(1+x_1x_3x_5)(x_1+x_3x_5)(x_3+x_1x_5)(x_5+x_1x_3)}}.$$

Then the parameters $\theta_2, \theta_4, \theta_6$ obtained by the star-triangle transformation are the unique angles in $(0, \frac{\pi}{2})$ such that

$$\forall i \in \{1,3,5\},\ \tan\theta_i \tan\theta_{i+3} = \frac{1}{k'} \tag{III.5}$$

where we labeled the angles modulo 6.

Remark III.21. This transformation may be expressed in different ways. The previous definition of k' comes naturally from the use of an *elliptic modulus* $k \in i\mathbb{R} \cup [0,1)$ such that $k^2 + k'^2 = 1$. Then we can define new angles $\theta'_1, \dots, \theta'_6$ by

$$\theta'_i = \frac{\pi \mathrm{F}(\theta_i, k)}{2\mathrm{K}(k)}.$$

where F is the elliptic integral of the first kind, and K the complete elliptic integral of the first kind. For this definition k can be seen as the only modulus such that the θ' angles satisfy

$$\theta'_1 + \theta'_3 + \theta'_5 = \frac{\pi}{2}. \tag{III.6}$$

In these parameters, the star-triangle transformation reads

$$\forall i \in \{1,3,5\},\ \theta'_{i+3} = \frac{\pi}{2} - \theta'_i. \tag{III.7}$$

Moreover, the trigonometric functions of θ angles are Jacobi elliptic functions of the θ' angles: let $\tau_i = \frac{2\mathrm{K}(k)}{\pi}\theta'_i$, then

$$\cos\theta_i = \mathrm{cn}\left(\tau_i, k\right),$$
$$\sin\theta_i = \mathrm{sn}\left(\tau_i, k\right).$$

The graphs $\Upsilon^\times$ corresponding to the star and to the triangle configurations are represented in Figure III.9. We show that when the angles θ are chosen so as to satisfy the star-triangle relations (III.5), the propagation equations "seen from the boundary vertices" $x_1, \dots, x_6$ are the same.

Proposition III.22. *Suppose that $\theta_1, \dots, \theta_6 \in (0, \frac{\pi}{2})$ satisfy the star-triangle relations* (III.5)*.*

Let $(x_1, x_2, x_3, x_4, x_5, x_6, y_1, y_3, y_5)$ be a solution of the propagation equations on the "triangle" graph of the left of Figure III.9. Then there exists a unique triplet (z_2, z_4, z_6) such that $(x_1, x_2, x_3, x_4, x_5, x_6, z_2, z_4, z_6)$ is a solution of the propagation equations on the "star" graph on the right.

Proof. It is easy to see that any values of (y_1, y_3, y_5) characterize uniquely the solution of the propagation equations on the triangle graph. Thus the set of possible vectors $(x_1, \dots, x_6)$ is

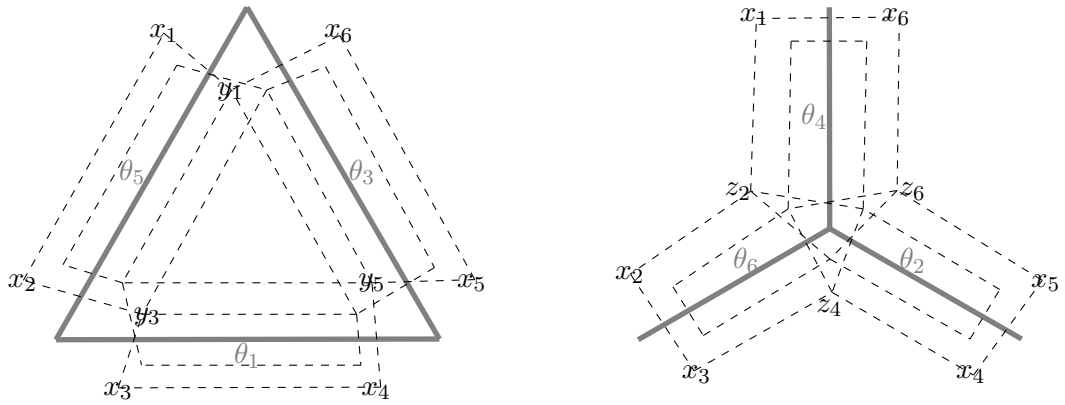

Figure III.9: Star-triangle transformation of $\Upsilon^{\times}$.

a 3-dimensional subspace V. By setting (y_1, y_3, y_5) to be the elements of the canonical basis of $\mathbb{C}^3$ and solving the propagation equations, we get a basis of V:

$$u_1 = \begin{pmatrix} 1/\cos\theta_5 \\ \tan\theta_5 \\ 0 \\ 0 \\ \tan\theta_3 \\ 1/\cos\theta_3 \end{pmatrix}, u_3 = \begin{pmatrix} \tan\theta_5 \\ 1/\cos\theta_5 \\ 1/\cos\theta_1 \\ \tan\theta_1 \\ 0 \\ 0 \end{pmatrix}, u_5 = \begin{pmatrix} 0 \\ 0 \\ \tan\theta_1 \\ 1/\cos\theta_1 \\ 1/\cos\theta_3 \\ \tan\theta_3 \end{pmatrix}.$$

Similarly, the set of values of $(x_1, \dots, x_6)$ for the star graph is a subspace V' with basis

$$v_2 = \begin{pmatrix} 1/\sin\theta_4 \\ 1/\sin\theta_6 \\ 1/\tan\theta_6 \\ 0 \\ 0 \\ 1/\tan\theta_4 \end{pmatrix}, v_4 = \begin{pmatrix} 0 \\ 1/\tan\theta_6 \\ 1/\sin\theta_6 \\ 1/\sin\theta_2 \\ 1/\tan\theta_2 \\ 0 \end{pmatrix}, v_6 = \begin{pmatrix} 1/\tan\theta_4 \\ 0 \\ 0 \\ 1/\tan\theta_2 \\ 1/\sin\theta_2 \\ 1/\sin\theta_4 \end{pmatrix}.$$

We want to show that these subspaces are equal. By dimensionality, we just need to show that $v_2, v_4, v_6 \in V$. We do it for v_2, the other cases being symmetric. We claim that

$$\frac{1}{\cos\theta_3 \tan\theta_4} u_1 + \frac{1}{\cos\theta_1 \tan\theta_6} u_3 - \frac{\tan\theta_1}{\tan\theta_6} u_5 = v_2.$$

This is checked immediately for the third and fourth entries; the fifth and sixth entries are similar after noting that by (III.5),

$$\frac{\tan\theta_1}{\tan\theta_6} = \frac{\tan\theta_3}{\tan\theta_4}. \tag{III.8}$$

The first and second entry are a bit more tedious. We detail the first one.

We want to show that

$$\frac{1}{\cos\theta_3 \tan\theta_4 \cos\theta_5} + \frac{\tan\theta_5}{\cos\theta_1 \tan\theta_6} = \frac{1}{\sin\theta_4}. \tag{III.9}$$

In terms of the elliptic τ_i variables from Remark III.21, this amounts to showing (we omit the elliptic parameter k):

$$\mathrm{nc}(\tau_3)\,\mathrm{cs}(\tau_4)\,\mathrm{nc}(\tau_5) + \mathrm{nc}(\tau_1)\mathrm{sc}(\tau_5)\,\mathrm{cs}(\tau_6) - \mathrm{ns}(\tau_4) = 0. \tag{III.10}$$

By (III.7), $\tau_4 = \mathrm{K}(k) - \tau_1$ and $\tau_6 = \mathrm{K}(k) - \tau_3$, and by (III.6), $\tau_1 = \mathrm{K}(k) - (\tau_3 + \tau_5)$. Thus we can express all the arguments in terms of τ_3, τ_5. Using the change of arguments in elliptic functions (see 16.8 in [AS64]), the right-hand side of (III.10) is equal to

$$\begin{aligned}
&\mathrm{nc}(\tau_3)\,\mathrm{nc}(\tau_5)\,\mathrm{cs}(\tau_3+\tau_5) + \mathrm{sc}(\tau_3)\mathrm{sc}(\tau_5)\,\mathrm{ds}(\tau_3+\tau_5) - \mathrm{ns}(\tau_3+\tau_5)\\
=&\,\mathrm{nc}(\tau_3)\,\mathrm{nc}(\tau_5)\,\mathrm{ns}(\tau_3+\tau_5)\times\\
&\quad(\mathrm{cn}(\tau_3+\tau_5) + \mathrm{sn}(\tau_3)\,\mathrm{sn}(\tau_5)\,\mathrm{dn}(\tau_3+\tau_5) - \mathrm{cn}(\tau_3)\,\mathrm{cn}(\tau_5))\,.
\end{aligned}$$

By 32(i) in Chapter 2 of [Law89], this is equal to zero. □

Remark III.23. From the previous proof, equations (III.8) and (III.9) imply

$$\cos(\theta_4) = \frac{\sin\theta_1 \cos\theta_3 \cos\theta_5}{\sin\theta_1 + \sin\theta_3 \sin\theta_5}.$$

This is enough to get the new angle θ_4 in terms of the initial one. Of course symmetric formulas exist for θ_2, θ_6. This a short and seemingly new way of writing the Ising star-triangle move.

We now have all the elements to prove the flip property.

Proof of Theorem III.7. We start with $A_0, A_1, \ldots, A_6$ a proper embedding of the left-hand side of Figure III.1. As uniqueness is a consequence of Proposition III.14, we just have to prove that there exists a point A_7 such that $A_1, A_2, \ldots, A_7$ is a proper embedding of the right-hand side.

By Proposition III.18, there exists $(x_1, x_2, x_3, x_4, x_5, x_6, y_1, y_3, y_5)$ a solution of the propagation equation as in the left-hand side of Figure III.9 such that the initial points $A_0, A_1, \ldots, A_6$ are the s-embedding of this solution. Hence by Proposition III.22, there exists (z_2, z_4, z_6) such that $(x_1, x_2, x_3, x_4, x_5, x_6, z_2, z_4, z_6)$ is a solution to the propagation equations the right-hand side of Figure III.9. Let us consider its s-embedding. It has the same boundary as the initial one, hence the points $A_1, \ldots, A_6$ are unchanged, and we have a new point A_7. It remains to prove that the three new 1-quads are proper.

As no three vertices of the hexagon are in a line, x_1/x_2 is not a real number; moreover the initial quad $A_1A_2A_3A_0$ is properly oriented. Hence we can apply Lemma III.19 to get the order of the arguments of x_1, x_2, y_3, y_1. By doing the same for the three initial quads, the order of the arguments of the variables x_i and y_i is that of the first part of Figure III.10.

Let us prove that the new quad $A_1A_2A_7A_6$ is properly oriented. By Lemma III.19, it is enough to prove that $\mathrm{Im}(x_6/x_1) > 0$. If this is not the case, then we are in the situation of the second configuration of Figure III.10, where all the arguments are included in a half-circle. Therefore we can get the order of the arguments of the x_i^2, as in the third Figure. However, as in the proof of Lemma III.19, the successive internal angles of the hexagon $A_1A_2A_3A_4A_5A_6$ can be expressed as the successive oriented angles in direct order in this last figure, hence their sum is 2π. This contradicts the fact that the hexagon is non-crossed, as the sum should be 4π.

By symmetry, the three new quads are properly oriented, which concludes the proof. □

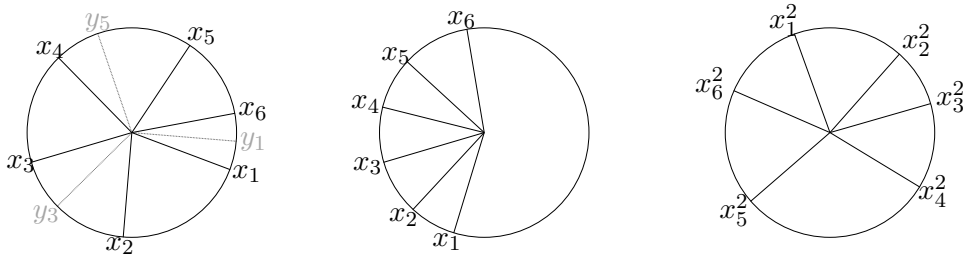

Figure III.10: The cyclic order of the arguments of the variables x_i and y_i.

III.4 Partial results for α-quads flip

In this part we make a few remarks related to the flip property for α-quads.

The fact that $A_0A_1A_2A_3$, $A_0A_3A_4A_5$ and $A_0A_5A_6A_1$ are α-quads implies that

$$A_1A_2^\alpha + A_3A_4^\alpha + A_5A_6^\alpha = A_2A_3^\alpha + A_4A_5^\alpha + A_6A_1^\alpha. \tag{III.11}$$

Define the curves

$$\begin{aligned} C_1 &= \{M \in \mathbb{R}^2 | MA_2^\alpha - MA_6^\alpha = A_1A_2^\alpha - A_1A_6^\alpha\} \\ C_3 &= \{M \in \mathbb{R}^2 | MA_4^\alpha - MA_2^\alpha = A_3A_4^\alpha - A_3A_2^\alpha\} \\ C_5 &= \{M \in \mathbb{R}^2 | MA_6^\alpha - MA_4^\alpha = A_5A_6^\alpha - A_5A_4^\alpha\}. \end{aligned}$$

By (III.11), we deduce that the intersection of any two of these curves is contained inside the third one, so A_7 could be taken to be any point in $C_1 \cap C_3$. However, it is not clear a priori why these curves should intersect.

Let us discuss briefly the nature of these curves.

Definition III.24. Let A, B, C be three distinct points in the plane, and let f be a symmetric homogeneous function. We call *f-construction curve with foci A, C going through B* the set

$$\{D \in \mathbb{R}^2 \mid f(AB, CD) = f(AC, BD)\}.$$

In some cases these curves are simple, for instance:

Lemma III.25. *For $f(x, y) = xy$ the f-construction curves are generalised circles (circles or straight lines).*

Proof. Suppose that in complex coordinates $A = 0$ and $C = 1$, then the curve can be seen as the set of $z \in \mathbb{C}$ such that $\left|\frac{z}{1-z}\right| =$ constant. Hence $Z = \frac{z}{1-z}$ is on a circle, and $z = \frac{Z}{1+Z}$ is the image of a circle by a Möbius transformation. □

Hence when $\alpha = 0$, the construction curves intersect in at most two points.

When $\alpha = 1$, the construction curves are generalised branches of hyperbolas, which are discussed in Section III.3.

When $\alpha = 2$, the construction curves are straight lines, more precisely the construction curve with foci A, C going through B is the line perpendicular to (AC) going through B. Hence the existence (and uniqueness) of an intersection point is also easy.

When α is a positive integer, the construction curves associated to $f(x,y) = x^\alpha + y^\alpha$ are branches of algebraic curves. For any $\beta \in \mathbb{R}$, the construction curves associated to the β-quadris (for which $f(x,y) = x^2 + y^2 + \beta xy$) are branches of algebraic curves of degree at most 4. This gives bounds on the number of intersection points of construction curves, as by Bézout's theorem two algebraic curves of respective degree n, m intersect in at most nm points.

Regarding existence and uniqueness of a proper intersection point, if we are in a regime of parameters where we have existence and uniqueness (such as $\alpha = 1$ or $\alpha = 2$) and we vary slightly α, then existence and uniqueness should be preserved, as the curves intersect in a transverse way. This means that a star-triangle move is well-defined for α close to 1 or close to 2 in some open region of the parameter space.

IV – On path partitions of the divisor graph

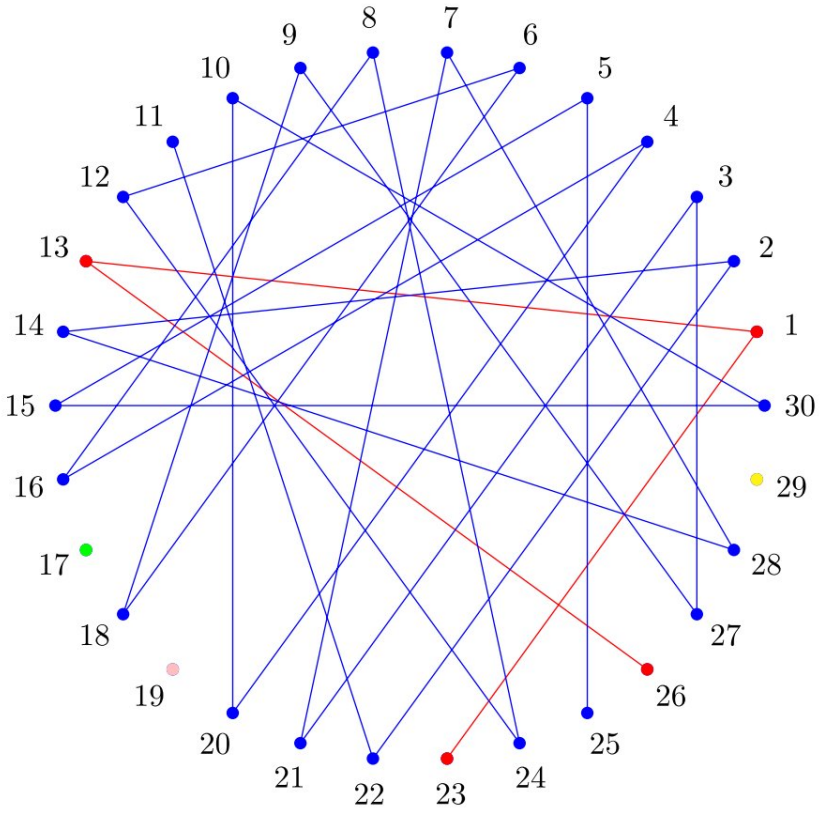

Picture by Roger Mansuy

Résumé

Il est établi que la plus longue chaîne dans le graphe divisoriel construit avec les entiers $\leq N$ a une longueur asymptotiquement $\asymp N/\log N$. Nous étudions les partitions de $\{1, 2, \ldots, N\}$ en un nombre *minimal* de chaînes, et nous montrons que dans une telle partition, la chaîne la plus longue peut avoir une longueur asymptotiquement $N^{1-o(1)}$.

Abstract

It is known that the longest simple path in the divisor graph that uses integers $\leq N$ is of asymptotic length $\asymp N/\log N$. We study the partitions of $\{1, 2, \ldots, N\}$ into a *minimal* number of paths of the divisor graph, and we show that in such a partition, the longest path can have length asymptotically $N^{1-o(1)}$.

IV.1 Introduction

The *divisor graph* is the unoriented graph whose vertices are the positive integers, and edges are the $\{a, b\}$ such that $a < b$ and a divides b. A *path* of length l in the divisor graph is a finite sequence $n_1, \ldots, n_l$ of pairwise distinct positive integers such that n_i is either a divisor or a multiple of n_{i+1}, for all i such that $1 \leq i < l$. Let $F(x)$ be the minimal cardinal of a partition of $\{1, 2, \ldots, \lfloor x \rfloor\}$ into paths of the divisor graph.

The asymptotic behaviour of $F(x)$ has been studied in [ES95, Sai03, Maz06, Cha08]. Thanks to the works of Mazet and Chadozeau, we know that there is a constant $c \in (\frac{1}{6}, \frac{1}{4})$ such that

$$F(x) = cx\left(1 + O\left(\frac{1}{\log\log x \ \log\log\log x}\right)\right). \tag{IV.1}$$

A partition of $\{1, 2, \ldots, N\}$ into paths of the divisor graph is said to be *optimal* if its cardinal is $F(N)$. We are interested in the length of the paths in an optimal partition.

Let us take the example $N = 30$ that was considered in [Pom83, Sai03]. It is known (see [Sai03]) that $F(30) = 5$, so that the following partition is optimal:

$$13, 26, 1, 11, 22, 2, 14, 28, 7, 21, 3, 27, 9, 18, 6, 12, 24, 8, 16, 4, 20, 10, 30, 15, 5, 25$$
$$17$$
$$19$$
$$23$$
$$29$$

Four of these five paths are singletons. In fact, at the end of the proof of Theorem 2 of [ES95], it is proven that the number of singletons in a (not necessarily optimal) partition is $\asymp N$ for N large enough.

Let us look at the longest paths in an optimal partition of $\{1, 2, \ldots, N\}$. Let $L(N)$ be the maximal path length, among all paths of all *optimal* partitions of $\{1, 2, \ldots, N\}$ into paths of the divisor graph. Let also $f(N)$ denote the maximal length of a path of the divisor graph that uses integers $\leq N$.

It is known that (Theorem 2 of [Sai98])

$$f(N) \asymp \frac{N}{\log N}. \tag{IV.2}$$

Of course $L(N) \leq f(N)$. In the previous example, four of the five paths are singletons, which implies that the longest path has maximal length. In other words $L(30) = f(30) = 26$. More generally, we know that for all $N \geq 1$,

$$F(N) \geq N - \lfloor N/2 \rfloor - \lfloor N/3 \rfloor \tag{IV.3}$$

(see [Sai03]). Inspired by the case $N = 30$, for any $N \in [1, 33]$ it is easy to construct a partition of $\{1, \ldots, N\}$ into $N - \lfloor N/2 \rfloor - \lfloor N/3 \rfloor$ paths, all of them but one being singletons. This shows that for $1 \leq N \leq 33$, (IV.3) is an equality and $L(N) = f(N) = \lfloor N/2 \rfloor + \lfloor N/3 \rfloor + 1$.

However for larger N the situation becomes more complicated. For N large enough there is no optimal partition with all paths but one being singletons. This can be deduced from

(IV.2) and the fact that the constant c in (IV.1) is less than 1. Still, it is natural to wonder if the equality $L(N) = f(N)$ holds for any $N \geq 1$.

We were unable to answer this question, but we looked for lower bounds on $L(N)$ and proved the following:

Theorem IV.1. *There is a constant $A \geq 0$ such that for all $N \geq 3$,*

$$L(N) \geq \frac{N}{\exp\left[\frac{(\log\log N)^2}{\log 2}\right](\log N)^A}.$$

Remark IV.2. In this form of the lower bound, it is tricky to find a decent, explicit value of A given by our method. However, if we allow for a constant factor, we show in the proof that there exists $C > 0$ such that for all N large enough,

$$L(N) \geq C\frac{N}{\exp\left[\frac{(\log\log N)^2}{\log 2}\right](\log N)^B}$$

for an effective $B \simeq 7.248$. With some optimization of parameters we managed to get $B \simeq 5.893$. However, notice that an improvement on the coefficient $\frac{1}{\log 2}$ would be more significant for the asymptotic.

To prove this we introduce a new function $H(x)$. For a real number $x \geq 1$ and two distinct integers $a, b \in [1, x]$, let $L_{a,b}(x)$ be the maximal length of a path having a and b as endpoints and belonging to an *optimal* partition of $\{1, 2, \ldots, \lfloor x \rfloor\}$. If there is no such path, we set $L_{a,b}(x) = 0$. Then we set

$$H(x) = \min L_{r',r}(x)$$

where the min is over all couples (r', r) of *prime* numbers such that

$$\frac{x}{3} < r \leq \frac{x}{2} < r' \leq x.$$

The theorem will be an easy consequence of the following.

Proposition IV.3. *There is a constant N_0 such that for any $N \geq N_0$, there is a set $\mathcal{P}(N)$ of prime numbers in $(3\sqrt{N\log N}, 4\sqrt{N\log N}]$, of cardinal $|\mathcal{P}(N)| \geq \frac{\sqrt{N}}{19(\log N)^{3/2}}$, such that*

$$H(N) \geq \sum_{p\in\mathcal{P}(N)} H\left(\frac{N}{p}\right). \tag{IV.4}$$

The technique used here is analogous to that of [Sai93] in the study of the longest path. More precisely, in [Sai93], $f^*(N)$ denotes the maximal length of a path that uses integers in $[\sqrt{N}, N]$. A quantity h^* is introduced, which is to f^* what H is to L in our case. The inequality (IV.4) is analogous to Buchstab's inequality (40) from [Sai93]. The corresponding lower bounds led to the proof that $f^*(N) \asymp N/\log N$ (Theorem 2 in [Sai98]).

The analogy can be pushed further: in both the proof of (IV.4) and of (40) in [Sai93], we borrow a technique used by Erdős, Freud and Hegyvári who proved the following asymptotic behaviour:

$$\min \max_{1\leq i\leq N-1} \operatorname{lcm}(a_i, a_{i+1}) = \left(\frac{1}{4} + o(1)\right)\frac{N^2}{\log N},$$

where the min is over all permutations $(a_1, a_2, \dots, a_N)$ of $\{1, 2, \dots, N\}$; see Theorem 1 of [EFH83]. In [EFH83] as in [Sai93] or in the present work, the proof goes through the construction of a sequence of integers by concatenating blocks whose largest prime factor is constant, and linking blocks together with separating integers. In [Sai93] as in the present work, these blocks take the form of sub-paths $p\mathcal{C}_{N/p}$, where the $\mathcal{C}_{N/p}$ is a path of integers $\leq N/p$ whose largest prime factor is $\leq p$.

It is worth mentioning that the article [EFH83] of Erdős, Freud and Hegyvári is the origin of all works related to the divisor graph.

IV.2 Notation

The letters p, q, q', r, r' will always denote generic prime numbers. For an integer $m \geq 2$, $P^-(m)$ denotes the smallest prime factor of m.

Let $N \geq 1$. A *path* of integers $\leq N$ of length l is a l-uple $\mathcal{C} = (a_1, a_2, \dots, a_l)$ of pairwise distinct positive integers $\leq N$, such that for all i with $1 \leq i \leq l-1$, a_i is either a divisor or a multiple of a_{i+1}. For convenience, we take $\mathcal{C}$ up to global flip, *i.e.* we identify $(a_1, \dots, a_l)$ with $(a_l, \dots, a_1)$. We will denote this path by $a_1 - a_2 - \cdots - a_l$ (or $a_l - \cdots - a_2 - a_1$). If b and c are integers such that $b = a_i$ and $c = a_{i\pm1}$ for some i, we say that b and c are *neighbours* (in $\mathcal{C}$).

When a partition $\mathcal{A}(N)$ of $\{1, 2, \dots, N\}$ is fixed, for any $n \in \{1, 2, \dots, N\}$ we will simply denote by $\mathcal{C}(n)$ the path that contains n in $\mathcal{A}(N)$.

A partition of $\{1, 2, \dots, N\}$ into paths is said to be *optimal* if it contains $F(N)$ paths (see the Introduction for the definition of F).

Let $\mathcal{C}$ be a path of integers $\leq N$ and $1 \leq n \leq N$. Then $\mathcal{C}$ is said to be *n-factorable* if all the integers of $\mathcal{C}$ are multiple of n. Then $\mathcal{C}$ can be written as $\mathcal{C} = n\mathcal{D}$ where $\mathcal{D}$ is a path of integers $\leq N/n$.

For integers $1 \leq n \leq N$ and a partition $\mathcal{A}(N)$ of $\{1, 2, \dots, N\}$, we say that n is *factoring* for $\mathcal{A}(N)$ if every path of $\mathcal{A}(N)$ that contains a multiple of n is n-factorable.

IV.3 Lemmas

Lemma IV.4. *Let $N \geq 1$ and $\mathcal{A}(N)$ be an optimal partition.*

(i) Let $1 \leq n \leq N$ with n factoring for $\mathcal{A}(N)$. Let $k = \lfloor N/n \rfloor$. There are exactly $F(k)$ paths in $\mathcal{A}(N)$ that contain a multiple of n. They are of the form $n\mathcal{D}_1, n\mathcal{D}_2, \dots, n\mathcal{D}_{F(k)}$ where $\mathcal{D}_1, \mathcal{D}_2, \dots, \mathcal{D}_{F(k)}$ is an optimal partition of $\{1, 2, \dots, k\}$.

(ii) Let $z > 1$ be a real number. Let $M_z(N)$ be the set of integers $m \leq N$ that are not *factoring for $\mathcal{A}(N)$ and such that*

$$m > \frac{N}{z} \quad \text{and} \quad P^-(m) > z.$$

Then

$$|M_z(N)| < \frac{2N}{z}.$$

Proof. (i) Since n is factoring, the paths in $\mathcal{A}(N)$ can be split in two subsets: those formed by the multiples of n, and those that do not contain any multiple of n. We write the first $\{n\mathcal{D}_1, n\mathcal{D}_2, \dots, n\mathcal{D}_g\}$. Thus $\mathcal{D}_1, \mathcal{D}_2, \dots, \mathcal{D}_g$ is a partition of the integers $\leq k = \lfloor N/n \rfloor$; this implies $g \geq F(k)$. We claim that this is an equality. Indeed, there exists an optimal partition $\mathcal{D}'_1, \mathcal{D}'_2, \dots, \mathcal{D}'_{F(k)}$ of k. If we had $g > F(k)$, we would be able to replace $\{n\mathcal{D}_1, n\mathcal{D}_2, \dots, n\mathcal{D}_g\}$ with $\{n\mathcal{D}'_1, n\mathcal{D}'_2, \dots, n\mathcal{D}'_{F(k)}\}$ in the initial partition $\mathcal{A}(N)$, thus getting a partition of n with fewer paths, which contradicts the optimality of $\mathcal{A}(N)$.

(ii) Let $m \in M_z(N)$. There exists a multiple of m that is a neighbour to non-multiple of m. Let $b(m)$ be the smallest multiple of m with that property, and let $c(m)$ be its smallest neighbour that is not a multiple of m. Then $c(m)$ has to be a divisor of $b(m)$. More precisely, if $b(m) = am$, then $c(m)$ can be written as $c(m) = \tilde{a}\tilde{m}$ with $\tilde{a}$ a divisor of a and $\tilde{m}$ a strict divisor of m. Since $P^-(m) > z$, $c(m) < N/z$.

Moreover, if m, m' are two distinct elements of $M_z(N)$, then

$$\operatorname{lcm}(m, m') \geq \min(mP^-(m'), m'P^-(m)) > \frac{N}{z} z = N.$$

so that there is no integer in $\{1, 2, \dots, N\}$ that is both a multiple of m and m'. As a result the map

$$\begin{aligned} b : M_z(N) &\to \{1, 2, \dots, N\} \\ m &\mapsto b(m) \end{aligned}$$

is an injection.

Moreover, any integer $c < N/z$ has at most two neighbours in $\mathbb{C}(c)$. Consequently the map

$$\begin{aligned} c : M_z(N) &\to \{1 \leq n < N/z\} \\ m &\mapsto c(m) \end{aligned}$$

is at-most-two-to-one. Thus

$$|M_z(N)| < \frac{2N}{z}.$$

□

Lemma IV.5. *There exists a constant N_1 such that for any $N \geq N_1$, there is a set $\widetilde{\mathcal{P}}(N)$ of prime numbers in $(3\sqrt{N \log N}, 4\sqrt{N \log N}]$ of cardinal*

$$|\widetilde{\mathcal{P}}(N)| \geq \sqrt{\frac{N}{\log N}}, \tag{IV.5}$$

such that for any prime numbers r, r' with

$$\frac{N}{3} < r \leq \frac{N}{2} < r' \leq N,$$

there exists an optimal partition $\mathcal{A}(N)$ of $\{1, 2, \dots, N\}$ that contains the paths r' and $2r - r$ and for which all the integers in $\widetilde{\mathcal{P}}(N)$ are factoring.

Proof. Let N_1 be such that for any $N \geq N_1$,

$$\pi\left(4\sqrt{N\log N}\right) - \pi\left(3\sqrt{N\log N}\right) - \frac{2}{3}\sqrt{\frac{N}{\log N}} \geq \sqrt{\frac{N}{\log N}}, \tag{IV.6}$$

$$\pi\left(\frac{N}{2}\right) - \pi\left(\frac{N}{3}\right) \geq 8. \tag{IV.7}$$

The existence of such a N_1 comes from the prime number theorem (more precisely the left-hand-side of (IV.6) is equivalent to $\frac{4}{3}\sqrt{\frac{N}{\log N}}$). We also take N_1 large enough so that

$$\left(3\sqrt{N\log N}, 4\sqrt{N\log N}\right] \cap \left(\frac{N}{3}, \frac{N}{2}\right] = \emptyset. \tag{IV.8}$$

Let $N \geq N_1$. We start by fixing an optimal partition $\mathcal{A}'(N)$. We apply Lemma IV.4 (ii) to $\mathcal{A}'(N)$ with $z = 3\sqrt{N\log N}$. All the prime numbers p in $(3\sqrt{N\log N}, 4\sqrt{N\log N}]$ that are not factoring are in $M_z(N)$, since they satisfy $p > 3\sqrt{N\log N} \geq \frac{N}{z}$ and $P^-(p) = p > z$, so there are at most $\frac{2}{3}\sqrt{\frac{N}{\log N}}$ of them. By removing these and using (IV.6), we get a set $\widetilde{\mathcal{P}}(N)$ of prime numbers in $(3\sqrt{N\log N}, 4\sqrt{N\log N}]$ that are factoring in $\mathcal{A}'(N)$, with cardinality

$$|\widetilde{\mathcal{P}}(N)| \geq \sqrt{\frac{N}{\log N}}.$$

We now change the notation slightly and fix two prime numbers r_0, r_0' such that

$$\frac{N}{3} < r_0 \leq \frac{N}{2} < r_0' \leq N.$$

Our goal is to go from $\mathcal{A}'(N)$ to a new optimal partition $\mathcal{A}(N)$ that contains the paths r_0' and $2r_0 - r_0$ *while maintaining the fact that the elements of* $\widetilde{\mathcal{P}}(N)$ *are factoring.*

Let us denote the set of prime numbers

$$\mathcal{R} = \left\{\frac{N}{3} < r \leq \frac{N}{2}\right\},$$

and $\mathcal{R}^*(\mathcal{A}'(N))$ the subset of $r \in \mathcal{R}$ such that r does not have 1 as a neighbour in $\mathcal{C}(r)$ and $2r$ does not have 1 nor 2 has a neighbour in $\mathcal{C}(2r)$. Then for any $r \in \mathcal{R}^*(\mathcal{A}'(N))$, since the only possible neighbour of r is $2r$ and reciprocally, by optimality the path $\mathcal{C}(r)$ is equal to $r - 2r$. Moreover, since 1 and 2 have at most two neighbours,

$$|\mathcal{R} \setminus \mathcal{R}^*(\mathcal{A}'(N))| \leq 4. \tag{IV.9}$$

Now we make it so that r_0' is a path. If it is not the case, since the only possible neighbour of r_0' is 1, $\mathcal{C}(r_0')$ is of the form $\mathcal{D} - r_0'$ with $\mathcal{D}$ a path ending in 1. We split this path into $\mathcal{D}$ on one side and r_0' on the other side. By (IV.9) and (IV.7), there is at least one element $r^* \in \mathcal{R}^*(\mathcal{A}'(N))$. We stick $\mathcal{D}$ to $\mathcal{C}(r^*)$, thus forming the path $\mathcal{D} - \mathcal{C}(r^*)$. This is possible because $\mathcal{D}$ ends in 1. Let $\mathcal{A}''(N)$ be this new partition. The total number of paths has not changed so $\mathcal{A}'(N)$ is still optimal, furthermore it contains the path r_0', and the elements of $\widetilde{\mathcal{P}}(N)$ are still factoring because the integers in the paths that changed were not multiples of any $p \in \widetilde{\mathcal{P}}(N)$.

The subset $\mathcal{R}^*(\mathcal{A}''(N))$ might differ from $\mathcal{R}^*(\mathcal{A}'(N))$ by one element, but it still satisfies (IV.9) and its elements r still satisfy that $\mathcal{C}(r)$ is equal to $r-2r$. If $r_0 \in \mathcal{R}^*(\mathcal{A}''(N))$, we can set $\mathcal{A}(N) = \mathcal{A}''(N)$ and the proof is over. We now suppose that $r_0 \notin \mathcal{R}^*(\mathcal{A}''(N))$.

By (IV.9) and (IV.7), there are at least four elements r_1, r_2, r_3, r_4 in $\mathcal{R}^*(\mathcal{A}''(N))$. We cut the path $\mathcal{C}(1)$ into one, two or three paths, one of them being the singleton 1 (we will see later that we get in fact three paths). Such a move will be called an *extraction* of the integer 1. We similarly *extract* the integer 2. We now use these integers 1 and 2 to stick together the paths $r_i - 2r_i$ by forming

$$r_1 - 2r_1 - 1 - 2r_2 - r_2 \quad \text{and} \quad r_3 - 2r_3 - 2 - 2r_4 - r_4.$$

We thus get a new partition $\mathcal{A}(N)$. Its number of paths is less or equal to that of $\mathcal{A}''(N)$, so it is still optimal (this shows in particular that 1 and 2 were not endpoints of their paths). It also satisfies $r_0 \in \mathcal{R}^*(\mathcal{A}(N))$ since 1 and 2 are not linked to r_0 nor $2r_0$, so that it contains the path $r_0 - 2r_0$, as well as r_0', and the elements of $\widetilde{\mathcal{P}}(N)$ are still factoring. □

IV.4 Proof of the Proposition

Let N_1 be the constant introduced in the proof of Lemma IV.5. We fix a N_0 such that

$$N_0 \geq N_1^4 \tag{IV.10}$$

and such that for all $N \geq N_0$,

$$\begin{aligned} \frac{1}{2}\sqrt{\frac{N}{\log N}} &\geq \pi\left(\frac{1}{4}\sqrt{\frac{N}{\log N}}\right) - \pi\left(\frac{1}{6}\sqrt{\frac{N}{\log N}}\right) \\ &\geq \pi\left(\frac{1}{8}\sqrt{\frac{N}{\log N}}\right) - \pi\left(\frac{1}{9}\sqrt{\frac{N}{\log N}}\right) \\ &\geq \left\lfloor \frac{\sqrt{N}}{37(\log N)^{3/2}} \right\rfloor \geq \frac{\sqrt{N}}{38(\log N)^{3/2}} + \frac{1}{2} \geq 5 \end{aligned} \tag{IV.11}$$

and

$$4\sqrt{\log N} \leq N^{1/4}. \tag{IV.12}$$

The existence of such a N_0 is again an easy consequence of the prime number theorem. Also note that since $N_0 \geq N_1$, (IV.8) still holds.

Let $N \geq N_0$. We chose a set $\widetilde{\mathcal{P}}(N)$ according to Lemma IV.5. Let us denote

$$I = \left\lfloor \frac{1}{37} \frac{\sqrt{N}}{(\log N)^{3/2}} \right\rfloor.$$

By (IV.5) and (IV.11) we can chose $2I$ elements in $\widetilde{\mathcal{P}}(N)$, which we denote as

$$p_1, p_2, \ldots, p_{2I}.$$

We set $\mathcal{P}(N) = \{p_1, \ldots, p_{2I-1}\}$. By (IV.11) again, $|\mathcal{P}(N)| \geq \frac{\sqrt{N}}{19(\log N)^{3/2}}$. It remains to prove that this set $\mathcal{P}(N)$ satisfies (IV.4).

Let r, r' be two prime numbers such that

$$\frac{N}{3} < r \leq \frac{N}{2} < r' \leq N. \tag{IV.13}$$

By the property of $\widetilde{\mathcal{P}}(N)$ in Lemma IV.5, there exists an optimal partition $\mathcal{A}'(N)$, that contains the paths r' and $2r - r$, for which the elements of $\widetilde{\mathcal{P}}(N)$ (and in particular the elements of $\mathcal{P}(N)$) are factoring.

We denote two sets of prime numbers

$$\mathcal{Q}(N) = \left\{ \frac{1}{9}\sqrt{\frac{N}{\log N}} < q \leq \frac{1}{8}\sqrt{\frac{N}{\log N}} \right\},$$
$$\mathcal{Q}'(N) = \left\{ \frac{1}{6}\sqrt{\frac{N}{\log N}} < q' \leq \frac{1}{4}\sqrt{\frac{N}{\log N}} \right\}.$$

For all $(p, q, q') \in \widetilde{\mathcal{P}}(N) \times \mathcal{Q}(N) \times \mathcal{Q}'(N)$ we have

$$\frac{N}{3} < pq \leq \frac{N}{2}, \tag{IV.14}$$
$$\frac{N}{2} < pq' \leq N. \tag{IV.15}$$

We focus on the factoring prime number p_{2I}. For any $q \in \mathcal{Q}(N)$, because of (IV.14) the only possible neighbours of $p_{2I}q$ are p_{2I} and $2p_{2I}q$. Similarly, the only possible neighbours of $2p_{2I}q$ are $p_{2I}, 2p_{2I}$ or $p_{2I}q$. But p_{2I} and $2p_{2I}$ can be linked to at most 4 elements of type $p_{2I}q$ or $2p_{2I}q$. By (IV.11) we know that $|\mathcal{Q}(N)| \geq 5$, so there exists a $q_{2I} \in \mathcal{Q}(N)$ for which neither $p_{2I}q_{2I}$ nor $2p_{2I}q_{2I}$ is a neighbour of p_{2I} or $2p_{2I}$. As a result, the only possible neighbour for $p_{2I}q_{2I}$ is $2p_{2I}q_{2I}$, and reciprocally. By optimality, $\mathcal{A}'(N)$ contains the path $p_{2I}q_{2I} - 2p_{2I}q_{2I}$.

Using (IV.11) we can chose

- I elements of $\mathcal{Q}'(N)$ which we write as

$$q_1, q_3, \ldots, q_{2I-1}; \tag{IV.16}$$

- $I - 1$ elements of $\mathcal{Q}(N) \setminus \{q_{2I}\}$ which we write as

$$q_2, q_4, \ldots, q_{2I-2}. \tag{IV.17}$$

Let i be such that $1 \leq i \leq 2I - 1$. Then the prime number p_i is factoring for $\mathcal{A}'(N)$ so by Lemma IV.4 (i) the paths of $\mathcal{A}'(N)$ that contain multiples of p_i are of the form

$$p_i\mathcal{C}_{i,1}, p_i\mathcal{C}_{i,2}, \ldots, p_i\mathcal{C}_{i,F(N/p_i)}$$

where $\mathcal{C}_{i,1}, \mathcal{C}_{i,2}, \ldots, \mathcal{C}_{i,F(N/p_i)}$ is an optimal partition of $\{1, 2, \ldots, \lfloor N/p_i \rfloor\}$. By our choice of indices (IV.16),(IV.17), one of the elements q_i, q_{i+1} is in $\mathcal{Q}'(N)$, we rename it $\widetilde{q_i}$, and the other is in $\mathcal{Q}(N)$, we rename it $\widetilde{q_{i+1}}$. Using (IV.14),(IV.15) we get

$$\frac{N}{3p_i} < \widetilde{q_{i+1}} \leq \frac{N}{2p_i} < \widetilde{q_i} \leq \frac{N}{p_i}.$$

Using (IV.12) and (IV.10), we have $N/p_i \geq N^{1/4} \geq N_0^{1/4} \geq N_1$. Hence we can apply Lemma IV.5 with N/p_i instead of N. We deduce that there exists an optimal partition of $\{1, 2, \dots, \lfloor N/p_i \rfloor\}$ that contains the paths $\widetilde{q_i}$ and $\widetilde{q_{i+1}} - 2\widetilde{q_{i+1}}$. By extracting 1 in that partition, we can stick these two paths together into $\widetilde{q_i} - 1 - 2\widetilde{q_{i+1}} - \widetilde{q_{i+1}}$ while keeping an optimal partition. To sum up, we know now that there is an optimal partition of the integers $\leq N/p_i$ containing a path that has q_i and q_{i+1} as endpoints.

Let $\mathcal{D}_{i,1}, \mathcal{D}_{i,2}, \dots, \mathcal{D}_{i,F(N/p_i)}$ be an optimal partition of the integers $\leq N/p_i$, with $\mathcal{D}_{i,1}$ having q_i, q_{i+1} as endpoints and of maximal length $L_{q_i,q_{i+1}}(N/p_i)$. We can transform $\mathcal{A}'(N)$ by replacing the paths $(p_i\mathcal{C}_{i,j})_{1\leq j\leq F(N/p_i)}$ by $(p_i\mathcal{D}_{i,j})_{1\leq j\leq F(N/p_i)}$. In this way we get a new optimal partition $\mathcal{A}''(N)$ that contains all the paths $p_i\mathcal{D}_{i,1}$ for $1 \leq i \leq 2I-1$, as well as r', $2r - r$, and $p_{2I}q_{2I} - 2p_{2I}q_{2I}$.

By extracting the integers 1, 2 and the q_i for $2 \leq i \leq 2I$, we construct the path of Figure IV.1 while keeping an optimal partition of $\{1, 2, \dots, N\}$.

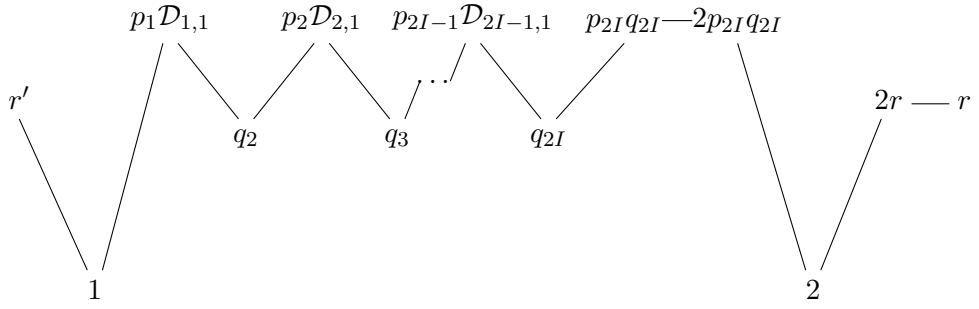

Figure IV.1: A long path with endpoints r', r.

Its length is larger than

$$\sum_{i=1}^{2I-1} L_{q_i,q_{i+1}}(N/p_i) \geq \sum_{p\in\mathcal{P}(N)} H(N/p_i).$$

This being true for any r, r' satisfying (IV.13), we get

$$H(N) \geq \sum_{p\in\mathcal{P}(N)} H(N/p_i).$$

□

IV.5 Proof of the Theorem

Let us fix a constant $N_2 = 2^{2^{k_0}} \geq N_0$, where N_0 is the constant introduced in the proof of the Proposition. Let $B = 1 + \log_2(76)$. We chose a constant $C_0 > 0$ such that for all $N \leq 2^{2^{k_0+2}}$,

$$N \leq 4C_0 \exp\left[\frac{(\log\log N)^2}{\log 2}\right] (\log N)^B. \tag{IV.18}$$

We show by induction on $k \geq k_0 + 2$ that for all N such that

$$2^{2^{k_0}} < N \leq 2^{2^k},$$

we have

$$H(N) \geq \frac{N}{C_0 \exp\left[\frac{(\log\log N)^2}{\log 2}\right] (\log N)^B} \tag{IV.19}$$

Base case

Let N be such that $2^{2^{k_0}} < N \leq 2^{2^{k_0+2}}$, then we have $N > N_2 \geq N_0 \geq N_1^4$ (see (IV.10)) with N_1 the constant of Lemma IV.5. Let r, r' be two prime numbers such that

$$\frac{N}{3} < r \leq \frac{N}{2} < r' \leq N.$$

Lemma IV.5 implies that there is an optimal partition $\mathcal{A}(N)$ of $\{1, 2, \ldots, N\}$ which contains the paths r' and $2r - r$. By extracting 1, we can stick them into $r' - 1 - 2r - r$ while keeping an optimal partition. This implies that $H(N) \geq 4$, and (IV.18) yields the base case.

Induction step

Let $k \geq k_0 + 2$. We suppose that (IV.19) holds for all $N \in \left(2^{2^{k_0}}, 2^{2^k}\right]$.

Let N be such that $2^{2^k} < N \leq 2^{2^{k+1}}$. Since $k \geq k_0 + 2$, we also have $N^{1/4} > 2^{2^{k_0}}$.

Let $p \in (3\sqrt{N \log N}, 4\sqrt{N \log N}]$. By (IV.12), we have

$$2^{2^{k_0}} < N^{1/4} \leq \frac{N}{p} \leq \sqrt{N} \leq 2^{2^k}.$$

By using the induction hypothesis on N/p, we get

$$\begin{aligned} H\left(\frac{N}{p}\right) &\geq \frac{N}{C_0 p \exp\left[\frac{(\log\log(N/p))^2}{\log 2}\right] (\log(N/p))^B} \\ &\geq \frac{N}{C_0 p \exp\left[\frac{(\log\log\sqrt{N})^2}{\log 2}\right] (\log\sqrt{N})^B} \\ &= \frac{2^{B-1}(\log N)^2 N}{C_0 p \exp\left[\frac{(\log\log N)^2}{\log 2}\right] (\log N)^B}. \end{aligned}$$

Hence by using the Proposition and the definition of B,

$$\begin{aligned} H(N) &\geq \sum_{p \in \mathcal{P}(N)} H\left(\frac{N}{p}\right) \\ &\geq \frac{|\mathcal{P}(N)|}{\max \mathcal{P}(N)} \, \frac{2^{B-1}(\log N)^2 N}{C_0 \exp\left[\frac{(\log\log N)^2}{\log 2}\right] (\log N)^B} \\ &\geq \frac{2^{B-1}}{76} \frac{N}{C_0 \exp\left[\frac{(\log\log N)^2}{\log 2}\right] (\log N)^B} \\ &= \frac{N}{C_0 \exp\left[\frac{(\log\log N)^2}{\log 2}\right] (\log N)^B}. \end{aligned}$$

This concludes the induction step.

Finally, since $L(N) \geq 1$ for all $N \geq 1$, we get the Theorem by choosing $A = \max(A_0, A_1)$, where A_0 is a constant such that for all $N \geq N_2$,

$$C_0 \, (\log N)^B \leq (\log N)^{A_0}$$

and A_1 is a constant such that for all $3 \leq N < N_2$,

$$N \leq \exp\left[\frac{(\log\log N)^2}{\log 2}\right] (\log N)^{A_1}.$$

□

Contributions

[1] P. Melotti; "The free-fermionic $C_2^{(1)}$ loop model, double dimers and Kashaev's recurrence"; Journal of Combinatorial Theory, Series A **158**, p. 407 – 448 (2018). ISSN 0097-3165. http://www.sciencedirect.com/science/article/pii/S009731651830058X.

[2] P. Melotti; "The free-fermion eight-vertex model: couplings, bipartite dimers and Z-invariance"; ArXiv e-prints (2018)ArXiv:1811.02026.

[3] P. Melotti & E. Saias; "On path partitions of the divisor graph"; ArXiv e-prints (2018)ArXiv:1807.07783.

[4] T. Bourgeat, J. Bringer, H. Chabanne, R. Champenois, J. Clément, H. Ferradi, M. Heinrich, P. Melotti, D. Naccache & A. Voizard; "New Algorithmic Approaches to Point Constellation Recognition"; dans "ICT Systems Security and Privacy Protection", p. 80–90 (Springer Berlin Heidelberg) (2014). https://doi.org/10.1007%2F978-3-642-55415-5_7.

[5] T. Bourgeat, M. Heinrich, P. Melotti & J.-M. Robert; "A probabilistic Hadwiger-Nelson problem"; ArXiv e-prints (2015)ArXiv:1501.02441.

Bibliography

[AS64] M. Abramowitz and I. A. Stegun. *Handbook of Mathematical Functions with Formulas, Graphs, and Mathematical Tables*. Dover, New York, ninth dover printing, tenth gpo printing edition, 1964.

[ABS03] V. Adler, A. Bobenko, and Y. Suris. Classification of Integrable Equations on Quad-Graphs. The Consistency Approach. *Communications in Mathematical Physics*, 233(3):513–543, Feb 2003.

[ABS04] V. Adler, A. Bobenko, and Y. B. Suris. Geometry of the Yang-Baxter Maps: pencils of conics and quadrirational mappings. *Communications in Analysis and Geometry*, 12(5):967–1008, 2004.

[AN94] M. Aizenman and B. Nachtergaele. Geometric aspects of quantum spin states. *Communications in Mathematical Physics*, 164(1):17–63, Jul 1994.

[Ako11] A. V. Akopyan. *Geometry in figures*. Createspace, 2011.

[AB26] J. W. Alexander and G. B. Briggs. On types of knotted curves. *Annals of Mathematics*, 28(1/4):562–586, 1926.

[AT43] J. Ashkin and E. Teller. Statistics of Two-Dimensional Lattices with Four Components. *Physical Review*, 64:178–184, September 1943.

[Ass17] M. Assis. The 16-vertex model and its even and odd 8-vertex subcases on the square lattice. arXiv:1702.02110, 2017.

[BBT03] O. Babelon, D. Bernard, and M. Talon. *Introduction to Classical Integrable Systems*. Cambridge Monographs on Mathematical Physics. Cambridge University Press, 2003.

[BDS16] J. Baik, P. Deift, and T. Suidan. *Combinatorics and random matrix theory*, volume 172 of *Graduate Studies in Mathematics*. American Mathematical Society, Providence, RI, 2016.

[BP11] Y. Baryshnikov and R. Pemantle. Asymptotics of multivariate sequences, part III: Quadratic points. *Advances in Mathematics*, 228(6):3127 – 3206, 2011.

[Bax72] R. J. Baxter. Partition function of the eight-vertex lattice model. *Annals of Physics*, 70(1):193 – 228, 1972.

[Bax73] R. J. Baxter. Eight-vertex model in lattice statistics and one-dimensional anisotropic Heisenberg chain. I. Some fundamental eigenvectors. *Annals of Physics*, 76(1):1–24, 1973.

[Bax78] R. J. Baxter. Solvable Eight-Vertex Model on an Arbitrary Planar Lattice. *Philosophical Transactions of the Royal Society of London A: Mathematical, Physical and Engineering Sciences*, 289(1359):315–346, 1978.

[Bax82] R. J. Baxter. *Exactly solved models in statistical mechanics*. Academic Press, London, 1982.

[Bax86] R. J. Baxter. Free-fermion, checkerboard and Z-invariant lattice models in statistical mechanics. *Proc. R. Soc. Lond. A*, 404(1826):1–33, 1986.

[BKW76] R. J. Baxter, S. B. Kelland, and F. Y. Wu. Equivalence of the Potts model or Whitney polynomial with an ice-type model. *Journal of Physics A: Mathematical and General*, 9(3):397–406, mar 1976.

[BPAY88] R. J. Baxter, J. H. H. Perk, and H. Au-Yang. New solutions of the star-triangle relations for the chiral Potts model. *Physics Letters A*, 128(3):138 – 142, 1988.

[Baz85] V. V. Bazhanov. Trigonometric Solution of Triangle Equations and Classical Lie Algebras. *Phys. Lett.*, B159:321–324, 1985.

[BS85a] V. V. Bazhanov and Y. G. Stroganov. Hidden symmetry of free fermion model. *Theoretical and Mathematical Physics*, 62(3):253–260, 1985.

[BS85b] V. V. Bazhanov and Y. G. Stroganov. Hidden symmetry of free fermion model. II. Partition function. *Theoretical and Mathematical Physics*, 63(2):519–527, 1985.

[BS85c] V. V. Bazhanov and Y. G. Stroganov. Hidden symmetry of free fermion model. III. Inversion relations. *Theoretical and Mathematical Physics*, 63(3):604–611, 1985.

[BCJ18] V. Beffara, S. Chhita, and K. Johansson. Airy point process at the liquid-gas boundary. *Ann. Probab.*, 46(5):2973–3013, 09 2018.

[Bel79] A. A. Belavin. Exact solution of the two-dimensional model with asymptotic freedom. *Physics Letters B*, 87(1):117 – 121, 1979.

[BPZ84] A. A. Belavin, A. M. Polyakov, and A. B. Zamolodchikov. Infinite Conformal Symmetry in Two-Dimensional Quantum Field Theory. *Nucl. Phys.*, B241:333–380, 1984. [,605(1984)].

[Bet31] H. Bethe. Zur Theorie der Metalle. *Zeitschrift für Physik*, 71(3):205–226, Mar 1931.

[Bol68] L. Boltzmann. *Wissenschaftliche Abhandlungen von Ludwig Boltzmann. I. Band (1865–1874); II. Band (1875–1881); III. Band (1882–1905)*. Herausgegeben von Fritz Hasenöhrl. Chelsea Publishing Co., New York, 1968.

[BdT10] C. Boutillier and B. de Tilière. The critical Z-invariant Ising model via dimers: the periodic case. *Probability Theory and Related Fields*, 147(3):379–413, Jul 2010.

[BdT11] C. Boutillier and B. de Tilière. The critical Z-Invariant Ising model via dimers: locality property. *Communications in Mathematical Physics*, 301(2):473–516, Jan 2011.

[BdT12] C. Boutillier and B. de Tilière. Statistical mechanics on isoradial graphs. In J.-D. Deuschel, B. Gentz, W. König, M. von Renesse, M. Scheutzow, and U. Schmock, editors, *Probability in Complex Physical Systems*, pages 491–512, Berlin, Heidelberg, 2012. Springer Berlin Heidelberg.

[BdTR17] C. Boutillier, B. de Tilière, and K. Raschel. The Z-invariant massive Laplacian on isoradial graphs. *Inventiones mathematicae*, 208(1):109–189, Apr 2017.

[BdTR18] C. Boutillier, B. de Tilière, and K. Raschel. The Z-invariant Ising model via dimers. *Probability Theory and Related Fields*, Jul 2018.

[BdT14] C. Boutillier and B. de Tilière. Height representation of XOR-Ising loops via bipartite dimers. *Electron. J. Probab.*, 19:33 pp., 2014.

[CT83] B. Carlson and J. Todd. The Degenerating Behavior of Elliptic Functions. *SIAM Journal on Numerical Analysis*, 20(6):1120–1129, 1983.

[CS04] G. D. Carroll and D. Speyer. The Cube Recurrence. *Electr. J. Comb.*, 11(1), 2004.

[Cay61] A. Cayley. XXVII. Note on the theory of determinants. *The London, Edinburgh, and Dublin Philosophical Magazine and Journal of Science*, 21(139):180–185, 1861.

[Cha08] A. Chadozeau. Sur les partitions en chaînes du graphe divisoriel. *Periodica Mathematica Hungarica*, 56(2):227–239, 2008.

[Che17] D. Chelkak. Planar Ising model at criticality: state-of-the-art and perspectives. *arXiv preprint*, 2017. arXiv:1712.04192.

[CCK17] D. Chelkak, D. Cimasoni, and A. Kassel. Revisiting the combinatorics of the 2D Ising model. *Annales de l'Institut Henri Poincaré D*, 4(3):309–385, 2017.

[CGS16] D. Chelkak, A. Glazman, and S. Smirnov. Discrete stress-energy tensor in the loop O(n) model. *arXiv e-prints*, April 2016.

[CS12] D. Chelkak and S. Smirnov. Universality in the 2D Ising model and conformal invariance of fermionic observables. *Inventiones mathematicae*, 189(3):515–580, 2012.

[CDC13] D. Cimasoni and H. Duminil-Copin. The critical temperature for the Ising model on planar doubly periodic graphs. *Electron. J. Probab.*, 18:18 pp., 2013.

[CR07] D. Cimasoni and N. Reshetikhin. Dimers on surface graphs and spin structures. I. *Communications in Mathematical Physics*, 275(1):187–208, 2007.

[CR08] D. Cimasoni and N. Reshetikhin. Dimers on surface graphs and spin structures. II. *Communications in Mathematical Physics*, 281(2):445, 2008.

[CKP01] H. Cohn, R. Kenyon, and J. Propp. A variational principle for domino tilings. *Journal of the American Mathematical Society*, 14(2):297–346, 2001.

[dGLR13] J. de Gier, A. Lee, and J. Rasmussen. Discrete holomorphicity and integrability in loop models with open boundaries. *J. Stat. Mech.*, 1302:P02029, 2013.

[dT07] B. de Tilière. Quadri-tilings of the plane. *Probability Theory and Related Fields*, 137(3):487–518, Mar 2007.

[dT18] B. de Tilière. The Z-Dirac and massive Laplacian operators in the Z-invariant Ising model. *ArXiv e-prints*, December 2018.

[Dei19] P. Deift. Fifty Years of KdV: An Integrable System. *arXiv e-prints*, page arXiv:1902.10267, Feb 2019.

[DFMS97] P. Di Francesco, P. Mathieu, and D. Senechal. *Conformal Field Theory*. Graduate Texts in Contemporary Physics. Springer-Verlag, New York, 1997.

[DFSG14] P. Di Francesco and R. Soto-Garrido. Arctic curves of the octahedron equation. *Journal of Physics A: Mathematical and Theoretical*, 47(28):285204, 2014.

[DF68] R. L. Dobrushin and H. C. Folguera. The description of a random field by means of conditional probabilities and conditions of its regularity. *Theory of Probability and its Applications*, 13:197–224, 1968.

[Dod66] C. L. Dodgson. Condensation of determinants, being a new and brief method for computing their arithmetical values. *Proceedings of the Royal Society of London*, 15:150–155, 1866.

[DMS$^+$96] N. P. Dolbilin, A. S. Mishchenko, M. A. Shtan'ko, M. I. Shtogrin, and Y. M. Zinoviev. Homological properties of dimer configurations for lattices on surfaces. *Functional Analysis and Its Applications*, 30(3):163–173, Jul 1996.

[DMNS81] E. Domany, D. Mukamel, B. Nienhuis, and A. Schwimmer. Duality relations and equivalences for models with O(N) and cubic symmetry. *Nuclear Physics B*, 190:279–287, August 1981.

[Dri88] V. G. Drinfel'd. Quantum groups. *Journal of Soviet Mathematics*, 41(2):898–915, Apr 1988.

[Dub11a] J. Dubédat. Exact bosonization of the Ising model. arXiv:1112.4399, Dec 2011.

[Dub11b] J. Dubédat. Topics on abelian spin models and related problems. *Probab. Surveys*, 8:374–402, 2011.

[DCLM18] H. Duminil-Copin, J.-H. Li, and I. Manolescu. Universality for the random-cluster model on isoradial graphs. *Electron. J. Probab.*, 23:70 pp., 2018.

[DCL17] H. Duminil-Copin and M. Lis. On the double random current nesting field. *arXiv e-prints*, page arXiv:1712.02305, Dec 2017.

[DRSV14] B. Duplantier, R. Rhodes, S. Sheffield, and V. Vargas. Critical Gaussian multiplicative chaos: convergence of the derivative martingale. *The Annals of Probability*, 42(5):1769–1808, 2014.

[DS11] B. Duplantier and S. Sheffield. Liouville quantum gravity and KPZ. *Inventiones mathematicae*, 185(2):333–393, 2011.

[Dut80] V. N. Dutyshev. Two-dimensional isotopic model of a fermion field with broken SU(2) symmetry. *Soviet Journal of Experimental and Theoretical Physics*, 51:671, April 1980.

[ES88] R. G. Edwards and A. D. Sokal. Generalization of the Fortuin-Kasteleyn-Swendsen-Wang representation and Monte Carlo algorithm. *Phys. Rev. D*, 38:2009–2012, Sep 1988.

[EKLP92] N. Elkies, G. Kuperberg, M. Larsen, and J. Propp. Alternating-Sign Matrices and Domino Tilings (Part II). *Journal of Algebraic Combinatorics*, 1(3):219–234, Nov 1992.

[Epi66] G. Epifanov. Reduction of a plane graph to an edge by a star-triangle transformation. In *Soviet. Math. Doklady*, volume 166, pages 13–17, 1966.

[EFH83] P. Erdős, R. Freud, and N. Hegyvári. Arithmetical properties of permutations of integers. *Acta Mathematica Hungarica*, 41(1):169–176, 1983.

[ES95] P. Erdős and E. Saias. Sur le graphe divisoriel. *Acta Arithmetica*, 73(2):189–198, 1995.

[Fad95] L. Faddeev. Instructive history of the quantum inverse scattering method. *Acta Applicandae Mathematica*, 39(1):69–84, Jun 1995.

[FW69] C. Fan and F. Y. Wu. Ising model with Second-Neighbor Interaction. I. Some Exact Results and an Approximate Solution. *Phys. Rev.*, 179:560–569, Mar 1969.

[FW70] C. Fan and F. Y. Wu. General Lattice Model of Phase Transitions. *Phys. Rev. B*, 2:723–733, Aug 1970.

[Fel73a] B. Felderhof. Diagonalization of the transfer matrix of the free-fermion model. II. *Physica*, 66(2):279 – 297, 1973.

[Fel73b] B. Felderhof. Diagonalization of the transfer matrix of the free-fermion model. III. *Physica*, 66(3):509 – 526, 1973.

[Fel73c] B. Felderhof. Direct diagonalization of the transfer matrix of the zero-field free-fermion model. *Physica*, 65(3):421 – 451, 1973.

[FP93] T. A. Feo and J. S. Provan. Delta-Wye transformations and the efficient reduction of two-terminal planar graphs. *Operations Research*, 41(3):572–582, 1993.

[Fis61] M. E. Fisher. Statistical mechanics of dimers on a plane lattice. *Phys. Rev.*, 124:1664–1672, Dec 1961.

[Fis66] M. E. Fisher. On the Dimer Solution of Planar Ising Models. *Journal of Mathematical Physics*, 7(10):1776–1781, 1966.

[FZ02a] S. Fomin and A. Zelevinsky. Cluster algebras. I. Foundations. *J. Amer. Math. Soc.*, 15(2):497–529 (electronic), 2002.

[FZ02b] S. Fomin and A. Zelevinsky. The Laurent phenomenon. *Advances in Applied Mathematics*, 28(2):119 – 144, 2002.

[FZ03] S. Fomin and A. Zelevinsky. Cluster algebras. II. Finite type classification. *Invent. Math.*, 154(1):63–121, 2003.

[FR37] R. H. Fowler and G. S. Rushbrooke. An attempt to extend the statistical theory of perfect solutions. *Trans. Faraday Soc.*, 33:1272–1294, 1937.

[GM02] W. Galleas and M. J. Martins. Yang-Baxter equation for the asymmetric eight-vertex model. *Physical Review E*, 66(4):047103, October 2002.

[GL99] A. Galluccio and M. Loebl. On the Theory of Pfaffian Orientations. I. Perfect Matchings and Permanents. *Electr. J. Comb.*, 6, 1999.

[GGKM67] C. S. Gardner, J. M. Greene, M. D. Kruskal, and R. M. Miura. Method for Solving the Korteweg-deVries Equation. *Phys. Rev. Lett.*, 19:1095–1097, Nov 1967.

[GGKM74] C. S. Gardner, J. M. Greene, M. D. Kruskal, and R. M. Miura. Korteweg-deVries equation and generalization. VI. Methods for exact solution. *Comm. Pure Appl. Math.*, 27:97–133, 1974.

[Geo17] T. George. Limit shapes for cube groves with periodic conductances. arXiv:1711.00790, Nov 2017.

[Gib02] J. W. Gibbs. *Elementary principles in statistical mechanics developed with especial reference to the rational foundation of thermodynamics.* New York :C. Scribner,, 1902.

[GK13] A. B. Goncharov and R. Kenyon. Dimers and cluster integrable systems. *Ann. Sci. Éc. Norm. Supér. (4)*, 46(5):747–813, 2013.

[GHS70] R. B. Griffiths, C. A. Hurst, and S. Sherman. Concavity of Magnetization of an Ising Ferromagnet in a Positive External Field. *Journal of Mathematical Physics*, 11:790–795, March 1970.

[GM13] G. R. Grimmett and I. Manolescu. Inhomogeneous bond percolation on square, triangular and hexagonal lattices. *Ann. Probab.*, 41(4):2990–3025, 07 2013.

[Hir77] R. Hirota. Nonlinear Partial Difference Equations. II. Discrete-Time Toda Equation. *Journal of the Physical Society of Japan*, 43:2074, 11 1977.

[HLW75] C. S. Hsue, K. Y. Lin, and F. Y. Wu. Staggered eight-vertex model. *Phys. Rev. B*, 12:429–437, Jul 1975.

[Hur66] C. A. Hurst. New approach to the Ising problem. *Journal of Mathematical Physics*, 7(2):305–310, 1966.

[IC09] Y. Ikhlef and J. Cardy. Discretely holomorphic parafermions and integrable loop models. *Journal of Physics A: Mathematical and Theoretical*, 42(10):102001, 2009.

[Isi25] E. Ising. Contribution to the Theory of Ferromagnetism. *Z. Phys.*, 31:253–258, 1925.

[JK04] J. L. Jacobsen and J. Kondev. Conformal field theory of the Flory model of polymer melting. *Physical Review E : Statistical, Nonlinear, and Soft Matter Physics*, 69:066108, 2004.

[Jim86] M. Jimbo. Quantum R matrix for the generalized Toda system. *Comm. Math. Phys.*, 102(4):537–547, 1986.

[JM94] M. Jimbo and T. Miwa. *Algebraic analysis of solvable lattice models*, volume 85. American Mathematical Soc., 1994.

[JPS98] W. Jockusch, J. Propp, and P. Shor. Random Domino Tilings and the Arctic Circle Theorem. *arXiv Mathematics e-prints*, page math/9801068, Jan 1998.

[Joh05] K. Johansson. The arctic circle boundary and the Airy process. *Ann. Probab.*, 33(1):1–30, 01 2005.

[Jor55] H. Jordan. Eine Bemerkung Über die Monotonie von sn(tK). *Archiv der Mathematik*, 6(3):185–187, Mar 1955.

[Jos11] M. Josefsson. When is a tangential quadrilateral a kite? *Forum Geom.*, 11, 2011.

[Jos12] M. Josefsson. Characterizations of orthodiagonal quadrilaterals. *Forum Geom.*, 12:13–25, 2012.

[KW52] M. Kac and J. C. Ward. A Combinatorial Solution of the Two-Dimensional Ising Model. *Phys. Rev.*, 88:1332–1337, Dec 1952.

[KC71] L. P. Kadanoff and H. Ceva. Determination of an Operator Algebra for the Two-Dimensional Ising Model. *Phys. Rev. B*, 3:3918–3939, Jun 1971.

[KW71] L. P. Kadanoff and F. J. Wegner. Some critical properties of the eight-vertex model. *Phys. Rev. B*, 4:3989–3993, Dec 1971.

[Kas96] R. M. Kashaev. On discrete three-dimensional equations associated with the local Yang-Baxter relation. *Letters in Mathematical Physics*, 38(4):389–397, 1996.

[Kas61] P. W. Kasteleyn. The statistics of dimers on a lattice : I. The number of dimer arrangements on a quadratic lattice. *Physica*, 27:1209–1225, December 1961.

[Kas63] P. W. Kasteleyn. Dimer Statistics and Phase Transitions. *Journal of Mathematical Physics*, 4(2):287–293, 1963.

[Kas67] P. W. Kasteleyn. Graph theory and crystal physics. *Graph Theory and Theoretical Physics*, pages 43–110, 1967.

[Kau49] B. Kaufman. Crystal Statistics. II. Partition Function Evaluated by Spinor Analysis. *Phys. Rev.*, 76:1232–1243, Oct 1949.

[KO49] B. Kaufman and L. Onsager. Crystal Statistics. III. Short-Range Order in a Binary Ising Lattice. *Phys. Rev.*, 76:1244–1252, Oct 1949.

[Ken99] A. E. Kennelly. The equivalence of triangles and three-pointed stars in conducting networks. *Electrical World and Engineer*, 34(12):413–414, 1899.

[Ken97] R. Kenyon. Local statistics of lattice dimers. *Annales de l'Institut Henri Poincaré (B) Probability and Statistics*, 33(5):591 – 618, 1997.

[Ken02] R. Kenyon. The Laplacian and Dirac operators on critical planar graphs. *Inventiones mathematicae*, 150(2):409–439, Nov 2002.

[Ken05] R. Kenyon. Dimer problems. *Encyclopedia of Mathematical Physics, ed. J.-P. Françoise, GL Naber, TS Tsun,(Academic Press, Amsterdam, 2006)*, 2005.

[Ken09] R. Kenyon. Lectures on dimers. statistical mechanics, 191–230. *IAS/Park City Math. Ser*, 16, 2009.

[Ken12] R. Kenyon. The Laplacian on planar graphs and graphs on surfaces. In *Current developments in mathematics, 2011*, pages 1–55. Int. Press, Somerville, MA, 2012.

[Ken19] R. Kenyon. Determinantal spanning forests on planar graphs. *The Annals of Probability*, 47(2):952–988, 2019.

[KLRR18] R. Kenyon, W. Y. Lam, S. Ramassamy, and M. Russkikh. Dimers and Circle patterns. *arXiv e-prints*, page arXiv:1810.05616, Oct 2018.

[KO06] R. Kenyon and A. Okounkov. Planar dimers and Harnack curves. *Duke Math. J.*, 131(3):499–524, 02 2006.

[KOS06] R. Kenyon, A. Okounkov, and S. Sheffield. Dimers and amoebae. *Annals of mathematics*, pages 1019–1056, 2006.

[KP16] R. Kenyon and R. Pemantle. Double-dimers, the Ising model and the hexahedron recurrence. *Journal of Combinatorial Theory, Series A*, 137:27 – 63, 2016.

[KPW00] R. Kenyon, J. Propp, and D. Wilson. Trees and matchings. *The Electronic Journal of Combinatorics [electronic only]*, 7:Research paper R25, 34 p., 2000.

[KS05] R. Kenyon and J.-M. Schlenker. Rhombic embeddings of planar quad-graphs. *Trans. Amer. Math. Soc.*, 357(9):3443–3458, 2005.

[KS13] S. Khachatryan and A. Sedrakyan. On the Solutions of the Yang-Baxter Equations with General Inhomogeneous Eight-Vertex R-Matrix: Relations with Zamolodchikov's Tetrahedral Algebra. *Journal of Statistical Physics*, 150(1):130–155, Jan 2013.

[KW41] H. A. Kramers and G. H. Wannier. Statistics of the Two-Dimensional Ferromagnet. Part I. *Physical Review*, 60:252–262, August 1941.

[Kri81] I. M. Krichever. Baxter's equations and algebraic geometry. *Functional Analysis and Its Applications*, 15(2):92–103, Apr 1981.

[LR69] O. E. Lanford and D. Ruelle. Observables at infinity and states with short range correlations in statistical mechanics. *Comm. Math. Phys.*, 13(3):194–215, 1969.

[Law89] D. F. Lawden. *Jacobi's Elliptic Functions*. Springer New York, New York, NY, 1989.

[LSW04] G. F. Lawler, O. Schramm, and W. Werner. Conformal invariance of planar loop-erased random walks and uniform spanning trees. *Ann. Probab.*, 32(1B):939–995, 2004.

[Lax68] P. D. Lax. Integrals of nonlinear equations of evolution and solitary waves. *Comm. Pure Appl. Math.*, 21:467–490, 1968.

[Lea19] A. Leaf. The Kashaev equation and related recurrences. *SIGMA Symmetry Integrability Geom. Methods Appl.*, 15:012, 64 pages, 2019.

[Len20] W. Lenz. Beitrag zum Verständnis der magnetischen Erscheinungen in festen Körpern. *Z. Phys.*, 21:613–615, 1920.

[Lie67] E. H. Lieb. Residual Entropy of Square Ice. *Phys. Rev.*, 162:162–172, Oct 1967.

[Lin76] K. Y. Lin. Staggered eight-vertex model on the Kagome lattice. *Journal of Physics A: Mathematical and General*, 9(4):581, 1976.

[Lin84] K. Y. Lin. Eight-vertex model on a ruby lattice. *Journal of Physics A: Mathematical and General*, 17(16):3201, 1984.

[LW77] K. Y. Lin and I. P. Wang. Staggered eight-vertex model with four sublattices. *Journal of Physics A: Mathematical and General*, 10(5):813, 1977.

[Lis17] M. Lis. Circle patterns and critical Ising models. *arXiv preprint*, 2017. arXiv:1712.08736.

[LSFW08] D. Lucarelli, A. Saksena, R. Farrell, and I.-J. Wang. Distributed inference for network localization using radio interferometric ranging. *Wireless Sensor Networks*, pages 52–73, 2008.

[LW16] T. Lupu and W. Werner. A note on Ising random currents, Ising-FK, loop-soups and the Gaussian free field. *Electron. Commun. Probab.*, 21:7 pp., 2016.

[Maz06] P. Mazet. Recouvrements hamiltoniens de certains graphes. *European Journal of Combinatorics*, 27(5):739 – 749, 2006.

[McC10] B. M. McCoy. *Advanced statistical mechanics*, volume 146. Oxford University Press, 2010.

[MW14] B. M. McCoy and T. T. Wu. *The two-dimensional Ising model*. Dover Publications, Inc., Mineola, NY, second edition, 2014. Corrected reprint of [MR3618829], with a new preface and a new chapter (Chapter XVII).

[McN18] N. McNew. Counting primitive subsets and other statistics of the divisor graph of $\{1, 2, \ldots n\}$. *arXiv e-prints*, August 2018.

[Mer01] C. Mercat. Discrete Riemann surfaces and the Ising model. *Communications in Mathematical Physics*, 218(1):177–216, 2001.

[MS16] J. Miller and S. Sheffield. Imaginary geometry I: interacting SLEs. *Probability Theory and Related Fields*, 164(3-4):553–705, 2016.

[Nie84] B. Nienhuis. Critical behavior of two-dimensional spin models and charge asymmetry in the Coulomb gas. *Journal of Statistical Physics*, 34(5):731–761, Mar 1984.

[Ons44] L. Onsager. Crystal Statistics. I. A Two-Dimensional Model with an Order-Disorder Transition. *Phys. Rev.*, 65:117–149, Feb 1944.

[Pau35] L. Pauling. The structure and entropy of ice and of other crystals with some randomness of atomic arrangement. *Journal of the American Chemical Society*, 57(12):2680–2684, 1935.

[Pei36] R. Peierls. On Ising's model of ferromagnetism. *Mathematical Proceedings of the Cambridge Philosophical Society*, 32(3):477–481, 1936.

[PW13] R. Pemantle and M. C. Wilson. *Analytic Combinatorics in Several Variables*. Cambridge University Press, New York, NY, USA, 2013.

[PAY06] J. H. H. Perk and H. Au-Yang. Yang-Baxter Equations. In J. P. Françoise, G. L. Naber, and S. T. Tsou, editors, *Encyclopedia of mathematical physics*, volume 5, pages 465–473. Elsevier, 2006.

[PS05] T. K. Petersen and D. Speyer. An arctic circle theorem for Groves. *Journal of Combinatorial Theory, Series A*, 111(1):137 – 164, 2005.

[Pom83] C. Pomerance. On the longest simple path in the divisor graph. *Congr. Numer.*, 40:291–304, 1983.

[Pro01] J. Propp. The Many Faces of Alternating-Sign Matrices. In *DMTCS Proceedings vol. AA, Discrete Models: Combinatorics, Computation, and Geometry (DM-CCG 2001)*, pages 43–58, 2001.

[Rei27] K. Reidemeister. Elementare Begründung der Knotentheorie. *Abhandlungen aus dem Mathematischen Seminar der Universität Hamburg*, 5(1):24–32, Dec 1927.

[Res10] N. Reshetikhin. Lectures on the integrability of the six-vertex model. *Exact methods in low-dimensional statistical physics and quantum computing*, pages 197–266, 2010.

[RV14] R. Rhodes and V. Vargas. Gaussian multiplicative chaos and applications: a review. *Probability Surveys*, 11, 2014.

[RHHB98] C. Richard, M. Höffe, J. Hermisson, and M. Baake. Random tilings: concepts and examples. *Journal of Physics A: Mathematical and General*, 31(30):6385, 1998.

[Sai93] E. Saias. Sur l'utilisation de l'identité de Buchstab. In S. David, editor, *Séminaire de Théorie des Nombres de Paris 1991-1992*, pages 217–245. Birkaüser, 1993.

[Sai98] E. Saias. Applications des entiers à diviseurs denses. *Acta Arithmetica*, 83(3):225–240, 1998.

[Sai03] E. Saias. Etude du graphe divisoriel 3. *Rendiconti del Circolo Matematico di Palermo*, 52(3):481–488, 2003.

[SS78] B. D. Saunders and H. Schneider. Flows on graphs applied to diagonal similarity and diagonal equivalence for matrices. *Discrete Mathematics*, 24(2):205 – 220, 1978.

[Sch71] T. C. Schelling. Dynamic models of segregation. *J. Math. Sociol.*, 1(2):143–186, 1971.

[Sch00] O. Schramm. Scaling limits of loop-erased random walks and uniform spanning trees. *Israel Journal of Mathematics*, 118(1):221–288, Dec 2000.

[She07] S. Sheffield. Gaussian free fields for mathematicians. *Probability theory and related fields*, 139(3-4):521–541, 2007.

[Sla41] J. C. Slater. Theory of the Transition in KH2PO4. *The Journal of Chemical Physics*, 9(1):16–33, 1941.

[Smi01] S. Smirnov. Critical percolation in the plane: conformal invariance, Cardy's formula, scaling limits. *Comptes Rendus de l'Académie des Sciences-Series I-Mathematics*, 333(3):239–244, 2001.

[Smi10] S. Smirnov. Conformal invariance in random cluster models. I. Holomorphic fermions in the Ising model. *Ann. of Math. (2)*, 172(2):1435–1467, 2010.

[SW01] S. Smirnov and W. Werner. Critical exponents for two-dimensional percolation. *Mathematical Research Letters*, 8:729–744, 2001.

[SUAW82] K. Sogo, M. Uchinami, Y. Akutsu, and M. Wadati. Classification of Exactly Solvable Two-Component Models. *Progress of Theoretical Physics*, 68:508–526, August 1982.

[Spe07] D. E. Speyer. Perfect matchings and the octahedron recurrence. *Journal of Algebraic Combinatorics*, 25(3):309–348, 2007.

[Spo91] H. Spohn. *Large Scale Dynamics of Interacting Particles*. Texts and monographs in physics. Springer-Verlag, 1991.

[Sut67] B. Sutherland. Exact solution of a two-dimensional model for hydrogen-bonded crystals. *Phys. Rev. Lett.*, 19:103–104, Jul 1967.

[Sut70] B. Sutherland. Two-Dimensional Hydrogen Bonded Crystals without the Ice Rule. *Journal of Mathematical Physics*, 11(11):3183–3186, 1970.

[Tem74] H. N. V. Temperley. Enumeration of graphs on a large periodic lattice. In *Combinatorics (Proc. British Combinatorial Conf., Univ. Coll. Wales, Aberystwyth, 1973)*, pages 155–159. London Math. Soc. Lecture Note Ser., No. 13. Cambridge Univ. Press, London, 1974.

[TF61] H. N. V. Temperley and M. E. Fisher. Dimer problem in statistical mechanics-an exact result. *The Philosophical Magazine: A Journal of Theoretical Experimental and Applied Physics*, 6(68):1061–1063, 1961.

[Tes00] G. Tesler. Matchings in Graphs on Non-orientable Surfaces. *Journal of Combinatorial Theory, Series B*, 78(2):198 – 231, 2000.

[Thu90] W. P. Thurston. Conway's tiling groups. *Amer. Math. Monthly*, 97(8):757–773, 1990.

[Tut63a] W. T. Tutte. A census of planar maps. *Canadian Journal of Mathematics*, 15:249–271, 1963.

[Tut63b] W. T. Tutte. How to draw a graph. *Proc. London Math. Soc. (3)*, 13:743–767, 1963.

[Val04] L. G. Valiant. Holographic algorithms. In *45th Annual IEEE Symposium on Foundations of Computer Science*, pages 306–315, Oct 2004.

[vdW41] B. L. van der Waerden. Die lange Reichweite der regelmäßigen Atomanordnung in Mischkristallen. *Zeitschrift für Physik*, 118(7):473–488, Jul 1941.

[Vie18] R. S. Vieira. Solving and classifying the solutions of the Yang-Baxter equation through a differential approach. Two-state systems. *Journal of High Energy Physics*, 2018(10):110, Oct 2018.

[Wan45] G. H. Wannier. The statistical problem in cooperative phenomena. *Reviews of Modern Physics*, 17(1):50, 1945.

[WN93] S. O. Warnaar and B. Nienhuis. Solvable lattice models labelled by Dynkin diagrams. *Journal of Physics A: Mathematical and General*, 26(10):2301, 1993.

[Weg72] F. J. Wegner. Duality relation between the Ashkin-Teller and the eight-vertex model. *Journal of Physics C: Solid State Physics*, 5(11):L131, 1972.

[Wer04] W. Werner. Random Planar Curves and Schramm-Loewner Evolutions. In *Lectures on probability theory and statistics*, pages 107–195. Springer, 2004.

[Wu71] F. W. Wu. Ising model with four-spin interactions. *Phys. Rev. B*, 4:2312–2314, Oct 1971.

[Wu69] F. Y. Wu. Exact Solution of a Model of an Antiferroelectric Transition. *Phys. Rev.*, 183:604–607, Jul 1969.

[WL75] F. Y. Wu and K. Y. Lin. Staggered ice-rule vertex model—The Pfaffian solution. *Phys. Rev. B*, 12:419–428, Jul 1975.

[XSR08] X. Xu, S. Sahni, and N. S. V. Rao. On basic properties of localization using distance-difference measurements. In *2008 11th International Conference on Information Fusion*, pages 1–8, 2008.

[Yam18] M. Yamazaki. Cluster-enriched Yang–Baxter equation from SUSY gauge theories. *Letters in Mathematical Physics*, 108(4):1137–1146, Apr 2018.

[Zam79] A. B. Zamolodchikov. Z4-symmetric factorizeds-matrix in two space-time dimensions. *Communications in Mathematical Physics*, 69(2):165–178, Jun 1979.

Paul MELOTTI **28 juin 2019**

Sujet : Modèles intégrables de spins, vertex et boucles

Résumé : Cette thèse porte sur divers problèmes de mécanique statistique, liée à l'étude des modèles intégrables. Dans ces modèles, l'existence de symétries particulières, exprimées par exemple par les équations de Yang-Baxter ou transformations "triangle-étoile", permettent de donner des formules exactes pour les observables d'intérêt.
Dans un premier temps, nous étudions la transformation triangle-étoile du modèle d'Ising, reformulée par Kashaev en une équation d'évolution polynomiale. Nous montrons que cette évolution fait apparaître des objets combinatoires : les modèles de boucles $C_2^{(1)}$. Nous montrons de plus des résultats de formes limites et des calculs d'énergie libre pour ces modèles de boucles.
Dans un second temps, nous développons la compréhension du modèle des "huit sommets", qui généralise les modèles de glace. Nous montrons que dans le régime des fermions libres, ces modèles peuvent être compris via des modèles de dimères bipartis, et des fortes structures d'intégrabilité de ces derniers. Nous en déduisons des constructions de mesures de Gibbs et des corrélations en volume infini, notamment pour des régimes Z-invariants sur des graphes isoradiaux.
Enfin, nous proposons des interprétations des équations de Yang-Baxter en géométrie discrète, via des plongements particuliers de graphes.

Mots clés : Mécanique statistique, modèles intégrables, équations de Yang-Baxter, Triangle-étoile, modèles de spins, modèles vertex, modèles de boucles, fermions libres.

Subject : Integrable spin, vertex and loop models

Abstract: This thesis deals with several problems in statistical mechanics, related to the study of integrable models. In these models, some particular symmetries, like those expressed by the Yang-Baxter equations or "star-triangle" transformations, lead to the existence of exact formulas for observables of interest.
In a first part, we study the star-triangle transformation of the Ising model, recast into a singe polynomial evolution equation by Kashaev. We show that this evolution creates combinatorial objects: $C_2^{(1)}$ loop models. We show some limit shapes results and compute the free energy of these loop models.
In a second part, we develop the study of the "eight-vertex" model, that generalises ice models. In the free-fermion regime, we translate these models into dimers on a bipartite graph, and use the strong integrability structures of these. We deduce the construction of Gibbs measures and correlations in infinite volume, in particular for Z-invariant regimes on isoradial graphs.
Finally, we suggest interpretations of the Yang-Baxter equations in discrete geometry, via particular embeddings of graphs.

Keywords : Statistical mechanics, integrable models, Yang-Baxter equations, star-triangle, spin models, vertex models, loop models, free fermions.